TESIS DE LA UNIVERSIDAD DE ZARAGOZA
2025
228

Lorenzo Arnal Vallés

Cyclometalated N-Heterocyclic Carbenes and Pyrazoles/Pyrazolates: Well-suited Ligands for Pt(II) Complexes with Outstanding Luminescence and Redox Properties

Director/es
Sicilia Martínez, María Violeta
Fuertes Lorda, Sara

ISSN 2254-7606

Prensas de la Universidad
Universidad Zaragoza

Universidad de Zaragoza
Servicio de Publicaciones

ISSN 2254-7606

Universidad Zaragoza
1542

Tesis Doctoral

CYCLOMETALATED N-HETEROCYCLIC CARBENES AND PYRAZOLES/PYRAZOLATES: WELL-SUITED LIGANDS FOR PT(II) COMPLEXES WITH OUTSTANDING LUMINESCENCE AND REDOX PROPERTIES

Autor

Lorenzo Arnal Vallés

Director/es

Sicilia Martínez, María Violeta
Fuertes Lorda, Sara

UNIVERSIDAD DE ZARAGOZA
Escuela de Doctorado

Programa de Doctorado en Química Inorgánica

2023

Departamento de Química Inorgánica
Universidad Zaragoza
Instituto de Síntesis Química y Catálisis Homogénea
CSIC
Consejo Superior de Investigaciones Científicas

Cyclometalated N-Heterocyclic Carbenes and Pyrazoles/Pyrazolates: Well-suited Ligands for Pt(II) Complexes with Outstanding Luminescence and Redox Properties.

Lorenzo Arnal Vallés

Tesis Doctoral

Memoria presentada para optar al grado de Doctor con Mención Internacional por la Universidad de Zaragoza

Departamento de Química Inorgánica

Facultad de Ciencias – ISQCH

Universidad de Zaragoza - CSIC

Cyclometalated N-Heterocyclic Carbenes and Pyrazoles/Pyrazolates: Well-suited Ligands for Pt(II) Complexes with Outstanding Luminescence and Redox Properties.

Memoria presentada por Lorenzo Arnal Vallés, Graduado en Química y Máster Universitario en Química Molecular y Catálisis Homogénea, para optar al grado de Doctor en Ciencias Químicas con "Mención de Doctorado Internacional" por la Universidad de Zaragoza.

Esta Tesis Doctoral se presenta en la modalidad de tesis por compendio de publicaciones, e incluye cinco artículos publicados en revistas científicas internacionales que se encuentran indexadas en el Journal Citations Reports. Todas ellas pertenecen al primer cuartil (Q1) dentro de su categoría.

Las publicaciones incluidas en la Tesis son las siguientes:

1.- Lorenzo Arnal, Sara Fuertes, Antonio Martín, Violeta Sicilia. The Use of Cyclometalated NHCs and Pyrazoles for the Development of Fully Efficient Blue Pt^{II} Emitters and Pt/Ag Clusters. *Chemistry - A European Journal* **2018**, *24* (37), 9377-9384. DOI: 10.1002/chem.201800646. IF: 5.160, Chemistry, Multidisciplinary 37/172

2.- Violeta Sicilia, Lorenzo Arnal, Daniel Escudero, Sara Fuertes, Antonio Martín. Chameleonic Photo- and Mechanoluminescence in Pyrazolate-Bridged NHC Cyclometalated Platinum Complexes. *Inorganic Chemistry* **2021**, *60* (16), 12274-12284. DOI: 10.1021/acs.inorgchem.1c01470. IF: 5.436, Chemistry Inorganic & Nuclear 5/45

3.- Lorenzo Arnal, Sara Fuertes, Antonio Martín, Miguel Baya, Violeta Sicilia. A Cyclometalated N-Heterocyclic Carbene: The Wings of the First Pt_2(II,II) Butterfly Oxidized by CHI_3. *Chemistry – A European Journal* **2018**, *24* (70), 18743-18748. DOI: 10.1002/chem.201804013. IF: 5.160, Chemistry, Multidisciplinary 37/172

4.- Violeta Sicilia, Lorenzo Arnal, Sara Fuertes, Antonio Martin, Miguel Baya. Metal-Metal Cooperation in the Oxidation of a Flapping Platinum Butterfly by Haloforms: Experimental and Theoretical Evidence. *Inorganic Chemistry* **2020**, *59* (17), 12586-12594. DOI: 10.1021/acs.inorgchem.0c01701. IF: 5.165, Chemistry Inorganic & Nuclear 5/45

5.- Lorenzo Arnal, Daniel Escudero, Sara Fuertes, Antonio Martín, Violeta Sicilia. High-Valent Pyrazolate-Bridged Platinum Complexes: A Joint Experimental and Theoretical Study. *Inorganic Chemistry* **2022**, *61* (32), 12559-12569. DOI: 10.1021/acs.inorgchem.2c01441. IF: 5.436 (2021), Chemistry Inorganic & Nuclear 5/45

VIOLETA SICILIA MARTÍNEZ, Catedrática de Universidad del Departamento de Química Inorgánica de la Facultad de Ciencias de la Universidad de Zaragoza

SARA FUERTES LORDA, Investigadora Distinguida del CSIC en el Instituto de Síntesis Química y Catálisis Homogénea (Universidad de Zaragoza – CSIC)

CERTIFICAN:

Que la presente Memoria titulada "Cyclometalated N-Heterocyclic Carbenes and Pyrazoles/Pyrazolates: Well-suited Ligands for Pt(II) Complexes with Outstanding Luminescence and Redox Properties" ha sido realizada en el Departamento de Química Inorgánica de la Universidad de Zaragoza y en el Instituto de Síntesis Química y Catálisis Homogénea (ISQCH) bajo su dirección y AUTORIZAN su presentación para que sea calificada como Tesis Doctoral en la modalidad de compendio de publicaciones. Asimismo, hacen constar la realización de una estancia de tres meses en la *Katholieke Universiteit Leuven* (Leuven, Bélgica), autorizando la solicitud a la mención internacional en el título de Doctor.

Zaragoza, 12 de enero de 2023.

Fdo. Prof. Dr. Violeta Sicilia Martínez Fdo. Dr. Sara Fuertes Lorda

A mis padres

A Pilar

Al resto de mi familia

Alguien dijo: *No olvides jamás el beneficio recibido*. Por ello quiero pararme un momento y dedicar las siguientes líneas a todos vosotros, a los que directa o indirectamente habéis hecho posible esta Tesis. Sin vosotros todo esto no habría sido posible.

En primer lugar, quiero agradecer a la Prof. Violeta Sicilia y a la Dr. Sara Fuertes por darme la oportunidad de realizar mi Tesis Doctoral bajo su dirección. Muchas gracias por la confianza que habéis depositado en mi todo este tiempo (ya son unos cuantos años), por vuestra continua ayuda, orientación, apoyo, cercanía y disponibilidad. Lo que empezó como un TFG inesperado para mí, ha llegado hasta esta Tesis Doctoral.

Me gustaría también agradecer al Prof. Daniel Escudero por acogerme en su grupo como uno más durante mi estancia en la KU Leuven. Muchas gracias por tu seguimiento constante, tu interés y disponibilidad tanto en los días que pudimos ir a la universidad como en el tiempo de confinamiento, reservándome todos los jueves a las 9 de la mañana.

Mi agradecimiento también al Dr. Antonio Martín por su imprescindible contribución en la resolución de las estructuras cristalinas, así como al Dr. Miguel Baya por la realización de algunos cálculos teóricos que han permitido apoyar los datos experimentales. Muchas gracias a los dos por vuestro apoyo, consejo y disponibilidad.

Quiero también darles las gracias a los profesores-investigadores del grupo, Prof. Juan Forniés, Dr. Babil Menjón, Prof. José María Casas, Prof. Irene Ara, Dr. Consuelo Fortuño, por su consejo, apoyo, disponibilidad y ayuda siempre que ha sido necesario.

Tampoco me olvido de los *Platineros* jóvenes presentes y pasados, Sara Jaime (que con su trabajo hizo el nuestro más fácil), Guille Arnal (mi primo el humilde), Sergio, Nacho, Nachito (y su positividad), Laura B. (en busca y captura), Laura F. (buscadora de respuestas), Irene (mi heredera folclórica), Juan, Samuel y las nuevas incorporaciones Jorge I (confiando en mí como codirector), Jorge II y Carmen (mis chicos del helado). También es necesaria una mención especial a los doctores Alberto Pérez (siempre dispuesto a conversar y mejor con un vino), David Campillo (que me instituyó como *Hombre del Renacimiento*), Daniel Joven (que no dudaba en venir a recordarme que tengo un pelazo las veces que fueran necesarias) y Antonio Gimeno (que me legó esa llave del RMN tan necesaria).

También a los culpables de mis excursiones a la otra punta del laboratorio (porque si vienen ellos les sale sarpullido), Joak y Alberto, y a la tercera planta, Isol (lo que unió una bufamanta, que no se separe).

I also want to thank *Computational Photochemistry Lab* at KU Leuven, for the warm welcome to the research group during the three months, especially every Tuesday in the online meetings.

Quiero agradecer a los servicios de análisis elemental y de espectroscopía de masas por su labor tan necesaria y en particular al servicio de RMN, a Rangel (Raquel y Ángel). Gracias por la disponibilidad, apoyo e intercambio de información con charlas en el 400 y el 500.

Hablando de RMN no me puedo olvidar del Dr. Ignacio Delso, para mí siempre Iñaki. Siempre estaré agradecido por la forma en la que me acercaste a esta técnica haciendo posible que en su momento fuera el *Usuario Avanzado más joven*. Gracias por tu disponibilidad para hablar y ayudarme en todo y por optimizarme experimentos como el ^{195}Pt-^{195}Pt {^{1}H} COSY (y… ¿por qué COSY?... Porque podemos).

También quiero dar las gracias a Cris, mi "*Jaca"* (que Cazadores une tanto), por todas esas conversaciones con confianza y que me llevó a conocer a más gente de la que no me olvido (aunque son muy de proteínas y no les gustan los metales), ¡Gracias *Juniors* de Almería!.

No me puedo olvidar de todos mis amigos de Huesca, mis orígenes, Elenita, Silvia, Pablo, Mel, Sergio, el Café de las 4, todos los de PJHU, y de todos los que he ido conociendo en Zaragoza y por España, Marcos, Adri, Nico, Isaí, "Dr." Marcos, mis Cerbunos y muchos otros.

Y por supuesto, a toda mi familia, que todos tienen parte de "culpa" de que haya llegado hasta aquí. Gracias por vuestro apoyo y vuestros consejos durante todo este tiempo.

Tengo claro que sin todos y cada uno de vosotros, tanto en lo científico como en lo personal, no sería el mismo.

Cada uno de nosotros necesita lo que la naturaleza nos da, cuando la naturaleza nos lo da.

Marco Aurelio

¡A todos muchísimas gracias!

Abstract

The chemistry and photophysics of mono- and dinuclear platinum (II) complexes with cyclometalated N-Heterocyclic carbenes and pyrazoles/pyrazolates ligands have been investigated in this PhD thesis. New bis-pyrazolyl compounds $[Pt(C\hat{}C^*_A)(RpzH)_2]X$, containing the NHC cyclometalated group $C\hat{}C^*_A$ ($CH\hat{}C^*_A$ = 1-(4-(ethoxycarbonyl)phenyl)-3-methyl-1*H*-imidazol-2-ylidene) were prepared as chloride, perchlorate or hexafluorophosphate salts. The photophysical properties of these compounds were studied and the lowest energy absorption and the blue emission of these compounds were mainly assigned to intraligand charge-transfer transition (^{1,3}ILCT) on the NHC. Quantum yield measurements in 5%wt PMMA films showed that these compounds are excellent blue emitters with values up to 100%.

These mononuclear compounds were used as precursors to prepare dinuclear pyrazolate bridging complexes $[\{Pt(C\hat{}C^*_A)(\mu\text{-}Rpz)\}_2]$ with a butterfly-like structure. Experimental and theoretical studies reveal the existence of two close-lying minima in both, the ground and the first excited triplet, states corresponding to the *butterfly-wing-spread* and the *butterfly-wing-folded* conformers which are characterized by long and short Pt-Pt distances, respectively. The very low barriers between the two minima support a fast interconversion process, resembling a *butterfly* flapping motion, that influences not only the photo- and mechanoluminescence properties but also the reactivity of these species.

The pyrazolate bridging complex $[\{Pt(C\hat{}C^*_A)(\mu\text{-}pz)\}_2]$ reacts with haloforms CHX_3 (X= Cl, Br, I) and haloalkanes RX (RX = MeI, BnBr, BnI) rendering dinuclear complexes with the same core $[\{Pt(C\hat{}C^*)(\mu\text{-}pz)\}_2]$ but different oxidation states Pt_2(III,III), Pt_2(III,III) ↔ Pt_2(II,IV) and Pt_2(IV,IV). Metal-metal cooperation seemed to be the key for the [2c, 2e] oxidation processes whose mechanisms were studied by DFT calculations.

Resumen

Los compuestos mono- y dinucleares de Platino (II) con ligandos carbeno N-heterocíclicos ciclometalados y pirazoles o pirazolatos como grupos auxiliares han sido el objeto de estudio en esta Tesis Doctoral. Se prepararon nuevos bis-pirazol compuestos [Pt(C^C*$_A$)(RpzH)$_2$]X, con el grupo NHC ciclometalado C^C*$_A$ (CH^C*$_A$ = 1-(4-(etoxicarbonil)fenil)-3-metil-1*H*-imidazol-2-ilideno) y diferentes contra-aniones (cloruro, perclorato o hexafluorofosfato). Se estudiaron las propiedades fotofísicas de estos complejos, en los que tanto la absorción de menor energía como la emisión se asignaron principalmente a transiciones intraligando (^{1,3}ILCT) centradas en el grupo NHC. Las medidas de rendimientos cuánticos en film de PMMA al 5% en peso alcanzaron valores cercanos al 100%, demostrando que son excelentes emisores de luz azul.

Utilizando estos compuestos mononucleares como precursores, se prepararon complejos dinucleares con puentes pirazolato [{Pt(C^C*$_A$)(μ-Rpz)}$_2$] que exhiben una estructura de tipo mariposa. Estudios experimentales y teóricos revelaron la coexistencia de dos mínimos energéticos tanto en el estado fundamental como en el primer estado excitado triplete, correspondientes a los confórmeros de tipo mariposa *"alas-extendidas*" o "*alas-plegadas*", caracterizados por distancias Pt-Pt largas o cortas, respectivamente. Las pequeñas barreras energéticas permiten un rápido proceso de interconversión, similar al aleteo de una *mariposa*, y que influye en las propiedades foto y mecanoluminiscentes así como en la reactividad de estas especies.

El compuesto [{Pt(C^C*$_A$)(μ-pz)}$_2$] reaccionó con haloformos CHX_3 (X= Cl, Br, I) y haloalcanos RX (RX = MeI, BnBr, BnI) dando lugar a complejos dinucleares con el mismo esqueleto [{Pt(C^C*)(μ-pz)}$_2$] pero diferentes estados de oxidación Pt_2(III,III), Pt_2(III,III) ↔ Pt_2(II,IV) y Pt_2(IV,IV). Los efectos de cooperación metal-metal fueron claves para los procesos de oxidación de [2c, 2e], cuyos mecanismos se estudiaron por cálculos DFT.

List of Abbreviatios

Techniques and Experiments

ATR	Attenuated total reflectance
COSY	Correlated Spectroscopy
CV	Cyclic Voltammetry
DCTB	*trans*-2-[3-(4-tert-butylphenyl)-2-methyl-2-propenylidene]malononitrile (MALDI matrix)
DRUV	Diffuse Reflectance UV-vis
HMQC	Heteronuclear Multiple Quantum Coherence
IR	Infrared
MALDI	Matrix-Assisted Laser Desorption/Ionization
NMR	Nuclear Magnetic Resonance
NOE	Nuclear Overhauser Effect
PLQY	Photoluminescence Quantum Yield
QY	Quantum Yield
UV	Ultraviolet

Ligands and Reagents

3,5-dmpzH	3,5-dimethylpyrazole
3,5-dppzH	3,5-diphenylpyrazole
4-MepzH	4-methylpyrazole
Bn	Benzyl
COD	Cycloocta-1,5-diene
Et	Ethyl
Gal·	Galvinoxyl Free Radical
Me	Methyl
NHC	N-Heterociclyc Carbene
^{n}Pr	Linear Propyl
Ph	Phenyl
PMMA	Poly(methyl methacrylate)
pzH	Pyrazole
^{t}Bu	*tert*-butyl

Luminescence and Computational calculations

BO	Bond Order
CIE coordinates	Commission Internationale de L'Éclaire coordinates
DFT / TD-DFT	Density Functional Theory / Time-Dependent Density Functional Theory
FO	Frontier Orbital
GS	Ground State
HOMO	Highest Occupied Molecular Orbital
IC	Internal Conversion
IL	Intraligand
ILCT	Intraligand Charge Transfer
ISC	Intersystem Crossing
LC	Ligand Center
LL'CT	Ligand to Ligand Charge Transfer
LUMO	Lowest Unoccupied Molecular Orbital
MC	Metal Center
MLCT	Metal to Ligand Charge Transfer
MMLCT	Metal-Metal to Ligand Charge Transfer
MO	Molecular Orbital
MUE	Mean Unsigned Error
NBO	Natural Bond Orbital
o.s.	Oscillator Strength
PCM	Polarizable Continuum Model
PES	Potential Energy Surface
PSC	Photostructural Change
SOC	Spin-Orbit Coupling
TS	Transition State
VR	Vibrational Relaxation

Others

LEC	Light Emitting Cell
OA	Oxidative Addition
PhOLED	Phosphorescent Organic Light Emitting Diodes
r.t.	Room Temperature
S_N2	Bi-Molecular Nucleophilic Substitution
T_g	Glass-Transition Temperature

Table of Contents

Introduction and Objectives

Phosphorescent Pt(II) complexes are a kind of photofunctional materials. An extensive research on them has been carried out in the last two decades, driven by their many challenging applications such as light-emitting devices (phosphorescent organic light emitting diodes, PhOLEDs and light emitting cells, LECs),[1-5] optical sensors,[6] photodynamic therapy[7-8] or biolabeling.[9-10] The emission efficiency in the visible spectral range, upon excitation with UV-light, is attributed to the strong spin−orbit coupling (SOC, ξ), induced by the heavy-metal atom (Pt, ξ: 4481 cm^{-1})[11] that facilitates both fast intersystem crossing (ISC) and formally spin-forbidden triplet radiative decay, leading to conversion rates up to 100% (Figure 1).

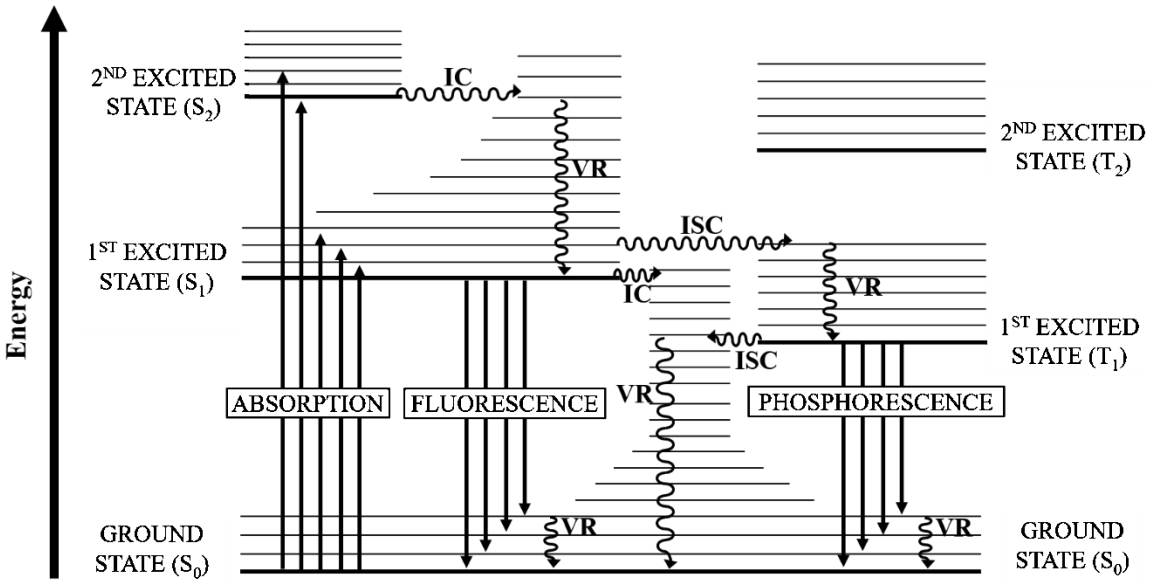

Figure 1. A simplified Jablonski diagram for conjugated organic molecules illustrating key processes: IC represents internal conversion; VR vibrational relaxation; ISC intersystem crossing

In square-planar d^8 complexes, like those of Pt(II), the simple ligand field splitting diagram for *d* orbitals has been represented in Figure 2.[12] The energies of the orbitals depend on the nature of the ligand set, with the dx^2-y^2 being always the highest.

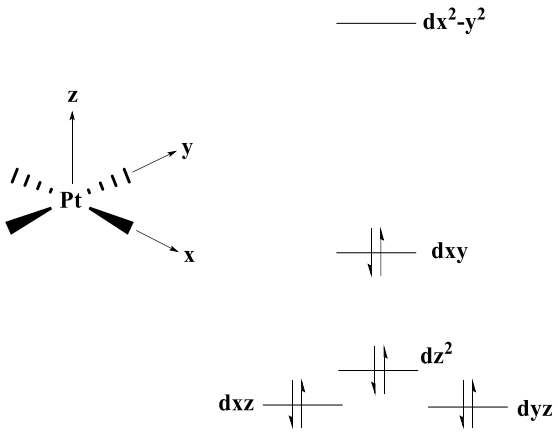

Figure 2. Simple ligand field splitting diagram for *d* orbitals in a square-planar Pt(II) complex.

In platinum (II) complexes with weak field ligands, light absorption leads to the population of the antibonding dx^2-y^2 orbital (Figure 3a), which use to be accompanied by elongation of Pt-L bonds, and severe geometrical distortions in the metal center (MC) excited state. Consequently, it promotes non-radiative deactivation and degradation *via* bond-breaking processes.

Keeping in mind the *Photoluminescence quantum yield* (PLQY, ϕ_{PL}) (ratio of the conversion of absorbed photons into emitted photons, expression in eq.1),[13] to get highly efficient phosphorescent complexes requires to minimize the non-radiative processes ($\sum k_{nr}$).

$$\phi_{PL} = k_r^T / \{k_r^T + \sum k_{nr}^T\} \text{ (eq.1)}$$

In the chemistry of platinum(II), a common approach for the design of efficient and stable phosphorescent systems is the incorporation of strong field ligands, with strong σ-donor/π-acceptor character, into the metal coordination sphere, such as C-deprotonated imines able to act as bidentate (C^N),[14-15] tridentate[14, 16] or tetradentate[14, 17] ligands. This kind of ligands raises the energy of the dx^2-y^2 orbital, preventing from population upon light absorption (Figure 3b). Moreover, they provide the complexes with rigidity and lower energy excited states, in such a way that their emissions arise from triplet metal perturbed intra-ligand charge transfer (^{3}ILCT, $\pi \rightarrow \pi^*$) and/or metal-to-ligand charge transfer (^{3}MLCT).

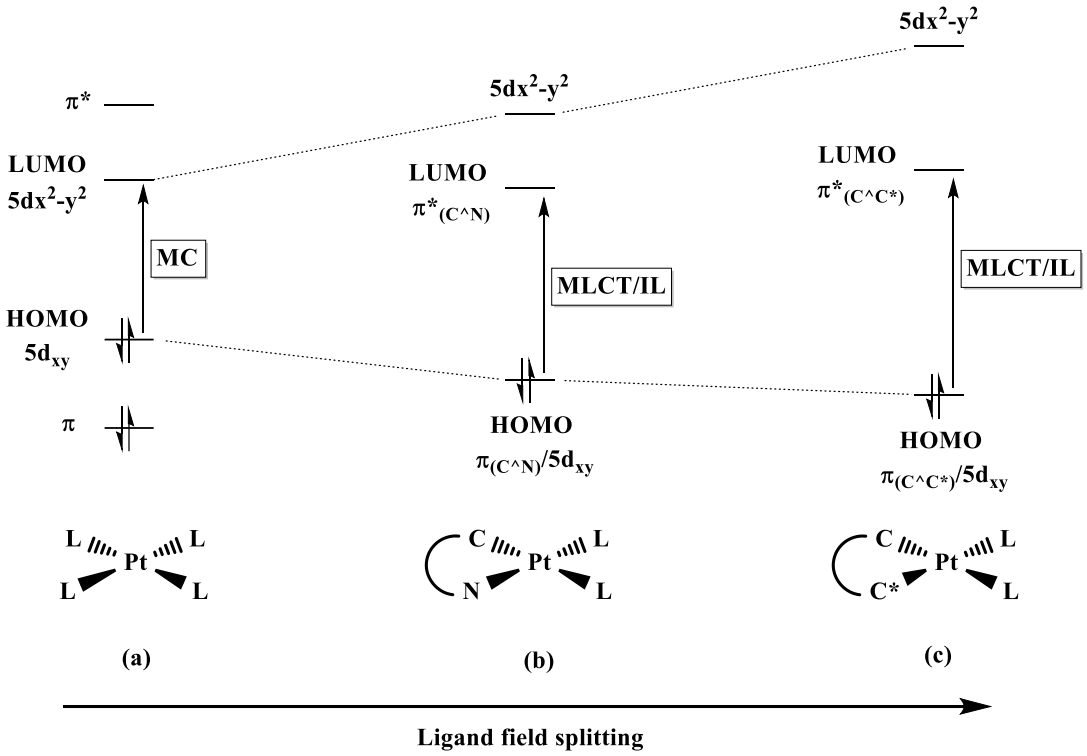

Figure 3. Simple MO diagram in a square-planar Pt(II) complex with weak field ligands(a); and strong field ligands as C^N (b) or C^C* (c).

In this context, cyclometalated N-heterocyclic carbenes (NHCs; C^C*) may surpass the high ligand-field splitting capacity of the C^N ligands because they form two σ M-C bonds (Figure 3c). Another consequence of the presence of strong carbon−metal bonds is the robustness and/or stability of the carbene complexes, which may provide long-term functional materials.[3, 18]

Prof. Thomas Strassner and co-coworkers have extensively investigated in this field. They developed a one-pot strategy (Scheme 1) to get *β*-diketonate complexes, [Pt(R-C^C*)(O^O)].[19-22]

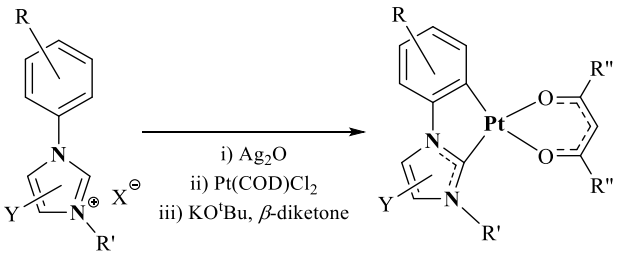

Scheme 1. Synthetic one pot strategy developed by Prof. Thomas Strassner et al.

By changing the nature of the R-C^C*, they have been able to tune the emission of these materials from blue to green-yellow.

Our group, with important contributions in the chemistry of Pt complexes with C,N-cyclometalated groups,[23-25] published its first paper in the field of cyclometalated NHCs "Pt(C^C*)" in 2015.[26] It describes a stepwise procedure to get a chloride-bridged complex with a cyclometalated NHC, [{Pt(Naph^C*)(μ-Cl)}$_2$] (HNaph^C*-*k*C*=3-methyl-1-(naphthalen-2-yl)-1*H*-imidazol-2-ylidene), which is represented in Scheme 2.

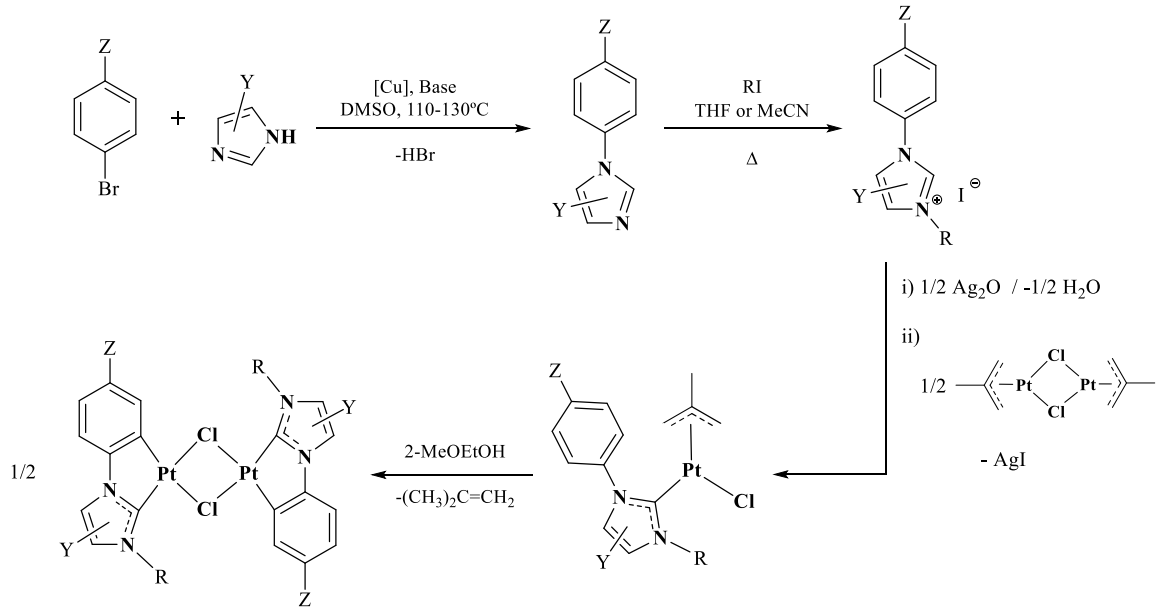

Scheme 2. Stepwise procedure for the synthesis of generic complexes [{Pt(C^C*)(μ-Cl)}$_2$].

This strategy was extended to get other similar complexes with different C^C* groups. Since the elimination of the chloride groups creates two available coordination positions, complexes [{Pt(C^C*)(μ-Cl)}$_2$] probed to be excellent precursors to get complexes with different kinds of ligands, [Pt(C^C*)LL']$^{0,+/-}$ (L, L' = Cyanide, isocyanide, phosphines, diphosphines, acac, dithiocarbamates). Therefore, the photoluminescence of these complexes can be now successfully tuned by varying either the cyclometalated groups or the ancillary ligands.

In the course of the research on Pt(II) complexes with cyclometalated NHCs "Pt(C^C*)", it was observed that the *trans* influence of the carbene (C*) and that of the metalated carbon atom (C_{Ar}) are very high, and not much different from one to another. That is why the synthesis of heteroleptic complexes, [Pt(C^C*)LL'], lead to mixtures of isomers, except when L= PPh_3, [Pt(C^C*)(PPh_3)L'] (L' = py, C≡N-Xyl, MMI (2-mercapto-1-methylimidazole)). In these cases, the greatest T[C_{Ar}/PPh_3)] (T= transphobia) accounts for the stereoselective formation of a unique isomer, the *trans*-(C*,PPh_3) one.[27] To avoid this problem, most of the prepared complexes in our group have either, two equal monodentate ancillary ligands or symmetrical bidentate ones. When the appended Z (Z-C^C*) is H or an electron-acceptor group (Z= CN, CO_2Et), it was possible to reach blue-emitters with high PLQYs in doped PMMA films: up to 70% in NBu_4[Pt(C^C*)($CN)_2$],[28] 93% in [Pt(C^C*)(PPh_3)L]PF_6[18] or [Pt(C^C*)(acac)],[29] and 95% in [Pt(C^C*)(P^P)]PF_6.[30-32] By contrast, those complexes containing Naph^C*, due to the more extended π system, are efficient emitters in the yellow spectral range. Many of these complexes have been proved in light- emitting devices.[18, 30, 32-33]

Objectives and Thesis Structure

Keeping in mind the interest in blue-light emitting systems, since blue light is an essential component of white light, this Thesis research was focused on the synthesis of platinum-based blue-light emitters. For that we used [{Pt(C^C*$_A$)(μ-Cl)}$_2$] (HC^C*$_A$= 1-(4-(ethoxycarbonyl)phenyl)-3-methyl-1*H*-imidazol-2-ylidene) as starting material and pyrazoles/ pyrazolates as auxiliary ligands, trying to combine the robustness of the Pt(C^C*) chromophore and the structural versatility of RpzH/Rpz ligands. This research explores a **thematic unit of knowledge** and resulted in the five publications listed at the beginning of this Memory. They show the synthesis, full characterization and deep study of the photophysical properties of highly efficient blue-light emitters, the mononuclear [Pt(C^C*)(RpzH)$_2$]$^+$ and the dinuclear complexes [{Pt(C^C*)(μ-Rpz)}$_2$] (RpzH = pyrazole (pzH), 4-methylpyrazole (4-MepzH), 3,5-

dimethylpyrazole (3,5-dmpzH), 3,5-diphenylpyrazole (3,5-dppzH)), with the former being used as precursors of the dinuclear Pt_2(II,II) complexes. In the course of this research we observed that the luminescence of the dinuclear systems quenched in contact with halogenated solvents. This quenching was proved to be due to the oxidation of these Pt_2(II,II) complexes to give metal-metal-bonded Pt_2(III,III) ones. Considering that the mechanisms of oxidation of Pt_2(II,II) complexes, with the metal centers held in proximity by bridging ligands, using haloforms had being scarcely explored (see Introduction of Chapter 2 in the Discussion),[34-35] we decided to study these processes and expand this research to alkyl halides, such as methyl iodide (MeI) and benzyl halides (BnBr and BnI). A joint experimental and theoretical study of the mechanisms accounted for this unexpected behavior and the formation of new high-valent pyrazolate-bridged platinum complexes, which were also fully characterized.

In the interest of providing a coherent discussion of the results, the **global discussion** of this Thesis has been split in the **Methodology** followed during this research and two chapters:

Chapter 1: Mono and Dinuclear Platinum (II) Emitters, contains information about the synthesis, characterization and luminescent properties of mononuclear (*Chem. Eur. J.* **2018**, *24*, 9377-9384) and dinuclear complexes (*Inorg. Chem.* **2021**, *60*, 12274-12284).

Chapter 2: Oxidation of the Flapping Platinum *Butterfly* [{Pt(C^C*$_A$)(μ-pz)}$_2$] by Halocarbons, contains information about the mechanisms of oxidation by haloforms (*Chem. Eur. J.*, **2018**, *24*, 18743-18748 and *Inorg. Chem.* **2020**, 59, 12586-12594) and alkyl halides (*Inorg. Chem.* **2022**, *61*, 12559-12569) of the dinuclear complexes.

This Memory contains also the **Conclusions** of the entire Thesis and ends with a list of **References**.

Publications

Heterocycles

The Use of Cyclometalated NHCs and Pyrazoles for the Development of Fully Efficient Blue Pt^{II} Emitters and Pt/Ag Clusters

Lorenzo Arnal,[b] Sara Fuertes,*[b] Antonio Martín,[b] and Violeta Sicilia*[a]

Abstract: New bis-pyrazole complexes [Pt(C^C*)(RpzH)$_2$]X, containing a cyclometalated N-heterocyclic carbene ligand (HC^C* = 1-(4-(ethoxycarbonyl)phenyl)-3-methyl-1*H*-imidazol-2-ylidene) were prepared as chloride (X = Cl^-, RpzH: 3,5-Me_2pzH **1a**, 4-MepzH **2a**, pzH **3a**), perchlorate (X = ClO_4^-, **1b**–**3b**), or hexafluorophosphate (X = PF_6^-, RpzH: 3,5-Me_2pzH **1c**) salts. The X-ray structure of **1a** showed that the Cl^- anion is trapped by the cation through two N–H···Cl bonds. In solution of methanol, acetone and THF at RT, **1a**–**3a** coexist in equilibrium with the corresponding [PtCl(C^C*)(RpzH)] (**B**) and RpzH species. In CH_2Cl_2, this equilibrium takes place just for **2a** and **3a**, but it is completely shifted to the left at 243 and 223 K for **2a** and **3a**, respectively. The low-lying absorption and emission bands were assigned to intraligand (ILCT) charge transfer on the NHC group. Quantum yield measurements in PMMA films revealed that **1b**, **2b** and **1c** are amongst the most efficient blue-light emitters, with values up to 100%. Proton abstraction from the coordinated 3,5-Me_2pzH in **1b** by NEt_3 and replacement by Ag^+ afforded a neutral [Pt_2Ag_2] cluster containing Pt→Ag dative bonds.

Introduction

Cyclometalated N-heterocyclic carbenes (NHCs) have been revealed to be useful groups in the production of efficient and stable phosphorescent transition metal complexes.[1] The presence of two strong carbon–metal bonds confers robustness and stability and may provide long-term functional materials.[2] In the chemistry of Pt^{II} they also induce high crystal field splitting, therefore reducing the photo- or thermal population of high-lying metal dd* states, which result in non-radiative deactivation and degradation via bond-breaking processes.[3] Since population of a high energy excited state is required for an efficient blue emission, the incorporation of strong field ligands such as NHCs is essential in the design of efficient blue-emitting compounds.[2d,e,h–j] Moreover, the use of bidentate cyclometalated NHCs ligands allows the emission tunability of the Pt^{II} complexes by varying either the substituents in the NHC or the nature of the ancillary groups.[1d,4] As an example, our previous work showed that Pt^{II} compounds containing cyclometalated N-heterocyclic carbenes (Scheme 1) were efficient emitters in the blue–yellow region of the visible spectra.[4]

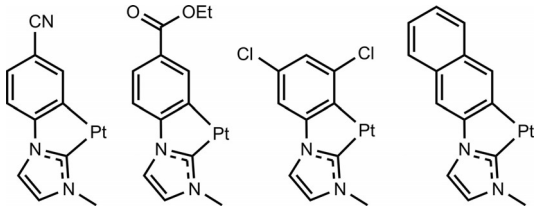

Scheme 1. Overview of cycloplatinated NHC based motifs reported by the authors.

Furthermore, there is significant interest in pyrazole (RpzH) complexes in fields such as medicine, because *cis*-dichlorobis(pyrazole)platinum(II)[5] and related compounds have been shown to have anticancer activity.[6] Pyrazole-based complexes are also useful in catalysis, and in hydrogenation and transfer hydrogenation processes through metal–ligand bifunctional cooperation.[7] Moreover, mononuclear pyrazole complexes are of interest in molecular architecture and luminescence. Pt^{II} complexes, such as [Pt(C≡CPh)$_2$(RpzH)$_2$],[8] [Pt(C^N)(RpzH)$_2$](PF$_6$),[9] [Pt(N^N)(RpzH)$_2$](PF$_6$)$_2$,[9a] [PtCl(3,5-Ph_2pzH)$_3$]Cl, [PtCl(3,5-Ph_2pz)(3,5-Ph_2pzH)$_2$], [Pt(3,5-Ph_2pz)(3,5-Me_2pzH)(3,5-Ph_2pzH)$_2$]Cl,[10] and [Pt(3,5-Me_2pzH)$_4$]Cl$_2$[11] are easily deprotonated and have been used as synthons for the synthe-

[a] *Dr. V. Sicilia*
Departamento de Química Inorgánica
Escuela de Ingeniería y Arquitectura de Zaragoza
Universidad de Zaragoza
Instituto de Síntesis QuímicayCatálisis Homogénea (ISQCH)
Campus Río Ebro, Edificio Torres Quevedo
50018 Zaragoza (Spain)
E-mail: sicilia@unizar.es

[b] *L. Arnal, Dr. S. Fuertes, Dr. A. Martín*
Departamento de Química Inorgánica, Facultad de Ciencias
Universidad de Zaragoza
Instituto de Síntesis QuímicayCatálisis Homogénea (ISQCH)
Pedro Cerbuna 12
50009 Zaragoza (Spain)
E-mail: sfuertes@unizar.es

Supporting information and the ORCID identification number(s) for the author(s) of this article can be found under: https://doi.org/10.1002/chem.201800646.

sis of a great variety of homo- and hetero-polynuclear ([PtM_2], [Pt_2M_2], M = Ag, Au) compounds. The 1,2-dihaptobridging Rpz ligands can hold metal atoms in close proximity while permitting a wide range of structures and intermetallic separations, with the strength of the metallophilic interactions affecting the emissive properties.[8,9]

Keeping this in mind, we decided to expand our work[4] to pyrazole complexes, to combine the robustness of the cyclometalated NHCs Pt^{II} chromophores and the structural versatility of RpzH ligands to achieve new stable and efficient photoluminescent compounds. As a result, we got the new mononuclear bis-pyrazole complexes [Pt(C^C*)(RpzH)$_2$]X, containing a cyclometalated NHC ligand (HC^C* = 1-(4-(ethoxycarbonyl)phenyl)-3-methyl-1*H*-imidazol-2-ylidene). They were isolated as chloride (Cl^-), perchlorate (ClO_4^-) or hexafluorophosphate (PF_6^-) salts, which were possible because of the availability of [{Pt(C^C*)(μ-Cl)}$_2$](**A**)[4b] as a starting material. Here, we describe their synthesis, characterization, and photophysical properties, explained in some cases with the aid of theoretical calculations (TD and DFT). Some of these compounds were found to be very efficient blue emitters with photoluminescent quantum yields (PLQY) up to 100%. The replacement of the proton in the coordinated pyrazoles of [Pt(C^C*)(3,5-Me_2pzH)$_2$]ClO_4 by Ag^+ allowed us to get a heteronuclear [Pt_2Ag_2] cluster and its luminescent properties have been compared with those of its precursor.

Results and Discussion

Synthesis and characterization of mononuclear bis-pyrazole Pt^{II} compounds

The new bis-pyrazole complexes [Pt(C^C*)(RpzH)$_2$]$^+$, containing a cyclometalated N-heterocyclic carbene ligand (HC^C* = 1-(4-(ethoxycarbonyl)phenyl)-3-methyl-1*H*-imidazol-2-ylidene) were prepared and isolated as the chloride (X = Cl^-, RpzH: 3,5-Me_2pzH **1a**, 4-MepzH **2a**, pzH **3a**), perchlorate (X = ClO_4^-, **1b**–**3b**), or hexafluorophosphate (X = PF_6^-, RpzH: 3,5-Me_2pzH **1c**) salts following the strategies indicated in Scheme 2.

Compounds **1a**, **2a** and **3a** were prepared by treatment of a suspension of **A** with 4.4 equivalents of the corresponding pyrazole ligand (RpzH) in acetone at room temperature (see Scheme 2 path a).

They were obtained from their solutions as pure solids in moderately good yield (61% **1a**, 64% **2a**, 60% **3a**) and fully characterized (see Experimental Section and Figures 1 and S1–S9). The proposed stoichiometry for them was later confirmed by single crystal X-ray diffraction of **1a** (see below Figure 1). In solution, the ^{1}H NMR spectrum in CD_2Cl_2 of **1a** (Figure S1) shows one set of signals corresponding to the C^C* group and two non-equivalent 3,5-Me_2pzH ligands. However the ^{1}H NMR spectra of **2a** and **3a** (Figures S3 and S4 (top)) showed the additional presence of the corresponding species [PtCl(C^C*)(RpzH)](**B**). Species **B** result also from the reaction of **A** with 2 equiv of RpzH. The *cis*-(C*,Cl) and *trans*-(C*,Cl) isomers appeared in ratios of 14:1 and 16:1 for 4-MepzH and pzH respectively (see Figure S8) and were identified on the bases of the ^{1}H NMR.[12] Species **B** would be formed from **2a**/**3a** by displacement of a RpzH ligand by the Cl^-, and co-exist in solution with **2a**/**3a** in a dynamic equilibrium, such as the represented in Scheme 3. In agreement with this, addition of 4-MepzH/pzH to a solution of compound **2a**/**3a** in CD_2Cl_2 shifts this equilibrium to the left and the signals attributed to **B** disappear (see Figures S3/S4 bottom).

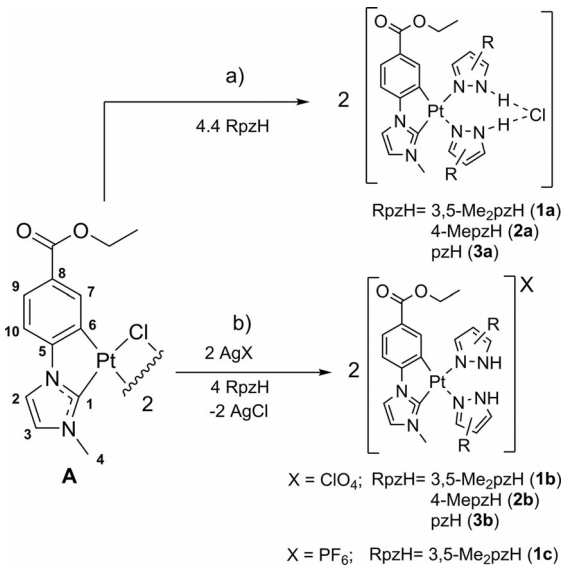

Scheme 2. Numbering scheme and synthetic pathways.

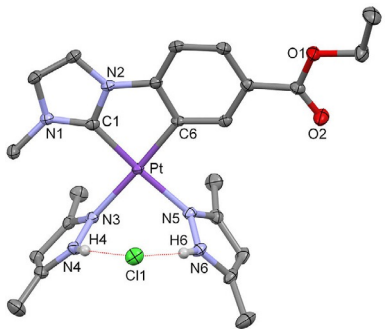

Figure 1. Molecular structure of **1a**. Ellipsoids are drawn at their 50% probability level; solvent molecules and hydrogen atoms were omitted for clarity. Selected bond lengths (Å) and angles (°) for **1a**·CH_2Cl_2: Pt(1)–C(1) = 1.964(3); Pt(1)–C(6) = 2.003(2); Pt(1)–N3 = 2.100(2); Pt(1)–N5 = 2.077(2); C(1)-Pt-C(6) = 80.17(10); C(6)-Pt-N(5) = 95.49(9); C(1)-Pt-N(3) = 96.76(9); N(5)-Pt-N(3) = 87.55(8).

Variable temperature ^{1}H NMR studies, carried out in CD_2Cl_2, for **2a** and **3a** showed that, as the temperature decreases, the amount of **B** decreases, in such a way that **2a** and **3a** are the only species in solution at temperatures equal to or below 243 and 223 K respectively (see Figures S5 and S6). Because the equilibrium represented in Scheme 3 becomes spontaneous ($\Delta G = \Delta H - T\Delta S < 0$) when the temperature raises and $\Delta S > 0$, the dissociation must be an endothermic process. The calculated values for ΔS (93.7 J k^{-1} mol^{-1} **2a**, 111.2 J k^{-1} mol^{-1} **3a**) and ΔH (ΔH = 26.5 KJ mol^{-1} **2a**, 30.3 KJ mol^{-1} **3a**) confirmed these statements (Figure S9). These results illustrate the higher basic-

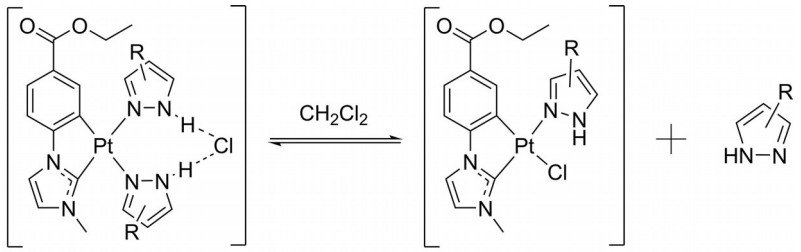

Scheme 3. Dynamic equilibria of **2a** and **3a** in CH_2Cl_2 solution at RT For **B** the major isomer is just represented.

ity of 3,5-Me_2pzH with respect to 4-MepzH and pzH in agreement with the pK_a value of their conjugate acids (3,5-Me_2pzH: 4.06, pzH: 2.83).[10] This equilibrium occurs also in methanol, acetone and THF for all the three compounds **1a**–**3a**, for THF being completely shifted to the right in such a way that just species **B** and RpzH are observed in the corresponding spectra.

The molecular structure of **1a**, determined from a single-crystal X-ray diffraction study, showed the *cis* arrangement of the two 3,5-Me_2pzH-κN ligands in the mononuclear complex and the presence of the chloride anion joined to the cation through two N–H···Cl hydrogen bonds (see Figure 1). The small bite angle of the cyclometalated ligand [80.17(10)°] together with the Pt–C6 and Pt–C1(C*) distances are similar to those found in other five-membered metalocycles of Pt^{II} with NHC ligands.[4a,d] These distances evidence the low *trans* influence of the 3,5-Me_2pzH ligands since them are shorter than those observed in complexes such as [Pt(NC-C^C*)(P P)]PF_6 (P^P = diphenylphosphino-ethane)[12] and [Pt(R-C^C*)(C≡NR′)$_2$]PF_6 (R = CN, CO_2Et; R′ = Xyl, *t*Bu).[4b] The Pt–N bond distances are rather long and similar to those found in complex *cis*-[Pt(C≡C)$_2$(Hdmpz)$_2$],[8] which is in agreement with the high *trans* influence of both C atoms (C1 and C6) of the EtO_2C-C^C*-κC,C* ligand, mainly the σ-bonded C_{Ar}(C6). The plane defined for the 5-membered metalocycle (Plane 1: Pt, C1, N2, C5, C6) is basically co-planar with the platinum coordination plane (Plane 2: Pt, C1, C6, N3, N5). However, the 3,5-Me_2pzH ligands are almost perpendicular to it with interplanar angles of 88.18(0.07)° and 80.34(0.06)° for planes 3 (N3, N4, C14–C16) and 4 (N5, N6, C19–C23) respectively, and they are also perpendicular one to another with the interplanar angle being 89.34(0.09)°.

The two 3,5-Me_2pzH ligands trap the chloride anion through two N–H···Cl hydrogen bonds, with the H4-Cl1-H6 angle being 79.22(1.22)°, almost the theoretical value (90°) for the lone electron pairs of the chloride ligand. The parameters corresponding to both, the two H bonds show values typical for this kind of interaction (H4···Cl1 = 2.3164 (361) Å, N4–H4···Cl1 = 162.39°, H6···Cl1 = 2.2662 (356) Å, N6–H6···Cl1 = 171.9°).[13]

In order to avoid the above analyzed chemical equilibria in solution and be able to study the optical properties of these new bis-pyrazole platinum complexes, we addressed their synthesis as salts of non-coordinating anions: ClO_4^- and PF_6^-. So, compounds **1b**, **2b**, **3b** and **1c** were prepared by treatment of a suspension of **A** with 2 equivalents of AgX (X = ClO_4 **1b**–**3b**, PF_6 **1c**) and 4 equivalents of the corresponding RpzH ligand in acetone at room temperature (see Scheme 1 path b). The workup of their corresponding solutions allowed them to be obtained in good yield (71% **1b**, 89% **2b**, 78% **3b**, 45% **1c**) and be characterized (see Experimental Section and Figures S10–S18 in the Supporting Information).

The strong IR absorptions due to ClO_4^- and PF_6^- anions for **1b**–**3b**, and **1c**; the corresponding $[Pt(C^C^*)(RpzH)_2]^+$ peak in their MALDI(+) mass spectra, molar conductivity[14] and their ^{1}H, ^{13}C{^{1}H} and ^{195}Pt{^{1}H} NMR spectra are in agreement with the proposed stoichiometry. For these compounds the NH resonances appear shifted upfield compared to those of **1a** (see Figure S18 for **1a**–**1c**), most surely due to differences in the H-bond interactions with the counteranion. Taking into account that stronger interactions lead to higher downfield shifting,[15] the H-bond interactions are significantly stronger in **1a** (NH···Cl) than in **1b** (NH···O–ClO_3) and **1c** (NH···F–PF_5).

In spite of their similarities while **1b**, **2b**, and **1c** are stable in CH_2Cl_2 solution at RT, **3b** partially evolves to give [{Pt(C^C*)(μ-pz)}$_2$] and free pzH. After one hour in CD_2Cl_2, the ratio **3b**: [{Pt(C^C*)(μ-pz)}$_2$] was 8:1. Once again this result illustrates the lower basicity of pzH with respect to 3,5-Me_2pzH and to 4-MepzH.[10]

Reactivity of [Pt(C^C*)(3,5-Me_2pzH)$_2$]ClO_4 (1b) towards Ag^I species to give the [Pt_2Ag_2] cluster, 4

The reactions of [Pt(C^C*)(3,5-Me_2pzH)$_2$]ClO_4 (**1b**) with $AgClO_4$ in 1:1 molar in the presence of NEt_3 resulted in the elimination of the two acidic hydrogen atoms and their replacement by Ag^I centers with the subsequent formation of the tetranuclear cluster [{Pt(C^C*)(3,5-Me_2pz)$_2$Ag}$_2$] (**4**) (see Experimental Section and Figures S19–S22). The absence of absorptions due to N–H bonds in the IR and the FAB+ mass spectra are in agreement with the single-crystal X-ray structure of **4** (see Figure 2, Table S1).

As can be seen, **4** is a tetranuclear [Pt_2Ag_2] cluster comprised of two "Pt(C^C*)(3,5-Me_2pz)$_2$Ag" subunits joined through Ag–N bonds and Ag···Ag interactions. Each subunit consists of one "Pt(C^C*)(3,5-Me_2pz)$_2$Ag" fragment with a 3,5-Me_2pz bridging the Pt and Ag centers located in close proximity.

The angle between the Pt–Ag vector and the platinum coordination plane (35.62°) in addition to the Pt–Ag distance are indicative of Pt→Ag dative bonds.[16] This Pt–Ag distance is

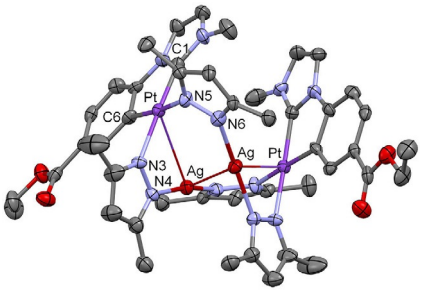

Figure 2. Molecular structure of compound **4**. Ellipsoids are drawn at their 50% probability level and hydrogen atoms were omitted for clarity. Selected bond lengths (Å) and angles (°): Pt–Ag, 3.2626(5); Ag–Ag#1, 3.2171(9); N4-Ag-N6#1, 169.2(2).

shorter than those observed in the related tetranuclear clusters $[Pt_2Ag_2(N^\wedge C)_2(Me_2pz)_4]^{0,2+}$ (N^C = ppy-, dfppy, bpy, $d_{Pt-Ag} > 3.4$ Å).[9a] The Ag center of each subunit completes its coordination environment with a N of a 3,5-Me_2pz belonging to the other Pt subunit with N-Ag-N angles close to 180°. Both silver centers interact with each other, with the Ag···Ag distance being 3.2171(9) Å, quite similar to those observed in other pyrazolate-bridged Pt/Ag clusters, which is indicative of argentophilic interactions.[9a,10,16]

In line with the X-ray structure, the ^{1}H NMR spectrum of freshly solutions of **4** in CD_2Cl_2 (RT, Figure S19; 183 K Figure S20) shows the expected resonances for half of the molecule with two sets of signals corresponding to the inequivalent pyrazolates of one "Pt(C^C*)(3,5-Me_2pz)$_2$" unit. Upon interaction with the silver center, all resonances shift upfield except that of H7 that moves to downfield and shows a moderately reduction of the ^3J(H,Pt) coupling constant from 59.2 Hz in **1b** to 51.2 Hz in **4**. This is in line with the existence of the Pt-M interactions in solution.[17] Also, ^{195}Pt NMR spectrum of **4** supports this statement, showing a signal at −3753 ppm in CD_2Cl_2 solution at 183 K (Figure S22) which is downfield-shifted when compared to that of **1b** (−3920 ppm, 298 K), in agreement with reported results.[9b,18]

Optical Properties

UV/Vis spectra and theoretical calculations

The absorption spectra of compounds **1a**–**1c**, **2b** and **3b** in CH_2Cl_2 (10^{-4} M) solutions (Table S2, Figure S23 and 3 for **1a**) exhibit intense absorptions at $\lambda < 300$ nm ($\varepsilon \geq 10^4$ M^{-1} cm^{-1}), normally attributed to intraligand (^{1}IL) transitions of the NHC ligand. They also display absorption bands at around 315 nm ($\varepsilon \sim 10^3$ M^{-1} cm^{-1}) with a shoulder in the range 340–360 nm. The absorptions of **1b** and **1c** at $\lambda > 300$ nm are very similar to each other, whereas that of **1a** appears slightly redshifted (Figure S23 (a)) indicating subtle differences because of the change in the counteranion. When comparing the perchlorate derivatives (**1b**–**3b**, Figure S23 (b)), we observed a great similarity in the lower-energy region of their spectra. Thus, it seems that the RpzH ligands do not much affect the absorption nor participate in the low energy transitions.

The absorptions at $\lambda > 300$ nm do not change either in CH_2Cl_2 at concentrations ranging from 10^{-3} to 10^{-6} M (see Figure S24 for **2b**) nor in different solvents (CH_2Cl_2, 2-MeTHF, and MeOH) at low concentration (10^{-4} M) (see Table S2 and Figure S25 for **1b**) indicating these absorptions to be due to transitions in the molecular species with no significant aggregation occurring within this concentration range and the absence of significant solvatochromism.

Diffuse reflectance spectra of powdery samples of **1a**–**1c**, **2a**, **2b** **3a**, and **3b** (Figure S26) show no significant differences with respect to those observed in CH_2Cl_2 solution in the range 200–400 nm. However, unlike them, they show weak and similar absorptions in the range 400–450 nm, which could be related with the intermolecular interactions absent in diluted solutions. Like in solution, the changes of both, the RpzH and the counteranion neither seem to have significant effect in the absorption properties in solid state at room temperature. When comparing the UV/Vis spectra of **4** with that of its precursor, **1b**, a lower energy band at ~350 nm appeared (see Figure S27 (a)). Diffuse reflectance spectrum of **4** resembles the UV/Vis one obtained from a freshly solution of **4** in CH_2Cl_2 (see Figure S27). Therefore, according to this and the NMR experiments, the Pt_2Ag_2 core is most likely kept in solution.

The time-dependent density functional theory (TD-DFT) results (Figure 3 and Table 1; Figure S28, and Tables S3–S6 in the Supporting Information) indicate that the HOMO→LUMO transition is the only contribution to the calculated spin-allowed

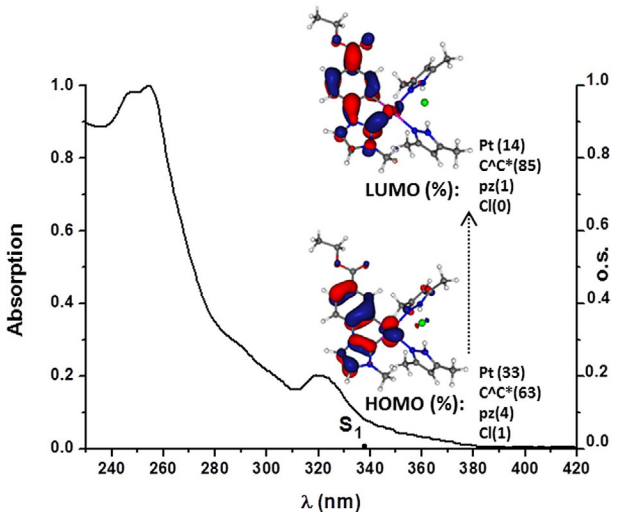

Figure 3. UV/Vis absorption spectrum, calculated transition in CH_2Cl_2 (bars) and calculated molecular orbitals for **1a**.

Table 1. S1 states calculated by TD-DFT in solution of CH_2Cl_2 (o.s. = oscillator strength).

Comp.	λ_{exc} (calc.) [nm]	o.s.	Transition [%]	Assignment
1a	337.8	0.0084	H→L (95)	ILCT, MLCT
1b	337.3	0.0064	H→L (96)	ILCT, MLCT
2b	334.8	0.0051	H→L (96)	ILCT, MLCT
3b	334.6	0.0059	H→L (96)	ILCT, MLCT

transition from S_0 to S_1 (see Table 1). The lowest energy calculated absorptions (S_1) fit well with the experimental ones (Figures 3 and S28).

Hence, the UV/Vis spectra of these compounds can be interpreted by focusing on the analysis of their molecular orbitals (MO) obtained by the DFT calculations, which show that the highest occupied molecular orbital (HOMO) and the lowest unoccupied molecular orbital (LUMO) are mainly centered on the NHC ligand (63–72% H; 76–85% L) and the Pt (27–33% H; 14–25% L) with a marginal contribution of the ancillary ligands (< 5%), which confirm that the Cl and the pyrazole ligands show barely any involvement in the crucial transition processes.

Also, the neutral or cationic nature of the compounds (**1a** vs. **1b**) appears to have very little effect on them. In view of the nature of the HOMO and LUMO, the lowest energy absorption in all compounds has been attributed to a metal-perturbed intraligand charge-transfer transition on the N-heterocyclic carbene (ILCT [(NHC)]) with a small metal-to-ligand charge-transfer contribution (MLCT).

Luminescence spectra

The emission spectra of compounds **1a**–**3a**, **1b**, **2b** and **1c** in rigid matrix (10^{-5} M CH_2Cl_2 solution at 77 K) or in poly(methyl methacrylate) (PMMA) films at 5 wt% are quite similar. They show highly structured emissions ($\lambda_{max} \approx 455$ nm) with vibronic spacings [ca. 1450 cm^{-1}] corresponding to the C=C/C=N stretches of the cyclometalated NHC ligands (see Figure 4 for **1b** Figure S29 and Table 2) with long emission lifetime decays (14–22 μs), typical of phosphorescent Pt^{II} systems. The emission energies are neither affected by the nature of the RpzH ligand nor the anion and are very similar to those of related compounds containing the same "(C^C*)Pt" fragment.[4b,c]

Thus, taking into account all these data and the TD-DFT calculations, these phosphorescent emissions are originated from the monomeric species and assigned mainly to intraligand charge transfer on the N-heterocyclic carbene (^{3}ILCT [(NHC)]).

Powdery solid samples of **1a**–**3a**, **1b**–**3b** and **1c** display bright blue emissions at 298 K (see Table 2 and Figure S30 for

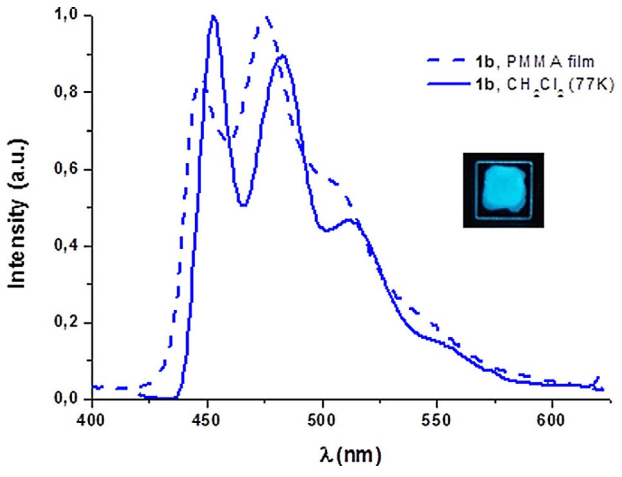

Figure 4. Normalized emission spectra of **1b**. Picture of **1b** taken under UV light (365 nm).

Table 2. Photophysical data for **1a**–**3a**, **1b**–**3b**, **1c** and **4**.

Comp	Media (*T*/K)	λ_{ex} [nm]	λ_{em} [nm]	τ [μs][b]	ϕ[c]
1a	CH_2Cl_2[a] (77)	322	454_{max}, 486, 514	14.0	
	PMMA Film	360	449, 476_{max}, 504		0.66
	Solid (298)	362	448, 475_{max}, 505, 540_{sh}	17.7	
2a[d]	CH_2Cl_2[a] (77)	325	453_{max}, 481, 520	14.9	
	Solid (298)	363	447, 477_{max}, 509, 546_{sh}		
3a[d]	CH_2Cl_2[a] (77)	325	454_{max}, 486, 518	12.3	
	Solid (298)	362	452, 483_{max}, 515, 550_{sh}		
1b	CH_2Cl_2[a] (77)	319	453_{max}, 483, 512, 553_{sh}	21.6	
	PMMA Film	360	447, 475_{max}, $505,540_{sh}$		1.00
	Solid (298)	360	463, 489_{max}, 517, 560_{sh}	13.4	0.33
2b	CH_2Cl_2[a] (77)	319	456_{max}, 488, 517	18.2	
	PMMA Film	360	446, 475_{max}, 500		0.99
	Solid (298)	370	458, 487_{max}, 516	10.1	
3b[e]	CH_2Cl_2[a] (77)	316	451_{max}, 481, 511, 555_{sh}	19.7	
	Solid (298)	366	460, 484_{max}, 515	15.9	
1c	CH_2Cl_2[a] (77)	319	454_{max}, 482, 512_{sh}	21.2	
	PMMA Film	360	455, 478_{max}, 512		1.00
	Solid (298)	370	461, 487_{max}, 518_{sh}	12.9	
4	CH_2Cl_2[a] (77)	340	453_{max}, 484, 512_{sh}	8.4	
	Solid (298)	360	454, 483_{max}, 510	6.4	0.51

[a] 10^{-5} M; [b] measurements at λ_{max}; [c] PMMA films in Ar atmosphere; [d] the dynamic equilibrium in solution hindered the PMMA film to be prepared conveniently for photophysical measurements. [e] QY in PMMA film has not been measured because **3b** evolves partially to [{Pt(C^C*)(μ-pz)}$_2$] in CH_2Cl_2 at RT.

1a–**1c**, **1b**–**3b**) exhibiting band profiles and lifetimes that resemble those obtained in rigid matrix of CH_2Cl_2.

As can be observed, the emission of powdery solid samples is slightly blueshifted when the counter anion is Cl^- (**1a**) instead of ClO_4^- (**1b**) or PF_6^- (**1c**). Luminescent mononuclear bis-pyrazole Pt^{II} compounds are very scarce in the literature. When comparing the emission properties of these mononuclear species with those of other bis-pyrazole compounds [Pt(fppz)(3,5-Me_2pzH)$_2$]Cl [fppzH = 3-(trifluoromethyl)-5-(2-pyridyl)pyrazole)][13c] and [(C^N)Pt(pz)$_2$BEt_2] [C^N = (2-(2,4-difluorophenyl)pyridyl],[19] some similarities concerning the emission profiles and lifetimes were found, but the photoluminescence quantum yields (PLQY) of our complexes in PMMA films (5 wt%) are far more higher with values up to 100%.

As observed in Table 2 and Figure 5, all emissions in PMMA films, except that of **1a** render QY values of 100% and Commission Internationale de L'Éclairage (CIE) coordinates of (0.15, 0.22) which are very close to the desirable ones for blue emitters (0.15, 0.15).[2j] These mononuclear bis-pyrazole compounds are amongst the best blue light emitters of Pt^{II} with QY values in PMMA film higher than the reported ones: [Pt(C^C*)(acac)] (Φ = 0.86,[2d] 0.90),[2e] [Pt(C*^C^C*)Cl] (Φ = 0.32)[2j] and [Pt(C^X-L^L')] [C^X = phenyl methyl imidazole; L^L' = phenoxy pyridine, Φ = 0.58; L^L' = carbazolyl pyridine, Φ = 0.89; C^X = phenyl pyrazole; L^L' = carbazolyl pyridine, Φ = 0.85].[2i] The emission efficiency of **1b**, **2b** and **1c** in PMMA films is in the range, but even larger than those of the related compounds [Pt(R-C^C*)(acac)] (QY = 0.98 R = CN, 0.93 R = CO_2Et in 5 wt% PMMA films).[4d] Undoubtedly, the presence of an electron-withdrawing substituent in the *para* position to the carbene fragment guarantees a high efficiency. In these bis-pyrazole

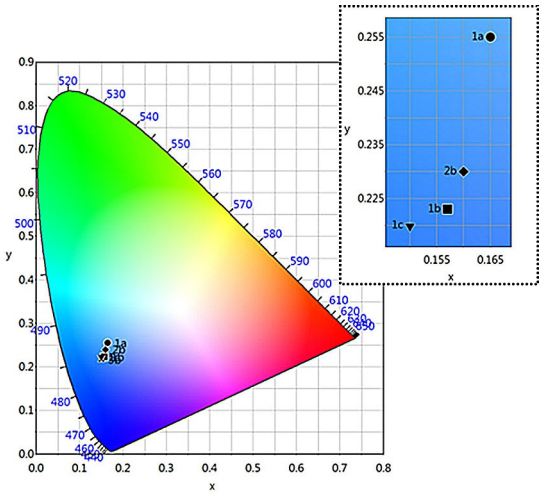

Figure 5. CIE 1931 chromaticity diagram with the (*x*, *y*) positions of the emissions of **1 a**–**1 c** and **2 b** in PMMA films.

compounds, the likely perpendicular disposition of the RpzH with respect to the Pt coordination plane will hinder the intermolecular Pt···Pt interactions, a fact that seems to lower the emission efficiency, as we observed in a previous report.[4d]

The most significant feature of **4**, regarding its emissive behavior, is the blueshift of the emission band of powdery solid in relation to that of its precursor, **1 b** (see Figure S31). This reflects the formation of the Pt→Ag dative bond since the electron density of the Pt center decreases upon bonding to Ag^+, lowering the energy of HOMO.[20] Likewise, there is a considerable reduction of the emission lifetime and an increase of the QY values from 0.33 (**1 b**) to 0.55 (**4**) in powdery solid samples. According to this and in line with similar compounds,[9] this emission has been assigned to a mixed ^{3}IL/^{3}MLCT emissive state.

Conclusions

The availability of the cyclometalated N-heterocyclic carbene compound [{Pt(C^C*)(μ-Cl)}$_2$](**A**) (HC^C* = 1-(4-(ethoxycarbonyl)phenyl)-3-methyl-1*H*-imidazol-2-ylidene) as starting material allowed to get the new bis-pyrazole complexes [Pt(C^C*)(RpzH)$_2$]X, as chloride (Cl^-), perchlorate (ClO_4^-) or hexafluorophosphate (PF_6^-) salts. Their behavior in CH_2Cl_2 solution at room temperature illustrates the higher basicity of the 3,5-Me$_2$pzH with respect to 4-MepzH and pzH and the dependence of the stability of these compounds on the solvent, RpzH and X nature. Then, among the chloride compounds, just [Pt(C^C*)(3,5-Me$_2$pzH)$_2$Cl](**1 a**) is stable in CH_2Cl_2 solution at RT while the 4-MepzH and pzH derivatives coexist with the corresponding [Pt(C^C*)(R-pzH)Cl](**B**) and RpzH species in a dynamic equilibria which can be avoided by lowering the temperature to around 220 K. In other solvents, such as methanol, acetone or THF this equilibrium takes place for all the three chloride compounds, even for **1 a**. Regarding the perchlorate compounds, [Pt(C^C*)(pzH)$_2$]ClO_4 partially evolves to give [Pt(C^C*)(μ-pz)}$_2$] and free pzH in solution at RT Experimental data and TD-DFT calculations showed that both, the anion and the substituent of the ancillary ligands (RpzH) do not deeply affect the nature of the emission of these compounds, which can be mainly assigned to intraligand charge transfer transitions on the N-heterocyclic carbene (^{3}ILCT [(NHC)]). The perchlorate and hexafluorophosphate derivatives (**1 b**, **2 b**, **1 c**) are fully efficient blue-light emitters with QY up to 100% in PMMA films. Compound **1 b** has been proved to behave as a useful synthon to reach the [Pt_2Ag_2] cluster, **4**, by the replacement of the acidic H of 3,5-Me$_2$pzH by Ag^+.

Experimental Section

Information describing materials, instrumental methods used for characterization, photophysical and spectroscopic studies, computational details concerning TD-DFT calculations, and X-ray structures are provided in the Supporting Information. All chemicals were used as supplied unless stated otherwise. The starting material [{Pt(μ-Cl)(C^C*)}$_2$] (**A**) was prepared following the literature procedure.[4b] 3,5-Me$_2$pzH, 4-MepzH, $AgClO_4$ were purchased from Sigma–Aldrich. pzH was purchased from Merck and $AgPF_6$ was purchased from fluorochem.

Synthesis of [Pt(C^C*)(3,5-Me$_2$pzH)$_2$Cl] (1 a)

3,5-Me$_2$pzH (46.5 mg, 0.48 mmol) was added to a suspension of **A** (100.0 mg, 0.11 mmol) in acetone (30 mL) at room temperature and the mixture stirred for 24 h. Subsequently, the solvent was removed under reduced pressure. The residue was treated with hexane/Et_2O (20:1 mL) and the resulting solid was filtered, and washed with hexane to give **1 a** as a yellow solid. Yield: 133.4 mg (61%). ^{1}H NMR (400 MHz, CD_2Cl_2, 25 °C): δ = 14.5 (s br, 1 H; NH), 14.3 (s br, 1 H; NH), 7.72 (dd, ^3J(H9,H10) = 8.1, ^4J (H9,H7) = 1.8, 1 H; H9), 7.48 (d, ^3J(H2,H3) = 2.1, 1 H; H2), 7.15 (d, ^3J (H10,H9) = 8.1, ^4J(H,Pt) = 23.5, 1 H; H10), 6.92 (d, ^4J(H9,H7) = 1.8, ^3J(H,Pt) = 57.5, 1 H; H7), 6.80 (d, ^3J(H3,H2) = 2.1, 1 H; H3), 6.05 (s, 1 H, H4′; 3,5-Me$_2$pzH), 5.98 (s, 1 H, H4″; 3,5-Me$_2$pzH), 4.22 (q, ^3J(H,H) = 7.1, 2 H, CH_2; CO_2Et), 2.97 (s, 3 H; H4), 2.38, 2.37, and 2.31 (s, 12 H, Me; 3,5-Me$_2$pzH), 1.29 ppm (t, ^3J(H,H) = 7.1, 3 H, CH_3; CO_2Et). ^{13}C{^{1}H} NMR (101 MHz, CD_2Cl_2, 25 °C): δ = 166.9 (s; CO_2Et), 155.5 (s; C1), 151.5 (s; C5), 149.6, 148.9, 143.3 and 143.1 (s, 4C, C3′, C3″, C5′, C5″; 3,5-Me$_2$pzH), 135.6 (s; C7), 129.0 and 127.4 (s, 2C; C6 and C8), 127.1 (s; C9), 123.0 (s; C3), 115.9 (s; C2), 110.9 (s; C10), 106.2 (s, C4′; 3,5-Me$_2$pzH), 106.0 (s, C4″; 3,5-Me$_2$pzH), 61.0 (s, CH_2; CO_2Et), 35.3 (s; C4), 14.9 and 14.7 (s, 2C, Me; 3,5-Me$_2$pzH), 14.5 (s, CH_3; CO_2Et), 11.3 ppm (s, 2C, Me; 3,5-Me$_2$pzH). ^{195}Pt{^{1}H} NMR (85.6 MHz, CD_2Cl_2, 25 °C): δ = −3889.6 ppm (s). IR (ATR): $\tilde{\nu}$ = 2917 (br m, NH), 1708 cm^{-1} (m, C=O). MS (MALDI+): *m/z* 616.3 $[M]^+$. Elemental analysis calcd (%) for $C_{23}H_{29}ClN_6O_2Pt$: C 42.37, H 4.48, N 12.89; found: C 42.01, H 4.29, N 12.88.

Synthesis of [Pt(C^C*)(4-MepzH)$_2$Cl] (2 a)

Complex **2 a** was synthesized following the same procedure used for **1 a** with 4-MepzH (22 μL, 0.27 mmol) and **A** (54 mg, 0.06 mmol). **2 a**, yellow solid. Yield: 35.0 mg (64%). ^{1}H NMR (400 MHz, CD_2Cl_2, −40 °C): δ = 14.7 (s br, 1 H; NH), 14.5 (s br, 1 H; NH), 7.70 (dd, ^3J(H9,H10) = 8.1, ^4J(H9,H7) = 1.7, 1 H; H9), 7.63 (s, 1 H; 4-MepzH), 7.61 (s, 1 H; 4-MepzH), 7.53 (s, 1 H; 4-MepzH), 7.51 (s, 1 H; 4-MepzH), 7.47 (d, ^3J(H2,H3) = 1.8, 1 H; H2), 7.14 (d, ^3J(H10,H9) = 8.1, 1 H; H10), 6.91 (d, ^4J(H7,H9) = 1.7, ^3J(H, Pt) = 51.3, 1 H; H7), 6.72 (d, ^3J(H3,H2) = 1.8, 1 H; H3),4.15 (q, ^3J(H,H) = 7.1, 2 H, CH_2; CO_2Et), 2.92 (s, 3 H; H4), 2.12 (s, 3 H, Me; 4-MepzH), 2.05 (s, 3 H, Me; 4-MepzH),

1.15 ppm (t, ^3J(H,H) = 7.1, 3H, CH_3; CO_2Et). $^{195}Pt\{^1H\}$ NMR (85.6 MHz, CD_2Cl_2, −40 °C): $\delta = -3874.1$ ppm (s). IR (ATR): $\tilde{\nu} = 2926$ (m, br, NH), 1703 cm^{-1} (m, C=O). MS (MALDI+): *m/z* 506.2 $[Pt(C\hat{}C^*)(4\text{-MepzH})]^+$. Elemental analysis calcd (%) for $C_{21}H_{25}ClN_6O_2Pt$: C 40.42, H 4.04, N 13.47; found: C 40.31, H 3.84, N 13.42.

Synthesis of [Pt(C^C*)(pzH)$_2$Cl] (3 a)

Complex **3 a** was synthesized following the same procedure used for **1 a** with pzH (20.6 mg, 0.30 mmol) and **A** (61.3 mg, 0.07 mmol). **3 a**, yellow solid. Yield: 31.4 mg (60 %). ^1H NMR (400 MHz, CD_2Cl_2, −60 °C): $\delta = 15.0$ (s br, 1H; NH), 14.9 (s br, 1H; NH), 7.89 (s, 1H; pzH), 7.85 (s, 1H; pzH), 7.75 (s, 1H; pzH), 7.73 (s, 1H; pzH), 7.68 (dd, ^3J(H9,H10) = 8.1, ^4J(H9,H7) = 1.4, 1H; H9), 7.57 (s, 1H; H2), 7.20 (d, ^3J(H10,H9) = 8.1, 1H; H10), 6.83 (d, ^4J(H7,H9) = 1.4, ^3J(H,Pt) = 50.5, 1H; H7), 6.64 (s,1H; H3), 6.51 (s, 1H; pzH), 6.44 (s, 1H; pzH), 4.13 (q, ^3J(H,H) = 6.9, 2H, CH_2; CO_2Et), 2.83 (s, 3H; H4), 1.23 ppm (t, ^3J(H,H) = 6.9, 3H, CH_3; CO_2Et). $^{195}Pt\{^1H\}$ NMR (85.6 MHz, CD_2Cl_2, −60 °C): $\delta = -3880.8$ ppm (s). IR (ATR): $\tilde{\nu} = 2975$ (m, br, NH), 1700 cm^{-1} (m, C=O). MS (MALDI+): *m/z* 492.2 $[Pt(C\hat{}C^*)(pzH)]^+$. Elemental analysis calcd (%) for $C_{19}H_{21}ClN_6O_2Pt$: C 38.29, H 3.55, N 14.10; found: C 37.97, H 3.42, N 13.71.

Synthesis of [Pt(C^C*)(3,5-Me$_2$pzH)$_2$]ClO$_4$ (1 b)

$AgClO_4$ (45.5 mg, 0.22 mmol) was added to a stirred suspension of **A** (100.0 mg, 0.11 mmol) in acetone (50 mL) in the dark at room temperature. After 2 h of reaction, 3,5-Me_2pzH (42.2 mg, 0.44 mmol) was added to the mixture and allowed to react for 16.5 h in the darkness. Then, the resulting suspension was filtered through Celite and the solvent was removed under reduced pressure. The residue was treated with hexane/Et_2O (20:1 mL) and filtered to give **1 b** as a pale yellow solid. Yield: 110.7 mg (71 %). ^1H NMR (400 MHz, CD_2Cl_2, 25 °C): $\delta = 11.8$ (s br, 1H; NH), 11.6 (s br, 1H; NH), 7.75 (dd, ^3J(H9,H10) = 8.1, ^4J(H9,H7) = 1.8, 1H; H9), 7.36 (d, ^3J(H2,H3) = 2.2, 1H; H2), 7.07 (d, ^3J(H10,H9) = 8.1, 1H; H10), 6.86 (d, ^3J(H3,H2) = 2.2, 1H; H3), 6.84 (d, ^4J(H7,H9) = 1.8, ^3J(H,Pt) = 59.2, 1H; H7), 6.13 (s, 1H, H4′; 3,5-Me_2pzH), 6.06 (s, 1H, H4″; 3,5-Me_2pzH), 4.22 (q, ^3J(H,H) = 7.1, 2H, CH_2; CO_2Et), 3.06 (s, 3H; H4), 2.41, 2.37, 2.36 and 2.34 (s, 12H, Me; 3,5-Me_2pzH), 1.29 ppm (t, ^3J(H,H) = 7.1, 3H, CH_3; CO_2Et). $^{13}C\{^1H\}$ NMR (101 MHz, CD_2Cl_2, 25 °C): $\delta = 166.7$ (s; *C*O_2Et), 155.0 (s; C1), 151.0 (s; C5), 150.2, 150.0 and 144.4 (s, 4C, C3′, C3″, C5′, C5″; 3,5-Me_2pzH), 135.6 (s; C7), 128.2 (s; C8), C6 is not detected, 127.5 (s; C9), 123.0 (s; C3), 115.7 (s; C2), 110.8 (s; C10), 106.8 (s, C4′; 3,5-Me_2pzH), 106.6 (s, C4″; 3,5-Me_2pzH), 61.1 (s, CH_2; CO_2Et), 35.5 (s; C4), 14.7 (s, 1C, Me; 3,5-Me_2pzH), 14,8 (s, 1C, Me; 3,5-Me_2pzH), 14.5 (s; CH_3, CO_2Et), 11.3 ppm (s, 2C; Me, 3,5-Me_2pzH). $^{195}Pt\{^1H\}$ NMR (85.6 MHz, CD_2Cl_2, 25 °C): $\delta = -3920.1$ ppm (s). IR (ATR): $\tilde{\nu} = 3140$ (m, br, NH), 1668 (m, C=O), 1060, 620 cm^{-1} (s, ClO_4). MS (MALDI+): *m/z* 616.2 $[M]^+$. Λ_M (5×10^{-4} M acetone solution): 103.5 $\Omega^{-1}cm^{-2}mol^{-1}$. Elemental analysis calcd (%) for $C_{23}H_{29}ClN_6O_6Pt$: C 38.58, H 4.08, N 11.73; found: C 38.49, H 4.05, N 11.80.

Synthesis of [Pt(C^C*)(4-MepzH)$_2$]ClO$_4$ (2 b)

$AgClO_4$ (45.5 mg, 0.22 mmol) was added to a stirred suspension of **A** (100.0 mg, 0.11 mmol) in acetone (50 mL) in the dark at room temperature. After 3 h, 4-MepzH (36 μL, 0.44 mmol) was added to the mixture and allowed to react for 14 h in the darkness. Then, the resulting suspension was filtered through Celite and the solvent was evaporated to dryness. The residue was treated with hexane/Et_2O (20/1 mL) and filtered, to give **2 b** as a pale yellow solid. Yield: 133.5 mg (89 %). ^1H NMR (400 MHz, CD_2Cl_2, 25 °C): $\delta =$ 12.2 (s br, 1H; NH), 12.0 (s br, 1H; NH), 7.76 (dd, ^3J(H9,H10) = 8.1, ^4J(H9,H7) = 1.9, 1H; H9), 7.65 (s, 1H, H3″; 4-MepzH), 7.64 (s, 1H, H3′; 4-MepzH), 7.59 (s, 1H, H5″; 4-MepzH), 7.54 (s, 1H, H5′; 4-MepzH), 7.35 (d, ^3J(H2,H3) = 2.1, 1H; H2), 7.07 (d, ^3J(H10,H9) = 8.1, 1H; H10), 6.90 (d, ^4J(H7,H9) = 1.7, ^3J(H7,Pt) = 58.5, 1H; H7), 6.85 (d, ^3J(H3,H2) = 2.1, 1H; H3), 4.22 (q, ^3J(H,H) = 7.1, 2H, CH_2; CO_2Et), 3.01 (s, 3H; H4), 2.16 (s, 3H, Me‘‘; 4-MepzH), 2.11 (s, 3H, Me″; 4-MepzH), 1.28 ppm (t, ^3J(H,H) = 7.1, 3H, CH_3; CO_2Et). $^{13}C\{^1H\}$ NMR (101 MHz, CD_2Cl_2, 25 °C): $\delta = 166.7$ (s; *C*O_2Et), 154.2 (s; C1), 151.4 (s; C5), 140.7(s, C5″; 4-MepzH), 140.6 (s, C5′; 4-MepzH), 135.6 (s; C7), 131.1 (s, C3″; 4-MepzH), 130.8 (s, C3′; 4-MepzH), 127.8 (s; C9), 127.5 (s, 2C; C6 and C8), 123.0 (s; C3), 118.6 (s, C4″; 4-MepzH), 118.3 (s; C4′, 4-MepzH), 115.7 (s; C2), 111.0 (s; C10), 61.2 (s, CH_2; CO_2Et), 35.8 (s; C4), 14.5 (s, CH_3; CO_2Et), 9.1 ppm (s, 2C, Me‘‘ and Me″; 4-MepzH). $^{195}Pt\{^1H\}$ NMR (85.6 MHz, CD_2Cl_2, 25 °C): $\delta = -3915.6$ (s). IR (ATR): $\tilde{\nu} = 3137$ (m, NH), 1655 (m, C=O), 1077, 623 cm^{-1} (s, ClO_4). MS (MALDI+): *m/z* 588.3 $[M]^+$. Λ_M (5×10^{-4} M acetone solution): 103.8 $\Omega^{-1}cm^{-2}mol^{-1}$. Elemental analysis calcd (%) for $C_{21}H_{25}ClN_6O_6Pt$: C 36.66, H 3.66, N 12.22; found: C 36.29, H 3.66, N 12.35.

Synthesis of [Pt(C^C*)(pzH)$_2$]ClO$_4$ (3 b)

Complex **3 b** was synthesized following the same procedure used for **2 b** with $AgClO_4$ (46.2 mg, 0.22 mmol), **A** (101.4 mg, 0.11 mmol) and pzH (30.0 mg, 0.44 mmol). **3 b**, white solid. Yield: 114.0 mg (78 %). ^1H NMR (400 MHz, CD_3OD, 25 °C): $\delta = 8.02$ (m, 2H; pzH), 7.93 (d, ^3J(H,H) = 1.9, 1H; pzH), 7.80 (m, 2H; H2 and H (pzH)), 7.75 (dd, ^3J(H9,H10) = 8.2, ^4J (H9,H7) = 1.7, 1H; H9), 7.31 (d, ^3J(H10,H9) = 8.2, 1H; H10), 7.22 (d, ^3J (H3,H2) = 2.1, 1H; H3), 7.01 (d, ^4J(H7,H9) = 1.7, ^3J(H,Pt) = 57.0, 1H; H7), 6.61 (m, 2H, H4′ and H4″; pzH), 4.23 (q, ^3J(H,H) = 7.1, 2H, CH_2; CO_2Et), 3.15 (s, 3H; H4), 1.30 ppm (t, ^3J(H,H) = 7.1, 3H, CH_3; CO_2Et). $^{13}C\{^1H\}$ NMR (101 MHz, CD_3OD, 25 °C): $\delta = 168.0$ (s; *C*O_2Et), 155.0 (s; C1), 152.9 (s; C5), 141.8 (s, 1C; pzH), 141.4 (s, 1C; pzH), 136.3 (s; C7), 132.7 (s, 1C; pzH), 132.6 (s, 1C; pzH), 128.4 (s; C9), 128.7 and 127.7 (s; C6 and C8), 124.4 (s; C3), 116.7 (s; C2), 111.7 (s; C10), 108.5 (s, 1C; pzH), 108.1 (s, 1C; pzH), 61.8 (s, CH_2; CO_2Et), 35.6 (s; C4), 14.5 ppm (s, CH_3; CO_2Et). $^{195}Pt\{^1H\}$ NMR (85.6 MHz, CD_3OD, 25 °C): $\delta = -3923.7$ ppm (s). IR (ATR): $\tilde{\nu} = 3134$ (m, br, NH), 1662 (m, C=O), 1086, 622 cm^{-1} (s, ClO_4). MS (ESI+): *m/z* 560.1 $[M]^+$. Λ_M (5×10^{-4} M acetone solution): 100.6 $\Omega^{-1}cm^{-2}mol^{-1}$. Elemental analysis calcd (%) for $C_{19}H_{21}ClN_6O_6Pt\cdot2H_2O$: C 32.79, H 3.62, N, 12.08; found: C 33.1, H 3.48, N 12.10.

Synthesis of [Pt(C^C*)(3,5-Me$_2$pzH)$_2$]PF$_6$ (1 c)

$AgPF_6$ (44.0 mg, 0.17 mmol) was added to a stirred suspension of **A** (80.0 mg, 0.09 mmol) in acetone (50 mL) in the darkness at room temperature. After 3 h, 3,5-Me_2pzH (33.79 mg, 0.35 mmol) was added to the mixture and allowed to react for 14 h in the darkness. Then, the resulting suspension was filtered through Celite and the solvent was evaporated to dryness. The residue was treated with hexane/Et_2O (20/1 mL) and filtered to give **1 c** as a pale yellow solid. Yield: 60.0 mg (45 %). ^1H NMR (300 MHz, CD_2Cl_2, 25 °C): $\delta =$ 11.0 (s br, 1H; NH), 10.9 (s br, 1H; NH), 7.76 (dd, ^3J(H9,H10) = 8.1, ^4J(H9,H7) = 1.5, 1H; H9), 7.37 (d, ^3J(H2,H3) = 1.9, 1H; H2), 7.08 (d, ^3J(H10,H9) = 8.1, ^4J(H,Pt) = 22.2, 1H; H10), 6.88 (d, ^3J(H3,H2) = 1.9, 1H; H3), 6.86 (s, ^3J(H,Pt) = 58.9, 1H; H7), 6.14 (s, 1H, H4′; 3,5-Me_2pzH), 6.07 (s, 1H, H4″; 3,5-Me_2pzH), 4.22 (q, ^3J(H,H) = 7.1, 2H, CH_2; CO_2Et), 3.07 (s, 3H; H4), 2.40, 2.34 (s, 12H, Me; 3,5-Me_2pzH), 1.29 ppm (t, ^3J(H,H) = 7.1, 3H, CH_3; CO_2Et). $^{195}Pt\{^1H\}$ NMR (85.6 MHz, CD_2Cl_2, 25 °C): $\delta = -3931.3$ ppm (s). IR (ATR): $\tilde{\nu} = 3150$ (m, NH), 1675 (m, C=O), 831, 555 cm^{-1} (s, PF_6). MS (MALDI+): *m/z* 616.2 $[M]^+$.

Λ_M (5×10^{-4} M acetone solution): 134.8 $\Omega^{-1}\,cm^{-2}\,mol^{-1}$. Elemental analysis calcd (%) for $C_{23}H_{29}F_6N_6O_2PPt$: C 36.27, H 3.84, N 11.04; found: C 36.09, H 3.80, N 11.02.

Synthesis of [{Pt(C^C*)(3,5-Me$_2$pz)Ag}$_2$] (4)

To a solution of **1b** (150 mg, 0.21 mmol) in methanol (10 mL) was added $AgClO_4$ (45 mg, 0.21 mmol) and excess of NEt_3 (0.5 mL, 3.58 mmol). The solution was stirred for 1 h at r.t. in the dark. The resulted yellow precipitate was collected, washed with methanol, and dried in vacuum. Yield 116 mg (78%). ^{1}H NMR (400 MHz, CD_2Cl_2, 25 °C): δ = 7.63 (dd, ^3J(H9,H10) = 8.1, ^4J(H9,H7) = 1.7, 2H; H9), 7.18 (d, ^3J(H2,H3) = 2.0, 2H; H2), 7.15 (d, ^4J(H7,H9) = 1.7, ^3J(H,Pt) = 51.2, 2H; H7), 6.88 (d, ^3J(H10,H9) = 8.1, 2H; H10), 6.57 (d, ^3J(H3,H2) = 2.0, 2H; H3), 6.01 (s, 2H, H4′; 3,5-Me$_2$pz), 5.78 (s, 2H, H4′; 3,5-Me$_2$pz), 4.21 (m, 4H; CH_2, CO_2Et), 2.41 (s, 6H; H4), 2.22 (s, 6H, Me; 3,5-Me$_2$pz), 2.21 (s, 6H, Me; 3,5-Me$_2$pz), 2.03 (s, 6H, Me; 3,5-Me$_2$pz), 1.70 (s, 6H, Me; 3,5-Me$_2$pz), 1.28 ppm (t, ^3J (H,H) = 7.1, 6H, CH_3; CO_2Et). ^{13}C{^{1}H} NMR (101 MHz, CD_2Cl_2, −90 °C): δ = 166.8 (s; CO_2Et), 159.0 (s; C1), 151.5 (s; C5), 148.2, 147.0, 146.1 (s; 3,5-Me$_2$pz), 137.1 (s; C7), 134.5 (s; C6), 126.3 (s; C8), 125.8 (s; C9), 122.5 (s; C3), 113.8 (s; C2), 109.6 (s; C10), 102.8 (s, C_4; 3,5-Me$_2$pz), 102.6 (s, C4′; 3,5-Me$_2$pz), 60.8 (s, CH_2; CO_2Et), 33.6 (s, C4), 14.2, 14.1, 14.0 (s, CH_3; CO_2Et and 3,5-Me$_2$pz), 13.6, 13.2 ppm (s, Me; 3,5-Me$_2$pz). ^{195}Pt{^{1}H} NMR (85.6 MHz, CD_2Cl_2, −90 °C): δ = −3753.5 (s). IR (ATR): $\tilde{\nu}$ = 1701 cm^{-1} (m, C=O). MS (MALDI+): *m/z* 627.2 [*M*-(3,5-Me$_2$pz)$_2$]$^{2+}$; 1349.3 [*M*-(3,5-Me$_2$pz)]$^+$; 1553.4 [*M*+Ag]$^+$. Elemental analysis calcd (%) for $C_{46}H_{54}Ag_2N_{12}O_4Pt_2$: C 38.24, H 3.77, N 11.63; found: C 38.00, H 3.63, N 11.54.

Acknowledgements

This work was supported by the Spanish Ministerio de Economía *y* Competitividad (MINECO)/FEDER (Project CTQ2015-67461-P led by Dr. Babil Menjón) and by the Gobierno de Aragón and Fondo Social Europeo (Grupo Consolidado E21: Química Inorgánica *y* de los Compuestos Organometálicos led by Dr. José M. Casas). The authors thank the Centro de Supercomputación de Galicia (CESGA) for generous allocation of computational resources.

Conflict of interest

The authors declare no conflict of interest.

Keywords: luminescence · metal–metal interactions · N-heterocyclic carbenes · platinum · pyrazole

[1] a) Z. Chen, L. Wang, S. Su, X. Zheng, N. Zhu, C.-L. Ho, S. Chen, W.-Y. Wong, *ACS Appl. Mater. Interfaces* **2017**, *9*, 40497 – 40502; b) I. Omae, *Coord. Chem. Rev.* **2016**, *310*, 154 – 169; c) T. von Arx, A. Szentkuti, T. N. Zehnder, O. Blacque, K. Venkatesan, *J. Mater. Chem. C* **2017**, *5*, 3765 – 3769; d) T. Strassner, *Acc. Chem. Res.* **2016**, *49*, 2680 – 2689.

[2] a) M. Bachmann, D. Suter, O. Blacque, K. Venkatesan, *Inorg. Chem.* **2016**, *55*, 4733 – 4745; b) H. Leopold, U. Heinemeyer, G. Wagenblast, I. Münster, T. Strassner, *Chem. Eur. J.* **2016**, *22*, 1 – 12; c) A. Tronnier, G. Wagenblast, I. Münster, T. Strassner, *Chem. Eur. J.* **2015**, *21*, 12881 – 12884 and references therein; d) Z. M. Hudson, C. Sun, M. G. Helander, Y. L. Chang, Z. H. Lu, S. N. Wang, *J. Am. Chem. Soc.* **2012**, *134*, 13930 – 13933; e) Y. Unger, D. Meyer, O. Molt, C. Schildknecht, I. Münster, G. Wagenblast, T. Strassner, *Angew. Chem. Int. Ed.* **2010**, *49*, 10214 – 10216; *Angew. Chem.* **2010**, *122*, 10412 – 10414; f) J. Lee, H. F. Chen, T. Batagoda, C. Coburn, P. I. Djurovich, M. E. Thompson, S. R. Forrest, *Nat. Mater.* **2016**, *15*, 92 – 99; g) G. J. Li, T. Fleetham, J. Li, *Adv. Mater.* **2014**, *26*, 2931 – 2936; h) T. Fleetham, G. J. Li, L. L. Wen, J. Li, *Adv. Mater.* **2014**, *26*, 7116 – 7121; i) X. C. Hang, T. Fleetham, E. Turner, J. Brooks, J. Li, *Angew. Chem. Int. Ed.* **2013**, *52*, 6753 – 6756; *Angew. Chem.* **2013**, *125*, 6885 – 6888; j) T. Fleetham, Z. X. Wang, J. Li, *Org. Electron.* **2012**, *13*, 1430 – 1435.

[3] A. F. Rausch, L. Murphy, J. A. G. Williams, H. Yersin, *Inorg. Chem.* **2012**, *51*, 312 – 319.

[4] a) S. Fuertes, H. Garcia, M. Peralvarez, W. Hertog, J. Carreras, V. Sicilia, *Chem. Eur. J.* **2015**, *21*, 1620 – 1631; b) S. Fuertes, A. J. Chueca, M. Perálvarez, P. Borja, M. Torrell, J. Carreras, V. Sicilia, *ACS Appl. Mater. Interfaces* **2016**, *8*, 16160 – 16169; c) S. Fuertes, A. J. Chueca, L. Arnal, A. Martín, U. Giovanella, C. Botta, V. Sicilia, *Inorg. Chem.* **2017**, *56*, 4829 – 4839; d) S. Fuertes, A. J. Chueca, A. Martín, V. Sicilia, *Cryst. Growth Des.* **2017**, *17*, 4336 – 4346.

[5] K. Sakai, Y. Tomita, T. Ue, K. Goshima, M. Ohminato, T. Tsubomura, K. Matsumoto, K. Ohmura, K. Kawakami, *Inorg. Chim. Acta* **2000**, *297*, 64 – 71.

[6] F. K. Keter, J. Darkwa, *Biometals* **2012**, *25*, 9 – 21.

[7] a) S. Kuwata, T. Ikariya, *Chem. Commun.* **2014**, *50*, 14290 – 14300; b) Y. Nakahara, T. Toda, A. Matsunami, Y. Kayaki, S. Kuwata, *Chem. Asian J.* **2018**, *13*, 73 – 80; c) Y. Suna, Y. Himeda, E. Fujita, J. T. Muckerman, M. Z. Ertem, *ChemSusChem* **2017**, *10*, 4535 – 4543.

[8] J. Forniés, S. Fuertes, A. Martín, V. Sicilia, E. Lalinde, M. T. Moreno, *Chem. Eur. J.* **2006**, *12*, 8253 – 8266.

[9] a) K. Nishihara, M. Ueda, A. Higashitani, Y. Nakao, Y. Arikawa, S. Horiuchi, E. Sakuda, K. Umakoshi, *Dalton Trans.* **2016**, *45*, 4978 – 4982; b) M. Ueda, S. Horiuchi, E. Sakuda, Y. Nakao, Y. Arikawa, K. Umakoshi, *Chem. Commun.* **2017**, *53*, 6405 – 6408.

[10] S. Akatsu, Y. Kanematsu, T.-A. Kurihara, S. Sueyoshi, Y. Arikawa, M. Onishi, S. Ishizaka, N. Kitamura, Y. Nakao, S. Sakaki, K. Umakoshi, *Inorg. Chem.* **2012**, *51*, 7977 – 7992.

[11] K. Umakoshi, K. Saito, Y. Arikawa, M. Onishi, S. Ishizaka, N. Kitamura, Y. Nakao, S. Sakaki, *Chem. Eur. J.* **2009**, *15*, 4238 – 4242.

[12] S. Fuertes, A. J. Chueca, V. Sicilia, *Inorg. Chem.* **2015**, *54*, 9885 – 9895.

[13] a) T. Steiner, *J. Phys. Chem. A* **1998**, *102*, 7041 – 7052; b) A. Martín, *J. Chem. Educ.* **1999**, *76*, 578 – 583; c) S.-Y. Chang, J.-L. Chen, Y. Chi, Y.-M. Cheng, G.-H. Lee, C.-M. Jiang, P.-T. Chou, *Inorg. Chem.* **2007**, *46*, 11202 – 11212; d) P. N. Fonteh, F. K. Keter, D. Meyer, I. A. Guzei, J. Darkwa, *J. Inorg. Biochem.* **2009**, *103*, 190 – 194.

[14] W. J. Geary, *Coord. Chem. Rev.* **1971**, *7*, 81 – 122.

[15] L. M. Epstein, E. S. Shubina, *Coord. Chem. Rev.* **2002**, *231*, 165 – 181.

[16] J. Forniés, V. Sicilia, J. M. Casas, A. Martín, J. A. López, C. Larraz, P. Borja, C. Ovejero, *Dalton Trans.* **2011**, *40*, 2898 – 2912 and references therein.

[17] a) S. Jamali, Z. Mazloomi, S. M. Nabavizadeh, D. Milic, R. Kia, M. Rashidi, *Inorg. Chem.* **2010**, *49*, 2721 – 2726; b) G. J. Arsenault, C. M. Anderson, R. J. Puddephatt, *Organometallics* **1988**, *7*, 2094 – 2097.

[18] a) D. E. Janzen, L. F. Mehne, D. G. VanDerveer, G. J. Grant, *Inorg. Chem.* **2005**, *44*, 8182 – 8184; b) T. Yamaguchi, F. Yamaguchizaki, T. Ito, *J. Am. Chem. Soc.* **2001**, *123*, 743 – 744; c) S. Fuertes, C. H. Woodall, P. R. Raithby, V. Sicilia, *Organometallics* **2012**, *31*, 4228 – 4240.

[19] B. Ma, J. Li, P. I. Djurovich, M. Yousufuddin, R. Bau, M. E. Thompson, *J. Am. Chem. Soc.* **2005**, *127*, 28 – 29.

[20] a) A. Díez, E. Lalinde, M. T. Moreno, *Coord. Chem. Rev.* **2011**, *255*, 2426 – 2447; b) M. C. Moret, P. J. Chen, *J. Am. Chem. Soc.* **2009**, *131*, 5675 – 5690; c) J. Forniés, S. Ibañez, A. Martin, M. Sanz, J. R. Berenguer, E. Lalinde, J. Torroba, *Organometallics* **2006**, *25*, 4331 – 4340.

Manuscript received: February 8, 2018
Revised manuscript received: May 1, 2018
Accepted manuscript online: May 15, 2018
Version of record online: June 5, 2018

Inorganic Chemistry

pubs.acs.org/IC Article

Chameleonic Photo- and Mechanoluminescence in Pyrazolate-Bridged NHC Cyclometalated Platinum Complexes

Violeta Sicilia,* Lorenzo Arnal, Daniel Escudero,* Sara Fuertes,* and Antonio Martin

Cite This: *Inorg. Chem.* 2021, 60, 12274−12284 Read Online

ACCESS | Metrics & More | Article Recommendations | Supporting Information

ABSTRACT: DFT investigations on the ground (GS) and the first triplet (T_1) excited state potential energy surfaces (PES) were performed on a new series of platinum-butterfly complexes, [{Pt(C^C*)(μ-Rpz)}$_2$] (Rpz: pz, **1**; 4-Mepz, **2**; 3,5-dmpz, **3**; 3,5-dppz, **4**), containing a cyclometalated NHC in their wings. The geometries of two close-lying local minima corresponding to butterfly spread conformers, **1s**−**4s**, and butterfly folded ones, **1f**−**4f**, with long and short Pt−Pt separations, respectively, were optimized in the GS and T_1 PES. A comparison of the GS and T_1 energy profiles revealed that an opposite trend is obtained in the relative stability of folded and spread conformers, the latter being more stabilized in their GS. Small ΔG (**s**/**f**) along with small-energy barriers in the GS support the coexistence of both kinds of conformers, which influence the photo- and mechanoluminescence of these complexes. In 5 wt % doped PMMA films in the air, these complexes exhibit intense sky-blue emissions (PLQY: 72.0−85.9%) upon excitation at $\lambda \leq 380$ nm arising from ^{3}IL/MLCT excited states, corresponding to the predominant **1s**−**4s** conformers. Upon excitation at longer wavelengths (up to 450 nm), the minor **1f**−**4f** conformers afford a blue emission as well, with PLQY still significant (40%−60%). In the solid state, the as-prepared powder of **4** exhibits a greenish-blue emission with QY ∼ 29%, mainly due to ^{3}IL/^{3}MLCT excited states of butterfly spread molecules, **4s**. Mechanical grinding resulted in an enhanced and yellowish-green emission (QY ∼ 51%) due to the ^{3}MMLCT excited states of butterfly folded molecules, **4f**, in such a way that the mechanoluminescence has been associated with an intramolecular structural change induced by mechanical grinding.

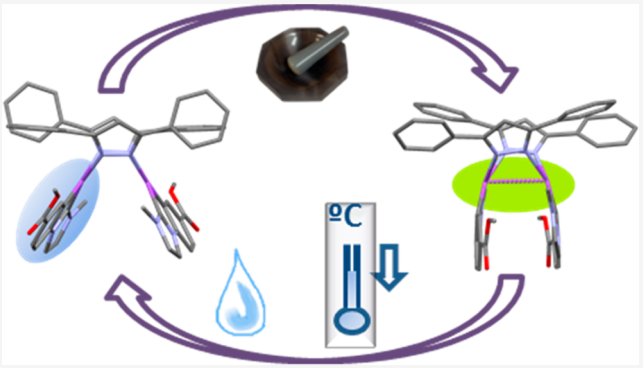

INTRODUCTION

Cyclometalated complexes of Pt(II) are characterized by outstanding photoluminescent properties,[1] arising from the radiative deactivation of triplet excited states, which are at the origin of many challenging applications such as optical sensors,[2] biological imaging,[3] or light emitting devices.[4] The planar geometry of the mononuclear complexes allows them to assemble through Pt···Pt and $\pi-\pi$ interactions. Recent computational investigations demonstrate that mononuclear complexes often possess very different photophysical properties than their aggregates. Thus, while mononuclear complexes are likely to deactivate nonradiatively through triplet metal-centered (^{3}MC) excited states,[5] the formation of the latter states is likely more hindered in condensed phases. Additionally, it was found that the formation of excimers in Pt(II) complexes is more favored than the formation of ground state aggregates.[6] As a result, the nature of the emissive triplet state changes from a monomer-based triplet emission to a triplet metal−metal-to-ligand charge transfer (^{3}MMLCT) like emission in the molecular ensembles, leading to red-shifted emissions.[7,8] This kind of platinum compound very often suffers the so-called aggregation-cause quenching (ACQ)[9] effect, which limits their applications. However, many transition metal complexes exhibit aggregation-induced phosphorescent emission (AIPE),[10−14] and they can successfully be used to achieve white light[15,16] or NIR[17,18] organic-light-emitting diodes by adjusting the doping concentration. The emission color strongly depends on the extent of these intermolecular interactions, and in their turn, on environmental factors able to affect them, such as temperature variations,[8] mechanical force,[12,19] or volatile solvent molecules embedded into the lattice.[2,20] Thus, these compounds become thermo-, mechano-, and/or vapoluminescent complexes, enlarging the technological interest of these smart functional materials.

Compared to mononuclear complexes, binuclear luminescent complexes have been less explored.[21−28] In binuclear Pt(II) cyclometalated compounds, the metallophilic inter-

Received: May 14, 2021
Published: August 2, 2021

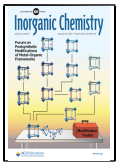

actions and thereto their luminescent properties can partially be controlled by selecting the bridging ligands, which result in different degrees of rigidity and steric hindrance.[21,23,24] Among them, platinum complexes with bridging pyrazolates have been deeply studied by Castellano,[25] Thompson,[26,27] and Ma[28] and co-workers. It was found that the Pt−Pt distance and the extent of the metallophilic interactions can be tuned by the bulkiness of the pyrazolate unit (butterfly body), in such a way that when the bulkiness increases, the cycloplatinated units (butterfly wings) are pushed closer together. As a result, the emission color of this kind of complexes can be tuned from blue to green or red.[23] In addition, in solution they exhibit sometimes a photoinduced structural change (PSC) on the lowest triplet-state potential energy surface (PES), resulting in a dramatic change of the Pt−Pt bond distance and thereto on the emission.[28] This unique butterfly-like structure allows the contraction of the Pt−Pt distance with temperature, thus leading to solid-state thermochromism and thermoluminescence. This is the case of $[\{Pt(ppy)(\mu\text{-}Ph_2pz)\}_2]$,[29] which at a low temperature exhibits monomer-based ^{3}LC/MLCT emission, and it changes to excimer-like ^{3}MMLCT emission above 160 K.

The cyclometalating groups play also an important role in the stability and the control of the photophysical properties.[30] In this sense, the platinum-butterfly complexes reported by Strassner et al., i.e., $[\{Pt(C^\wedge C^*)(\mu\text{-}Rpz)\}_2]$[31,32] are exemplary ones. They revealed that the cyclometalated N-heterocyclic carbenes (C^C*), forming two strong metal−carbon bonds, are excellent wingsa for the synthesis of highly efficient blue and orange emitters. In this field, we reported compound $[\{Pt(C^\wedge C^*)(\mu\text{-}pz)\}_2]$ (HC^C* = 1-(4-(ethoxy-carbonyl)-phenyl)-3-methyl-1H-imidazol-2-ylidene; pz: pyrazolate **1**) which undergoes two-center, two-electron [2c, 2e] oxidation in the presence of haloforms (CHX_3, X = Cl, Br, I).[33] Herein, we report three new complexes, $[\{Pt(C^\wedge C^*)(\mu\text{-}Rpz)\}_2]$ (Rpz: 4-methylpyrazolate (4-Mepz), **2**; 3,5-dimethylpyrazolate (3,5-dmpz), **3**; and 3,5-diphenylpyrazolate (3,5-dppz), **4**) bearing the same wings, C^C*, but different bodies (Rpz). Besides the experimental synthesis and characterization of compounds **1**−**4**, the intriguing luminescence and mechanoluminescence have been studied and deciphered with density functional theory (DFT) and time-dependent DFT (TD-DFT) investigations. For all of the complexes, two close-lying local minima corresponding to the folded (**f**) and spread (**s**) conformers were located on both the ground-state (GS) and the lowest adiabatic triplet excited state (T_1) PES. A low energy barrier for the thermal interconversion between both structures in the GS seems to be at the core of the stimuli-responsive luminescence of complex **4** in the solid state.

EXPERIMENTAL SECTION

Compounds $[\{Pt(EtO_2C{-}C^\wedge C^*)(\mu\text{-}Cl)\}_2]$ (**A**),[34] $[Pt(EtO_2C{-}C^\wedge C^*)(4\text{-}MepzH)_2]ClO_4$ (**B2**),[35] and $[\{Pt(EtO_2C{-}C^\wedge C^*)(\mu\text{-}pz)\}_2]$ (**1**)[36] were prepared as described elsewhere.

Synthesis of *syn*-/*anti*-$[\{Pt(EtO_2C{-}C^\wedge C^*)(\mu\text{-}4\text{-}Mepz)\}_2]$ (2). NEt_3 (0.5 mL, 3.62 mmol) was added to a solution of **B2** (133.5 mg, 0.19 mmol) in acetone (30 mL) at room temperature. After 2 h of reaction, the solvent was removed in vacuo to 2 mL. The solution was treated with H_2O (20 mL), filtered, and washed with H_2O to give **2**-*anti* (83%)/**2**-*syn*(17%) as a yellow solid. Yield: 73.7 mg, 75%. Anal. Calcd for $C_{34}H_{36}N_8O_4Pt_2$: C, 40.40; H, 3.59; N, 11.08. Found: C, 40.00; H, 3.75; N, 11.06. ^{1}H NMR data for **2**-*anti* (500 MHz, acetone-d_6): δ 8.02 (d, $^4J_{H7,H9}$ = 1.8, $^3J_{H7,Pt}$ = 55.1, 2H, H_7), 7.65 (d, $^3J_{H2,H3}$ = 2.1, 2H, H_2), 7.63 (dd, $^3J_{H9,H10}$ = 8.1, $^4J_{H9,H7}$ = 1.8, 2H, H_9), 7.50 (s, 2H, $H_{3'}$, 4-Mepz), 7.46 (s, 2H, $H_{5'}$, 4-Mepz), 7.18 (d, $^3J_{H10,H9}$ = 8.1, 2H, H_{10}), 7.06 (d, $^3J_{H3,H2}$ = 2.1, 2H, H_3), 4.23 (m, CH_2, CO_2Et), 3.35 (s, 6H, H_4), 2.12 (s, 6H, Me, 4-Mepz), 1.31 (t, $^3J_{H,H}$ = 7.1, 6H, CH_3, CO_2Et). ^{1}H NMR data for **2**-*syn*: δ 7.97 (d, $^4J_{H7,H9}$ = 1.8, 2H, H_7), 7.68 (d, $^3J_{H2,H3}$ = 2.1, 2H, H_2), 7.58 (dd, $^3J_{H9,H10}$ = 8.1, $^4J_{H9,H7}$ = 1.8, 2H, H_9), 7.54 (s, 2H, $H_{3'}$, 4-Mepz), 7.42 (s, 2H, $H_{5'}$, 4-Mepz), 3.63 (s, 6H, H_4), 1.35 (t, $^3J_{H,H}$ = 7.1, 6H, CH_3, CO_2Et). The rest of the signals appear overlapped with those of the **2**-*anti* isomer. $^{13}C\{^1H\}$ NMR plus HSQC and HMBC data for **2**-*anti* (125.75 MHz, acetone-d_6): δ 161.2 (C_1), 152.9 (C_5), 139.6 and 138.3 ($C_{3'}$ and $C_{5'}$), 136.3 (C_7), 133.8 and 126.8 (C_6 and C_8), 126.3 (C_9), 123.3 (C_3), 116.2 (C_2), 116.1 ($C_{4'}$), 110.9 (C_{10}), 60.7 (CH_2, CO_2Et), 36.5 (C_4), 14.6 (CH_3, CO_2Et), 9.5 (Me, 4-Mepz). $^{13}C\{^1H\}$ NMR plus HSQC and HMBC data for **2**-*syn* (125.75 MHz, acetone-d_6): δ = 160.3 (C_1), 123.1 (C_3), 36.7 (C_4). $^{195}Pt\{^1H\}$ NMR (108 MHz, acetone-d_6): δ −3775 (**2**-*anti*), −3785 (**2**-*syn*) ppm. (MS (MALDI+): *m*/*z* 1010.4 $[\{Pt(C^\wedge C^*)(\mu\text{-}4\text{-}Mepz)\}_2]$.

Synthesis of *syn*-/*anti*-$[\{Pt(EtO_2C{-}C^\wedge C^*)(\mu\text{-}3,5\text{-}dmpz)\}_2]$ (3). Compound **A** (106.3 mg, 0.12 mmol) was added to a solution containing NaO^{t}Bu (22.2 mg, 0.23 mmol) and 3,5-dmpzH (22.5 mg, 0.23 mmol) in acetone/EtOH (10 mL/5 mL). After 3 h of reaction at −10 °C, the solvent was removed to 3 mL under reduced pressure, filtered, and washed with 2 × 5 mL of H_2O to give **3**-anti(80%)/**3**-syn(20%) as a yellow solid. Yield: 70 mg, 58%. Anal. Calcd for $C_{36}H_{40}N_8O_4Pt_2$: C, 41.62; H, 3.88; N, 10.79. Found: C, 41.24; H, 4.02; N, 10.76. ^{1}H NMR data for **3**-*anti* (500 MHz, methylene chloride- d_2): δ 7.83 (d, $^4J_{H7,H9}$ = 1.7, $^3J_{H7,Pt}$ = 52.3, 2H, H_7), 7.67 (d, $^3J_{H9,H10}$ = 7.5, 2H, H_9), 7.20 (s, br, 2H, H_2), 6.94 (d, $^3J_{H10,H9}$ = 7.5, 2H, H_{10}), 6.67 (s, br, 2H, H_3), 6.11 (s, 2H, $H_{4'}$, dmpz), 4.24 (m, CH_2, CO_2Et), 3.33 (s, 6H, H_4), 2.32 and 2.27 (s, 12H, Me, dmpz), 1.35 (t, $^3J_{H,H}$ = 7.1, 6H, CH_3, CO_2Et). ^{1}H NMR data for **3**-*syn*: δ 6.13 and 6.04 (s, 2H, $H_{4'}$, dmpz), 3.58 (s, 6H, H_4). The rest of the signals appear overlapped with those of the **3**-*anti*.

$^{13}C\{^1H\}$ NMR plus HSQC and HMBC data for **3**-*anti* (125.75 MHz, methylene chloride-d_2): δ 160.7 (C_1), 152.2 (C_5), 146.7 ($C_{3'}$ and $C_{5'}$). 136.9 (C_7), 133.4 and 126.7 (C_6 and C_8), 125.9 (C_9), 122.1 (C_3), 115.4 (C_2), 110.2 (C_{10}), 104.6 ($C_{4'}$), 60.8 (CH_2, CO_2Et), 35.7 (C_4), 14.7 (CH_3, CO_2Et), 14.2 (Me, dmpz). $^{13}C\{^1H\}$ NMR plus HSQC and HMBC data for **3**-*syn* (125.75 MHz, methylene chloride-d_2): 160.2 (C_1), 35.8 (C_4). $^{195}Pt\{^1H\}$ NMR (108 MHz, methylene chloride- d_2): δ = −3771 ppm (**3**-*anti*), −3799 (**3**-*syn*) ppm. MS (MALDI+): *m*/*z* 1038.2 $[\{Pt(C^\wedge C^*)(\mu\text{-}dmpz)\}_2]$.

Synthesis of *syn*-/*anti*- $[\{Pt(EtO_2C{-}C^\wedge C^*)(\mu\text{-}3,5\text{-}dppz)\}_2]$ (4). $AgClO_4$ (52.7 mg, 0.25 mmol) was added to a stirred suspension of **A** (115.8 mg, 0.12 mmol) in acetone (30 mL) in the dark at room temperature. After 2 h of reaction, 3,5-dppzH (110.9 mg, 0.50 mmol) was added to the mixture and allowed to react overnight in the darkness. Then, the resulting suspension was filtered through Celite and concentrated to ca. 20 mL. NEt_3 (0.5 mL, 3.62 mmol) was added to the reaction mixture and stirred for 2 h. Then, the solvent was removed in vacuo. The residue was treated with cold MeOH (5 mL) and filtered to give **4**-*anti* (94%)/**4**-*syn* (6%) as a yellow solid. Yield: 90.0 mg, 74%. Anal. Calcd for $C_{56}H_{48}N_8O_4Pt_2$: C, 52.25; H, 3.76; N, 8.71. Found: C, 52.64; H, 3.90; N, 8.82. ^{1}H NMR data for **4**-*anti* (500 MHz, DMSO-d_6, 353 K): δ 8.59 (d, $^3J_{Ho,Hm}$ = 7.2, 4H, H_o), 8.25 (dd, $^3J_{Ho,Hm}$ = 7.2, $^4J_{Ho,Hp}$ = 1.8, 4H, H_o), 7.84 (s, br, 1H, $H_{C^\wedge C^*}$), 7.72−7.53 (m, 4H, $H_{C^\wedge C^*}$), 7.50−7.24 (m, 9H, H_{pz} and $H_{C^\wedge C^*}$), 7.20−7.03 (m, 8H, H_{pz} and $H_{C^\wedge C^*}$), 6.99 (s, br, 2H, H_{pz}), 4.18 (q, $^3J_{H,H}$ = 7.0, 4H, CH_2, CO_2Et), 3.18 (s, 6H, H_4), 1.29 (t, $^3J_{H,H}$ = 7.0, 6H, CH_3, CO_2Et). ^{1}H NMR data for **4**-*syn*: δ 3.32 (s, 6H, H_4). The rest of the signals appear overlapped with those of the **4**-*anti* isomer. $^{13}C\{^1H\}$ NMR plus HSQC and HMBC data for **4**-*anti* (125.75 MHz, DMSO-d_2,353 K): δ 155.5 (C_1), 135.1 ($C_{C^\wedge C^*}$), 132.7 (C_{pz}), 132.6 (C_{pz}), 127.6 (C_{pz}), 127.0 (C_{pz}), 126.8 ($C_{C^\wedge C^*}$), 126.7 (C_o), 125.4 (C_o), 124.7 ($C_{C^\wedge C^*}$), 124.5 ($C_{C^\wedge C^*}$), 122.1 ($C_{C^\wedge C^*}$), 109.7 ($C_{C^\wedge C^*}$), 103.2 ($C_{C^\wedge C^*}$), 59.3 (CH_2, CO_2Et), 34.3 (C_4), 13.6 (CH_3, CO_2Et). $^{195}Pt\{^1H\}$ NMR (108 MHz, DMSO-d_6, 353 K): δ −3680 ppm (**4**-*anti*). (MS (MALDI+): *m*/*z* 1286.5 $[\{Pt(C^\wedge C^*)(\mu\text{-}3,5\text{-}dppz)\}_2]$.

https://doi.org/10.1021/acs.inorgchem.1c01470
Inorg. Chem. 2021, 60, 12274−12284

Scheme 1. Synthetic Routes Followed for Compounds 1−4[c]

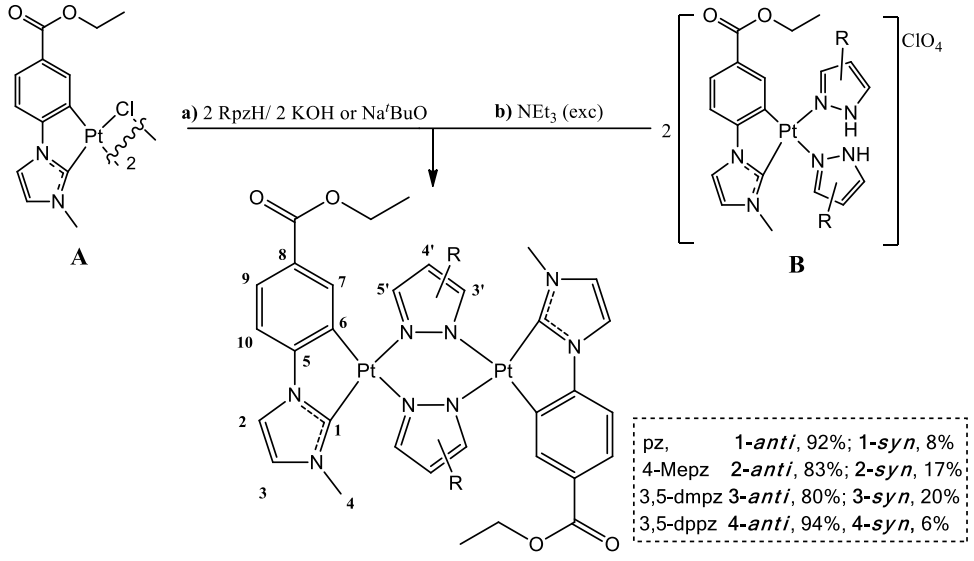

[a]−2 KCl (NaCl)/−2 H_2O (^{t}BuOH). [b]−2 $NHEt_3Rpz$/−2 $NHEt_3ClO_4$. [c]Just the major isomer "*anti*" appears, represented for clarity along with its numerical scheme for NMR analysis. Compound **1** is included for overview.

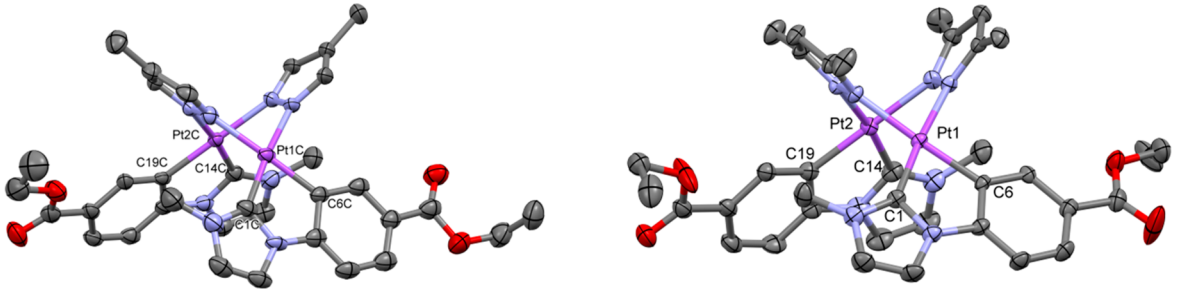

Figure 1. Molecular structures of **2A** (left) and **3** (right). Ellipsoids are drawn at their 50% probability level; solvent molecules and hydrogen atoms have been omitted for clarity.

RESULTS AND DISCUSSION

Compounds $[\{Pt(C\^C^*)(\mu\text{-Rpz})\}_2]$ (HC^C* = 1-(4-(ethoxycarbonyl) phenyl)-3-methyl-1*H*-imidazol-2-ylidene; Rpz: 4-methylpyrazolate (4-Mepz), **2**; 3,5-dimethylpyrazolate (3,5-dmpz), **3**; 3,5-diphenylpyrazolate (3,5-dppz), **4**) were prepared following path a (for **3**) or b (for **2** and **4**) in Scheme 1).

The inability to get compound **3** through path b is in agreement with the greater basicity of 3,5-dmpzH[37] with respect to pzH, 4-MepzH, and 3,5-dppzH, which prevents it from being removed from the coordination sphere of the platinum center (experimental details for **2**−**4** in the SI). All the complexes were obtained as a mixture of *syn*/*anti* isomers with respect to the relative orientation of the cyclometalated C^C* groups, with the anti-isomer being the predominant one, as can be seen in the ^{1}H and the ^{195}Pt{^{1}H} NMR spectra of **2**−**4** (Figures S1−S4). The single-crystal X-ray diffraction study of **2** and **3** confirmed the expected spread butterfly-like structure (Figure 1). Like compound **1**,[36] complex **2** showed three different molecules in the asymmetric unit (A, B, C) with intermetallic distances of 3.355(4) Å (**2A**), 3.224(3) Å (**2B**), and 3.156(3) Å (**2C**). However, complex **3** exhibited only one dinuclear molecule with an intermetallic separation of 3.131(17) Å, in the low range of distances observed in other platinum-butterfly complexes with the same body (3,5-dmpz) but bearing different wings (3.128−3.203 Å).[26,38−40] Unfortunately, no good quality crystals were obtained for **4**, but we could confirm the atom connectivity. Two different molecules with a Pt−Pt separation of 3.054 and 2.982 Å were found in the asymmetric unit. Therefore, once again it can be established that when the steric demand of the bridging pyrazolate increases the platinum centers are pushed closer together, like in other butterfly-like platinum complexes reported by Thompson et al.,[26] Umakoshi et al.,[40] and Strassner et al.[32] An extended description of these molecules has been included in the SI (see Table S2 and Figures S5−S7).

Theoretical Calculations. DFT calculations on the GS and the lowest adiabatic triplet excited state (T_1) PESs for **1**−**4** were performed, and the geometries of relevant stationary points, such as, e.g., local minima and transition states (TS), were optimized (see SI for computational details) accounting for solvent effects in THF.

For all of the complexes, the geometries of two close-lying local minima were optimized in the GS PES (see Figure S8 in SI) which corresponded to the butterfly spread structures **1s**−**4s** and the butterfly folded ones **1f**−**4f**. Those corresponding to the butterfly spread conformers **1s**−**4s** show long Pt−Pt

https://doi.org/10.1021/acs.inorgchem.1c01470
Inorg. Chem. 2021, 60, 12274−12284

distances (3.10 Å for **4s**, 3.10 Å for **3s**, <3.20 Å for **1s**, <3.22 Å for **2s**) and intramolecular C^C* separations (>4.5 Å) following the same trend as the one observed in the experimental values. Also, they are characterized by a small Pt−Pt bond order (BO: 0.036 **4s**, <0.106 **3s**, <0.110 **1s**, <0.111 **2s**). On the other hand, the GS optimized geometries corresponding to the butterfly folded conformers **1f**−**4f** are characterized by shorter Pt−Pt distances (2.96 Å for **4f**, <2.97 Å for **3f**, 2.97 Å for **1f**, <2.98 Å for **2f**) and intramolecular C^C* contacts (<3.8 Å) along with larger Pt−Pt bond orders (BO: 0.170 **4f**, 0.174 **3f**, <0.228 **1f**, <0.233 **2f**) than those of **1s**−**4s**. The computed energy profiles in the GS PES are shown in Figure 2. For all compounds, the conformers **1s**−**4s**,

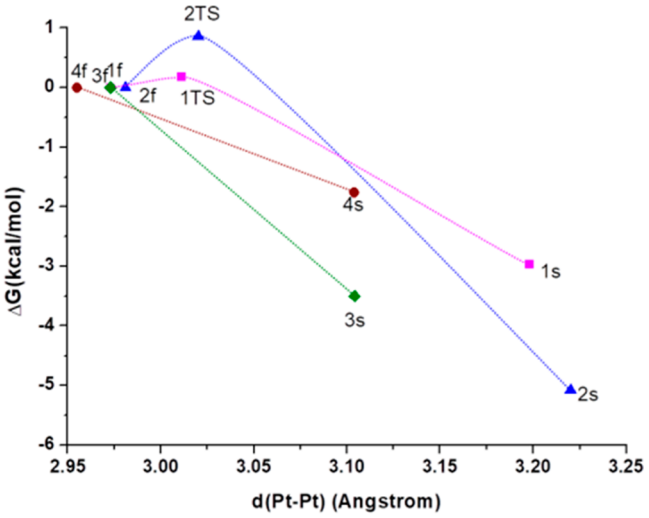

Figure 2. Calculated relative energy profile (PCM-M06/6-31G(d) and MWB60(Pt)) in the GS for the interconversion between the **1f**−**4f** and **1s**−**4s** conformers. Values calculated in THF.

featuring longer Pt−Pt distances, are more stable than the conformers **1f**−**4f** (Δ*G*: 0.076 eV (1.76 kcal/mol) for **4**, 0.129 eV (2.97 kcal/mol) for **1**, 0.152 eV (3.50 kcal/mol) for **3**, and 0.220 eV (5.08 kcal/mol) for **2**). Especially, this is remarkable for **2s**, which bears the longest Pt−Pt separation and the largest dihedral angle between the two platinum coordination planes. In addition, for complexes bearing bulkier Rpz units (**3** and **4**), their **3s** and **4s** minima are stabilized at shorter Pt−Pt distances than **1s** and **2s**.

Furthermore, for complexes **1** and **2**, we have successfully located the transition state (TS) associated with the interconversion between both conformers (see their optimized geometries in Figure S8). These TSs lie exemplarily 0.0077 eV (0.18 kcal/mol) above **1f** and 0.037 eV (0.86 kcal/mol) above **2f** (see Figure 2). Their optimized geometries display Pt−Pt distances which lie in between those found for the butterfly folded and butterfly spread optimized minima. In the case of **1**,[33] a small Δ*G* (**1s**/**1f**) value along with a small activation barrier supports, within the experimental error, a fast thermal equilibration in the ground state PES, thus resembling an intramolecular *butterfly flapping-like* motion.

These results are fully consistent with the presence of both conformers in solution, with the butterfly spread being the predominant one. Attempts to optimize the geometries of the TSs for the interconversion between conformers of complexes **3** and **4** were unsuccessful. In view of this piece of evidence, the flapping process likely occurs in a barrierless manner for the latter complexes.

Let us now discuss the results for the calculations on the lowest adiabatic triplet excited state (T_1) PES. The geometries of two local minima, i.e., **s**/**f**, were optimized for all of the complexes (Figure 3 and Figure S9 in the SI). The optimized

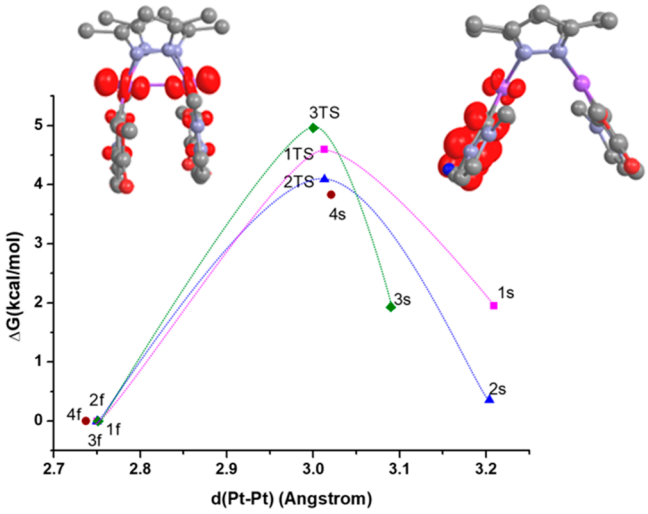

Figure 3. Calculated relative energy profile (PCM-M06/6-31G(d) and MWB60(Pt)) in the lowest adiabatic triplet excited state (T_1) for the interconversion between the **1f**−**4f** and **1s**−**4s** conformers. Values calculated in THF. Spin density distribution plots of **3f** (left) and **3s** (right).

geometries for the butterfly spread conformers, **1s**−**4s**, show Pt−Pt distances (3.02 Å for **4s**, <3.09 Å for **3s**, <3.20 Å for **2s**, <3.21 Å for **1s**) and Pt−Pt bond orders (BO: 0.116 **3s**, 0.110 **2s**, 0.102 **4s**, 0.099 **1s**), similar to those observed for most of them in the GS.

However, the T_1 optimized geometries for the butterfly folded conformers, **1f**−**4f**, exhibit intermetallic separations (2.74 Å for **4f**, <2.75 Å for **1f**−**3f**), which are shortened by ca. 0.22 Å with respect to those in the GS, and Pt−Pt bond orders (BO: 0.586 **4f**, 0.591 **3f**, 0.626 **2f**, 0.621 **1f**), which are increased by 0.4 with respect to those in the GS. The calculated spin density distribution for **1s**−**4s** indicates a mixed ^{3}IL/^{3}MLCT [π(C^C*) → π*(C^C*)]/[5d(Pt) → π*-(C^C*)] character for their T_1 states (see Figures 3 and S10) but a ^{3}MMLCT [dσ*(Pt−Pt) → π*(C^C*)] character for the T_1 states of **1f**−**4f**. Note that the changes in the Pt−Pt distances and the BO values from the GS to T_1 states in the butterfly folded conformers **1f**−**4f** almost agree with a one-electron excitation from the dσ*(Pt−Pt) orbital.

Like in the previously reported C,N-cycloplatinated butterfly-like complexes by Ma et al.,[28] as the steric bulk of the Rpz ligand increases, their spread-like minima (^{3}IL/^{3}MLCT) display shorter Pt−Pt bond distances (compare e.g., **1s** and **2s** vs **3s** and **4s** in Figure 3). Importantly, comparing the **1s**−**4s** and the **1f**−**4f** optimized geometries in their T_1 states, there is a considerable shortening of the Pt−Pt distances in the folded-like structures. The change of excited state character when going from the **1s**−**4s** minima (^{3}IL/^{3}MLCT) to the **1f**−**4f** ones (^{3}MMLCT) leads to an extra stabilization of the latter conformers[41] by 0.085 eV (1.95 kcal/mol), 0.015 eV (0.36 kcal/mol), 0.084 eV (1.93 kcal/mol), and 0.166 eV (3.83 kcal/mol) for complexes **1**−**4**,

https://doi.org/10.1021/acs.inorgchem.1c01470
Inorg. Chem. 2021, 60, 12274−12284

respectively. Note also that a certain amount of Pt−Pt bonding is only possible in the T_1 state but not in the GS.

All in all, a comparison of the GS and T_1 energy profiles reveals that an opposite trend is obtained in the relative stability of folded and spread conformers, the former being clearly more stabilized in their T_1 states, regardless of the steric hindrance of the bridging Rpz, but specially for complex **4**. In addition, we located the transition states (TSs) for the interconversion between conformers in the T_1 state for **1**−**3**, which are shown in Figure S9. These TSs all bear one imaginary frequency associated with the interconversion between both conformers. These TSs lie 0.115 eV (2.65 kcal/mol), 0.162 eV (3.73 kcal/mol), and 0.132 eV (3.04 kcal/mol) above the local minima **1s**−**3s**, respectively. These energy barriers for PSC are larger than those for the flapping-like intramolecular motion in the GS

The absorption properties of **1**−**4** were also investigated with PCM-TD-DFT calculations in the presence of THF (see details in the SI). The results are collected in Tables S3 and S4 and Figure S11. The frontier molecular orbitals (Figure S11) for **1s**−**4s** and **1f**−**4f** along with the energies of their lowest singlet excited states were also calculated (see inset of Figure 4 and Table S4 in SI). The lowest singlet excited states have predominant HOMO to LUMO character and can be described mainly as ^{1}MLCT/^{1}IL [5d(Pt) → π^*(C^C*)]/[π(C^C*) → π^*(C^C*)] for **1s**−**4s**, while some additional ^{1}MMLCT [dσ^*(Pt−Pt) →π^*(C^C*)] character is found for those of **1f**−**4f**. The vertical ΔSCF-M06 emission energies from the T_1 optimized geometries were calculated as well, rendering values of ca. 510 nm for **1s**−**4s** and of ca. 570 nm for **1f**−**4f** (see Table S4 in SI).

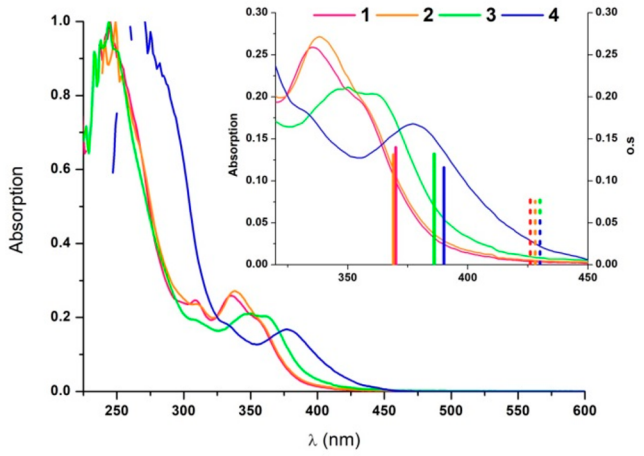

Figure 4. UV−visible spectra (path length: 1 mm) of **1**−**3** in 2-MeTHF 10^{-3} M and **4** in 2-MeTHF 10^{-5} M (path length: 1 cm). Inset: Expanded view of the UV−vis spectra along with the TD-M06/6-31G(d) and MWB60(Pt) $S_0 \rightarrow S_1$ transitions of the butterfly spread (solid bars) and butterfly folded (dashed bars) conformers.

Photophysical Properties. The absorption and emission properties of **1**−**4** were investigated and explained on the basis of the DFT calculations. The UV−vis spectra of **1**−**4** (Figure 4 and Table S26 in SI) do not show differences between diluted (10^{-5} M) and concentrated solutions (10^{-3} M). They show their lowest-energy absorption bands ($\varepsilon \sim 9 \times 10^3$ M^{-1} cm^{-1}) in the range 325−390 nm. These absorptions bands match the $S_0 \rightarrow S_1$ transitions calculated for the butterfly spread molecules **1s**−**4s** (see Figure 4), which are the predominant species according to the calculations.

However, in spite of the low contribution of the Rpz to the frontier molecular orbitals (FMOs), this absorption appears clearly red-shifted as the bulkiness of the R groups on the bridging pyrazolate increases. So, for species **3s** and **4s**, exhibiting shorter intermetallic distances and smaller interplanar angles in the GS, some ^{1}MMLCT [dσ^*(Pt−Pt) → π^*(C^C*)] character could be reasonably attributed (see Figures S8 and S11).

Diluted solutions (10^{-5} M) of **1**−**4** in 2-MeTHF were fast-cooled to 77 K. Upon excitation at $\lambda \leq 340$ nm, each of their emission spectra were characterized by highly structured emission bands with $\lambda_{max} \sim 450$ nm and vibronic spacings [~1450 cm^{-1}], likely corresponding to the C═C/C═N bond stretching modes of the cyclometalated NHC ligands (Figure 5, left). The emission energies are not affected by the nature of the Rpz ligands, and they are very similar to those observed in the mononuclear compounds bearing the same "(C^C*)Pt" fragment.[34,35,42,43]

The computed emission energies for the butterfly spread conformers, i.e., **1s**−**4s**, agree better with the experimental findings at 77 K than those calculated from **1f**−**4f**. Thus, these results highlight that the barriers for interconversion between **s**/**f** conformers at the T_1 state (see Figure 3) are large enough to prevent their thermal equilibrium at 77 K.

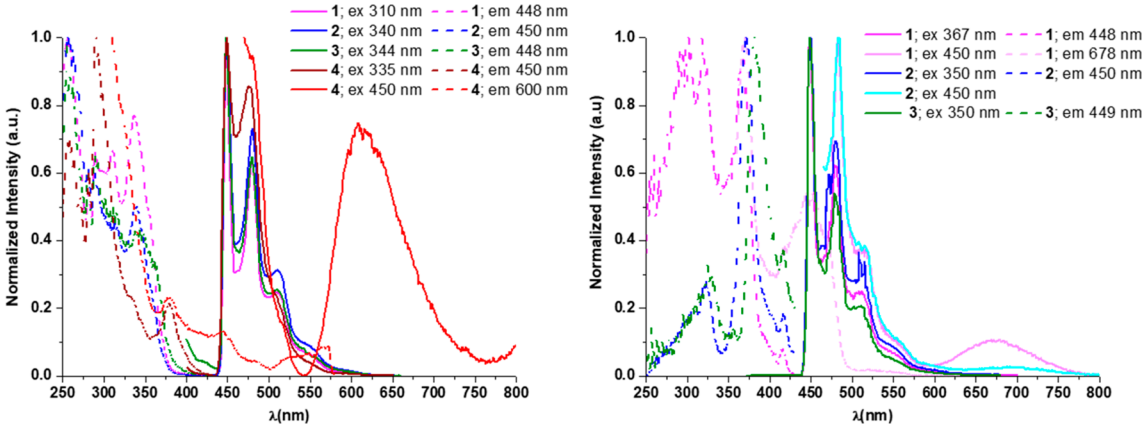

Figure 5. Normalized excitation (dotted lines) and emission (solid lines) spectra at 77 K under an Ar atmosphere. Left: **1**−**4** in 2-MeTHF 10^{-5} M. Right: **1**−**3** in 2-MeTHF 10^{-3} M.

https://doi.org/10.1021/acs.inorgchem.1c01470
Inorg. Chem. 2021, 60, 12274−12284

Table 1. Photophysical Data for 1−4 in PMMA Films and Solid State in the Air at 298 K

C	media	λ_{exc} (nm)	λ_{em} (nm)	CIE (x;y)	τ (μs)	φ(%)	k_r[b]	k_{nr}[c]
1	PMMA[a]	390	483_{max}, 517_{sh}, 567_{sh}	0.18; 0.32	3.7	20	5.4×10^4	21.6×10^4
	PMMA[a]	350	483_{max},517_{sh}, 567_{sh}	0.18; 0.32		72		
	solid	390	469, 527_{sh}, 556_{max}	0.41; 0.52	0.4 (20%)	3	2.5×10^4	79.2×10^4
					1.4 (80%)			
2	PMMA[a]	390	469, 485_{max}, 524_{sh}	0.16; 0.29	3.5	54	15.4×10^4	13.1×10^4
	PMMA[a]	370	473, 492_{max}, 536_{sh}	0.16; 0.27		83		
	solid	390	472, 527_{sh}, 559_{max}	0.41; 0.53	0.3 (22%)	3	3.2×10^4	103.2×10^4
					1.1 (78%)			
3	PMMA[a]	390	464, 484_{max}, 523_{sh}	0.15; 0.25	3.4	53	15.7×10^4	13.8×10^4
	PMMA[a]	380	464, 484_{max}, 523_{sh}	0.15; 0.25		79		
	solid	390	468, 487_{max}	0.19; 0.35	0.3 (32%)	16	30.1×10^4	158.1×10^4
					0.6 (68%)			
	ground	390	468, 492_{max}, 519	0.29; 0.47	0.2 (20%)	6	11.2×10^4	175.4×10^4
	solid				0.6 (80%)			
4	PMMA[a]	390	480_{max}	0.14; 0.26	2.2	69	31.7×10^4	14.1×10^4
	PMMA[a]	380	480_{max}	0.14; 0.26		86		
	solid	390	469,482_{max}, 553_{sh}	0.24; 0.37	0.5 (30%)	29	32.9×10^4	80.7×10^4
					1.1 (70%)			
	ground	390	553_{max}	0.39; 0.55	1.1 (33%)	51	28.3×10^4	27.2×10^4
	solid				2.2 (67%)			

[a]5 wt %. [b]Radiative decay rate constant given as $k_r = \varphi/\tau_{exp}$. [c]$k_{nr} = (1 - \varphi)/\tau_{exp}$.

Complexes **1** and **4** show additional excitation and emission bands at lower energies ($\lambda_{exc} \sim 450$ nm, $\lambda_{em} > 600$ nm), attributable to the butterfly folded molecules (calculated $S_1 \sim 426$ nm and $T_1 = 572$ nm for **1f**; $S_1 \sim 429$ nm and $T_1 = 570$ nm for **4f**), although for **1** they are only perceptible in concentrated solutions (10^{-3} M; Figure 5, right). The coexistence of butterfly spread and butterfly folded molecules for **1** and **4** is in accordance with the small ΔG value computed between the two conformers, **s**/**f** in the ground state (ΔG: 0.076 eV (1.76 kcal/mol) **4s**/**4f**, 0.129 eV (2.97 kcal/mol) **1s**/**1f**) within the margin of error for the calculation of the energies of similar complexes with the M06 functional (MUE = 2.48 kcal/mol, see SI). For complexes **2** and **3** because of the greater ΔG between them (0.220 eV (5.08 kcal/mol) **2s**/**2f**, 0.152 eV (3.50 kcal/mol) **3s**/**3f**), it seems to be more unlikely and undetectable at 77 K.

In 5 wt % doped PMMA films in the air, excitation of complexes **1**−**4** at $\lambda \leq 380$ nm affords intense sky-blue emissions with quantum yields of 72.0% **1**, 83.4% **2**, 79.0% **3**, and 85.9% **4** (see Table 1). These emissions match with those observed in 2-MeTHF (10^{-5} M) at 77 K. The slight blue shift in the emission spectra upon cooling is in accordance with an emissive state of ^{3}IL/ ^{3}MLCT character. The excitation of these films at longer wavelengths, up to 450 nm, render less intense but matched emission bands (see Figure 6; Table S27 and Figure S12 in the SI). The short radiative decay of these emissions at room temperature should be noted, which are similar to those observed in analogous complexes [{Pt(C^C*)-(μ-Rpz)}$_2$](HC^C* = 3-dibenzofuran-4-yl-1-methyl-3*H*-imidazol-2-ylidene, imidazopyridine-2-ylidene; R = H, Me, tBu)[31,32] but clearly shorter than those measured for mononuclear compounds containing the same "(C^C*)Pt" fragment.[42,43]

All of these pieces of evidence highlight a greater metallic contribution to the excited state and, then, a greater ^{3}MLCT character of the blue emissions of complexes **1**−**4** in PMMA films compared to those of the mononuclear complexes.[42,43]

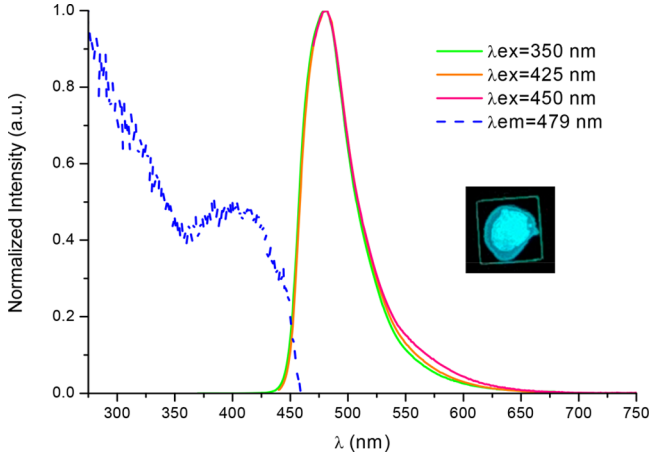

Figure 6. Normalized emission and excitation spectra of complex **4** in 5 wt % PMMA film in the air, Picture was taken under 365 nm UV light.

Note that the large radiative rate constant values (k_r, Table 1) support this. Also, compared to **2**−**4** ($k_r > 1.0 \times 10^5$ s^{-1}), a smaller radiative rate constant was obtained for **1** ($k_r = 1.0 \times 10^4$ s^{-1}), suggesting that the spin−orbit coupling (SOC) efficiency was lower because of a larger energy separation between the manifold of triplet and singlet states.[44] Exemplarily, from the absorption and the PMMA emission data, the energy differences between S_1 and T_1 ($\Delta E_{S-T} = 0.93$ eV **1**, 0.81 eV **2**; 0.75 eV **3**, 0.70 eV **4**) were found to follow the same trend observed for the k_r.

In solution at room temperature, compounds **1**−**4** are scarcely luminescent even in an argon atmosphere, a usual feature for blue-emitting Pt(II) complexes since the population of dd* states and formation of exciplexes are very common thermal quenching processes.[43] However, in a fluid solution of 2-MeTHF (10^{-5} M) at room temperature under an argon atmosphere (Figures S13 in SI), excitation in the low-energy absorption range ($\lambda \leq 380$ nm) renders for complexes **1** and **2**

https://doi.org/10.1021/acs.inorgchem.1c01470
Inorg. Chem. 2021, 60, 12274−12284

a weak emission from **1s** and **2s**, for complex **3** a dual emission with maxima at 456 and 552 nm, likely corresponding to **3s** and **3f**, and for complex **4** an emission with a maximum at 559 nm arising from **4f**, according to theoretical calculations.

In summary, photoexcitation of complexes **1**−**4** at λ < 380 nm allows the major **1s**−**4s** conformers to reach the high-energy ^{1}IL/MLCT excited state; then, by a rapid intersystem crossing (ISC), the ^{3}IL/MLCT (Ts) state will be populated, which is calculated to have a similar Pt−Pt separation than that of its corresponding ground state geometry (see Scheme 2). In

Scheme 2. Schematic Diagrams of Photophysical Processes Based on the Steady-State Excitation and Emission Spectra along with the Results of the Theoretical Investigations

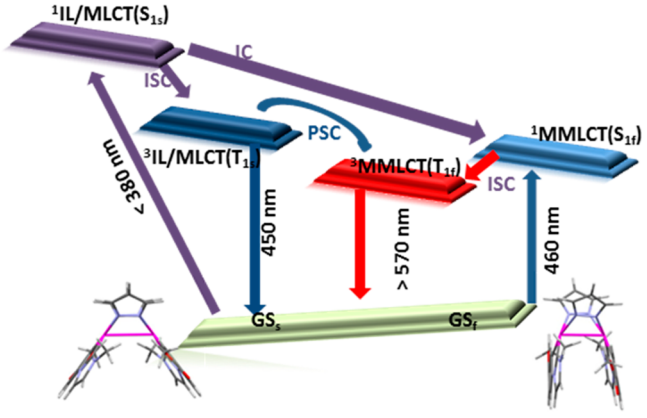

fluid solution, where the geometries of neither ground states nor those of the excited states are constrained, a photoinduced structural change (PSC) process between T_s and T_f conformers could happen depending on both, ΔG (T_f−T_s) and the PSC energy barrier.[28] In the case of **4**, the computed barrierless PSC process along with the large ΔG values (T_{4f}−T_{4s} = −0.166 eV, −3.83 kcal) leads to T_{4f} almost in an exclusive manner. This piece of evidence explains why the emission from T_{4f} is the only one observed experimentally. In the case of complex **3**, characterized by a smaller ΔG (T_{3f}−T_{3s} = −0.84 eV, −1.93 kcal) and a non-negligible PSC barrier (0.132 eV, 3.04 kcal), a thermal equilibrium between T_{3s} and T_{3f} is likely at room temperature, thus explaining its dual emission.

In the case of complex **2** with a lower ΔG (T_{2f}−T_{2s} = −0.015 eV, −0.36 kcal) but larger energy barrier (0.162 eV, 3.73 kcal/mol), the PSC seems not to take place and the emission arises only from T_{2s}. For complex **1**, with ΔG (T_{1f}/T_{1s}= 0.085 eV, 1.95 kcal) and the PSC energy barrier (0.115 eV, 2.65 kcal) on the same order of magnitude as those calculated for complex **3**, the PSC was expected to occur, but, the emission arises only from T_{1s}.

In this case, we recently reported that internal conversion (IC) from ^{1}IL/MLCT to ^{1}MMLCT competes with ISC to ^{3}IL/MLCT.[33] Therefore, a faster quenching of the $^{1/3}$MMLCT states of complex **1**, as compared to that occurring in complexes **3** and **4**, enabled by the lack of steric hindrance of the reactive positions in complex **1**, could account for the absence of this low-energy emission.

In rigid media (2-MeTHF 10^{-5} M at 77 K or PMMA films), photoexcitation of complexes **1**−**4** at λ < 380 nm leads in an analogous manner to the emission from the higher-lying triplet state ^{3}IL/MLCT, despite the greater stability of the ^{3}MMLCT state. This indicates that the energy barriers to connect the T_s/T_f wells are large enough to prevent the PSC in 2-MeTHF at 77 K, and it is also in agreement with PMMA being a rigid glass at r.t. (Tg = 378 K).[29] Notably, the frozen glass environment leads to a deceleration of the nonradiative pathways, thus leading to large PLQY values in PMMA films (see Table 1).

On the other hand, irradiation at λ > 400 nm will populate the low-energy states of the minor **1f**−**4f** conformers, ^{1}IL/MLCT with some ^{1}MMLCT character (see right panel in Scheme 2). A fast ISC to the close-lying triplet state ^{3}IL/MLCT[45] would lead to the high-energy emission, which is the only one observed in 5 wt % PMMA films of **1**−**4**. The low PLQYs when compared with those observed by irradiation at λ < 380 nm (see Table S27 and Figure S12 in SI) are in agreement with the low ratio of butterfly folded molecules in the samples but still being significant. Therefore, for complexes **2**−**4**, the existence of close-lying ^{1}IL/MLCT/MMLCT−^{3}IL/MLCT states makes it possible to get intense blue emissions (PLQY: 40%−60%) from doped films by irradiation with wavelengths in the visible region.

Mechanoluminescence in the Solid State. The as-prepared powders of **1** and **2** are scarcely emissive. They exhibit a weak (PLQY < 5%), broad, structureless emission centered at λ ∼ 555 nm (Table 1 and Figure S14) with a shoulder at λ ∼ 450 nm. The shape and energy of the main band could match with the one arising from the low-lying triplet state for the butterfly folded molecules that is the ^{3}MMLCT state. Yet, the role of excimeric $^3\pi$−π* states can not be fully disregarded, given the extended and numerous intermolecular π−π interactions observed in the single-crystal X-ray structures of **1** and **2** (see Figure S6) and the lower quantum yield of compounds **1** and **2** in solid state compared to those in 5 wt % PMMA films. Keeping in mind that other mononuclear Pt(II) compounds containing cyclometalated NHCs reported previously[42,46,47] exhibit a similar behavior mainly as a consequence of π−π intermolecular interactions, it seems likely that the emission of **1** and **2** arises from excimeric $^3\pi$−π* states with intermolecular π−π interactions affording efficient nonemissive deactivation channels[12] through an *aggregation-caused quenching* (ACQ) effect.[9,48] Neither the excitation nor the emission spectra of **1** and **2** exhibit changes after grinding the solids with a mortar and pestle (see Figure S15 for **2** as an example). However, complexes **3** and **4** exhibit mechanoluminescence in the solid state. After grinding, the pale-yellow solids do not visually change their colors, but their photoluminescence changes from blue to yellowish-green. Before being ground, a powdered sample of **3** exhibits a sky-blue emission, similar but weaker than that exhibited in PMMA film (5 wt %), which we attribute to ^{3}IL/MLCT. After grinding, the emission becomes green (Figure S16) due to the presence of an intense lower-energy band with λ ∼ 540 nm that could be assigned to the ^{3}MMLCT state of molecules with the butterfly folded configuration in accordance with the theoretical calculations. However, in view of the intermolecular π−π interactions observed in the single-crystal X-ray structure of **3** (see Figure S6) and the decreased PLQY upon grinding, the participation of excimeric $^3\pi$−π* states to the low-energy band cannot be ruled out.[9,48]

In case of compound **4**, photoexcitation of as-prepared powder leads to a greenish-blue emission with λ_{max} at 480 nm and an incipient shoulder at 553 nm that can be assigned to ^{3}IL/MLCT and ^{3}MMLCT emissions, respectively, in accord-

https://doi.org/10.1021/acs.inorgchem.1c01470
Inorg. Chem. 2021, 60, 12274−12284

ance with the theoretical calculations and with the ^{3}MMLCT emission observed for [{Pt(C^C*)(μ-NPh-CH-NPh)}$_2$] exhibiting a short Pt···Pt distance, of about 2.8 Å.[24] Mechanical grinding resulted in a suppression of the ^{3}IL/MLCT band along with an increase of the ^{3}MMLCT one and, unlike complex **3**, an enhancement of the PLQY (see Figure 7). As a result, the photoluminescence of powdery samples of **4** is intensified and changed from greenish-blue to yellowish-green upon grinding.

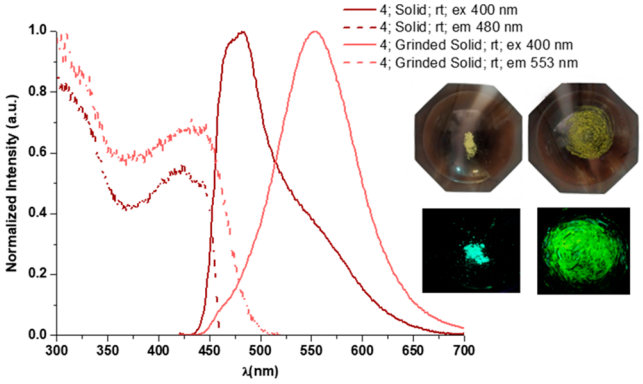

Figure 7. Normalized emission and excitation spectra of complex **4** in the solid state in the air at room temperature. Pictures were taken under 365 nm UV light.

From the excitation and emission spectra, it seems that the as-prepared powder of **4** shows phosphorescence from the two kinds of conformers, **4s** and **4f**, that from **4s** being predominant. This is in agreement with the butterfly spread conformer, **4s** being the major one in the GS and the fact that no PSC can take place in rigid media. Mechanical grinding seems to induce changes in the GS that somehow shorten the Pt−Pt distances and enforces the intramolecular Pt−Pt interactions, in such a way that in the ground solid, **4-g**, the phosphorescence arises mainly from **4f**.

Structural changes involving the intramolecular Pt−Pt separation in the GS as the origin of mechanoluminesce seems plausible on the bases of experimental and theoretical data, and once other causes were dismissed, like desolvation, since there is no solvent embedded in the solid (see CHN elemental analysis and NMR experiments) or intermolecular interactions, we proved that the luminescence spectrum of **4** in 40 wt % doped PMMA films match that at 5 wt % (see Figure S17), and its PLQY drops to 40%.

The ground solid, **4-g**, undergoes the reverse change partially upon cooling to 77 K, as deduced from the emission and excitation spectra collected at room temperature and 77 K (Figure S18).

Structural changes involving the intramolecular Pt−Pt separation in the GS were reported for the thermochromic platinum-butterfly compound [{Pt(ppy)(μ-Ph$_2$pz)}$_2$],[29] but those induced by mechanical grinding have never been reported. In this case, like in complex **4**, elongation of the Pt−Pt distance occurs when the temperature drops. Also, the transformations resulted to be reversible by the addition of THF, toluene, or diethyl ether to the ground samples of **3** and **4** that led to the recovery of the blue emission (see Figure 8 and S19), and thus presumably restoring the previous structure arrangement.

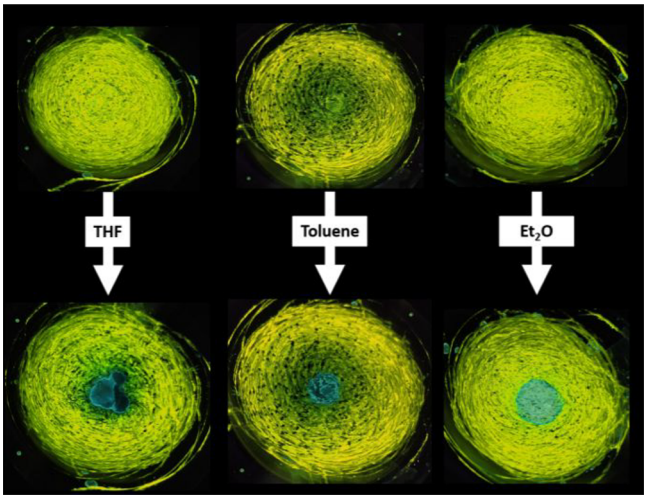

Figure 8. Photographic images of mechanical grinding samples of **4** in response to solvent treatment taken under 365 nm UV light

Therefore, it could be argued that the bulkiness of the μ-pyrazolates has a strong impact not only on the luminescence, but also on the mechanoluminiscence of these platinum butterflies in the solid state. As the bulkiness increases, the intermolecular $\pi-\pi$ interactions become more hindered, affording less efficient nonemissive deactivation channels and consequently a more efficient emission. In addition, as the steric demand of the μ-pyrazolates increases, the Pt−Pt interaction, enhanced by mechanical stimulation, causes a bathochromic shift of the emission (2750 cm^{-1} **4**) along with a remarkable increment of its PLQY.[49−54]

CONCLUSIONS

Photoluminescence and DFT calculations on a new series of platinum butterflies, [{Pt(C^C*)(μ-Rpz)}$_2$] (Rpz: pz **1**, 4-Mepz **2**, 3,5-dmpz **3**, 3,5-dppz **4**) containing a cyclometalated NHC in their wings, prove the presence of two conformers in the ground state at room temperature, the butterfly spread, **1s−4s** and the butterfly folded, **1f−4f** ones, which are characterized by long and short Pt−Pt separations, respectively. DFT calculations revealed that the former are the more stable in the GS but, in most of them, low ΔG (**s**/**f**) and low energy barriers in solution of THF support a fast thermal equilibration in the ground state PES, thus resembling an intramolecular *butterfly flapping-like* motion. By contrast, the butterfly folded, **1f−4f**, conformers are the more stable in the T$_1$PES. In 5 wt % doped PMMA films in the air, these complexes show intense sky-blue emissions (PLQY: 72.0−85.9%) upon excitation at $\lambda \leq 380$ nm mainly arising from an ^{3}IL/MLCT excited state, the first triplet state of the major butterfly spread conformer **1s−4s**, in accord with no PSC occurring in a rigid matrix. The existence of close-lying ^{1}IL/MLCT/MMLCT-^{3}IL/MLCT states for the **1f−4f** species enables the obtaining of intense blue emissions (PLQY: 40%−60%) under excitation with wavelengths in the visible region, up to 450 nm.

In addition, it could be argued that the bulkiness of the μ-pyrazolates has a strong impact on the luminescence and mechanoluminescence of these platinum butterflies in a solid state. In complexes **3** and **4**, the intermolecular $\pi-\pi$ interactions become more hindered than in complexes **1** and **2**, affording more efficient emissions. In addition, in the 3,5-

https://doi.org/10.1021/acs.inorgchem.1c01470
Inorg. Chem. 2021, 60, 12274−12284

dppz derivative, **4**, mechanical grinding causes a bathochromic shift of the emission from greenish-blue to yellowish-green along with a remarkable increment of its PLQY. This mechanoluminescence mechanism has been associated with an intramolecular structural change in the GS that somehow shortens the Pt−Pt distances and enhances the Pt−Pt interactions in such a way that the thermal butterfly flapping can be induced by mechanical grinding.

■ ASSOCIATED CONTENT

Supporting Information

The Supporting Information is available free of charge at https://pubs.acs.org/doi/10.1021/acs.inorgchem.1c01470.

General procedures and materials; crystallographic data; computational methods, NMR figures; description of single-crystal X-ray structures, DFT and PCM-DFT studies, additional figures for the photophysical study (DOCX)

Accession Codes

CCDC 2077779−2077780 contain the supplementary crystallographic data for this paper. These data can be obtained free of charge via www.ccdc.cam.ac.uk/data_request/cif, or by emailing data_request@ccdc.cam.ac.uk, or by contacting The Cambridge Crystallographic Data Centre, 12 Union Road, Cambridge CB2 1EZ, UK; fax: +44 1223 336033.

■ AUTHOR INFORMATION

Corresponding Authors

Violeta Sicilia − *Departamento de Quimica Inorganica, Escuela de Ingenieria y Arquitectura de Zaragoza, Instituto de Sintesis Quimica y Catalisis Homogenea (ISQCH), CSIC - Universidad de Zaragoza, 50018 Zaragoza, Spain;* orcid.org/0000-0002-0257-0483; Email: sicilia@unizar.es

Daniel Escudero − *Department of Chemistry, KU Leuven, 3001 Leuven, Belgium;* orcid.org/0000-0002-1777-8578; Email: daniel.escudero@kuleuven.be

Sara Fuertes − *Departamento de Quimica Inorganica, Facultad de Ciencias, Instituto de Sintesis Quimica y Catalisis Homogenea (ISQCH), CSIC - Universidad de Zaragoza, 50009 Zaragoza, Spain;* orcid.org/0000-0003-1812-3175; Email: sfuertes@unizar.es

Authors

Lorenzo Arnal − *Departamento de Quimica Inorganica, Facultad de Ciencias, Instituto de Sintesis Quimica y Catalisis Homogenea (ISQCH), CSIC - Universidad de Zaragoza, 50009 Zaragoza, Spain;* orcid.org/0000-0002-0283-9307

Antonio Martin − *Departamento de Quimica Inorganica, Facultad de Ciencias, Instituto de Sintesis Quimica y Catalisis Homogenea (ISQCH), CSIC - Universidad de Zaragoza, 50009 Zaragoza, Spain;* orcid.org/0000-0002-4808-574X

Complete contact information is available at: https://pubs.acs.org/10.1021/acs.inorgchem.1c01470

Author Contributions

The manuscript was written through contributions of all authors. All authors have given approval to the final version of the manuscript.

Funding

This work was supported by the Spanish Ministerio de Economia y Competitividad (Ministerio de Ciencia Innovacion y Universidades)/FEDER (Project PGC2018−094749−B-I00), by the Gobierno de Aragon (Grupo E17_20R: Quimica Inorganica y de los Compuestos Organometallicos), and by Internal Funds KU Leuven.

Notes

The authors declare no competing financial interest.

■ ACKNOWLEDGMENTS

This work was supported by the Spanish Ministerio de Economia y Competitividad (Ministerio de Ciencia Innovacion y Universidades)/FEDER (Project PGC2018-094749-B-I00), by the Gobierno de Aragon (Grupo E17_20R: Quimica Inorganica y de los Compuestos Organometallicos) and by Internal Funds KU Leuven. L.A. acknowledges the support of a grant from the Gobierno de Aragon.

■ REFERENCES

(1) Herberger, J.; Winter, R. F. Platinum Emitters with Dye-Based r-Aryl Ligands. *Coord. Chem. Rev.* **2019**, *400*, 213048.

(2) Shigeta, Y.; Kobayashi, A.; Yoshida, M.; Kato, M. Stability Tuning of Vapor-Adsorbed State of Vapochromic Pt(II) Complex by Introduction of Chiral Moiety. *Inorg. Chem.* **2019**, *58*, 7385−7392.

(3) Law, A. S. Y.; Lee, L. C. C.; Yeung, M. C. L.; Lo, K. K. W.; Yam, V. W. W. Amyloid Protein-Induced Supramolecular Self-Assembly of Water-Soluble Platinum(II) Complexes: A Luminescence Assay for Amyloid Fibrillation Detection and Inhibitor Screening. *J. Am. Chem. Soc.* **2019**, *141*, 18570−18577.

(4) Liao, J. L.; Chi, Y.; Wang, J. Y.; Chen, Z. N.; Tsai, Z. H.; Hung, W. Y.; Tseng, M. R.; Lee, G. H. Pt(II) Phosphors Featuring Both Dicarbene and Functional Biazolate Chelates: Synthesis, Luminescent Properties, and Applications in Organic Light-Emitting Diodes. *Inorg. Chem.* **2016**, *55*, 6394−6404.

(5) Pinter, P.; Strassner, T. Prediction of the Efficiency of Phosphorescent Emitters: A Theoretical Analysis of Triplet States in Platinum Blue Emitters. *Chem. - Eur. J.* **2019**, *25*, 4202−4205.

(6) Sukpattanacharoen, C.; Kumar, P.; Chi, Y.; Kungwan, N.; Escudero, D. Formation of Excimers in Isoquinolinyl Pyrazolate Pt(II) Complexes: Role of Cooperativity Effects. *Inorg. Chem.* **2020**, *59*, 18253−18263.

(7) Fornies, J.; Sicilia, V.; Borja, P.; Casas, J. M.; Diez, A.; Lalinde, E.; Larraz, C.; Martin, A.; Moreno, M. T. Luminescent Benzoquinolate-Isocyanide platinum(II) Complexes: Effect of Pt···Pt and π-π Interactions on their Photophysical properties. *Chem. - Asian J.* **2012**, *7*, 2813−2823.

(8) Saito, D.; Ogawa, T.; Yoshida, M.; Takayama, J.; Hiura, S.; Murayama, A.; Kobayashi, A.; Kato, M. Intense Red-Blue Luminescence Based on Superfine Control of Metal-Metal Interactions for Self-Assembled Platinum(II) Complexes. *Angew. Chem., Int. Ed.* **2020**, *59*, 18723−18730.

(9) Le Bras, L.; Chaitou, K.; Aloise, S.; Adamo, C.; Perrier, A. Aggregation-Caused Quenching versus Crystallization Induced Emission in thiazolo[5,4-b]thieno[3,2-e]-pyridine (TTP) Derivatives: Theoretical Insights. *Phys. Chem. Chem. Phys.* **2019**, *21*, 46−56.

(10) Alam, P.; Climent, C.; Alemany, P.; Laskar, R. "Aggregation-Induced Emission" of Transition Metal Compounds: Design, Mechanistic Insights and Applications. *J. Photochem. Photobiol., C* **2019**, *41*, 100317.

(11) Zhu, S.; Hu, J.; Zhai, S.; Wang, Y.; Xu, Z.; Liu, R.; Zhu, H. AIPE-Active Pt(II) Complexes with a Tunable Triplet Excited State: Design, Mechanochromism and Application in Anti-Counterfeiting. *Inorg. Chem. Front.* **2020**, *7*, 4677−4686.

(12) Martinez-Junquera, M.; Lara, R.; Lalinde, E.; Moreno, M. T. Isomerism, Aggregation-Induced Emission and Mechanochromism of

Isocyanide Cycloplatinated(II) Complexes. *J. Mater. Chem. C* **2020**, *8*, 7221−7233.
(13) Pinter, P.; Pittkowski, R.; Soellner, J.; Strassner, T. The Chameleonic Nature of Platinum(II) Imidazopyridine Complexes. *Chem. - Eur. J.* **2017**, *23*, 14173−14176.
(14) Pinter, P.; Mangold, H.; Stengel, I.; Münster, I.; Strassner, T. Enhanced Photoluminescence Quantum Yields through Excimer Formation of Cyclometalated Platinum(II) N-Heterocyclic Carbene Complexes. *Organometallics* **2016**, *35*, 673−680.
(15) Li, G.; Fleetham, T.; Li, J. Efficient and Stable White Organic Light-Emitting Diodes Employing a Single Emitter. *Adv. Mater.* **2014**, *26*, 2931−2936.
(16) Fleetham, T.; Li, J. Recent Advances in White Organic Light-Emitting Diodes Employing a Single-Emissive Material. *J. Photonics Energy* **2014**, *4*, 040991.
(17) Shafikov, M. Z.; Pander, P.; Zaytsev, A. V.; Daniels, R.; Martinscroft, R.; Dias, F. B.; Williams, J. A. G.; Kozhevnikov, V. N. Extended Ligand Conjugation and Dinuclearity as a Route to Efficient Platinum-based Near-Infrared (NIR) Triplet Emitters and Solution-Processed NIR-OLEDs. *J. Mater. Chem. C* **2021**, *9*, 127−135.
(18) Nisic, F.; Colombo, A.; Dragonetti, C.; Roberto, D.; Valore, A.; Malicka, J. M.; Cocchi, M.; Freeman, G. R.; Williams, J. A. G. Platinum(II) Complexes with Cyclometallated 5-π-Delocalized-Donor-1,3-di(2-pyridyl)benzene Ligands as Efficient Phosphors for NIR-OLEDs. *J. Mater. Chem. C* **2014**, *2*, 1791−1800.
(19) Liu, L.; Wang, X.; Wang, N.; Peng, T.; Wang, S. Bright, Multi-responsive, Sky-Blue Platinum(II) Phosphors Based on a Tetradentate Chelating Framework. *Angew. Chem.* **2017**, *129*, 9288−9292.
(20) Fornies, J.; Fuertes, S.; Lopez, J. A.; Martin, A.; Sicilia, V. New Water Soluble and Luminescent Platinum(II) Compounds, Vapochromic Behavior of $[K(H_2O)][Pt(bzq)(CN)_2]$, New Examples of the Influence of the Counterion on the Photophysical Properties of d^8 Square-Planar Complexes. *Inorg. Chem.* **2008**, *47*, 7166−7176.
(21) Puttock, E. V.; Walden, M. T.; Williams, J. A. G. The Luminescence Properties of Multinuclear Platinum Complexes. *Coord. Chem. Rev.* **2018**, *367*, 127−162.
(22) Zhang, Q. C.; Xiao, H.; Zhang, X.; Xu, L. J.; Chen, Z. N. Luminescent Oligonuclear Metal Complexes and the Use in Organic Light-Emitting Diodes. *Coord. Chem. Rev.* **2019**, *378*, 121−133.
(23) Chaaban, M.; Zhou, C.; Lin, H.; Chyi, B.; Ma, B. Platinum(II) Binuclear Complexes: Molecular Structures, Photophysical Properties, and Applications. *J. Mater. Chem. C* **2019**, *7*, 5910−5924.
(24) Leopold, H.; Tenne, M.; Tronnier, A.; Metz, S.; Munster, I.; Wagenblast, G.; Strassner, T. Binuclear C^C* Cyclometalated Platinum(II) NHC Complexes with Bridging Amidinate Ligands. *Angew. Chem., Int. Ed.* **2016**, *55*, 15779−15782.
(25) Brown-Xu, S. E.; Kelley, M. S. J.; Fransted, K. A.; Chakraborty, A.; Schatz, G. C.; Castellano, F. N.; Chen, L. X. Tunable Excited-State Properties and Dynamics as a Function of Pt-Pt Distance in Pyrazolate-Bridged Pt(II) Dimers. *J. Phys. Chem. A* **2016**, *120*, 543−550.
(26) Ma, B.; Li, J.; Djurovich, P. I.; Yousufuddin, M.; Bau, R.; Thompson, M. E. Synthetic Control of Pt···Pt Separation and Photophysics of Binuclear Platinum Complexes. *J. Am. Chem. Soc.* **2005**, *127*, 28−29.
(27) Ma, B.; Djurovich, P. I.; Garon, S.; Alleyne, B.; Thompson, M. E. Platinum Binuclear Complexes as Phosphorescent Dopants for Monochromatic and White Organic Light-Emitting Diodes. *Adv. Funct. Mater.* **2006**, *16*, 2438−2446.
(28) Zhou, C.; Tian, Y.; Yuan, Z.; Han, M.; Wang, J.; Zhu, L.; Tameh, M. S.; Huang, C.; Ma, B. Precise Design of Phosphorescent Molecular Butterflies with Tunable Photoinduced Structural Change and dual Emission. *Angew. Chem., Int. Ed.* **2015**, *54*, 9591−9595.
(29) Rachford, A. A.; Castellano, F. N. Thermochromic Absorption and Photoluminescence in $[\{Pt(ppy)(\mu\text{-}Ph_2pz)\}_2]$. *Inorg. Chem.* **2009**, *48*, 10865−10867.
(30) Chakraborty, A.; Deaton, J. C.; Haefele, A.; Castellano, F. N. Charge-Transfer and Ligand-Localized Photophysics in Luminescent Cyclometalated Pyrazolate-Bridged Dinuclear Platinum(II) Complexes. *Organometallics* **2013**, *32*, 3819−3829.
(31) Pinter, P.; Unger, Y.; Strassner, T. Cyclometalated NHC Platinum(II) Complexes with Bridging Pyrazolates: Enhanced Photophysics of Binuclear Blue Emitters. *Chem. Photo Chem.* **2017**, *1*, 113−115.
(32) Pinter, P.; Soellner, J.; Strassner, T. Photophysical Properties of Phosphorescent Mono- and Bimetallic Platinum(II) Complexes with C^C* Cyclometalating NHC Ligands. *Organometallics* **2021**, *40*, 557−563.
(33) Sicilia, V.; Arnal, L.; Fuertes, S.; Martin, A.; Baya, M. Metal-Metal Cooperation in the Oxidation of a Flapping Platinum Butterfly by Haloforms: Experimental and Theoretical Evidence. *Inorg. Chem.* **2020**, *59*, 12586−12594.
(34) Fuertes, S.; Chueca, A. J.; Peralvarez, M.; Borja, P.; Torrell, M.; Carreras, J.; Sicilia, V. White Light Emission from Planar Remote Phosphor Based on NHC Cycloplatinated Complexes. *ACS Appl. Mater. Interfaces* **2016**, *8*, 16160−16169.
(35) Arnal, L.; Fuertes, S.; Martin, A.; Sicilia, V. The Use of Cyclometalated NHCs and Pyrazoles for the Development of Fully Efficient Blue Pt^{II} Emitters and Pt/Ag Clusters. *Chem. - Eur. J.* **2018**, *24*, 9377−9384.
(36) Arnal, L.; Fuertes, S.; Martin, A.; Baya, M.; Sicilia, V. A Cyclometalated N-Heterocyclic Carbene: The Wings of the First Pt_2(II, II) Butterfly Oxidized by CHI_3. *Chem. - Eur. J.* **2018**, *24*, 18743−18748.
(37) Akatsu, S.; Kanematsu, Y.; Kurihara, T.-A.; Sueyoshi, S.; Arikawa, Y.; Onishi, M.; Ishizaka, S.; Kitamura, N.; Nakao, Y.; Sakaki, S.; Umakoshi, K. Syntheses and Luminescent Properties of 3,5-Diphenylpyrazolato-Bridged Heteropolynuclear Platinum Complexes. The Influence of Chloride Ligands on the Emission Energy Revealed by the Systematic Replacement of Chloride Ligands by 3,5-Dimethylpyrazolate. *Inorg. Chem.* **2012**, *51*, 7977−7992.
(38) Umakoshi, K.; Kimura, K.; Kim, Y. H.; Tsukimoto, Y.; Arikawa, Y.; Onishi, M.; Ishizaka, S.; Kitamura, N. Pyrazolato- and 3,5-Dimethylpyrazolato-Bridged Dinuclear Platinum(II), Palladium(II), and Their Mixed-Metal Complexes of 2,2′-Bipyrimidine. Syntheses, Structures, and Luminescent Properties. *Bull. Chem. Soc. Jpn.* **2010**, *83*, 1504−1510.
(39) Ghavale, N.; Wadawale, A.; Dey, S.; Jain, V. K. Synthesis, Structures and Spectroscopic Properties of Platinum Complexes Containing Orthometalated 2-Phenylpyridine. *J. Organomet. Chem.* **2010**, *695*, 1237−1245.
(40) Moon, S.; Horiuchi, S.; Sakuda, E.; Ito, A.; Arikawa, Y.; Umakoshi, K. Synthesis and Photophysical Properties of Butterfly-Shaped Dinuclear Pt(II) Complex Having NHC-Based Chelate Ligands. *Inorg. Chim. Acta* **2019**, *493*, 43−48.
(41) Saito, K.; Nakao, Y.; Sakaki, S. Theoretical Study of Pyrazolate-Bridged Dinuclear Platinum(II) Complexes: Interesting Potential Energy Curve of the Lowest Energy Triplet Excited State and Phosphorescence Spectra. *Inorg. Chem.* **2008**, *47*, 4329−4337.
(42) Sicilia, V.; Fuertes, S.; Chueca, A. J.; Arnal, L.; Martin, A.; Peralvarez, M.; Botta, C.; Giovanella, U. Highly Efficient Platinum-Based Emitters for Warm White Light Emitting Diodes. *J. Mater. Chem. C* **2019**, *7*, 4509−4516.
(43) Fuertes, S.; Chueca, A. J.; Martin, A.; Sicilia, V. New NHC Cycloplatinated Compounds. Significance of the Cyclometalated Group on the Electronic and Emitting Properties of Biscyanide Compounds. *J. Organomet. Chem.* **2019**, *889*, 53−61.
(44) Ogawa, T.; Sameera, W. M. C.; Saito, D.; Yoshida, M.; Kobayashi, A.; Kato, M. Phosphorescence Properties of Discrete Platinum(II) Complex Anions Bearing N-Heterocyclic Carbenes in the Solid State. *Inorg. Chem.* **2018**, *57*, 14086−14096.
(45) Kim, P.; Kelley, M. S.; Chakraborty, A.; Wong, N. L.; Van Duyne, R. P.; Schatz, G. C.; Castellano, F. N.; Chen, L. X. Coherent Vibrational Wavepacket Dynamics in Platinum(II) Dimers and Their Implications. *J. Phys. Chem. C* **2018**, *122*, 14195−14204.

(46) Jaime, S.; Arnal, L.; Sicilia, V.; Fuertes, S. Cyclometalated NHCs Pt(II) Compounds with Chelating P^P and S^S Ligands: From Blue to White Luminescence. *Organometallics* **2020**, *39*, 3695−3704.
(47) Sicilia, V.; Arnal, L.; Chueca, A. J.; Fuertes, S.; Babaei, A.; Igual Muñoz, A. M.; Sessolo, M.; Bolink, H. J. Highly Photoluminescent Blue Ionic Platinum-Based Emitters. *Inorg. Chem.* **2020**, *59*, 1145−1152.
(48) Zhao, Z.; Zhang, H.; Lam, J. W. Y.; Tang, B. Z. Aggregation-Induced Emission: New Vistas at the Aggregate Level. *Angew. Chem., Int. Ed.* **2020**, *59*, 9888−9907.
(49) Ku, H.-Y.; Tong, B.; Chi, Y.; Kao, H.-C.; Yeh, C.-C.; Chang, C.-H.; Lee, G.-H. Luminescent Pt(II) Complexes Bearing Dual Isoquinolinyl Pyrazolates: Fundamentals and Applications. *Dalton Trans.* **2015**, *44*, 8552−8563.
(50) Ni, J.; Wang, Y.-G.; Wang, H. i.-H.; Xu, L.; Zhao, Y.-Q.; Pan, Y.-Z.; Zhang, J.-J. Thermo- and Mechanical-Grinding-Triggered Color and Luminescence Switches of the Diimine-Platinum(II) Complex with 4-bromo-2,2'-bipyridine. *Dalton Trans.* **2014**, *43*, 352−360.
(51) Zhang, X.; Zhang, L.-Y.; Wang, J.-Y.; Dai, F.-R.; Chen, Z.-N. Two-Step Phosphorescent Mechanochromism Due to Intramolecular Deformation. *J. Mater. Chem. C* **2020**, *8*, 715−720.
(52) Genovese, D.; Aliprandi, A.; Prasetyanto, E. A.; Mauro, M.; Hirtz, M.; Fuchs, H.; Fujita, Y.; Uji-I, H.; Lebedkin, S.; Kappes, M.; De Cola, L. Mechano- and Photochromism from Bulk to Nanoscale: Data Storage on Individual Self-Assembled Ribbons. *Adv. Funct. Mater.* **2016**, *26*, 5271−5278.
(53) Ni, J.; Zhang, X.; Qiu, N.; Wu, Y.-H.; Zhang, L.-Y.; Zhang, J.-J.; Chen, Z.-N. Mechanochromic Luminescence Switch of Platinum(II) Complexes with 5-Trimethylsilylethynyl-2,2'-bipyridine. *Inorg. Chem.* **2011**, *50*, 9090−9096.
(54) Han, A.; Du, P.; Sun, Z.; Wu, H.; Jia, H.; Zhang, R.; Liang, Z.; Cao, R.; Eisenberg, R. Reversible Mechanochromic Luminescence at Room Temperature in Cationic Platinum(II) Terpyridyl Complexes. *Inorg. Chem.* **2014**, *53*, 3338−3344.

https://doi.org/10.1021/acs.inorgchem.1c01470
Inorg. Chem. 2021, 60, 12274−12284

Metallacycles

A Cyclometalated N-Heterocyclic Carbene: The Wings of the First Pt_2(II,II) Butterfly Oxidized by CHI_3

Lorenzo Arnal,[b] Sara Fuertes,*[b] Antonio Martín,[b] Miguel Baya,[b] and Violeta Sicilia*[a]

Dedicated to Professor Ernesto Carmona on the occasion of his 70th birthday

Abstract: The X-ray study on a single crystal of the butterfly-like complex [{Pt(C^C*)(μ-pz)}$_2$] (**1**), containing a cyclometalated N-heterocyclic carbene ligand as wings (HC^C* = 1-(4-(ethoxycarbonyl)phenyl)-3-methyl-1*H*-imidazol-2-ylidene), showed three molecules in the asymmetric unit with intermetallic separations (Å) of 3.2294(4) (**1A**), 3.2834(4) (**1B**), and 3.1208(6) (**1C**). From the reaction of **1** with excess of CHI_3 in the air and the sunlight, complex [{Pt(C^C*)(μ-pz)I)}$_2$] (**2**) (d_{Pt-Pt} = 2.6079(2) Å) was obtained as the major product, while [IPt(C^C*)(μ-pz)$_2$Pt(C^C*)CHI$_2$] (**3**) (d_{Pt-Pt} = 2.6324(3) Å) was obtained as the major product under argon atmosphere in the dark. Experimental and theoretical investigations showed that an easily accessible radical-like mechanism operates under thermal conditions, with dioxygen acting as an efficient radical (R$^•$) scavenger. The oxidation of a Pt_2(II,II) "butterfly" by CHI_3 to give metal–metal bonded Pt_2(III,III) compounds is described now for the first time.

Introduction

The oxidative addition (OA) reaction is a fundamental process in organometallic chemistry with significant implications in many important catalytic reactions.[1] The use of unsaturated dinuclear metal complexes can lead to reaction pathways and products not possible from mononuclear ones because of the cooperative effects between the two adjacent metals.[2] The mechanisms of OA of a range of halocarbons (RX) to d^8 rhodium and iridium dinuclear bis-pyrazolate complexes have been proved to proceed through a bimetallic S_N2 pathway yielding metal–metal bonded M_2(II,II) compounds.[3] Other times it follows a radical-like mechanism[4] or a monometallic S_N2 pathways, the latter resulting in the mixed valence M^I–M^{III} compounds.[5] The mechanism of these reactions depends on many factors, such as the metal, the ligands or the nature of the added molecule,[6] and sometimes requires visible or UV-light, especially for chloroalkanes.[7] In the case of pyrazolate-bridged dinuclear Pt^{II} complexes, the chemistry has been focused on butterfly-like complexes such as [{Pt(N^N)(μ-Rpz)}$_2$] (N^N = diimines or pyridylpyrazolate),[8] [{Pt(C^N)(μ-Rpz)}$_2$] (C^N: C,N-cyclometalated ligand)[9] and [{Pt(C^C*)(μ-Rpz)}$_2$][10] due to their phosphorescent behavior. Many studies addressed the control of the bulkiness of the pyrazolate bridge (the butterfly body) and the bulk and electronic properties of the C^N (the butterfly wings), as the way to control the Pt···Pt distance and then, the nature of the emissive state (^{3}IL/^{3}MLCT or ^{3}MMLCT) and the color of the emission (from greenish-blue to orangish-red).[9]

To our knowledge, two-center two-electron [2c, 2e] oxidation processes of Pt_2(II,II) complexes with halocarbons (RX) to give the corresponding Pt_2(III,III)X_2 or Pt_2(III,III)RX have been described for lantern- or half-lantern complexes, such as $[Pt(pop)_4]^{4-}$ (pop = pyrophosphite),[11] $[Pt_2(pyt)_4]$,[12] $[Pt_2(ppy)_2(pyt)_2]$,[13] and $[Pt_2(bzq)_2(\mu\text{-}N^S)_2]$,[14] all of them with intermetallic distances of ca. 2.9 Å. However, for bis-pyrazolate complexes,[8,9a–c,15] with intermetallic separations ranging from 3.4863(6) to 3.0457(7) Å (except in complex with C^N = 2-(2,4-difluorophenyl)pyridyl and Rpz = 3,5-bis(*tert*-butyl)pyrazolate, d_{Pt-Pt} = 2.8343(6) Å), this kind of reaction has been never reported. Herein, we show compound [{Pt(C^C*)(μ-pz)}$_2$] (**1**) as the first "platinum-butterfly" ever oxidized by halocarbons, such as CHI_3. In the wings: a cyclometalated N-heterocyclic carbene ligand, C^C*. The mechanism of the [2c, 2e] oxidation of **1** has been elucidated experimentally and explained with the aid of theoretical calculations.

[a] *Dr. V. Sicilia*
Departamento de Química Inorgánica
Escuela de Ingeniería y Arquitectura de Zaragoza
Universidad de Zaragoza
Instituto de Síntesis Química y Catálisis Homogénea (ISQCH)
Campus Río Ebro, Edificio Torres Quevedo, 50018 Zaragoza (Spain)
E-mail: sicilia@unizar.es

[b] *L. Arnal, Dr. S. Fuertes, Dr. A. Martín, Dr. M. Baya*
Instituto de Síntesis Química y Catálisis Homogénea (ISQCH)
Departamento de Química Inorgánica
Universidad de Zaragoza-CSIC
C/ Pedro Cerbuna 12, 50009 Zaragoza (Spain)
E-mail: sfuertes@unizar.es

Supporting information and the ORCID identification number(s) for the author(s) of this article can be found under: https://doi.org/10.1002/chem.201804013.

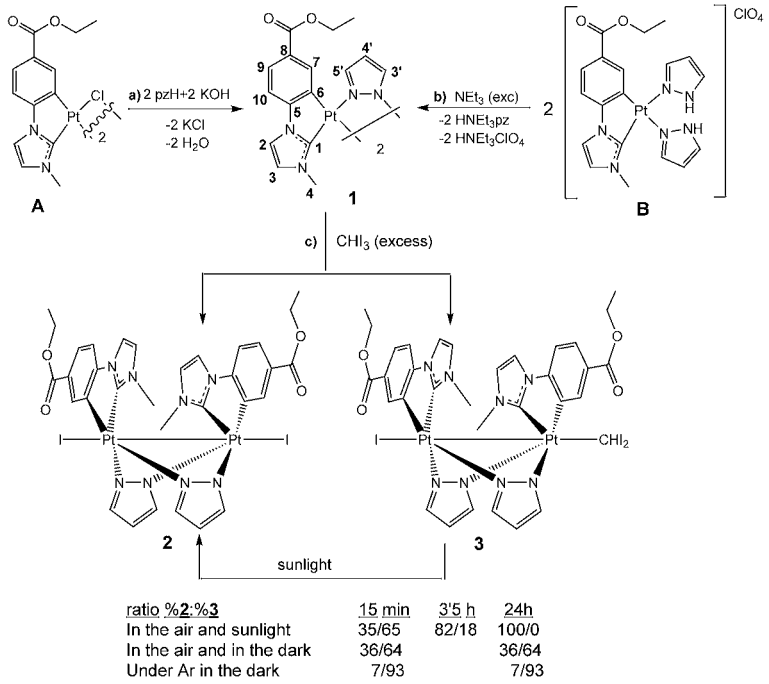

Scheme 1. Reaction pathways involving synthesis and reactivity of **1** including the Numerical Scheme for NMR purposes.

Results and Discussion

Compound **1** was prepared by two paths, from [{Pt(C^C*)(μ-Cl)}$_2$][16] or [Pt(C^C*)(pzH)$_2$]ClO$_4$[17] as a mixture of *syn*/*anti* isomers with respect to the relative orientation of the two cyclometalating C^C* ligands (see Scheme 1 paths a, b). The composition of **1**, with the *anti* isomer being the major one (^{1}H and ^{195}Pt{^{1}H} NMR spectra in Figures S1 and S2 in Supporting Information), is in agreement with the DFT ground-state (S_0) calculations, which showed the *anti* isomer to be 3.1 kcal mol^{-1} lower in energy than the *syn* one (See Figure S3 in Supporting Information).[9f] The synthesis of **1** was also performed at −10 °C and in refluxing acetone following path b, always providing mixtures of isomers with little differences in the *syn*/*anti* ratio. Variable-temperature NMR spectra of **1** in [D$_8$]THF (298 K, 318 K, 323 K, and 323 K) or [D$_6$]benzene (298 K, 318 K, 338 K, and 343 K) showed no change in the *syn*/*anti* ratio (see Figures S4 and S5 in the Supporting Information). Therefore, it seems that these two diastereoisomers (*syn*/*anti*), once formed, do not transform one into the other, even at 343 K. The X-ray study on a single crystal of **1** showed three butterfly-like molecules (A, B, C; see Table 1 and Figure 1 and Figure S6 in Supporting Information) in the asymmetric unit with intermetallic separations of 3.2294(4) Å (**1A**), 3.2834(4) Å (**1B**) and 3.1208(6) Å (**1C**), each of them shorter than those observed in other platinum "butterflies" with the same body (pz) but different wings (3.231–3.486 Å).[8,9a–c,15] In each of them, **1A**–**1C**, the molecule shows a dinuclear structure comprised of two "Pt(EtO$_2$C-C^C*)" metallocycles bridged by two pz ligands and displaying an *anti* arrangement of the C^C* groups. The six-membered ring Pt$_2$N$_4$ has the typical boat-like conformation with an angle between the Pt-N-N-Pt fragments of about 82°

Table 1. Selected bond lengths (Å) and angles (°) for **1·0.5 tol·0.16 OEt$_2$**.

	1A	1B	1C
Pt(1)–C(1)	1.964(7)	1.964(6)	1.961(6)
Pt(1)–C(6)	2.003(6)	2.003(7)	2.007(6)
Pt(1)–N(5)	2.055(5)	2.043(5)	2.057(5)
Pt(1)–N(7)	2.092(5)	2.083(5)	2.089(5)
Pt···Pt	3.2294(4)	3.2834(4)	3.1210(3)
Pt(2)–C(14)	1.966(7)	1.956(6)	1.951(6)
Pt(2)–C(19)	2.013(6)	2.012(6)	2.020(6)
Pt(2)–N(6)	2.086(5)	2.082(5)	2.094(5)
Pt(2)–N(8)	2.043(5)	2.051(5)	2.064(5)
C(1)-Pt(1)-C(6)	80.0(3)	80.0(3)	80.3(3)
C(1)-Pt(1)-N(7)	100.5(3)	101.3(2)	100.2(2)
C(6)-Pt(1)-N(5)	94.8(2)	94.6(2)	94.8(2)
N(5)-Pt(1)-N(7)	84.8(2)	84.1(2)	84.4(2)
C(14)-Pt(2)-C(19)	80.0(3)	79.7(3)	80.5(3)
C(14)-Pt(2)-N(6)	100.8(3)	99.8(2)	98.6(2)
C(19)-Pt(2)-N(8)	95.1(2)	94.2(2)	95.5(2)
N(6)-Pt(2)-N(8)	84.2(2)	86.17(19)	85.3(2)

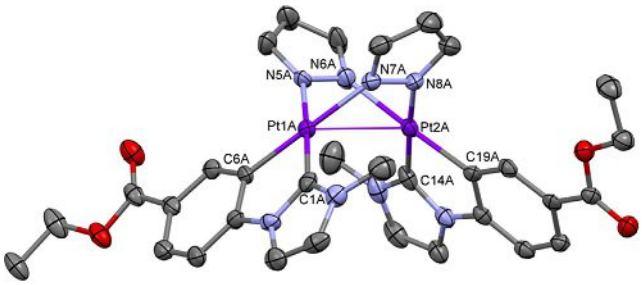

Figure 1. Molecular structure of complex **1A**. Ellipsoids are drawn at their 50% probability level; solvent molecules and hydrogen atoms have been omitted for clarity.

(82.27(13)° **1A**, 80.21(14)° **1B**, 83.64(14)° **1C**) and an angle between the best least-squares planes of the platinum environments [Pt1,C1,C6,N5,N7; Pt2,C14,C19,N6,N8] of ca. 70° (73.84(18)° **1A**, 78.96(15)° **1B**, 66.68(13)° **1C**). The angles between the Pt–Pt line and both metal coordination planes are close to 35° (36.55(13)° Pt(1) and 37.41(12)° Pt(2) **1A**, 35.95(9)° Pt(1) and 43.24(11)° Pt(2) **1B**, 33.40(10)° Pt(1) and 33.51(8)° Pt(2) **1C**). In the molecule, each Pt center lies in a distorted square planar coordination environment as a consequence of the small bite angle of the EtO_2C-C^C* cyclometalated ligand ca 80°. These angles and the Pt–C_{Ar} and Pt–C* distances are similar to those found in other compounds containing five-membered cycloplatinated N-heterocyclic carbenes.[16–18] The Pt–N bond lengths are also similar to those found in dinuclear bis-pyrazolate-bridge complexes containing ligands with high *trans* influence.[9a,15,19]

The reaction of **1** (*syn*/*anti* mixture) with an excess of CHI_3 (molar ratio 1:4, see Scheme 1 path c) in the air and in sunlight rendered $Pt_2(III,III)I_2$ as the major species, with complex [{Pt(C^C*)(μ-pz)I)}$_2$] (**2**), with an *anti* arrangement of the C^C* groups, being precipitated and separated from the mixture in a 41% yield. However, under Ar atmosphere, the reaction was observed to render species "$Pt_2(III,III)I(CHI_2)$" almost selectively. Compound [IPt(C^C*)(μ-pz)$_2$Pt(C^C*)(CHI_2)](**3**), with an *anti* arrangement of the C^C* groups, was in this case precipitated and separated from the mixture in a 43% yield. Compounds **2** and **3** were fully characterized (see Experimental Section, Figures 2, 3, and 4 and Figures S7–S19 in Supporting Information). Their X-ray structures showed for both, **2** and **3** (see Figure 2) the expected boat-like shape of the molecule and also, the shortening of the intermetallic distance (d_{Pt-Pt}: 2.6079(2) Å **2**, 2.6324(3) Å **3**) with respect to **1** due to the formation of a Pt^{III}–Pt^{III} bond.[12,14,20] These distances are shorter than the observed in the mixed-valent $Pt^{III}Pt^{III}Pt^{II}$ complex [Pt_3Br_2(μ-pz)$_6$] ($d_{Pt(III)-Pt(III)}$ = 2.7787(8) Å).[21] In these complexes each Pt^{III} center has a distorted octahedral environment with the axial positions occupied by an X fragment (I **2**, I and CHI_2 **3**) and the other Pt^{III} center with the X-Pt-Pt angles close to 165°. The Pt–Pt distance in **3** (2.6324(3) Å) is slightly longer than that in **2** (2.6079(2) Å) (see Table 2), likely due to the larger *trans* influence of the CHI_2 fragment when compared to the I one. The Pt–I distances are also in the range of those found in other Pt^{III} complexes.[14,20b,e,f] In the two complexes, **2** and **3**, the "Pt(EtO_2C-C^C*)" metallocycles display an *anti*-arrangement of the Pt–C* bonds (C1-Pt1-Pt2-C14 torsion angles are 82.25(17)° **2** and 79.65 (31)° **3**), the six-membered ring Pt_2N_4 has the typical boat-like conformation (the angle between the Pt-N-N-Pt fragments being 89.25(6)° for **2** and 89.32(9)° for **3**). In each complex, the equatorial platinum coordination planes are non-parallel and form interplanar angles close to 40° (37.58(9)° **2**, 40.19(14)° **3**) quite smaller than those observed for complexes **1A**–**1C** (66.68(13)–78.96(15)°), which undoubtedly must be a consequence of the metal–metal bond formation. It also affects the angles between the Pt coordination planes and the Pt–Pt line [18.03(7)° Pt1, 19.59(6)° Pt2 **2** and 21.30(11)° Pt1, 18.89(10)° Pt2 **3**] that became smaller than those in **1** (close to 36°).

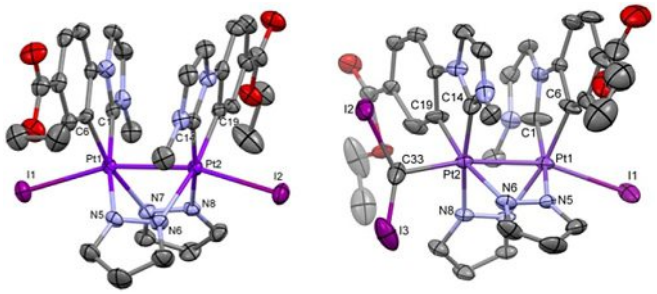

Figure 2. Molecular structure of complex (a) **2·1.75 Me_2CO** and (b) **3**. Ellipsoids are drawn at their 50% probability level; solvent molecules and hydrogen atoms have been omitted for clarity.

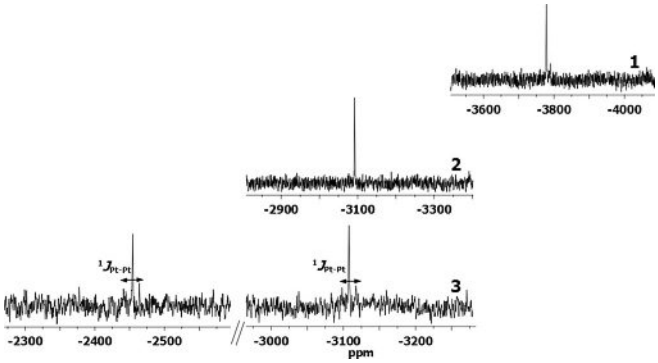

Figure 3. $^{195}Pt\{^1H\}$ NMR spectra of **1**([D_6]acetone), **2** and **3** (CD_2Cl_2).

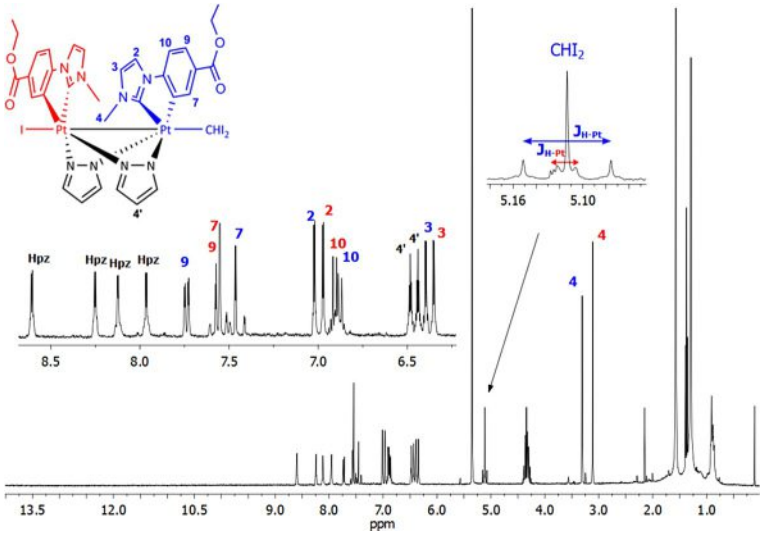

Figure 4. ^1H NMR spectrum of **3** in CD_2Cl_2 (sample prepared in the dark).

The increased oxidation state of Pt in **2** and **3** is evident from the significant downfield shift of the ^{195}Pt NMR signals with respect to that of **1** (see Figure 3). The presence of two widely separated ^{195}Pt signals at −2454 and −3107 ppm in the

Table 2. Selected bond lengths (Å) and angles (°) for for **2·1.75 Me_2CO** and **3·0.25 Me_2CO.**

	2·1.75 Me_2CO	**3·0.25 Me_2CO**
Pt(1)–C(1)	1.983(4)	1.992(7)
Pt(1)–C(6)	2.031(4)	2.012(6)
Pt(1)–N(5)	2.086(3)	2.055(5)
Pt(1)–N(7)	2.117(3)	2.105(5)
Pt(1)–I(1)	2.7030(3)	2.8066(5)
Pt–Pt	2.6079(2)	2.6324(3)
Pt(2)–C(14)	1.991(4)	1.960(6)
Pt(2)–C(19)	2.025(4)	2.014(6)
Pt(2)–N(8)	2.075(3)	2.065(5)
Pt(2)–N(6)	2.115(3)	2.128(5)
Pt(2)–X′	2.7176(3) X′ = I(2)	2.145(8) X′ = CHI_2
C(1)-Pt(1)-C(6)	79.64(16)	79.6(3)
C(1)-Pt(1)-N(7)	96.79(14)	98.6(3)
C(6)-Pt(1)-N(5)	96.45(14)	95.3(3)
N(5)-Pt(1)-N(7)	85.17(13)	84.91(18)
I(1)-Pt1-Pt2	163.328(10)	162.412(14)
C(14)-Pt(2)-C(19)	79.97(16)	80.4(3)
C(14)-Pt(2)-N(6)	98.38(15)	96.9(3)
C(19)-Pt(2)-N(8)	94.71(14)	94.7(2)
N(6)-Pt(2)-N(8)	85.71(13)	85.7(2)
X′-Pt2-Pt1	164.776(10) X′ = I(2)	167.85(18) X′ = CHI_2

$^{195}Pt\{^1H\}$ NMR spectrum of **3** in CD_2Cl_2 evidences the non-equivalence of the two Pt fragments within this diplatinum(III) complex. In spite of its low solubility, platinum satellites could be also detected with a $^1J_{Pt,Pt}$ coupling constant of 1674 Hz, which is similar to the one observed for $[Pt_2(pop)_4MeI]$ ($^1J_{Pt,Pt}$ = 1550 Hz).[11b] Structurally significant is also the singlet corresponding to the CHI_2 fragment at 5.11 ppm, which displays the expected ^{195}Pt satellite pattern ($^2J_{Pt,H}$ = 30.2 Hz, $^3J_{Pt,H}$ = 5.9 Hz) for its structure (see ^1H NMR spectrum in Figure 4).

The mechanism of this unexpected [2c, 2e] oxidation process was studied. To do that **1** was reacted with CHI_3 in a 1:4 molar ratio in $[D_6]$acetone in NMR tubes in different conditions and the reactions followed by ^1H NMR spectroscopy (see Scheme 1). In the air, **1** was completely reacted in 15 min to give a mixture of **2** and **3**. However, while in the reaction performed in the dark the mixture remained unchanged for at least 24 h (see Figure S20), in that performed in the sunlight, after 24 h complex **3** was completely transformed into the dihalocomplex **2** and minor unknown species (see Figure S21).

Under Ar atmosphere in the dark, compound **1** was completely reacted in 1 h to render **3** in about a 93% but, the formation of **2** is also evident (see Figure S22). The mixture also remains unchanged for at least 24 h. So, the simultaneous formation of **2** and **3** in this reaction suggests a radical pathway for the thermal addition process.[11b]

Comparative experiments were performed under Ar atmosphere in the dark with and without the trapping alkyl reagent galvinoxyl (Gal•). They showed that the reaction of **1** with CHI_3 in the presence of Gal• resulted to be slower than in the absence of it (in 1 h, most amount of **1** remains unreacted). After 24 h, **1** is completely reacted, being the ratio **2**:**3** bigger with Gal•, than without it (Figure S22). In spite of the fact that in the air the formation of quite small quantities of iodine (generated by O_2) and its subsequent addition to **1** can be not absolutely ruled out, the experimental results are in agreement with a radical pathway [Eq. (1)–(4)] in which O_2 (or Gal•) acts as an efficient radical trap (R•), increasing the ratio **2**:**3**.

$$Pt_2 + RI \rightarrow Pt_2I^{\bullet} + R^{\bullet} \quad (1)$$

$$Pt_2 + R^{\bullet} \rightarrow Pt_2R^{\bullet} \quad (2)$$

$$Pt_2I^{\bullet} + RI \rightarrow Pt_2I_2 + R^{\bullet} \quad (3)$$

$$Pt_2R^{\bullet} + RI \rightarrow Pt_2RI + R^{\bullet} \quad (4)$$

To gain more in-depth knowledge about the thermal reaction of the dimer **1** and CHI_3, we carried out theoretical calculations (see computational details in the Supporting Information). Thus, we have considered four conceptually different metal oxidation pathways: *i*) a classical S_N2 addition of iodoform to the Pt^{II}–Pt^{II} dimer; *ii*) an iodine transfer from iodoform to the Pt^{II}–Pt^{II} dimer; *iii*) an electron-transfer from the Pt^{II}–Pt^{II} dimer to iodoform and; *iv*) an OA via singlet–triplet crossover processes (see Scheme 2 and Scheme S1 in the Supporting Information). DFT calculations indicate that the pathways involving spin crossover processes and triplet state (T1) Pt–Pt species (paths *iva* and *ivb* in Scheme S1) can be ruled out under thermal conditions, so they will not be further discussed here. In contrast, the formation of either the Pt-Pt···CHI_3 or the Pt-Pt···$ICHI_2$ adducts as reaction intermediates are energetically feasible (Scheme 2). Interestingly, even though the S_N2 addition pathway (*i*) appears energetically accessible ($\Delta G^{\ddagger}$ = 23.6 kcal

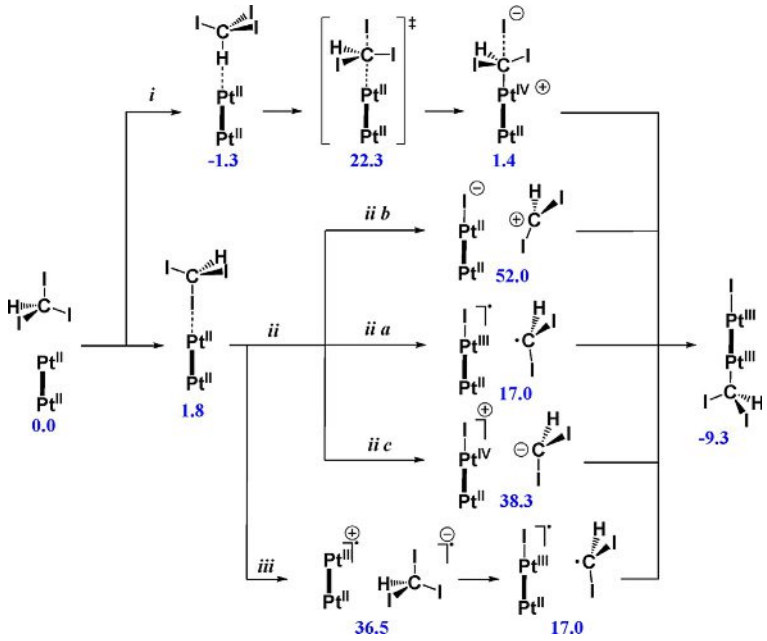

Scheme 2. Single-state DFT-calculated pathways and energy barriers (kcal mol^{-1} in blue) for the conversion of **1** to **3**.

mol^{-1}), iodine-atom transfer to the platinum dimer (*iia*) is clearly favored ($\Delta G^0 = 17.0$ kcal mol^{-1}) and therefore emerges as the most likely reaction mechanism. Other variants as iodide transfer (*iib*), iodine-cation transfer (*iic*) and electron transfer from the platinum dimer to the iodoform (*iii*) are energetically disfavored processes.

DFT calculations show that pathway *iia* is energetically compatible with the experimental results, that is, with a fast reaction which is completed in minutes. This means that the formation of the Pt^{III}–Pt^{III} compound **3** proceeds via a homolytic breakage of the I–C bond[22] in a S_0 [Pt-Pt···$ICHI_2$] adduct. Furthermore, the concomitant generation of radicals in the reaction media is consistent with the observed formation of the diiodide derivative **2** and also with the variable outcomes observed in the reactions carried out under argon atmosphere or in the presence of O_2 or galvinoxyl.

Conclusion

In summary this paper shows the first reported "platinum butterfly" ever oxidized by halocarbons (CHI_3) to give metal–metal bonded platinum(III) complexes, Pt_2(III,III)I_2 and Pt_2(III,III)I(CHI_2). In the wings: a cyclometalated N-heterocyclic carbene ligand, C^C*. The thermal addition seems to follow a radical-like pathway, with O_2 acting as an efficient radical trap (R·), likely due to the easily accessible Pt_2-promoted homolytic I–C bond breakage of iodoform. By controlling the reaction conditions it was possible to get Pt_2(III,III)I_2 and Pt_2(III,III)I(CHI_2) species almost selectively. Preliminary studies on the mechanism and reactivity of **1** towards other halocarbons, such as $CHBr_3$, $CHCl_3$ or CH_2Cl_2 indicate that under ambient conditions the behavior is quite similar, which indicates the inconvenience of treating this kind of compound with halogenated solvents.

Experimental Section

Information describing Instrumental methods used for characterization, details concerning DFT calculations and X-ray structure determination are provided in the Supporting Information. The starting materials [{Pt(μ-Cl)(EtO_2C-C^C*)}$_2$] (**A**)[16] and [Pt(EtO_2C-C^C*)(pzH)$_2$]ClO_4 (**B**)[17] were prepared following the literature procedure. pzH was purchased from MERCK.

Synthesis of *syn*/anti-[{Pt(C^C*)(μ-pz)}$_2$] (1)

Method A: Compound **A** (100.0 mg, 0.11 mmol) was added to a solution containing KOH (13.6 mg, 0.22 mmol) and pzH (14.8 mg, 0.22 mmol) in acetone/EtOH (16 mL/8 mL). After 24 h of reaction at r.t. the solvent was removed under reduced pressure, filtered and washed with 2×5 mL of H_2O to give **1-*anti* (92%)/1-*syn* (8%)** as a yellow solid. Yield: 66 mg, 62%. **Method B**: NEt_3 (0.5 mL, 3.62 mmol) was added to a solution of **B** (120 mg, 0.18 mmol) in acetone (40 mL) at r.t. After 2 h of reaction the solvent was removed in vacuo. The residue was treated with MeOH (5 mL), filtered, and washed to give **1-*anti* (86%)/1-*syn* (14%)** as a yellow solid. Yield: 60 mg, 68%. Anal. Calcd for $C_{32}H_{32}N_8O_4Pt_2$: C, 39.11; H, 3.28; N, 11.40. Found: C, 38.72; H, 3.34; N, 11.26. ^{1}H NMR data for **1-*anti*** (500 MHz, [D$_6$]acetone): $\delta = 7.97$ (d, $^4J_{H7,H9} = 1.7$, $^3J_{H7,Pt} = 54.2$, 2H, H_7), 7.72 (d, $^3J_{H,H} = 1.7$, 2H, pz), 7.96 (d, $^3J_{H2,H3} = 2.1$, 2H, H_2), 7.68 (d, $^3J_{H,H} = 2.0$, 2H, pz), 7.65 (dd, $^3J_{H9,H10} = 8.1$, $^4J_{H9,H7} = 1.8$, 2H, H_9), 7.22 (d, $^3J_{H10,H9} = 8.1$, 2H, H_{10}), 7.11 (d, $^3J_{H3,H2} = 2.1$, 2H, H_3), 6.38 (t, $^3J_{H,H} = 2.0$, 2H, $H_{4'}$, pz), 4.23 (q, $^3J_{H,H} = 7.1$, 4H, CH_2, CO_2Et), 3.32 (s, 6H, H_4), 1.29 (t, $^3J_{H,H} = 7.1$, 6H, CH_3, CO_2Et). ^{1}H NMR data for **1-*syn***: $\delta = 7.92$ (d, $^4J_{H7,H9} = 1.7$, 2H, H_7), 7.60 (dd, $^3J_{H9,H10} = 8.1$, $^4J_{H9,H7} = 1.8$, 2H, H_9), 6.41 (t, 1H, $^3J_{H,H} = 1.7$) and 6.30 (t, $^3J_{H,H} = 1.7$, 1H) ($H_{4'}$ and $H_{4''}$, pz); the rest of the signals appear overlapped with those of the **1-*anti*** isomer. ^{195}Pt{^{1}H} NMR (85.6 MHz, [D$_6$]acetone): $\delta = -3778$ (s) **1-*anti***; $\delta = -3789$ (s) **1-*syn***. MS (MALDI+): *m/z* 981.1 [{Pt(C^C*)(μ-pz)}$_2$]

Synthesis of [{Pt(C^C*)(μ-pz)I)}$_2$] (2)

CHI_3 (83.4 mg, 0.21 mmol) was added to a solution of **1** (51.4 mg, 0.052 mmol) in acetone (15 mL) at r.t and sunlight. After 8 h of reaction the resulting suspension was concentrated to a volume of ca. 5 mL, filtered and washed with *n*-hexane (20 mL) to give **2** as a dark orange solid. Yield: 26 mg, 41%. Anal. Calcd for $C_{32}H_{32}I_2N_8O_4Pt_2$: C, 31.08; H, 2.61; N, 9.06. Found: C, 30.76; H, 2.57; N, 8.76. ^{1}H NMR data (400 MHz, CD_2Cl_2): $\delta = 7.98$ (d, $^3J_{H,H} = 1.9$, $^4J_{H,Pt} = 12.3$, 2H), 7.82 (d, $^3J_{H,H} = 1.9$, $^4J_{H,Pt} = 10.4$, 2H) [$H_{3'}$and $H_{5'}$, pz], 7.54 (dd, $^3J_{H9,H10} = 8.3$, $^4J_{H9,H7} = 1.6$, 2H, H_9), 7.47 (d, $^4J_{H9,H7} = 1.6$, $^4J_{H7,Pt} = 40.4$, 2H, H_7), 6.97 (d, $^3J_{H3,H2} = 1.8$, 2H, H_2), 6.89 (d, $^3J_{H10,H9} = 8.3$, 2H, H_{10}), 6.37 (d, $^3J_{H3,H2} = 1.8$, 2H, H_3), 6.35 (t, $^3J_{H,H} = 1.9$, 2H, $H_{4'}$, pz), 4.37–4.22 (m, 4H, CH_2, CO_2Et), 3.22 (s, 6H, H_4), 1.33 (t, $^3J_{H,H} = 6.9$, 6H, CH_3 (CO_2Et)). ^{13}C{^{1}H} NMR plus HMBC and HSQC (101 MHz, CD_2Cl_2): $\delta = 166.4$ (s, 2C, *C*O_2Et), 147.0 (s, 2C, C_5), 146.7 (s, 2C, C_1), 139.4 (s, 2C) and 138.3 (s, 2C) [$C_{3'}$ and $C_{5'}$, pz], 134.0 (s, 2C, C_7), 127.3 (s, 2C, C_9), 127.3 (s, 2C) and 124.2 (s, 2C) [C_6 and C_8, pz], 123.4 (s, 2C, C_2), 114.9 (s, 2C, C_3), 111.2 (s, 2C, C_{10}), 106.5 (s, 2C, $C_{4'}$), 61.5 (s, 2C, CH_2, CO_2Et), 37.5 (s, 2C, C_4), 14.6 (s, 2C, CH_3 (CO_2Et)). ^{195}Pt{^{1}H} NMR (85.6 MHz, CD_2Cl_2): $\delta = -3092.1$ (s). MS (MALDI+): *m/z* 1109.1 [{Pt(C^C*)(μ-pz)}$_2$I]$^+$

Synthesis of [IPt(C^C*)(μ-pz)$_2$Pt(C^C*)CHI_2] (3)

CHI_3 (25.0 mg, 0.06 mmol) was added in the dark to a solution of **1** (50.0 mg, 0.05 mmol) in degassed acetone (5 mL) at r.t under an argon atmosphere. After 30 min of reaction, an orange precipitate was filtered off and washed with *n*-hexane (5 mL) to give **3** as an orange solid. Yield: 30 mg, 43%. Anal. Calcd for $C_{33}H_{33}I_3N_8O_4Pt_2$: C, 28.79; H, 2.42; N, 8.14. Found: C, 28.56; H, 2.47; N, 7.82. ^{1}H NMR data (400 MHz, CD_2Cl_2): $\delta = 8.60$ (d, $^3J_{H,H} = 2.3$, $^3J_{H,Pt} = 5.0$, 1H, pz), 8.24 (d, $^3J_{H,H} = 2.2$, $^3J_{H,Pt} = 6.6$, 1H, pz), 8.12 (d, $^3J_{H,H} = 1.9$, $^3J_{H,Pt} = 11.1$, 1H, pz), 7.96 (d, $^3J_{H,H} = 2.1$, $^3J_{H,Pt} = 9.2$, 1H, pz), 7.73 (dd, $^3J_{H9,H10} = 8.1$, $^4J_{H9,H7} = 1.7$, 1H, H_9 (Pt-CHI_2)), 7.55 (dd, $^3J_{H9,H10} = 7.5$, $^4J_{H9,H7} = 1.8$, 1H, H_9 (Pt-I)), 7.54 (m, partially overlapped with H_9, $^3J_{H,Pt} = 44.9$, 1H, H_7 (Pt-I)), 7.46 (d, $^3J_{H,H} = 2.3$, $^3J_{H,Pt} = 44.8$, 1H, H_7 (Pt-CHI_2)), 7.02 (d, $^3J_{H3,H2} = 2.2$, $^4J_{H,Pt} = 5.0$, 1H, H_2 (Pt-CHI_2)), 6.97 (d, $^3J_{H3,H2} = 2.2$, 1H, H_2 (Pt-I)), 6.94 (d, $^3J_{H10,H9} = 8.2$, 1H, H_{10} (Pt-I)), 6.87 (d, $^3J_{H10,H9} = 8.8$, 1H, H_{10} (Pt-CHI_2)), 6.47 (t, $^3J_{H,H} = 2.2$, 1H, $H_{4'}$, pz), 6.43 (t, $^3J_{H,H} = 2.1$, 1H, $H_{4'}$, pz), 6.40 (d, $^3J_{H3,H2} = 2.1$, $^4J_{H,Pt} = 6.8$, 1H, H_3, (Pt-CHI_2)), 6.35 (d, $^3J_{H3,H2} = 2.2$, $^4J_{H,Pt} = 6.9$, 1H, H_3, (Pt-I)), 5.11 (s, $^2J_{Pt,H} = 30.4$, $^3J_{Pt,H} = 5.9$, 1H, C*H*I_2), 4.25–4.41 (m, 4H, CH_2, CO_2Et), 3.31 (s, $^4J_{Pt,H} = 4.3$, 3H, H_4 (Pt-CHI_2)), 3.11 (s, 3H, H_4 (Pt-I)), 1.36 (t, 6H, CH_3 (CO_2Et)). ^{13}C{^{1}H} NMR plus HMBC and HSQC (101 MHz, CD_2Cl_2): $\delta = 141.4$, 140.1, 133.8 and 131.6 (s, 4C, CH, pz), 132.8 (s, 1C, C_7), 128.1 (s, 1C, C_9), 126.2 (s, 2C, C_7 and C_9), 123.7 (s, 1C, C_3 (Pt-CHI_2)), 121.9 (s, 1C, C_3 (Pt-I)), 111.8 (s, 1C, C_{10}), 110.5 (s, 1C, C_{10}), 105.9 (m, 2C, $C_{4'}$), 61.6 (s, 2C, CH_2, CO_2Et), 61.3 (s, 2C, CH_2, CO_2Et), 37.4 and 37.2 (s, 2C, C_4), 14.6 (s, 6C, CH_3 (CO_2Et)). The rest of signals are not detected due to solubility issues.^{195}Pt{^{1}H} NMR (85.6 MHz, CD_2Cl_2): $\delta = -2454$ (s, $^1J_{Pt,Pt} = 1674$ Hz, Pt-CHI_2) and -3107 ppm (s, Pt-I). MS (MALDI+): *m/*

z 1109.1 [{Pt(EtO_2C-C^C*)(μ-pz)}$_2$I], 1249.0 [{Pt(EtO_2C-C^C*)(μ-pz)}$_2$$CHI_2$]

Acknowledgements

This work was supported by the Spanish Ministerio de Economía *y* Competitividad (MINECO)/FEDER (Project CTQ2015-67461-P led by Dr. Babil Menjón) and by the Gobierno de Aragón and Fondo Social Europeo (Grupo E17_17R: Química Inorgánica *y* de los Compuestos Organometálicos led by Dr. José M. Casas). The authors thank the Instituto de Biocomputación *y* Física de Sistemas Complejos (BIFI) and Centro de Supercomputación de Galicia (CESGA) for generous allocation of computational resources.

Conflict of interest

The authors declare no conflict of interest.

Keywords: bridging pyrazolate · cyclometalated NHC · dinuclear Pt^{III} · molecular butterfly · oxidative addition

[1] J. P. Collman, L. S. Hegedus, J. R. Norton, R. G. Finke, *Principles and Applications of Organotransition Metal Chemistry*, University Science Books, Mill Valley, CA, **1987**.

[2] a) D. C. Powers, E. Lee, A. Ariafard, M. S. Sanford, B. F. Yates, A. J. Canty, T. Ritter, *J. Am. Chem. Soc.* **2012**, *134*, 12002 – 12009; b) D. R. Hartline, M. Zeller, C. Uyeda, *J. Am. Chem. Soc.* **2017**, *139*, 13672 – 13675; c) I. G. Powers, C. Uyeda, *ACS Catal.* **2017**, *7*, 936 – 958.

[3] a) L. A. Oro, E. Sola, J. A. López, F. Torres, A. Elduque, F. J. Lahoz, *Inorg. Chem. Commun.* **1998**, *1*, 64 – 67; b) D. O. K. Fjeldsted, S. R. Stobart, M. J. Zaworotko, *J. Am. Chem. Soc.* **1985**, *107*, 8258 – 8259; c) J. L. Atwood, K. A. Beveridge, G. W. Bushnell, K. R. Dixon, D. T. Eadie, S. R. Stobart, M. J. Zaworotko, *Inorg. Chem.* **1984**, *23*, 4050 – 4057.

[4] a) M. A. Casado, J. J. Pérez-Torrente, M. A. Ciriano, I. T. Dobrinovitch, F. J. Lahoz, L. A. Oro, *Inorg. Chem.* **2003**, *42*, 3956 – 3964; b) P. Kalck, J.-J. Bonnet, *Organometallics* **1982**, *1*, 1211 – 1216.

[5] a) M. K. Kolel-Veetil, A. L. Rheingold, K. J. Ahmed, *Organometallics* **1993**, *12*, 3439 – 3446; b) T. G. Schenck, C. R. C. Milne, F. J. Sawyer, B. Bosnich, *Inorg. Chem.* **1985**, *24*, 2338 – 2344.

[6] a) D. H. Nguyen, F. J. Modrego, J. M. Cetina-Casas, D. Gómez-Bautista, M. V. Jiménez, R. Castarlenas, F. J. Lahoz, L. A. Oro, J. J. Pérez-Torrente, *Organometallics* **2012**, *31*, 6395 – 6407; b) C. Tejel, M. A. Ciriano, A. J. Edwards, F. J. Lahoz, L. A. Oro, *Organometallics* **2000**, *19*, 4968 – 4976; c) C. Tejel, M. A. Ciriano, J. A. López, F. J. Lahoz, L. A. Oro, *Organometallics* **2000**, *19*, 4977 – 4984.

[7] J. V. Caspar, H. B. Gray, *J. Am. Chem. Soc.* **1984**, *106*, 3029 – 3030.

[8] a) K. Sakai, T. Sato, T. Tsubomura, K. Matsumoto, *Acta Crystallogr. Sect. C* **1996**, *52*, 783 – 786; b) K. Umakoshi, K. Kimura, Y. H. Kim, Y. Tsukimoto, Y. Arikawa, M. Onishi, S. Ishizaka, N. Kitamura, *Bull. Chem. Soc. Jpn.* **2010**, *83*, 1504 – 1510; c) N. Ghavale, A. Wadawale, S. Dey, V. K. Jain, *J. Organomet. Chem.* **2010**, *695*, 1237 – 1245; d) S.-W. Lai, M. C. W. Chan, K.-K. Cheung, S.-M. Peng, C.-M. Che, *Organometallics* **1999**, *18*, 3991 – 3997; e) Q.-F. Sun, K. M.-C. Wong, L.-X. Liu, H.-P. Huang, S.-Y. Yu, V. W.-W. Yam, Y.-Z. Li, Y.-J. Pan, K.-C. Yu, *Inorg. Chem.* **2008**, *47*, 2142 – 2154; f) S.-Y. Chang, J.-L. Chen, Y. Chi, Y.-M. Cheng, G.-H. Lee, C.-M. Jiang, P.-T. Chou, *Inorg. Chem.* **2007**, *46*, 11202 – 11212.

[9] a) B. Ma, J. Li, P. I. Djurovich, M. Yousufuddin, R. Bau, M. E. Thompson, *J. Am. Chem. Soc.* **2005**, *127*, 28 – 29; b) B. Ma, P. I. Djurovich, S. Garon, B. Alleyne, M. E. Thompson, *Adv. Funct. Mater.* **2006**, *16*, 2438 – 2446; c) A. Chakraborty, J. C. Deaton, A. Haefele, F. N. Castellano, *Organometallics* **2013**, *32*, 3819 – 3829; d) S. E. Brown-Xu, M. S. J. Kelley, K. A. Fransted, A. Chakraborty, G. C. Schatz, F. N. Castellano, L. X. Chen, *J. Phys. Chem. A* **2016**, *120*, 543 – 550; e) M. Han, Y. Tian, Z. Yuan, L. Zhu, B. Ma, *Angew. Chem. Int. Ed.* **2014**, *53*, 10908 – 10912; *Angew. Chem.* **2014**, *126*, 11088 – 11092; f) C. Zhou, Y. Tian, Z. Yuan, M. Han, J. Wang, L. Zhu, M. S. Tameh, C. Huang, B. Ma, *Angew. Chem. Int. Ed.* **2015**, *54*, 9591 – 9595; *Angew. Chem.* **2015**, *127*, 9727 – 9731; g) C. Zhou, L. Yuan, Z. Yuan, N. K. Doyle, T. Dilbeck, D. Bahadur, S. Ramakrishnan, A. Dearden, C. Huang, B. Ma, *Inorg. Chem.* **2016**, *55*, 8564 – 8569.

[10] P. Pinter, Y. Unger, T. Strassner, *ChemPhotoChem* **2017**, *1*, 113 – 115.

[11] a) C.-M. Che, W. P. Schaefer, H. B. Gray, M. K. Dickson, P. B. Stein, D. M. Roundhill, *J. Am. Chem. Soc.* **1982**, *104*, 4253 – 4255; b) D. M. Roundhill, M. K. Dickson, S. J. Atherton, *J. Organomet. Chem.* **1987**, *335*, 413 – 422.

[12] K. Umakoshi, I. Kinoshita, A. Ichamura, S. Ooi, *Inorg. Chem.* **1987**, *26*, 3551 – 3556.

[13] T. Koshiyama, A. Omura, M. Kato, *Chem. Lett.* **2004**, *33*, 1386 – 1387.

[14] V. Sicilia, M. Baya, P. Borja, A. Martín, *Inorg. chem.* **2015**, *54*, 7316 – 7324.

[15] J. R. Berenguer, A. Díez, E. Lalinde, M. T. Moreno, S. Ruiz, S. Sánchez, *Organometallics* **2011**, *30*, 5776 – 5792.

[16] S. Fuertes, A. J. Chueca, M. Perálvarez, P. Borja, M. Torrell, J. Carreras, V. Sicilia, *ACS Appl. Mater. Interfaces* **2016**, *8*, 16160 – 16169.

[17] L. Arnal, S. Fuertes, A. Martín, V. Sicilia, *Chem. Eur. J.* **2018**, *24*, 9377 – 9384.

[18] a) S. Fuertes, A. J. Chueca, L. Arnal, A. Martín, U. Giovanella, C. Botta, V. Sicilia, *Inorg. Chem.* **2017**, *56*, 4829 – 4839; b) S. Fuertes, A. J. Chueca, A. Martín, V. Sicilia, *Cryst. Growth Des.* **2017**, *17*, 4336 – 4346.

[19] a) L. R. Falvello, J. Fornies, A. Martin, V. Sicilia, P. Villarroya, *Organometallics* **2002**, *21*, 4604 – 4610; b) C.-K. Koo, Y.-M. Ho, C.-F. Chow, M. H.-W. Lam, T.-C. Lau, W.-Y. Wong, *Inorg. Chem.* **2007**, *46*, 3603 – 3612.

[20] a) C. M. Che, F. H. Herbstein, W. P. Schaefer, R. E. Marsh, H. B. Gray, *J. Am. Chem. Soc.* **1983**, *105*, 4604 – 4607; b) K. A. Alexander, S. A. Bryan, F. R. Fronczek, W. C. Fultz, A. L. Rheingold, D. M. Roundhill, P. Stein, S. F. Watkins, *Inorg. Chem.* **1985**, *24*, 2803 – 2808; c) R. Aoki, A. Kobayashi, H. C. Chang, M. Kato, *Bull. Chem. Soc. Jpn.* **2011**, *84*, 218 – 225; d) M. A. Bennett, S. K. Bhargava, E. C. C. Cheng, W. H. Lam, T. K. M. Lee, S. H. Priver, J. Wagler, A. C. Willis, V. W. W. Yam, *J. Am. Chem. Soc.* **2010**, *132*, 7094 – 7103; e) V. Sicilia, J. Forniés, J. M. Casas, A. Martín, J. A. López, C. Larraz, P. Borja, C. Ovejero, D. Tordera, H. Bolink, *Inorg. Chem.* **2012**, *51*, 3427 – 3435; f) V. Sicilia, P. Borja, J. M. Casas, S. Fuertes, A. Martín, *J. Organomet. Chem.* **2013**, *731*, 10 – 17.

[21] K. Umakoshi, T. Kojima, Y. H. Kim, M. Onishi, Y. Nakao, S. Sakaki, *Chem. Eur. J.* **2006**, *12*, 6521 – 6527.

[22] J. L. G. Wade, *Organic Chemistry, Fourth Edition*, Prentice-hall, Inc., New yersey, **1999**.

Manuscript received: August 4, 2018

Accepted manuscript online: October 1, 2018

Version of record online: November 15, 2018

Inorganic Chemistry

pubs.acs.org/IC Article

Metal–Metal Cooperation in the Oxidation of a Flapping Platinum Butterfly by Haloforms: Experimental and Theoretical Evidence

Violeta Sicilia,* Lorenzo Arnal, Sara Fuertes,* Antonio Martín, and Miguel Baya

Cite This: *Inorg. Chem.* 2020, 59, 12586–12594 Read Online

ACCESS | Metrics & More | Article Recommendations | Supporting Information

ABSTRACT: The model **1**-DFT for the butterfly complex [{Pt(C^C*)(μ-pz)}$_2$] (**1**; HC^C* = 1-(4-(ethoxycarbonyl)phenyl)-3-methyl-1*H*-imidazol-2-ylidene) shows two minima in the potential energy surface of the ground state in acetone solution: the butterfly-wing-spreading molecules **1-s**, ($d_{Pt-Pt} \approx 3.20$ Å) and the wing-folding molecules **1-f** ($d_{Pt-Pt} \leq 3.00$ Å). Both minima are very close in energy ($\Delta G° = 1.7$ kcal/mol) and are connected through a transition state, which lies only 1.9 kcal/mol above **1-s** and 0.2 kcal/mol above **1-f**. These very low barriers support a fast interconversion process, resembling a *butterfly flapping*, and the presence of both conformers in acetone solution. However, the **1-f** ratio is so low that it is undetectable in the excitation and emission spectra of **1** in 2-MeTHF of diluted solutions (10^{-5} M) at 77 K, while it is seen in more concentrated solutions (10^{-3} M). In acetone solution, **1** undergoes a [2c, 2e] oxidation by CHX_3 (X = Cl, Br) in the sunlight to render the Pt_2(III,III) compounds [{Pt(C^C*)(μ-pz)X)}$_2$] (X = Cl (**2-Cl**), Br (**2-Br**)). In concentrated solutions, **1** can react with $CHCl_3$ under blue light to give **2-Cl** and with $CHBr_3$ in the dark, the latter rendering the compound [BrPt(C^C*)(μ-pz)$_2$Pt(C^C*)$CHBr_2$] (**3-Br**) or mixtures of **2-Br** and **3-Br** if the reaction is performed under an argon atmosphere or in the air, respectively. Mechanistic studies showed that in concentrated solutions the oxidation processes follow a radical mechanism being the MMLCT-based species **1-f**, those which trigger the reaction of **1** with $CHBr_3$ and $CHCl_3$. In the ground state (S_{0f}), it promotes the thermal oxidation of **1** by $CHBr_3$ and in the first singlet excited state (S_{1f}) the blue-light-driven photooxidation of **1** by $CHCl_3$. Complexes, **2-Cl**, **2-Br**, and **3-Br** were selectively obtained and fully characterized, showing Pt–Pt distances (ca. 2.6 Å) shorter than that of the starting complex, **1**. They are, together with the analogous [{Pt(C^C*)(μ-pz)I)}$_2$] and [IPt(C^C*)(μ-pz)$_2$Pt(C^C*)CHI_2], the only dinuclear metal–metal-bonded $Pt^{III}(\mu\text{-pz})_2Pt^{III}$ compounds reported to date.

INTRODUCTION

Cooperative effects between the adjacent d^8 metal centers of dinuclear complexes have been reported to facilitate the formation of stabilizing metal–metal bonds in the intermediates of catalytic reactions, involving oxidative addition–reductive elimination processes, which allows pathways and products unavailable from mononuclear complexes.[1] Pd_2(III,III) or Rh_2(II,II) species are some examples of low-energy transition states for C–H functionalization[2,3] or alkene hydroformylation[4] reactions, respectively. In the chemistry of dinuclear platinum(II) complexes it is well-known that $[Pt_2(POP)_4]^{4-}$ (POP = pyrophosphito) exhibits a rich luminescence and photochemistry associated with the presence of Pt···Pt interactions, resulting in short intermetallic separation (2.925 Å). This complex undergoes thermal two-center–two-electron [2c, 2e] oxidative addition (OA),[5] but the diradical excited state $^3[5d\sigma^* \rightarrow 6p\sigma]$, with enhanced metal–metal-bonding interactions, is the active species for the photoinduced dehydrogenation of alcohols to aldehydes/ketones.[6]

Furthermore, the half-lantern compound [{Pt(bzq)(μ-N^S)}$_2$] (bzq = benzo[*h*]quinoline, HN^S = 2-mercaptopyrimidine) also undergoes [2c, 2e] thermal oxidative addition (OA) of CH_3I and haloforms CHX_3 (X = Br, I), but the MMLCT $5d\sigma^* \rightarrow \pi^*$(bzq) excited state, available upon excitation with green LEDs, is the active state for the photooxidation of [{Pt(bzq)(μ-N^S)}$_2$] with $CHCl_3$.[7]

In this sense, pyrazolate ligands have a proven ability to hold two metal atoms in close proximity, while they permit a wide range of intermetallic separations. Cooperative effects between the two metal centers have been reported for the [2c, 2e] OA of many electrophiles to Ir_2(I,I) bis-pyrazolate bridging complexes.[8] In the case of pyrazolate-bridged dinuclear Pt(II) complexes [2c, 2e] OA reactions have been never reported. The chemistry has been focused on complexes such as [{Pt(N^E)(μ-Rpz)}$_2$]$^{2+}$ (E = N, diimines or pyridylpyrazolate; E = C, pyridyl-NHC),[9−15] [{Pt(C^N)(μ-Rpz)}$_2$] (C^N = C,N-cyclometalated ligand),[16−23] and [{Pt(C^C*)(μ-Rpz)}$_2$] (C^C* = phenyl-NHC)[24] due to their phosphorescent behavior. Most studies have addressed the control of the photoluminescence properties of the complexes [{Pt(C^N)(μ-Rpz)}$_2$], dubbed "molecular butterflies", by tuning the Pt···Pt

Received: June 9, 2020
Published: August 20, 2020

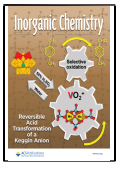

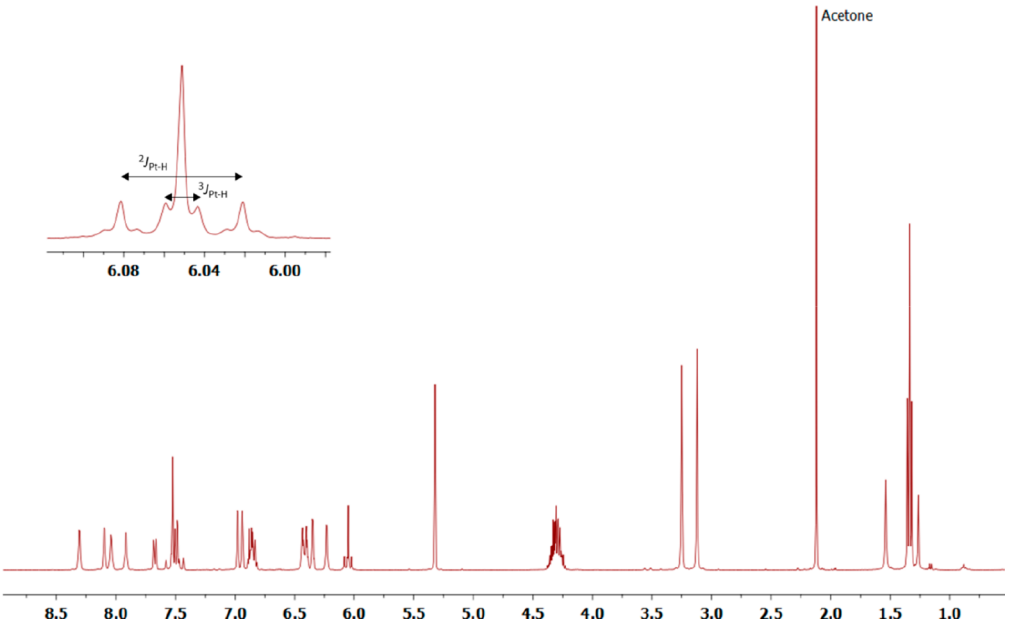

Figure 1. ^{1}H NMR spectrum of **3-Br** in CD_2Cl_2.

separation; they can be modulated by controlling the bulkiness of the bridging pyrazolates (the butterfly body) and the bulkiness and electronic properties of the C^N group (the butterfly wings).[16−23]

In the course of our research we prepared the butterfly compound $[\{Pt(C^C^*)(\mu\text{-pz})\}_2]$ (**1**) (HC^C* = 1-(4-(ethoxycarbonyl)phenyl)-3-methyl-1*H*-imidazol-2-ylidene), and the reaction mechanism of **1** with CHI_3 was deeply studied.[25] To complete this piece of chemistry, we studied the reaction of **1** with $CHCl_3$ and $CHBr_3$ and the mechanisms of the thermal oxidation and photooxidation of **1** with $CHBr_3$ and $CHCl_3$ both experimentally and theoretically. Our results showed that the C^C* basicity and the cooperative effects between the two adjacent metal centers in the Pt_2(II,II) species are crucial to promote the C−X (X = Cl, Br) activation. Furthermore, the oxidation products $[\{Pt(C^C^*)(\mu\text{-pz})X)\}_2]$ (X = Cl (**2-Cl**), Br (**2-Br**)) and $[BrPt(C^C^*)(\mu\text{-pz})_2Pt(C^C^*)CHBr_2]$ (**3-Br**) have been fully characterized, including their X-ray single-crystal structures.

EXPERIMENTAL SECTION

General information about procedures and instrumentation, NMR spectra for characterization, DFT and TD-DFT calculations, and X-ray structure determinations (CCDC 1985166−1985168) are available in the Supporting Information. The starting material $[\{Pt(C^C^*)(\mu\text{-pz})\}_2]$ (**1**) was prepared byfollowing the published procedure and isolated in a 1/9 *syn*/*anti* ratio.[25]

Synthesis and Characterization of *syn*-/*anti*-[{Pt(EtO$_2$C-C^C*)(μ-pz)Cl)}$_2$] (2-Cl). Compound **A** (67.9 mg, 0.069 mmol) was allowed to react in $CHCl_3$ (15 mL) in ambient light at rt for 7.5 h. The resulting yellow solution was concentrated to ∼5 mL, and 10 mL of hexane was added to the residue to give **2-Cl**-*anti* (96%)/ 2-Cl-*syn* (4%) as a yellow solid. Yield: 65 mg, 89%. Anal. Calcd for $C_{32}H_{32}Cl_2N_8O_4Pt_2$: C, 36.47; H, 3.06; N, 10.63. Found: C, 36.03; H, 2.83; N, 10.36. ^{1}H NMR data for **2-Cl**-*anti* (400 MHz, methylene chloride-d_2; *J* values in Hz): δ 7.97−7.92 (m, 2H, $H_{3'}$, pz), 7.86−7.81 (m, 2H, $H_{5'}$, pz), 7.58 (dd, $^3J_{H9,H10}$ = 8.2, $^4J_{H9,\ H7}$ = 1.7, 2H, H_9), 7.50 (d, $^4J_{H7,H9}$ = 1.7, $^3J_{H7,Pt}$ = 39.6, 2H, H_7), 6.99 (d, $^3J_{H3,H2}$ = 2.2, 2H, H_2), 6.90 (d, $^3J_{H10,H9}$ = 8.2, 2H, H_{10}), 6.42−6.36 (m, 4H, $H_{4'}$(pz) and H_3), 4.30 (q, $^3J_{H,H}$ = 7.1, 4H, CH_2, CO_2Et), 3.30 (s, 6H, H_4), 1.33 (t, $^3J_{H,H}$ = 7.1, 6H, CH_3, CO_2Et). ^{1}H NMR data for **2-Cl**-*syn*: δ 3.63 (s, 6H, H_4); other resonances were not detected. $^{13}C\{^1H\}$ NMR plus HMBC and HSQC for **2-Cl**-*anti* (101 MHz, methylene chloride-d_2): δ 166.3 (s, 2C, CO_2Et), 146.7 (s, 2C, C_1), 136.7 and 134.7 (s, 4C, CH, pz), 133.7 (s, 2C, H_7), 127.8 (s, 2C, C_9), 123.6 (s, 2C, C_3), 115.1 (s, 2C, C_2), 111.4 (s, 2C, C_{10}), 106.3 (s, 2C, $C_{4'}$), 61.6 (s, 2C, CH_2, CO_2Et), 37.1 (s, 2C, C_4), 14.8 (s, 2C, CH_3, CO_2Et). $^{195}Pt\{^1H\}$ NMR (85.6 MHz, methylene chloride-d_2): δ −2441 ppm. MS (MALDI+): *m*/*z* 982.3 $[\{Pt(EtO_2C\text{-}C^C^*)(\mu\text{-pz})\}_2]$, 1017.2 $[\{Pt(EtO_2C\text{-}C^C^*)(\mu\text{-pz})\}_2Cl]^+$. MS (MALDI−): *m*/*z* 1089.3 $[\{Pt(EtO_2C\text{-}C^C^*)(\mu\text{-pz})Cl\}_2Cl]^-$.

Synthesis and Characterization of *syn*-/*anti*-[{Pt(EtO$_2$C-C^C*)(μ-pz)Br)}$_2$] (2-Br). $CHBr_3$ (38 μL, 0.10 mmol) was added to a solution of **1** (43 mg, 0.044 mmol) in acetone (10 mL) and allowed to react in ambient light at rt for 2 h. Then the solvent was removed under vacuum, the residue was treated with hexane, and this solution was filtered to give **2-Br**-*anti* (96%)/ 2-Br-*syn* (4%) as a yellowish orange solid. Yield: 45 mg, 90%. Anal. Calcd for $C_{32}H_{32}Br_2N_8O_4Pt_2$: C, 33.64; H, 2.82; N, 9.81. Found: C, 33.29; H, 2.86; N, 9.31. ^{1}H NMR data for **2-Br**-*anti* (400 MHz, methylene chloride-d_2; *J* values in Hz): δ 8.00−7.95 (m, 2H, $H_{3'}$, pz), 7.87−7.82 (m, 2H, $H_{5'}$, pz), 7.56 (dd, $^3J_{H9,H10}$ = 8.1, $^4J_{H9,H7}$ = 1.7, 2H, H_9), 7.49 (d, $^4J_{H7,H9}$ = 1.7, $^3J_{H7,Pt}$ = 40.0, 2H, H_7), 6.98 (d, $^3J_{H3,H2}$ = 2.2, 2H, H_2), 6.90 (d, $^3J_{H10,H9}$ = 8.2, 2H, H_{10}), 6.40−6.34 (m, 4H, $H_{4'}$(pz) and H_3), 4.30 (q, $^3J_{H,H}$ = 7.1, 4H, CH_2, CO_2Et), 3.28 (s, 6H, H_4), 1.33 (t, $^3J_{H,H}$ = 7.1, 6H, CH_3, CO_2Et). ^{1}H NMR data for **2-Br**-*syn*: δ 3.60 (s, 6H, H_4); other resonances were not detected. $^{13}C\{^1H\}$ NMR plus HMBC and HSQC for **2-Br**-*anti* (101 MHz, methylene chloride-d_2): δ 166.3 (s, 2C, CO_2Et), 147.1 (s, 2C, C_5), 146.4 (s, 2C, C_1), 137.3 and 135.7 (s, 4C, CH, pz), 133.8 (s, 2C, C_7), 127.6 (s, 2C, C_9), 127.5 and 124.3 (s, 4C, C_6 and C_8), 123.5 (s, 2C, C_3), 115.1 (s, 2C, C_2), 111.3 (s, 2C, C_{10}), 106.3 (s, 2C, $C_{4'}$), 61.6 (s, 2C, CH_2, CO_2Et), 37.1 (s, 2C, C_4), 14.6 (s, 2C, CH_3, CO_2Et). $^{195}Pt\{^1H\}$ NMR (85.6 MHz, methylene chloride-d_2): δ −2675 ppm. MS (MALDI+): *m*/*z* 982.2 $[\{Pt(EtO_2C\text{-}C^C^*)(\mu\text{-pz})\}_2]$, 1063.2 $[\{Pt(EtO_2C\text{-}C^C^*)(\mu\text{-pz})\}_2Br]^+$.

Synthesis and Characterization of *anti*-[BrPt(EtO$_2$C-C^C*)(μ-pz)$_2$Pt(EtO$_2$C-C^C*)(CHBr$_2$)] (3-Br). $CHBr_3$ (29.0 μL, 0.33 mmol) was added in the dark to a solution of **A** (81.4 mg, 0.08 mmol) in degassed acetone (7 mL) at rt under an argon atmosphere and allowed to react for 30 min. Then the solvent was removed under vacuum, the residue was treated with *n*-hexane, and this solution was filtered to give **3-Br** as a yellow solid. Yield: 70.4 mg, 69%. Anal. Calcd for $C_{33}H_{33}Br_3N_8O_4Pt_2$: C, 32.08; H, 2.69; N, 9.07. Found: C, 32.40; H, 2.96; N, 8.67. ^{1}H NMR data (400 MHz, methylene chloride-d_2; *J*

https://dx.doi.org/10.1021/acs.inorgchem.0c01701
Inorg. Chem. 2020, 59, 12586−12594

values in Hz): δ 8.31 (d, $^3J_{H,H}$ = 2.2, $^3J_{H,Pt}$ = 5.0, 1H, pz), 8.10 (d, $^3J_{H,H}$ = 2.3, $^3J_{H,Pt}$ = 5.6, 1H, pz), 8.04 (d, $^3J_{H,H}$ = 1.7, $^3J_{H,Pt}$ = 10.2, 1H, pz), 7.92 (d, $^3J_{H,H}$ = 2.0, $^3J_{H,Pt}$ = 10.3, 1H, pz), 7.67 (dd, $^3J_{H9,H10}$ = 8.2, $^4J_{H9,H7}$ = 1.6, 1H, H_9), 7.52 (m, $^3J_{H,Pt}$ = 44.0, 1H, H_7 partially overlapped with H_9), 7.51 (m, 1H, H_9 partially overlapped with H_7), 7.48 (d, $^3J_{H,H}$ = 1.6, $^3J_{H,Pt}$ = 40.0, 1H, H_7), 6.98 (d, $^3J_{H3,H2}$ = 2.2, $^4J_{H,Pt}$ = 4.3, 1H, H_2 (Pt-$CHBr_2$)), 6.94 (d, $^3J_{H3,H2}$ = 2.1, 1H, H_2 (Pt−Br)), 6.91−6.81 (m, 2H, H_{10}), 6.43 (t, $^3J_{H,H}$ = 2.1, 1H, $H_{4'}$, pz), 6.40 (t, $^3J_{H,H}$ = 2.2, 1H, $H_{4'}$, pz), 6.35 (d, $^3J_{H3,H2}$ = 2.2, $^4J_{H,Pt}$ = 6.6, 1H, H_3 (Pt-$CHBr_2$)), 6.23 (d, $^3J_{H3,H2}$ = 2.1, $^4J_{H,Pt}$ = 7.2, 1H, H_3, (Pt−Br)), 6.05 (s, $^2J_{Pt,H}$ = 24.2, $^3J_{Pt,H}$ = 6.3, 1H, C*H*Br_2), 4.38−4.22 (m,4H, CH_2, CO_2Et), 3.25 (s, 3H, H_4 (Pt-$CHBr_2$)), 3.12 (s, 3H, H_4 (Pt−Br)), 1.34 (t, 6H, $^3J_{H,H}$ = 7.1, CH_3 (CO_2Et)). $^{13}C\{^1H\}$ NMR plus HMBC and HSQC (101 MHz, methylene chloride-d_2): δ 166.7 and 166.1 (s, 2C, CO_2Et), 152.1 (s, 1C, C_1 (Pt-Br)), 148.7 (s, 1C, C_1 (Pt-$CHBr_2$)), 139.0, 137.4, 135.4, and 133.0 (s, 4C, *C*H, pz), 133.8 (s, 1C, C_7), 132.9 (s, 1C, C_7), 127.8 (s, 1C, C_9), 126.6 (s, 1C, C_9), 123.9 (s, 1C, C_3 (Pt-$CHBr_2$)), 122.8 (s, 1C, C_3 (Pt−Br)), 114.7 (s, 1C, C_2 (Pt-$CHBr_2$)), 114.4 (s, 1C, C_2 (Pt-Br)), 111.6 (s, 1C, C_{10}), 110.7 (s, 1C, C_{10}), 106.1 (m, 2C, $C_{4'}$), 61.6 and 61.3 (s, 2C, CH_2, (CO_2Et)), 37.2 and 37.0 (s, 2C, C_4), 14.7 and 14.6 (s, 2C, CH_3, (CO_2Et)). $^{195}Pt\{^1H\}$ NMR (85.6 MHz, methylene chloride-d_2): δ −2443 (s, $^1J_{Pt,Pt}$ = 1633 Hz, Pt-$CHBr_2$) and −2799 ppm (s, Pt−Br). MS (MALDI+): *m*/*z* 1062.0 [{Pt(EtO_2C-C^C*)(μ-pz)}$_2$Br], 1154.9 [{Pt(EtO_2C-C^C*)(μ-pz)}$_2$$CHBr_2$].

RESULTS AND DISCUSSION

Reactivity of 1 with Haloforms (CHX_3, X = Br, Cl): Synthesis and Characterization of New Metal−Metal-Bonded Pt_2(III,III) Complexes. Compound **1** is thermally stable in $CHCl_3$ solution in the air and in the dark at both room and reflux temperatures and also in refluxing toluene in the presence of $CHCl_3$ (1/4) for at least 7 h. However, the exposure of a solution of **1** (1/9 *syn*/*anti* ratio) in $CHCl_3$ in the air to sunlight leads to its photochemical oxidation, rendering [{Pt(C^C*)(μ-pz)Cl)}$_2$] (**2-Cl**). On the other hand, the reaction of **1** with $CHBr_3$ (1/2.2) at room temperature in the air and sunlight rendered the complex Pt_2(III,III)Br_2 (**2-Br**), but it surprisingly led to the compound [BrPt(C^C*)(μ-pz)$_2$Pt(C^C*)$CHBr_2$] (**3-Br**) in the dark under an argon atmosphere (see Figure 1, Scheme 1, and the Experimental Section).

Scheme 1. Reaction Pathways and Numbering Scheme for NMR Purposes[a]

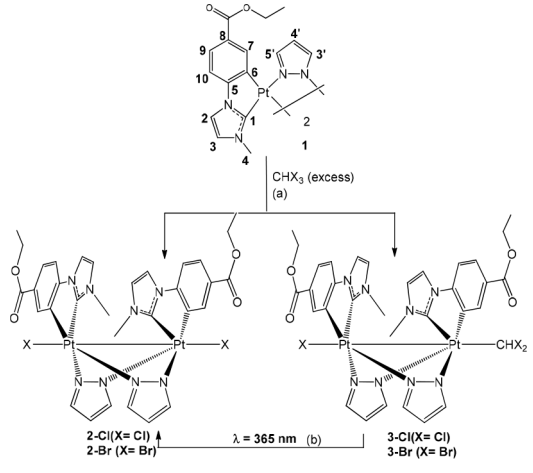

[a]For clarity, only the major isomer (*anti*) has been represented.

Compounds **2-Cl**/**2-Br** and **3-Br** were isolated as yellow (**2-Cl, 3-Br**) or orange (**2-Br**) solids in very good yields mostly as the *anti* isomer and then were fully characterized (see the Experimental Section, Figures 1 and 2, and Figures S1−S15 in the Supporting Information). However, compound **3-Cl** could be identified by ^{1}H and ^{195}Pt NMR from the reaction mixtures performed under an argon atmosphere (see Figures S16 and S17 in the Supporting Information). The higher oxidation state of **2-Cl**/**2-Br** and **3-Cl**/**3-Br** with respect to compound **1** can be inferred from the considerable reductions of the $^3J_{Pt,H7}$ coupling constants from 54 Hz in **1** to ca. 40 Hz[26−28] and from the relevant downfield shifts ($\Delta\delta$(Pt) = 979−1337 ppm) of their ^{195}Pt NMR signals from **1** ($\delta(^{195}Pt)$ = −3778 ppm) (see Figures S17 and S18 in the Supporting Information).[29] Structurally relevant for **3-Cl**/**3-Br** is the presence of two separated ^{195}Pt signals ($^1J_{Pt,Pt}$ = 1633 Hz for **3-Br**), which evidence the existence of two nonequivalent Pt(III) fragments within these complexes (Figures S17 and S18 in the Supporting Information). In addition, the ^{1}H NMR spectra of **3-Cl**/**3-Br** show a singlet corresponding to the Pt-CHX_2 fragment (6.59 ppm, **3-Cl**; 6.05 ppm, **3-Br**), which in the case of **3-Br** displays the expected ^{195}Pt satellite pattern in accord with its dinuclear Pt_2(III,III) formulation ($^2J_{Pt,H}$ = 24.4 Hz, $^3J_{Pt,H}$ = 6.5 Hz) (Figure 1).

These NMR features resembled those observed for [IPt(C^C*)(μ-pz)$_2$Pt(C^C*)CHI_2][25] and [Pt_2(pop)$_4$MeI] ($^1J_{Pt,Pt}$ = 1550 Hz).[30]

The molecular structures of **2-Cl**, **2-Br**, and **3-Br**, determined by single-crystal X-ray crystallography (see Figure 2 and the Supporting Information for a full description) were quite similar to those of [{Pt(C^C*)(μ-pz)I)}$_2$] and [IPt(C^C*)(μ-pz)$_2$Pt(C^C*)CHI_2], respectively.[25] As far as we know, these are the only dinuclear metal−metal-bonded $Pt^{III}(\mu\text{-pz})_2Pt^{III}$ compounds reported to date.

Experimental Data for the Mechanistic Study of the Reactivity of 1 with CHX_3 (X = Cl, Br). The oxidation of **1** with $CHCl_3$ requires light to occur, as is the case for most oxidations of Pt(II) complexes by chlorocarbons.[7,31−33] The reaction mechanism was investigated by reacting **1** (8×10^{-3} M) with $CHCl_3$ (1/5 molar ratio) in acetone-d_6 in NMR tubes under different conditions and following the reactions by ^{1}H NMR spectroscopy (see Scheme 1 and Table 1). Comparative experiments were performed simultaneously to avoid differences in the temperature. Two samples were prepared in the dark under an argon atmosphere, one of them with and the other without galvinoxyl (Gal$^\bullet$), and irradiated with a 365 nm UV lamp (see Figure S20). These experiments showed that Gal$^\bullet$ slows down the reaction and allows the selective formation of the species **2-Cl**, pointing to a radical mechanism, with Gal$^\bullet$ acting as a radical (R$^\bullet$) scavenger.[30,33] The role of O_2 as a radical trap in the reactions performed in the air was confirmed, since an aerated sample rendered **2-Cl** as the only oxidized species (see Figure S21) as well.

Additionally, we observed that in the air the reaction occurs by irradiation with blue LEDs (λ_{max} = 457 nm), but not with green (λ_{max} = 510 nm) or red (λ_{max} = 631 nm) LEDs (see Figure S22), rendering **2-Cl** as the unique Pt_2(III,III) species. In this case the reaction goes more quickly than that under 365 nm UV light (see Table 1, Figure S23, and Table S3 for more details). Moreover, aerated diluted solutions (10^{-5} M) of **1** in acetone-d_6 did not react with $CHCl_3$ under blue LEDs but they did under 365 nm UV light to give **2-Cl** (Figure S24).

https://dx.doi.org/10.1021/acs.inorgchem.0c01701
Inorg. Chem. 2020, 59, 12586−12594

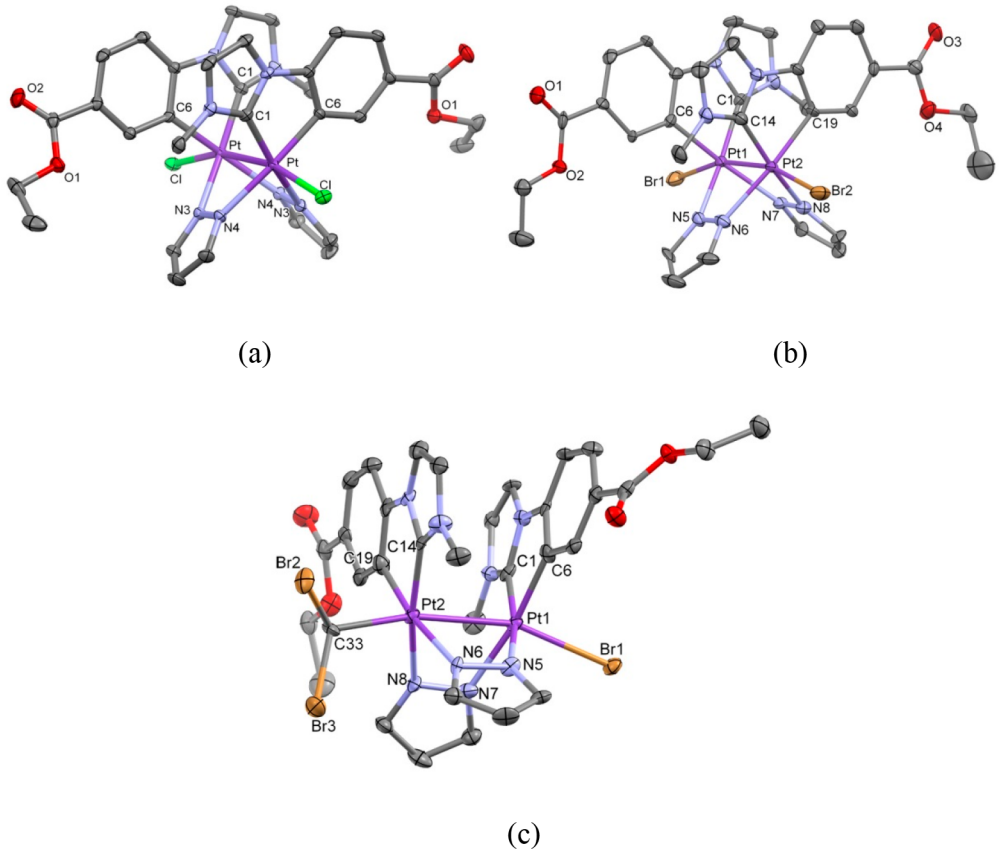

Figure 2. Molecular structures of complexes **2-Cl** (a), **2-Br** (b), and **3-Br** (c). Ellipsoids are drawn at the 50% probability level; solvent molecules and hydrogen atoms have been omitted for clarity. d_{Pt-Pt}: 2.57446(18) Å (**2-Cl**), 2.5849(6) Å (**2-Br**), 2.6302(4) Å (**3-Br**).

Table 1. Data Corresponding to the Reaction of 1 (8×10^{-3} M) with CHX_3 (X = Cl, Br)

$CHCl_3$ ratio (%) **1**/**2-Cl**/**3-Cl**			$CHBr_3$ ratio (%) **1**/**2-Br**/**3-Br**		
15 min	8 h	24 h	15 min	3.5 h	24 h
Ar/λ = 365 nm			Ar/dark		
89/8/3		35/33/32	0/0/100	0/0/100	0/0/100
Ar/λ = 365 nm (Gal*)			Ar/dark (Gal*)		
100/0/ 0		82/18/0	100/0/0	100/0/0	100/0/0
air/λ = 365 nm			air/dark		
83/17/0	34/66/0	0/100/0	86/9/5	81/14/5	74/18/8
air/457 nm blue LEDs			air/sunlight		
80/20/0	8/92/0	0/100/0	0/71/29	0/92/8	0/100/0
air/457 nm blue LEDs/anthracene					
	7/93/0	0/100/0			

On the other hand, the reaction of a concentrated solution of **1** (8×10^{-3} M) with oxygen-free $CHBr_3$ (1/4 molar ratio in acetone-d_6) in the dark under an Ar atmosphere is complete in 15 min, to give selectively **3-Br** (*syn*/*anti* mixture), which remained unchanged under the experimental conditions for at least 24 h. However, in the air, the reaction was less selective than that under Ar, rendering mixtures of **2-Br** and **3-Br** (see Scheme 1, Table 1, and Figure S25). These results pointed as well to a radical pathway for step a (Scheme 1), in which O_2 acts as a radical ($R^{\bullet}$) trap, increasing the amount of **2-Br** in the reaction mixture. In contrast, under the same ambient conditions a diluted solution (10^{-4}–10^{-5} M) of **1** did not react with $CHBr_3$ even after 45 h (Figure S26), while it did under 365 nm UV light (Figure S27) in 45 min to render **2-Br**.

Considering the selective formation of **3-Br** by reaction of **1** with $CHBr_3$ under an Ar atmosphere in the dark and the fast and selective transformation of **1** into **2-Br** when the reaction proceeds in the air and the sunlight (see the Experimental Section and Table 1), we investigated for the first time the role of both light and O_2 in the transformation of **3-Br** into **2-Br** (path b in Scheme 1). With that purpose, we prepared first two reaction experiments containing **3-Br** (obtained from **1** and $CHBr_3$ under argon in the dark) in J. Young NMR tubes. Subsequently, one of the samples was freeze–pump–thaw degassed and placed under an O_2 atmosphere (1 atm). Then, both samples were irradiated with UV light (λ = 365 nm) for 5 min, rendering **2-Br**/**3-Br** mixtures in different ratios (28%/72% in the oxygen-free sample and 64%/36% in the oxygen-containing sample) (Figure S28). When it is kept in mind that under Ar in the dark compound **3-Br** remained unchanged for at least 24 h, the selective transformation of **3-Br** into **2-Br** is clearly promoted by UV light with O_2 not being required but making the process faster. In a thorough analysis of the ^{1}H NMR spectra, it was possible to identify a singlet at 6.66 ppm in the oxygen-free sample corresponding to 1,1,2,2-tetrabromoethane ($C_2H_2Br_4$) generated by R–R coupling (Figure S28). To prove the radical mechanism of path b, two samples containing **3-Br** (obtained from **1** and $CHBr_3$, 1/4 molar ratio, under argon in the dark) were prepared and then Gal$^{\bullet}$ was added to one of them. After irradiation with a 365 nm UV light just the Gal$^{\bullet}$-free sample showed the signal corresponding to 1,1,2,2-tetrabromoethane ($C_2H_2Br_4$) (Figure S29) and a faster transformation of **3-Br** into **2-Br**. Therefore, under an Ar atmosphere, the photochemical bond homolysis of the Pt–C

https://dx.doi.org/10.1021/acs.inorgchem.0c01701
Inorg. Chem. 2020, 59, 12586–12594

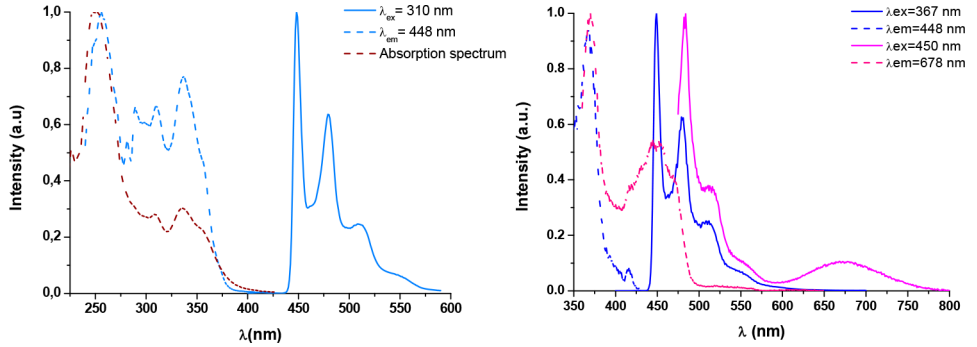

Figure 3. (left) Absorption spectrum (garnet dotted plot) of **1** in 2-MeTHF (10^{-4} M) at rt and the excitation (sky-blue dotted plot) and emission (blue solid plot) spectra of **1** in 2-MeTHF (under Ar, 10^{-5} M) at 77 K. (right) Excitation (dotted plots) and emission (solid plots) spectra of **1** in 2-MeTHF (10^{-3} M) under Ar at 77 K.

($CHBr_2$) bond in **3-Br** promoted by UV irradiation[34] followed by Br abstraction from $CHBr_3$ could account for the selective formation of **2-Br**.

To shed light on the concentration-dependent reactivity of **1** with CHX_3 (X = Cl, Br), we recorded the excitation and emission spectra for diluted (10^{-5} M) and concentrated (10^{-3} M) solutions of **1** in 2-MeTHF and explained them on the basis of theoretical calculations, as can be seen in the following.

Emission Spectra and Theoretical Calculations on Complex 1. The excitation and emission spectra of diluted (10^{-5} M) and concentrated (10^{-3} M) solutions of **1** in 2-MeTHF under an Ar atmosphere at 77 K can be seen in Figure 3. For a diluted solution of **1** (see Figure 3, left) just one excited state at high energy (S_{1s}, λ_{max} = 355 nm, tail to 380 nm; T_{1s}, λ_{max} = 450 nm) is perceptible, which can be reached by irradiation with a 365 nm UV light. In a concentrated solution of **1** (see Figure 3, right), an additional excited state at low energy appears (S_{1f}, λ_{max} = 450 nm; T_{1f}, λ_{max} = 678 nm) by irradiation in the range 450−470 nm.

In view of the experimental results and taking into account the different Pt···Pt distances observed for complex **1** (three independent molecules in the asymmetric unit with Pt−Pt separations of 3.1210(3), 3.2294(4), and 3.2834(4) Å were found in a single-crystal X-ray diffraction study of **1**)[25] we studied the potential energy surface (PES) of the S_0 model complex **1**-DFT in acetone solution as a function of the Pt−Pt distance. Interestingly we found two stationary points (see Figure 4), characterized as local minima showing quite different geometries: a butterfly-spreading structure, **1-s**, and a butterfly-folding structure, **1-f** (Figure 4). **1-s** shows a long Pt−Pt distance of 3.212 Å and long intramolecular C−C distances between the C^C* groups in the wings ($d \geq 4.83$ Å). Conversely, **1-f** shows a short Pt−Pt distance of 2.98 Å and short intramolecular C−C contacts between the C^C* groups in the wings (3.624−3.843 Å). Both structures are very close in energy in the PES ($\Delta G°$ = 1.7 kcal/mol). Furthermore, we have located a transition state, connecting both structures, with one negative frequency associated with the butterfly-spreading, butterfly-folding intramolecular dynamics. The transition state connecting both minima presents intermediate parameters, with a Pt−Pt distance of 3.012 Å and long intramolecular C−C contacts between the C^C* groups ($d \geq 3.93$ Å), and lies only 1.9 kcal/mol above **1-s** and 0.2 kcal/mol above **1-f**. These very low barriers support a fast thermally induced structural change in the ground state, likely through a dynamics resembling an intramolecular butterfly flapping, and are fully consistent with the presence of both conformations of **1** in acetone solution.

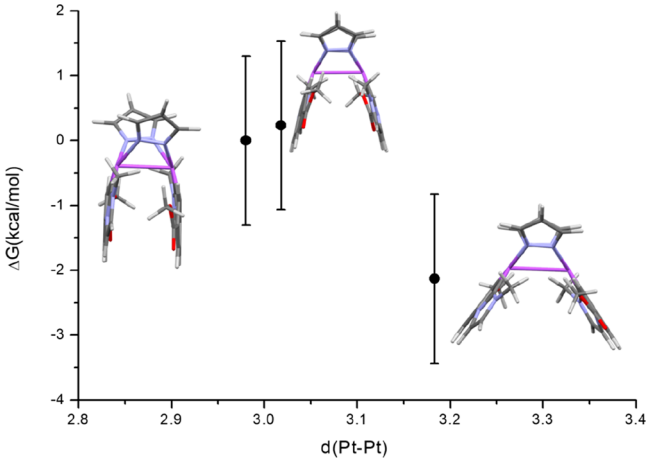

Figure 4. Calculated energy profile for the butterfly-spreading−butterfly-folding structures (**1-s** and **1-f**) interconversion of the S_0 state of the dinuclear complex **1-DFT** in acetone, including the transition state (Ts). MUE (M06) = 2.48 kcal/mol.[35]

The calculated S_{1s} value (367 nm) of the butterfly wing-spreading structure **1-s** mostly corresponds to the HOMO−LUMO transition (93%) at the S_0 geometry (see Tables S4 and S5 and Figure S30). In view of the population analysis (%) of the frontier molecular orbitals (FMOs), S_{1s} is ^{1}LC/^{1}MLCT in nature. We also optimized the lowest triplet state of **1-s** (T_{1s}) in acetone solution (see Figure 5). It showed a Pt−Pt distance (3.178 Å) and a Pt−Pt bond order (0.11) quite similar to those (3.212 Å, 0.10) in the ground state (S_{0s}). Furthermore, both the spin density distribution (see Figure 5) and the calculated energy ($\Delta E_{T1s-S0s}$ = 2.738 eV, 453 nm) for T_{1s} support its ^{3}IL/^{3}MLCT nature, indicating **1-s** molecules are responsible for the high-energy absorption/emission (S_{1s}, λ_{max} = 355 nm, tail to 380 nm; T_{1s}, λ_{max} = 450 nm) bands observed for solutions of **1** in 2-MeTHF.

In addition, we optimized the ground (S_{0f}) and the lowest triplet (T_{1f}) states of the butterfly wing-folded structure, **1-f**, in acetone solution (see Figure 5 and the Supporting Information). Unlike T_{1s}, T_{1f} showed a Pt−Pt distance of 2.746 Å, clearly shorter than that in the ground state S_{0f}, 2.98 Å, in agreement with the increased bonding character between the metal centers (BO = 0.62 (T_{1f}), 0.22 (S_{0f})). These two parameters and the spin density distribution calculated for T_{1f} (Figure 5) are in accordance with a mainly $^{1/3}$MMLCT ($d\sigma^*$(Pt−Pt) → π^*(C^C*)) nature of the lower energy excited states of species **1-f** (see Tables S4 and S5, Figure 5,

https://dx.doi.org/10.1021/acs.inorgchem.0c01701
Inorg. Chem. 2020, 59, 12586−12594

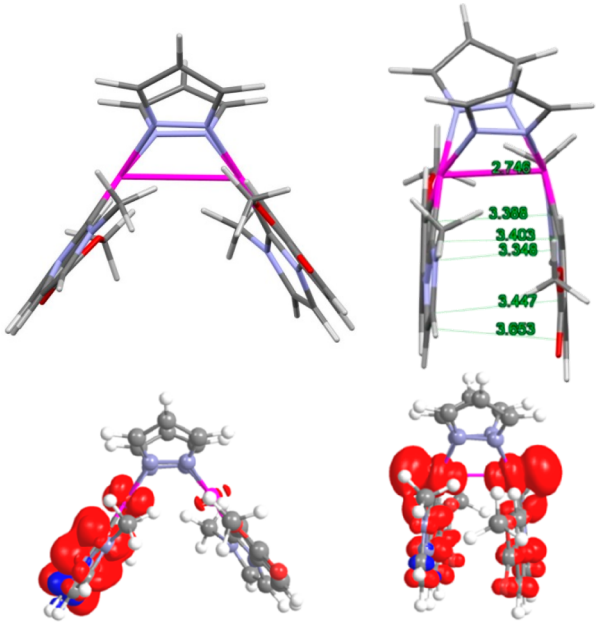

Figure 5. (top) Calculated structures in acetone solutions of T_{1s} (left) and T_{1f} (right): (bottom) Spin density distribution for T_{1s} (left) and T_{1f} (right).

and Figure S30). This is due to the interactions through the d_{z^2} orbital of the two platinum atoms located in close proximity and will be somehow affected by the intramolecular $\pi-\pi$ interactions. These results agree with the $^{1/3}$MMLCT excited states of **1-f** to be the origin of the low-energy excitation (λ_{max} = 450 nm) and emission (λ_{max} = 678 nm) bands observed for concentrated solutions of **1** in 2-MeTHF.

The possibility of low-lying excited states due to intermolecular $\pi-\pi$ interactions was ruled out, since the low-energy excitation and emission bands of **1** in concentrated (10^{-3} M) solutions (Figure S31, bottom) differ from those in the solid state, where extensive intermolecular $\pi-\pi$ interactions are expected (see the X-ray molecular packing of **1** in Figure S31, top). Thus, it leads us to consider the low-energy excitation and emission bands observed for concentrated (10^{-3} M) solutions of **1** are most likely due to the $^{1/3}$MMLCT excited states of **1-f** rather than to aggregates. The coexistence of molecules with short and long intramolecular Pt−Pt distances was proposed by Thompson to explain the EL for devices using [{Pt(C^N)(μ-pz)}$_2$] (C^N = 2-(4′,6′-difluorophenyl)pyridinato-*N*,$C^{2'}$, pz = pyrazolate) as the dopant in high concentration (70 wt %) or as a neat film.[17]

Then, our excitation/emission spectra and theoretical calculations pointed to the existence of both kinds of molecules, **1-s** and **1-f**, in acetone solutions. However, the ΔG value ($\Delta G_{1\text{-}f} - \Delta G_{1\text{-}s}$ = 1.7 kcal/mol) for the **1-s** ↔ **1-f** transformation predicts a **1-f** ratio of 6% at 298 K, being much lower as the temperature is decreased.[36] At 77 K the **1-f** ratio seems to be as low, as in diluted solutions of **1** the low-energy emission of **1-f** is undetectable but can be detected in more concentrated solutions (Figure 3).

In addition, considering the [2c, 2e] oxidation of the butterfly Pt_2(II,II) complexes [{Pt(C^N)(μ-pz)}$_2$], by haloforms (CHX_3, X = Cl, Br, I) had been never described, we performed the NBO charge distributions analysis on both the compound [{Pt(C^C*)(μ-pz)}$_2$] (**1**) and the analogous [{Pt(C^N)(μ-pz)}$_2$] (C^N = 2-phenylpyridinate) at the DFT/M06/SDD/6-31G* level of theory in acetone solution. These calculations showed the atomic charges on the platinum centers of **1** to be +0.273 (**1-f**) and +0.288 (**1-s**) while those on the platinum centers of [{Pt(C^N)(μ-pz)}$_2$] are +0.407. The lower value observed in the C^C* derivative is attributable to the greater donor ability of C^C* with respect to C^N[37] and could contribute to the easier oxidation of this butterfly compound, **1**.

Discussion of the Reactivity of 1 with CHX_3 (X = Cl, Br). The results showed above indicated that diluted solutions of **1** (10^{-5}, 10^{-4} M) react with CHX_3 (X = Cl, Br) under 365 nm UV light, but at higher concentrations of **1** (8×10^{-3} M) in acetone, the reaction can be initiated by heat (X = Br) or blue light (X = Cl, $\lambda_{exc} \approx$ 460 nm), following a radical process (path a in Scheme 1) to render species **2**, **3**, or a mixture of both, depending on the ambient conditions. In addition, under UV light species **3** convertd into **2** following a radical pathway (path b in Scheme 1) as well, which explains how in ambient light **1** converts completely into **2-Cl**/**2-Br** in the presence of excess CHX_3 (X = Cl, Br).

Since the reaction of **1** with $CHCl_3$ is driven by 365 nm UV light ([**1**] = 10^{-5} M) or blue light ([**1**] = 8×10^{-3} M), a haloform-initiated radical pathway[38] can be excluded. Instead, the reaction should be initiated by platinum-based excited species, generated by irradiation of complex **1**. Thus, under the experimental conditions, when a concentrated sample of **1** (8×10^{-3} M solution in acetone-d_6) was irradiated with blue LEDs (λ_{max} = 457 nm) the ^{1}MMLCT of species **1-f** (S_{1f}) was reached (Scheme 2) and then the ^{1}MMLCT or ^{3}MMLCT

Scheme 2. Schematic Diagram of Energy Levels for the Ground and Excited States: Photophysical Processes Based on the Steady-State Excitation and Emission Spectra along with Theoretical Calculations

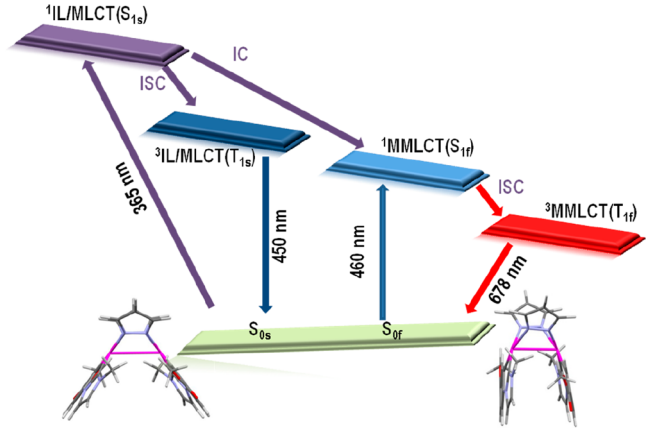

(reached by an ISC process) excited states would likely initiate the fast reaction with $CHCl_3$. To discern between the singlet/triplet nature of the reactive [**1-f**]* species, we used anthracene as a quencher of the triplet excited states (E_S < 350 nm, E_T = 681 nm).[39] For that, two samples (8×10^{-3} M **1** and $CHCl_3$, 1/5) were prepared in the air under blue LEDs, one of them with and the other one without anthracene (0.08 M).

In both samples, the exciting light (λ_{max} = 457 nm) must be completely absorbed by complex **1**. By ^{1}H NMR we observed that after 2, 6, and 8 h the unreacted amounts of **1** were ca. 51%, 16%, and 8%, respectively, in both samples, with no visible differences between them (Table 1 and Table S3). On

https://dx.doi.org/10.1021/acs.inorgchem.0c01701
Inorg. Chem. 2020, 59, 12586−12594

Scheme 3. Comparative DFT-Calculated Pathways and Energy Barriers (ΔG, kcal/mol) for the Thermal Conversion of 1 (S_{0s}) into 2-Cl/Br and 3-Cl/Br following a S_N2 (i) or a Radical Mechanism (ii)[a]

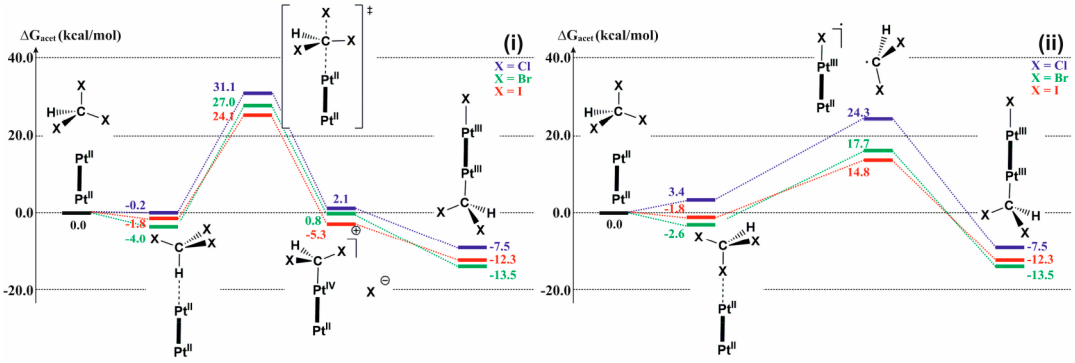

[a]The values corresponding to the reaction of **1** with CHI_3 have been included for an overall picture of these reactions. MUE (M06) = 2.48 kcal/mol.

the other hand, we observed that the presence of anthracene quenches the ^{3}MMLCT phosphorescence of **1** upon excitation at 460 nm (Figure S32). Since anthracene quenches the ^{3}MMLCT phosphorescence of **1** but not its photoreaction with $CHCl_3$, ^{1}[**1-f**]* species, ^{1}MMLCT in nature, seems to be the reactive species (Scheme 2). These results agree with the observed effect of O_2 (E_{T1} = 1192 nm, E_{T2} = 773 nm) quenching the phosphorescence of **1** (see Figure S33) upon excitation at 400 nm but not the photoreaction with $CHCl_3$ (see Table 1 and Scheme 1). Thus, under blue light, the species ^{1}[**1-f**]* would interact with $CHCl_3$, undergoing dissociation into $Pt_2Cl^{\bullet}$ and $CHCl_2^{\bullet}$, as the first step of the radical reaction.

At high concentration (8×10^{-3} M) in acetone under a 365 nm UV light the photooxidation rate of **1** is lower than that under blue light. In this case, irradiation will lead to the high-energy ^{1}IL/MLCT excited state. Then, by ISC or IC the ^{1}IL/MLCT state can populate the ^{3}IL/MLCT or ^{1}MMLCT excited state, respectively, since the last two lie very close in energy (Scheme 2). If ^{1}MMLCT corresponding to **1-f** species are those that induce the reaction and are just partially populated, this would account for the slower oxidation observed under 365 nm UV light (see Scheme 2) with respect to the blue-light-driven reaction.

On the other hand, the thermal oxidation of **1** with $CHBr_3$ takes place in a concentrated solution of **1** (8×10^{-3} M) in acetone but not in diluted solution (10^{-4} M) even after 45 h, presumably because in concentrated solutions of **1** the MMLCT-based species [**1-f**] will initiate a thermal radical process, while the almost negligible presence of such species in diluted solutions slows down the thermal reaction dramatically, in such a way that after 45 h no reaction was observed.

Theoretical calculations confirmed that a radical pathway through the homolytic breakage of the Br−C bond in a S_0 [Pt−Pt−BrCHBr$_2$] adduct is clearly the most favored option, among the proposed ones, for the thermal oxidation of **1** (see Scheme S1, path *ii*, and Scheme 3).

Furthermore, the concomitant generation of $Pt_2Br^{\bullet}$ and $^{\bullet}CHBr_2$ ($R^{\bullet}$) radicals is consistent with the simultaneous formation of Pt_2Br_2 (**2-Br**) and Pt_2Br ($CHBr_2$) (**3-Br**) species (eqs 1−4). The role of O_2 as a radical ($R^{\bullet}$) trap can justify the greater amount of **2-Br** in the reaction mixture when the reaction is performed in the air with respect to that performed under an argon atmosphere.

$$Pt_2 + RBr \rightarrow Pt_2Br^{\bullet} + R^{\bullet} \quad (1)$$

$$Pt_2 + R^{\bullet} \rightarrow Pt_2R^{\bullet} \quad (2)$$

$$Pt_2Br^{\bullet} + RBr \rightarrow Pt_2Br_2 + R^{\bullet} \quad (3)$$

$$Pt_2R^{\bullet} + RBr \rightarrow Pt_2RBr + R^{\bullet} \quad (4)$$

DFT calculations show a gradation for the X transfer process (Scheme 3ii), which is increasingly favored with the heavier haloforms. Whereas the calculated barrier for the reaction with CHI_3 supports an easy process happening under a wide diversity of conditions, the barrier for the reaction with $CHBr_3$ seems high enough as to be sensitive to other kinetic factors such as the concentration of reagents, in good agreement with experimentally observed trends. Finally, the reaction with chloroform shows the highest barrier and experimentally does not occur under thermal conditions. In this case, the S_{1f} species, reached by irradiation, will trigger the photooxidation of **1** with $CHCl_3$ to give Pt_2(III,III) complexes following a radical mechanism.

CONCLUSION

This paper shows the [2c, 2e] oxidation of the butterfly complex [{Pt(C^C*)(μ-pz)}$_2$] (**1**) by CHX_3 (X = Cl, Br) in acetone solution, which under controlled ambient conditions leads to the selective synthesis of the compounds [{Pt(C^C*)(μ-pz)X}$_2$] (X = Cl (**2-Cl**), Br (**2-Br**)) and [Pt_2(C^C*)$_2$(μ-pz)$_2$Br(CHBr$_2$)] (**3-Br**). Together with the analogous iodo derivatives [{Pt(C^C*)(μ-pz)I)}$_2$] and [IPt(C^C*)(μ-pz)$_2$Pt(C^C*)CHI$_2$], they are the only dinuclear metal−metal-bonded $Pt^{III}(\mu\text{-pz})_2Pt^{III}$ compounds reported to date.

The oxidation of **1** by CHX_3 (X = Cl, Br) under UV light takes place in either diluted (10^{-5} M) or concentrated (8×10^{-3} M) solutions of **1** in acetone to give compounds **2-Cl**/**2-Br**. However, in concentrated solutions the oxidation of **1** is possible in the dark ($CHBr_3$) or under blue-light ($CHCl_3$) irradiation. Our theoretical results show the existence of two minima in the PES of the ground state (S_0) of the model **1**-DFT in acetone solution: the butterfly wing-spreading molecules **1-s** and the wing-folding molecules **1-f**. They are very close in energy (ΔG° = 1.7 kcal/mol) and are connected through a low barrier transition state (TS), which supports a fast interconversion process resembling an intramolecular butterfly flapping and the presence of both kinds of molecules

https://dx.doi.org/10.1021/acs.inorgchem.0c01701
Inorg. Chem. 2020, 59, 12586−12594

in acetone solution. The experimental results point to a radical mechanism, with the MMLCT-based **1-f** species being those which trigger the heat- or blue-light-driven photooxidation of **1** with $CHBr_3$ and $CHCl_3$, respectively. The C^C* basicity and the cooperative effects between the two adjacent metal centers located in close proximity in the **1-f** species appear to be crucial in promoting the homolytic C−X (X = Cl, Br) bond breaking, which constitutes the first step of the radical mechanism of the oxidation of **1** by CHX_3 (X = Cl, Br).

■ ASSOCIATED CONTENT

Supporting Information

The Supporting Information is available free of charge at https://pubs.acs.org/doi/10.1021/acs.inorgchem.0c01701.

Experimental details of the general procedures and instrumentation, crystallographic data, and computational methods, NMR spectra for characterization and mechanistic studies, single-crystal X-ray structures and description, emission spectra and theoretical calculations, and additional figures as described in the text (PDF)

Accession Codes

CCDC 1985166−1985168 contain the supplementary crystallographic data for this paper. These data can be obtained free of charge via www.ccdc.cam.ac.uk/data_request/cif, or by emailing data_request@ccdc.cam.ac.uk, or by contacting The Cambridge Crystallographic Data Centre, 12 Union Road, Cambridge CB2 1EZ, UK; fax: +44 1223 336033.

■ AUTHOR INFORMATION

Corresponding Authors

Violeta Sicilia − *Departamento de Química Inorgánica, Escuela de Ingeniería y Arquitectura de Zaragoza, Instituto de Síntesis Química y Catálisis Homogénea (ISQCH), CSIC-Universidad de Zaragoza, 50018 Zaragoza, Spain;* orcid.org/0000-0002-0257-0483; Email: sicilia@unizar.es

Sara Fuertes − *Departamento de Química Inorgánica, Facultad de Ciencias, Instituto de Síntesis Química y Catálisis Homogénea (ISQCH), CSIC-Universidad de Zaragoza, 50009 Zaragoza, Spain;* orcid.org/0000-0003-1812-3175; Email: sfuertes@unizar.es

Authors

Lorenzo Arnal − *Departamento de Química Inorgánica, Facultad de Ciencias, Instituto de Síntesis Química y Catálisis Homogénea (ISQCH), CSIC-Universidad de Zaragoza, 50009 Zaragoza, Spain;* orcid.org/0000-0002-0283-9307

Antonio Martín − *Departamento de Química Inorgánica, Facultad de Ciencias, Instituto de Síntesis Química y Catálisis Homogénea (ISQCH), CSIC-Universidad de Zaragoza, 50009 Zaragoza, Spain;* orcid.org/0000-0002-4808-574X

Miguel Baya − *Departamento de Química Inorgánica, Facultad de Ciencias, Instituto de Síntesis Química y Catálisis Homogénea (ISQCH), CSIC-Universidad de Zaragoza, 50009 Zaragoza, Spain;* orcid.org/0000-0002-2492-625X

Complete contact information is available at: https://pubs.acs.org/10.1021/acs.inorgchem.0c01701

Notes

The authors declare no competing financial interest.

■ ACKNOWLEDGMENTS

This work was supported by the Spanish Ministerio de Economía y Competitividad (Ministerio de Ciencia Innovación y Universidades)/FEDER (Project PGC2018-094749-B-I00), the Gobierno de Aragón (Grupo E17_20R: Química Inorgánica y de los Compuestos Organometálicos), and FEDER 2014-2020 (Construyendo Europa desde Aragón). The authors thank the Instituto de Biocomputación y Física de Sistemas Complejos (BIFI) and Centro de Supercomputación de Galicia (CESGA) for generous allocation of computational resources. The authors thank Dr. M. V. Collados, at the University of Zaragoza for spectra of the LEDs used in this work and Prof. Daniel Escudero at the KU Leuven for its guidance with theoretical calculations. L.A. acknowledges the support of a grant from the Gobierno de Aragón. S.F. thanks the Spanish National Research Council for Grant No. 2018801070-PIE-147.

■ REFERENCES

(1) Powers, I. G.; Uyeda, C. Metal−Metal Bonds in Catalysis. *ACS Catal.* **2017**, *7*, 936−958.

(2) Powers, D. C.; Ritter, T. Bimetallic Pd(III) Complexes in Palladium-Catalysed Carbon−Heteroatom Bond Formation. *Nat. Chem.* **2009**, *1*, 302−309.

(3) Powers, D. C.; Ritter, T. Bimetallic Redox Synergy in Oxidative Palladium Catalysis. *Acc. Chem. Res.* **2012**, *45*, 840−850.

(4) Fernando, R. G.; Gasery, C. D.; Moulis, M. D.; Stanley, G. G. *Homo- and Heterobimetallic Complexes in Catalysis:Cooperative Catalysis*; Springer International: Cham, Switzerland, 2016; pp 1−29.

(5) Che, C.-M.; Schaefer, W. P.; Gray, H. B.; Dickson, M. K.; Stein, P. B.; Roundhill, D. M. Novel Binuclear Platinum(III) Octaphosphite Complexes. *J. Am. Chem. Soc.* **1982**, *104*, 4253−4255.

(6) Roundhill, D. M.; Gray, H. B.; Che, C.-M. Pyrophosphito-bridged Diplatinum Chemistry. *Acc. Chem. Res.* **1989**, *22*, 55−61.

(7) Sicilia, V.; Baya, M.; Borja, P.; Martín, A. Oxidation of Half-Lantern Pt_2(II,II) Compounds by Halocarbons. Evidence of Dioxygen Insertion into a Pt(III)-CH_3 Bond. *Inorg. Chem.* **2015**, *54*, 7316−7324.

(8) Tejel, C.; Ciriano, M. A.; Edwards, A. J.; Lahoz, F. J.; Oro, L. A. Metal Basicity of Dirhodium and Diiridium Complexes Induced by Isocyanide Ligands. Model for the Oxidative-Addition reaction of Methyl Iodide with Dinuclear Complexes. *Organometallics* **1997**, *16*, 45−53 and references therein..

(9) Sakai, K.; Sato, T.; Tsubomura, T.; Matsumoto, K. Di-(m-pyrazolato-N:N')-bis[(2,2′-bipyridineN,N')platinum(II)] Bis-(tetrafluoroborate) Monohydrate. *Acta Crystallogr., Sect. C: Cryst. Struct. Commun.* **1996**, *C52*, 783−786.

(10) Umakoshi, K.; Kimura, K.; Kim, Y. H.; Tsukimoto, Y.; Arikawa, Y.; Onishi, M.; Ishizaka, S.; Kitamura, N. Pyrazolato- and 3,5-Dimethylpyrazolato-Bridged Dinuclear Platinum(II), Palladium(II), and Their Mixed-Metal Complexes of 2,2′-Bipyrimidine. Syntheses, Structures, and Luminescent Properties. *Bull. Chem. Soc. Jpn.* **2010**, *83*, 1504−1510.

(11) Ghavale, N.; Wadawale, A.; Dey, S.; Jain, V. K. Synthesis, Structures and Spectroscopic Properties of Platinum Complexes Containing Orthometalated 2-phenylpyridine. *J. Organomet. Chem.* **2010**, *695*, 1237−1245.

(12) Lai, S.-W.; Chan, M. C. W.; Cheung, K.-K.; Peng, S.-M.; Che, C.-M. Synthesis of Organoplatinum Oligomers by Employing N-Donor Bridges with Predesigned Geometry: Structural and Photophysical Properties of Luminescent Cyclometalated Platinum(II) Macrocycles. *Organometallics* **1999**, *18*, 3991−3997.

(13) Sun, Q.-F.; Wong, K. M.-C.; Liu, L.-X.; Huang, H.-P.; Yu, S.-Y.; Yam, V. W.-W.; Li, Y.-Z.; Pan, Y.-J.; Yu, K.-C. Self-Assembly, Structures, and Photophysical Properties of 4,4′-Bipyrazolate-Linked Metallo-Macrocycles with Dimetal Clips. *Inorg. Chem.* **2008**, *47*, 2142−2154.

(14) Chang, S.-Y.; Chen, J.-L.; Chi, Y.; Cheng, Y.-M.; Lee, G.-H.; Jiang, C.-M.; Chou, P.-T. Blue-Emitting Platinum(II) Complexes Bearing both Pyridylpyrazolate Chelate and Bridging Pyrazolate Ligands: Synthesis, Structures, and Photophysical Properties. *Inorg. Chem.* **2007**, *46*, 11202−11212.
(15) Moon, S.; Horiuchi, S.; Sakuda, E.; Ito, A.; Arikawa, y.; Umakoshi, K. Synthesis and Photophysical Properties of Butterfly-Shaped Dinuclear Pt(II) Complex Having NHC-based Chelate Ligands. *Inorg. Chim. Acta* **2019**, *493*, 43−48.
(16) Ma, B.; Li, J.; Djurovich, P. I.; Yousufuddin, M.; Bau, R.; Thompson, M. E. Synthetic Control of Pt···Pt Separation and Photophysics of Binuclear Platinum Complexes. *J. Am. Chem. Soc.* **2005**, *127*, 28−29.
(17) Ma, B. W.; Djurovich, P. I.; Garon, S.; Alleyne, B.; Thompson, M. E. Platinum Binuclear Complexes as Phosphorescent Dopants for Monochromatic and White Organic Light-Emitting Diodes. *Adv. Funct. Mater.* **2006**, *16*, 2438−2446.
(18) Chakraborty, A.; Deaton, J. C.; Haefele, A.; Castellano, F. N. Charge-Transfer and Ligand-Localized Photophysics in Luminescent Cyclometalated Pyrazolate-Bridged Dinuclear Platinum(II) Complexes. *Organometallics* **2013**, *32*, 3819−3829.
(19) Brown-Xu, S. E.; Kelley, M. S. J.; Fransted, K. A.; Chalcraborty, A.; Schatz, G. C.; Castellano, F. N.; Chen, L. X. Tunable Excited-State Properties and Dynamics as a Function of Pt-Pt Distance in Pyrazolate-Bridged Pt(II) Dimers. *J. Phys. Chem. A* **2016**, *120*, 543−550.
(20) Han, M. G.; Tian, Y.; Yuan, Z.; Zhu, L.; Ma, B. W. A Phosphorescent Molecular "Butterfly" that undergoes a Photoinduced Structural Change allowing Temperature Sensing and White Emission. *Angew. Chem., Int. Ed.* **2014**, *53*, 10908−10912.
(21) Zhou, C.; Tian, Y.; Yuan, Z.; Han, M.; Wang, J.; Zhu, L.; Tameh, M. S.; Huang, C.; Ma, B. Precise Design of Phosphorescent Molecular Butterflies with Tunable Photoinduced Structural Change and dual Emission. *Angew. Chem., Int. Ed.* **2015**, *54*, 9591−9595.
(22) Zhou, C. K.; Yuan, L.; Yuan, Z.; Doyle, N. K.; Dilbeck, T.; Bahadur, D.; Ramakrishnan, S.; Dearden, A.; Huang, C.; Ma, B. W. Phosphorescent Molecular Butterflies with Controlled Potential-Energy Surfaces and Their Application as Luminescent Viscosity Sensor. *Inorg. Chem.* **2016**, *55*, 8564−8569.
(23) Saito, K.; Nakao, Y.; Sakaki, S. Theoretical Study of Pyrazolate-Bridged Dinuclear Platinum(II) Complexes: Interesting Potential Energy Curve of the Lowest Energy Triplet Excited State and Phosphorescence Spectra. *Inorg. Chem.* **2008**, *47*, 4329−4337.
(24) Pinter, P.; Unger, Y.; Strassner, T. Cyclometalated N-Heterocyclic Carbene Platinum(II) Complexes with Bridging Pyrazolates: Enhanced Photophysical Properties of Binuclear Blue Emitters. *Chemphotochem* **2017**, *1*, 113−115.
(25) Arnal, L.; Fuertes, S.; Martín, A.; Baya, M.; Sicilia, V. A Cyclometalated N-Heterocyclic Carbene: The Wings of the First Pt_2(II,II) Butterfly Oxidized by CHI_3. *Chem. - Eur. J.* **2018**, *24*, 18743−18748.
(26) Nabavizadeh, S. M.; Sepehrpour, H.; Kia, R.; Rheingold, A. L. Bis(diphenylphosphino)acetylene as Bifunctional Ligand in Cycloplatinated Complexes: Synthesis, Characterization, Crystal Structures and Mechanism of MeI Oxidative Addition. *J. Organomet. Chem.* **2013**, *745*−*746*, 148−157.
(27) Nabavizadeh, S. M.; Aseman, M. D.; Ghaffari, B.; Rashidi, M.; Hosseini, F. N.; Azimi, G. Kinetics and Mechanism of Oxidative Addition of MeI to Binuclear Cycloplatinated Complexes Containing Biphosphine Bridges: Effects of ligands. *J. Organomet. Chem.* **2012**, *715*, 73−81.
(28) Jamali, S.; Nabavizadeh, S. M.; Rashidi, M. Binuclear Cyclometalated Organoplatinum Complexes Containing 1,1′-Bis-(diphenylphosphino)ferrocene as Spacer Ligand: Kinetics and Mechanism of MeI Oxidative Addition. *Inorg. Chem.* **2008**, *47*, 5441−5452.
(29) Pregosin, P. S. Platinum-195 nuclear magnetic resonance. *Coord. Chem. Rev.* **1982**, *44*, 247−291.
(30) Roundhill, D. M.; Dickson, M. K.; Atherton, S. J. Thermal and photochemical addition of alkyl and aryl halides to tetrakis(μ-pyrophosphito) diplatinum(II) tetraanion. *J. Organomet. Chem.* **1987**, *335*, 413−422.
(31) Ciriano, M. A.; Pérez-Torrente, J. J.; Oro, L. A. Synthesis and reactivity of binuclear 7-azaindolate complexes of iridium: II. Oxidative-addition reactions of halogens and halocarbons to $[\{Ir(\mu\text{-aza})(CO)_2\}_2]$. *J. Organomet. Chem.* **1993**, *445*, 273−281.
(32) Caspar, J. V.; Gray, H. B. Photoinduced oxidative addition chemistry of bis(1,5-cyclooctadiene)bis(μ -pyrazolyl)diiridium(I). *J. Am. Chem. Soc.* **1984**, *106*, 3029−3030.
(33) Vogler, A.; Kunkely, h. Photooxidation of 1,2-dithiolene Complexes of Nickel, Palladium and Platinum in Chloroform. *Inorg. Chem.* **1982**, *21*, 1172−1175.
(34) van Slageren, J.; Klein, A.; Zalis, S. Ligand-to-ligand charge transfer states and photochemical bond homolysis in metal-carbon bonded platinum complexes. *Coord. Chem. Rev.* **2002**, *230*, 193−211.
(35) Wang, Y.; Verma, P.; Jin, X.; Truhlar, D. G.; He, X. Revised M06 Density Functional for Main-Group and Transition-Metal Chemistry. *Proc. Natl. Acad. Sci. U. S. A.* **2018**, *115*, 10257−10262.
(36) From the expression $\Delta G^{\circ}/-RT = \ln[\mathbf{1\text{-}f}]/[\mathbf{1\text{-}s}]$, it can be deduced that as the temperature is decreased [**1-f**] decreases as well.
(37) Fuertes, S.; Chueca, A. J.; Martín, A.; Sicilia, V. New NHC Cycloplatinated Compounds. Significance of the cyclometalated Group on the Electronic and emitting Properties of Biscyanide Compounds. *J. Organomet. Chem.* **2019**, *889*, 53−61.
(38) Hoggard, P. E.; Vogler, A. The photooxidation of tetrachloroplatinate(II) in chloroform. *Inorg. Chim. Acta* **2003**, *348*, 229−232.
(39) Sandrini, D.; Maestri, M.; Balzani, V.; Chassot, L.; von Zelewsky, A. Photochemistry of the Orthometalated cis-Bis-[2-(2-thienyl)pyridine]platinum(II) Complex in halocarbon Solvents. *J. Am. Chem. Soc.* **1987**, *109*, 7720−7724.

https://dx.doi.org/10.1021/acs.inorgchem.0c01701
Inorg. Chem. 2020, 59, 12586−12594

Inorganic Chemistry

pubs.acs.org/IC

Article

High-Valent Pyrazolate-Bridged Platinum Complexes: A Joint Experimental and Theoretical Study

Lorenzo Arnal, Daniel Escudero,* Sara Fuertes,* Antonio Martin, and Violeta Sicilia*

Cite This: *Inorg. Chem.* 2022, 61, 12559−12569

Read Online

ACCESS | Metrics & More | Article Recommendations | Supporting Information

ABSTRACT: Complexes $[\{Pt(C\hat{}C^*)(\mu\text{-pz})\}_2]$ ($HC\hat{}C^*_A$ = 1-(4-(ethoxycarbonyl)phenyl)-3-methyl-1*H*-imidazol-2-ylidene **1a**, $HC\hat{}C^*_B$ = 1-phenyl-3-methyl-1*H*-imidazol-2-ylidene **1b**) react with methyl iodide (MeI) at room temperature in the dark to give compounds $[\{Pt^{IV}(C\hat{}C^*)Me(\mu\text{-pz})\}_2(\mu\text{-I})]I$ ($C\hat{}C^*_A$ **2a**, $C\hat{}C^*_B$ **2b**). The reaction of **1a** with benzyl bromide (BnBr) in the same conditions afforded $[Br(C\hat{}C^*_A)Pt^{III}(\mu\text{-pz})_2Pt^{III}(C\hat{}C^*_A)Bn]$ (**5a**), which by heating in BnBr(l) became $[\{Pt^{IV}(C\hat{}C^*_A)Bn(\mu\text{-pz})\}_2(\mu\text{-Br})]Br$ (**6a**). Experimental investigations and density functional theory (DFT) calculations on the mechanisms of these reactions from **1a** revealed that they follow a S_N2 pathway in the two steps of the double oxidative addition (OA). Based on the DFT investigations, species such as $[(C\hat{}C^*_A)Pt^{III}(\mu\text{-pz})_2Pt^{III}(C\hat{}C^*_A)R]X$ (RX = MeI **Int-Me**, BnBr **Int-Bn**) and $[(C\hat{}C^*_A)Pt^{II}(\mu\text{-pz})_2Pt^{IV}(C\hat{}C^*_A)(R)X]$ (RX = MeI **Int′-Me**, BnBr **Int′-Bn**) were proposed as intermediates for the first and the second OA reactions, respectively. In order to put the mechanisms on firmer grounds, **Int-Me** was prepared as $[(C\hat{}C^*_A)Pt^{III}(\mu\text{-pz})_2Pt^{III}(C\hat{}C^*_A)Me]BF_4$ (**3a′**) and used to get $[I(C\hat{}C^*_A)Pt^{III}(\mu\text{-pz})_2Pt^{III}(C\hat{}C^*_A)Me]$ (**4a**), $[(C\hat{}C^*_A)Pt^{II}(\mu\text{-pz})_2Pt^{IV}(C\hat{}C^*_A)(Me)I]$ (**Int′-Me**), and $[\{Pt^{IV}(C\hat{}C^*)Me(\mu\text{-pz})\}_2(\mu\text{-I})]BF_4$ (**2a′**). The single-crystal X-ray structures of **2a**, **2b**, **3a′**, and **5a** along with the mono- and bi-dimensional ^1H and $^{195}Pt\{^1H\}$ NMR spectra of all the named species allowed us to compare structural and spectroscopic data for high-valent complexes with the same core $[\{Pt(C\hat{}C^*)(\mu\text{-pz})\}_2]$ but different oxidation states.

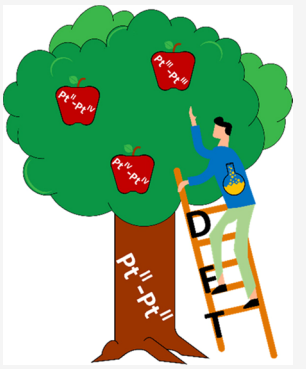

INTRODUCTION

Oxidative addition (OA)−reductive elimination processes on d^8 transition metal complexes account for many organic transformations.[1−5] High-valent metal−metal-bonded binuclear species play very often a key role as intermediates.[6−9] Compared to those of $Rh_2(I,I)$ and $Ir_2(I,I)$, the mechanisms of OA reactions of haloalkanes (RX) to $Pt_2(II,II)$ complexes have been scarcely studied. In the case of $Pt_2(II,II)$ complexes with the metal atoms far away from each other, the OA reactions follow monometallic pathways.[10−12] However, if the metal centers are held in proximity by bridging ligands, different kinds of mono- or bimetallic mechanisms can operate. In lantern- or half-lantern-shaped complexes, exhibiting short intermetallic separation (<3.0 Å), it is well known that the $[Pt_2(POP)_4]^{4-}$ (POP = pyrophosphite, d_{Pt-Pt} = 2.925 Å) complex undergoes thermal two-electron two-center [2e, 2c] OA of RI (R = Me, Et, ^{n}Pr, ^{i}Pr, n-pentyl) following a radical mechanism, although contribution of a S_N2-type one cannot be excluded for MeI.[13] Furthermore, the half-lantern compound $[\{Pt(bzq)(\mu\text{-N}\hat{}S)\}_2]$ [bzq = benzo[*h*]quinoline, HN^S = 2-mercaptopyrimidine] also undergoes [2e, 2c] thermal OA of CH_3I and CHX_3 (X = Br, I) following a bimetallic S_N2 or radical mechanism.[14] On the other hand, complexes $[Pt_2Me_2(C\hat{}N)_2(\mu\text{-P}\hat{}P)]$ [C^N = 2-phenylpyridyl-H, benzo[*h*]quinoline; P^P = dppf (1,1′-bis(diphenylphosphino)ferrocene), dppa (1,1′-bis(diphenylphosphino)acetylene)],[11,12,15] and *cis,cis*-$[Me_2Pt(\mu\text{-NN})(\mu\text{-dppm})PtMe_2]$ (NN = phthalazine, dppm = bis(diphenylphosphino)methane), with flexible bridging ligands, reacted with MeI in two steps, via a monometallic S_N2 mechanism. As a result, the diplatinum(IV) derivatives $[Pt_2Me_4I_2(C\hat{}N)_2(\mu\text{-P}\hat{}P)]$ and $[Me_3Pt(\mu\text{-I})_2(\mu\text{-dppm})PtMe_3]$ were obtained.[16]

Pyrazolates are a kind of adaptative bridging ligands. Because they have a proven ability to hold two metal atoms in close proximity while enabling a wide range of intermetallic separations; they allow for different kinds of OA mechanisms. For instance, haloalkanes such as CH_3I or CH_2I_2 add to $[\{Ir^I(\mu\text{-pz})\}_2]$ complexes following mostly a bimetallic S_N2[17−19] or radical[20,21] mechanisms, leading to metal−metal-bonded $Ir_2(II,II)$ complexes. Monometallic S_N2[22,23] pathways resulting in mixed valence Ir(I)−Ir(III) compounds have sometimes been proven. The $Ir_2(II,II)$ species, once rarely formed, undergo further OA; when this happens, no metal−metal-bonded Ir(III)−Ir(III) compounds were obtained.[24,25] In the field of pyrazolate-bridged $Pt_2(II,II)$ complexes, we observed that $[\{Pt^{II}(C\hat{}C^*_A)(\mu\text{-pz})\}_2]$ ($HC\hat{}C^*_A$ = 1-(4-(ethoxycarbonyl)-

Received: April 27, 2022
Published: August 3, 2022

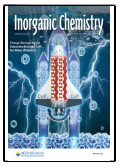

https://doi.org/10.1021/acs.inorgchem.2c01441
Inorg. Chem. 2022, 61, 12559−12569

phenyl)-3-methyl-1*H*-imidazol-2-ylidene **1a**) reacted with haloforms, CHX_3 (X = Cl, Br, I), following a radical mechanism. Complexes $[\{Pt(C\hat{}C^*_A)(\mu\text{-pz})X\}_2]$, $[XPt(C\hat{}C^*_A)(\mu\text{-pz})_2Pt(C\hat{}C^*_A)CHX_2]$ or mixtures of both were obtained, depending mostly on the environmental conditions (argon atmosphere, oxygen or light).[26,27] In depth mechanistic investigations evidenced that complex **1a** exists in solution in two forms: the butterfly-wing-spreading form **1a**−**s** characterized by long intermetallic distances and the wing-folding one **1a**−**f**, with short ones. These two conformers interconvert one into the other, resembling a butterfly flapping process. Species **1a**−**f** are those which trigger the reaction with haloforms in the ground state (S_0) with $CHBr_3$ and CHI_3 or in the excited state S_1 with $CHCl_3$.[27] These results highlighted the relevance of metal−metal cooperativity to enable the oxidation of **1a**. These findings, along with the importance of high-valent organometallic complexes in many organic synthesis, encouraged us to widen the scope of our earlier investigations, exploring the reactivity of **1a** and the analogous complex $[\{Pt^{II}(C\hat{}C^*_B)(\mu\text{-pz})\}_2]$ ($HC\hat{}C^*_B$ = 1-phenyl-3-methyl-1*H*-imidazol-2-ylidene (**1b**) toward other halogenated species, such as methyl iodide (MeI) and benzyl bromide (BnBr). Supported by density functional theory (DFT) studies on the OA mechanisms, we were able to prepare dinuclear complexes with different oxidation states: Pt_2(III,III), Pt_2(III,III) ↔ Pt_2(II,IV) and Pt_2(IV,IV). They allowed us to substantiate the modeled mechanisms and to compare their structural and spectroscopic data.

EXPERIMENTAL SECTION

General information about instrumentation, X-ray structure determinations (CCDC 2160386−2160389), DFT computational details with Figure S1, and NMR spectra for characterization are available in the Supporting Information.

Compounds $[\{Pt(C\hat{}C^*_A)(\mu\text{-pz})\}_2]$ (**1a**),[26] and $[\{Pt(C\hat{}C^*_B)(\mu\text{-Cl})\}_2]$ (**B**)[28] were prepared as described elsewhere. MeI, BnBr, Hpz, and $AgClO_4$ were used as purchased from Acros Organics, Fluka, Merck, and Aldrich, respectively. NMR spectra were recorded at r.t., except if a different value is indicated. Data are given according to Figure 1.

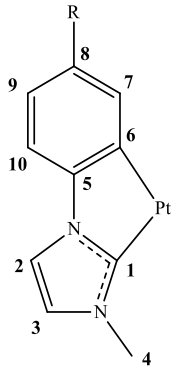

R = $EtCO_2$ ($C\hat{}C^*_A$); H ($C\hat{}C^*_B$)

Figure 1. Numerical scheme for NMR purposes.

Synthesis of $[\{Pt(C\hat{}C^*_B)(\mu\text{-pz})\}_2]$ (1b). $AgClO_4$ (55.1 mg, 0.263 mmol) was added to a stirred suspension of **B** (102.1 mg, 0.132 mmol) in acetone (40 mL) in the dark at room temperature. After 2.5 h, pzH (35.8 mg, 0.527 mmol) was added to the mixture and allowed to react for 18.5 h in the darkness. Then, the resulting suspension was filtered through Celite and the solution was concentrated to 50 mL. Afterward, NEt_3 (0.5 mL, 3.62 mmol) was added to the solution at r.t. and allowed to react for 2 h. The suspension was concentrated to 15 mL, and the solid was filtered and washed with 2 mL of acetone to give **1b** as a white solid. Yield: 74.0 mg, 0.088 mmol, 67%. Anal. calcd for $C_{26}H_{24}N_8Pt_2$: C, 37.23; H, 2.88; N, 13.36. Found: C, 37.22; H, 2.98; N, 12.97. ^{1}H NMR (400 MHz, DMSO-d_6): δ = 7.43 (d, $^3J_{2,3}$ = 1.6, 2H, H_2), 7.25 (s, 2H, H_{pz}), 7.16 (s, 2H, H_{pz}), 6.82 (d, $J_{H,H}$ = 7.4, 2H, H_{Ar}), 6.76 (d, 2H, H_3), 6.63 (d, $J_{H,H}$ = 7.3, 2H, H_{Ar}), 6.50 (t, $J_{H,H}$ = 7.4, 2H, H_{Ar}), 6.35 (t, $J_{H,H}$ = 7.0, 2H, H_{Ar}), 5.88 (s br, 2H, H_{pz}), 2.72 (s, 6H, H_4). ^{1}H−^{195}Pt HMQC NMR (85.6 MHz, DMSO-d_6): δ = −3767.4 (s).

Synthesis of $[\{Pt(C\hat{}C^*_A)Me(\mu\text{-pz})\}_2(\mu\text{-I})]I$ (2a). CH_3I (26 μL, 0.403 mmol) was added to a solution of **1a** (98.9 mg, 0.101 mmol) in anhydrous CH_2Cl_2 (5 mL) under argon atmosphere in the dark. After 14 h of reaction, the precipitate was filtered, washed with Et_2O (4 × 10 mL), and dried to give **2a** as a white solid. Yield: 117.8 mg; 0.093 mmol; 92%. Anal. calcd for $C_{34}H_{38}I_2N_8O_4Pt_2$: C, 32.24; H, 3.02; N, 8.85. Found: C, 31.84; H, 2.82; N, 8.45. ^{1}H NMR (400 MHz, CD_2Cl_2, 248 K): δ = 7.97 (s, $^3J_{H,Pt}$ = 37.7, 2H, H_7), 7.94 (d, $^3J_{9,10}$ = 8.2, 2H, H_9), 7.87−7.73 (m, 6H, H_{pz} and H_2), 7.47 (d, $^3J_{10,9}$ = 8.2, 2H, H_{10}), 7.34 (d, $^3J_{3,2}$ = 1.8, 2H, H_3), 6.50 (s br, 2H, H_{pz}), 4.27 (q, $^3J_{H,H}$ = 6.9, 4H, OCH_2CH_3), 3.52 (s, 6H, H_4), 1.78 (s, $^2J_{H,Pt}$ = 65.5, 6H, Pt-CH_3), 1.31 (t, $^3J_{H,H}$ = 6.9, 6H, OCH_2CH_3). ^{13}C{^{1}H} NMR plus HMBC and HSQC (101 MHz, CD_2Cl_2, 248 K): δ = 165.7 (s, 2C, C═O), 146.3 (s, 2C, C_5), 142.1 (s, 2C, $^1J_{C,Pt}$ = 1126.2, C_1), 140.1 and 139.2 (4C, C_{pz}), 133.3 (s, 2C, C_7), 128.4 (s, 2C, C_9), 125.5 (s, 1C, C_3), 117.5 (s, 1C, C_2), 113.6 (s, 2C, C_{10}), 107.6 (s, 2C, C_{pz}), 61.5 (s, 2C, OCH_2CH_3), 38.1 (s, 2C, C_4), 14.3 (s, 2C, OCH_2CH_3), 11.6 (s, $^1J_{C,Pt}$ = 502.2, 2C, Pt-CH_3). ^{195}Pt{^{1}H} NMR (85.6 MHz, CD_2Cl_2, 248 K): δ = −2688.0 (s). MS (MALDI+): m/z = 1138.88 $[\{Pt(C\hat{}C^*_A)(CH_3)(\mu\text{-pz})\}_2(\mu\text{-I})]^+$. IR (ATR, cm^{-1}) υ = 1698 (m, C═O).

Synthesis of $[\{Pt(C\hat{}C^*_B)Me(\mu\text{-pz})\}_2(\mu\text{-I})]I$ (2b). CH_3I (18 μL, 0.2862 mmol) was added to a suspension of **1b** (60 mg, 0.072 mmol) in anhydrous DMF (5 mL) under argon atmosphere in the dark. After 8 h of reaction, 100 mL of Et_2O was added and the precipitate was filtered, washed with Et_2O (5 × 10 mL), and dried to give **2b** as a white solid. Yield: 70.7 mg; 0.063 mmol; 88%. Anal. calcd for $C_{28}H_{30}I_2N_8Pt_2$: C, 29.96; H, 2.69; N, 9.98. Found: C, 29.76; H, 2.62; N, 9.65. ^{1}H NMR (400 MHz, CD_2Cl_2): δ = 7.78 (m, 4H, H_{pz}), 7.70 (d, $^3J_{2,3}$ = 2.0, 2H, H_2), 7.41−7.24 (m, 8H, H_3 and H_{Ar}), 7.13 (m, 2H, H_{Ar}), 6.47 (m, 2H, H_{pz}), 3.52 (s, 6H, H_4), 1.80 (s, $^2J_{H,Pt}$ = 66.1, 6H, Pt-CH_3). ^{1}H−^{195}Pt HMQC NMR (85.6 MHz, CD_2Cl_2): δ = −2664.4 (s). MS (MALDI+): m/z = 994.07 $[\{Pt(C\hat{}C^*_B)(CH_3)(\mu\text{-pz})\}_2(\mu\text{-I})]^+$.

Synthesis of $[(C\hat{}C^*_A)Pt(\mu\text{-pz})_2Pt(C\hat{}C^*_A)Me]BF_4$ (3a′). Me_3OBF_4 (49.3 mg, 0.320 mmol) was added to a solution of **1a** (262.0 mg, 0.267 mmol) in anhydrous CH_2Cl_2 (15 mL) under argon atmosphere in the dark at −25 °C. After 2 h of reaction, the solution was dried in vacuo. The residue was treated with 20 mL of dried Et_2O, and the resulting solid was filtered, washed with Et_2O (2 × 20 mL), and dried to give **3a′** as a brown solid. Yield: 244.8 mg; 0.226 mmol; 85%. Anal. calcd for $C_{33}H_{35}BF_4N_8O_4Pt_2{\cdot}2CH_2Cl_2$: C, 33.51; H, 3.13; N, 8.93. Found: C, 33.27; H, 3.10; N, 9.33. ^{1}H NMR (400 MHz, CD_2Cl_2): δ = 7.92 (d, $^3J_{H,H}$ = 2.1, 1H, H_{pz}), 7.85−7.77 (m, 3H, 2H_{pz}, and H_9 [Pt−Me]), 7.74 (d, $^3J_{H,H}$ = 2.1, 1H, H_{pz}), 7.66 (dd, $^3J_{9,10}$ = 8.2, $^4J_{9,7}$ = 1.6, 1H, H_9 [Pt]), 7.52 (d, $^4J_{7,9}$ = 1.6, $^3J_{H,Pt}$ = 41.2, 1H, H_7[Pt]), 7.50 (d, $^4J_{7,9}$ = 1.6, $^3J_{H,Pt}$ = 51.7, 1H, H_7 [Pt−Me]), 7.43 (d, $^3J_{2,3}$ = 2.0, 1H, H_2 [Pt−Me]), 7.24−7.16 (m, 2H, H_{10} [Pt−Me] and H_2 [Pt]), 7.03 (d, $^3J_{10,9}$ = 8.1, 1H, H_{10} [Pt]), 6.60−6.52 (m, 3H, 2H_{pz} and H_3), 6.37 (d, $^3J_{3,2}$ = 2.1, 1H, H_3 [Pt]), 4.38−4.23 (m, 4H, OCH_2CH_3), 3.17 (s, 3H, H_4 [Pt−Me]), 3.05 (s, 3H, H_4 [Pt]), 2.42 (s, $^2J_{H,Pt}$ = 70.7, $^3J_{H,Pt}$ = 14.7, 3H, [Pt-CH_3]), 1.40−1.30 (m, 6H, OCH_2CH_3). ^{13}C{^{1}H} NMR plus HMBC and HSQC (101 MHz, CD_2Cl_2): δ = 166.5 (s, 1C, C═O), 166.0 (s, 1C, C═O), 153.8 (s, 1C, $^1J_{C,Pt}$ = 1391.4, C_1 [Pt]), 150.4 (s, 1C, C_5 [Pt]), 147.2 (s, 1C, C_5 [Pt−Me]), 144.5 (s, 1C, $^1J_{C,Pt}$ = 1179.2, C_1 [Pt−Me]), 140.2 (s, 1C, C_{pz}), 137.9 (s, 1C, C_{pz}), 135.9 and 135.5 (s, 4C, C_{pz}), 134.7 (s, 1C, C_7 [Pt]), 133.2 (s, 1C, C_7 [Pt−Me]), 129.8 (s, 1C, C_9 [Pt−Me]), 129.6 (s, 1C, C_9 [Pt]), 124.8 (s, 1C, C_3 [Pt−Me]), 123.6 (s, 1C, C_3 [Pt]), 117.4 (s, 1C, C_2 [Pt−Me]), 116.8 (s, 1C, C_2 [Pt]), 113.7 (s, 1C, C_{10} [Pt−Me]), 112.1 (s, 1C, C_{10} [Pt]), 107.8 and 107.7 (s, 2C, C_{pz}), 61.9 and 61.8 (s, 2C, OCH_2CH_3), 37.2 (s, 1C, C_4 [Pt−Me]), 37.0 (s, 1C, C_4 [Pt]), 14.6 and 14.5 (s, 2C, OCH_2CH_3), −1.9 (s, $^1J_{C,Pt}$ = 411.2, 1C, Pt-CH_3). ^{19}F NMR (376 MHz, CD_2Cl_2): δ = −151.4 (m, 4F,

https://doi.org/10.1021/acs.inorgchem.2c01441
Inorg. Chem. 2022, 61, 12559−12569

Scheme 1. Reaction Pathway for OA Reactions of MeI to 1a and 1b

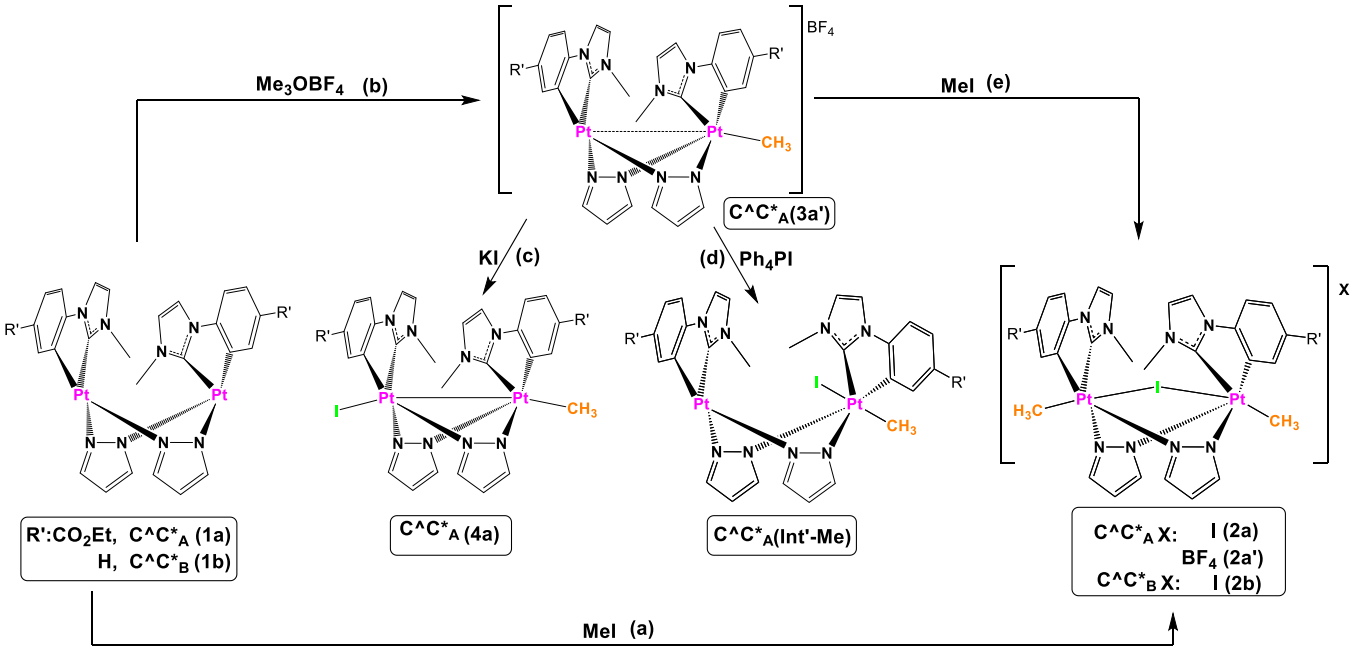

BF_4). $^{195}Pt\{^1H\}$ NMR (85.6 MHz, CD_2Cl_2): δ = −2589.2 (s, $^1J_{Pt,Pt}$ = 1023.4, Pt−Me), −3064.2 (s, Pt). MS (MALDI+): m/z = 997.2 $[(C\hat{}C^*_A)Pt(\mu\text{-}pz)_2Pt(C\hat{}C^*_A)CH_3]^+$. IR (ATR, cm^{-1}) υ = 1702 (m, C═O), 1043, 1012 and 519 (s, BF_4).

Synthesis of [I(C^C*$_A$)Pt(μ-pz)$_2$Pt(C^C*$_A$)Me] (4a). KI (33.6 mg, 0.202 mmol) was added to a solution of **3a′** (109.8 mg, 0.101 mmol) in MeCN (3 mL) in the dark at −25 °C. After 3 h of reaction, the suspension was filtered and the solid was washed with water (7 × 10 mL) and dried to give **4a** as a yellow solid. Yield: 44.0 mg; 0.039 mmol; 39%. Anal. calcd for $C_{33}H_{35}IN_8O_4Pt_2$: C, 35.54; H, 3.14; N, 9.96. Found: C, 35.88; H, 2.88; N, 9.65. ^1H NMR (400 MHz, CD_2Cl_2, 223 K): δ = 8.01 (d, $^3J_{H,H}$ = 2.0, 1H, H_{pz}), 7.89 (d, $^3J_{H,H}$ = 2.0, 1H, H_{pz}), 7.72 (d, $^3J_{H,H}$ = 2.0, 1H, H_{pz}), 7.64 (d, $^3J_{H,H}$ = 2.0, 1H, H_{pz}), 7.61 (dd, $^3J_{9,10}$ = 8.2, $^4J_{9,7}$ = 1.6, 1H, H_9 [Pt−Me]), 7.53 (d, $^4J_{7,9}$ = 1.6, $^3J_{H,Pt}$ = 58.7, 1H, H_7 [Pt−I]), 7.44−7.33 (m, 2H, H_9 [Pt−I] and H_7[Pt−Me]), 7.04 (d, $^3J_{2,3}$ = 2.1, 1H, H_2 [Pt−Me]), 6.89 (d, $^3J_{10,9}$ = 8.2, 1H, H_{10} [Pt−Me]), 6.84 (d, $^3J_{2,3}$ = 2.1, 1H, H_2 [Pt−I]), 6.93 (d, $^3J_{10,9}$ = 8.2, 1H, H_{10} [Pt−I]), 6.38−6.30 (m, 3H, H_{pz} and H_3 [Pt−Me]), 6.15 (d, $^3J_{3,2}$ = 2.0, 1H, H_3 [Pt−I]), 4.35−4.10 (m, 4H, OCH_2CH_3), 3.04 (s, 3H, H_4 [Pt−I]), 3.01 (s, 3H, H_4 [Pt−Me]), 1.48 (s, $^2J_{H,Pt}$ = 61.0, $^3J_{H,Pt}$ = 14.5, 3H, Pt-CH_3), 1.32−1.24 (m, 6H, OCH_2CH_3). $^{13}C\{^1H\}$ NMR plus HMBC and HSQC (101 MHz, CD_2Cl_2, 223 K): δ = 166.3 (s, 1C, C═O), 165.8 (s, 1C, C═O), 153.0 (s, $^1J_{C,Pt}$ = 1358.7, 1C, C_1 [Pt−I]), 147.8 (s, 1C, C_5), 147.5 (s, $^1J_{C,Pt}$ = 1153.6, 1C, C_1 [Pt−Me]), 145.7 (s, 1C, C_5), 140.5, 139.1 and 134.3 (s, 3C, C_{pz}), 132.9 (s, 1C, C_7 [Pt−I]), 132.0 (s, 1C, C_7 [Pt−Me]), 131.7 (s, 1C, C_{pz}), 128.1, 127.1, 126.2 and 125.2 (C_6, C_6, C_8 and C_8), 126.4 (s, 1C, C_9 [Pt−Me]), 125.3(s, 1C, C_9 [Pt−I]), 123.0 (s, 1C, C_3 [Pt−Me]), 121.7 (s, 1C, C_3 [Pt−I]), 114.1 (s, 1C, C_2 [Pt−Me]), 113.7 (s, 1C, C_2 [Pt−I]), 111.1 (s, 1C, C_{10} [Pt−Me]), 110.0 (s, 1C, C_{10} [Pt−I]), 105.6 (m, 2C, C_{pz}), 61.1 and 60.9 (s, 2C, OCH_2CH_3), 36.6 and 36.5 (s, 2C, C_4, [Pt−Me] and [Pt−I]), 14.1 (s br, 2C, OCH_2CH_3), −16.0 (s, $^1J_{C,Pt}$ = 467.1, 1C, Pt-CH_3). $^{195}Pt\{^1H\}$ NMR (85.6 MHz, CD_2Cl_2, 223 K): δ = −2848.2 (s, $^1J_{Pt,Pt}$ = 1239.8, Pt−Me), −3018.8 (s, Pt−I). MS (MALDI+): m/z = 997.2 $[(C\hat{}C^*_A)Pt(\mu\text{-}pz)_2Pt(C\hat{}C^*_A)(CH_3)]^+$. IR (ATR, cm^{-1}) υ = 1699 (m, C═O).

Synthesis of Int′-Me. PPh_4I (83.4 mg, 0.179 mmol) was added to a solution of **3a′** (97.0 mg, 0.089 mmol) in anisole (5 mL) in the dark at 30 °C, and the mixture was allowed to react for 2 h. Then, the solvent was removed under vacuum and the residue was treated with H_2O. The resulting yellow solid was identified as $[(C\hat{}C^*_A)Pt(\mu\text{-}pz)_2(C\hat{}C^*_A)\text{-}PtI(CH_3)]$ (**Int′-Me**) by ^1H and ^{195}Pt NMR, although anisole and PPh_4BF_4 were detected as impurities. ^1H NMR (400 MHz, 223 K, CD_2Cl_2): δ = 8.10−6.00 (16 H_{Ar} of **Int′-Me** and H_{Ar} of PPh_4), 4.33−4.07 (m, 4H, OCH_2CH_3), 3.75 (s, OCH_3, anisole), 3.49 and 3.19 (s, 6H, H_4), 1.75 (s, $^2J_{H,Pt}$ = 65.9, 3H, [Pt-CH_3]). $^{195}Pt\{^1H\}$ NMR (85.6 MHz, 223 K, CD_2Cl_2): δ = −2697.0 (s, Pt^{IV}), −3776.0 (s, Pt^{II}).

Synthesis of [Br(C^C*$_A$)Pt(μ-pz)$_2$Pt(C^C*$_A$)Bn] (5a). BnBr (33 μL, 0.277 mmol) was added to a solution of **1a** (68.0 mg, 0.069 mmol) in MeCN (20 mL) in the dark. After 3.5 h of reaction, the solvent was removed under vacuum. The residue was treated with a mixture of Et_2O and *n*-hexane (1:20) to give **5a** as an orange solid. Yield: 74.0 mg; 0.064 mmol; 93%. Anal. calcd for $C_{39}H_{39}BrN_8O_4Pt_2$: C, 40.60; H, 3.41; N, 9.71. Found: C, 40.32; H, 3.36; N, 9.68. ^1H NMR (400 MHz, CD_2Cl_2, 248 K): δ = 7.97 (d, $^3J_{H,H}$ = 1.8, 1H, H_{pz}), 7.91 (d, $^3J_{H,H}$ = 1.8, 1H, H_{pz}), 7.78 (d, $^3J_{H,H}$ = 2.1, 1H, H_{pz}), 7.65 (dd, $^3J_{9,10}$ = 8.2, $^4J_{9,7}$ = 1.7, 1H, H_9 [Pt−Bn]), 7.50 (d, $^4J_{7,9}$ = 1.7, $^3J_{H,Pt}$ = 43.3, 1H, H_7 [Pt−Bn]), 7.44 (d, $^4J_{7,9}$ = 1.7, $^3J_{H,Pt}$ = 45.2, 1H, H_7 [Pt−Br]), 7.39 (dd, $^3J_{9,10}$ = 8.2, $^4J_{9,7}$ = 1.7, 1H, H_9 [Pt−Br]), 7.16 (d, $^3J_{H,H}$ = 2.1, 1H, H_{pz}), 7.06−6.98 (m, 1H, H_{para}), 6.89−6.80 (m, 5H, H_2, H_2, H_{10} [Pt−Bn] and H_{meta}), 6.78−6.68 (m, 3H, H_{10} [Pt−Br] and H_{orto}), 6.40 (pt, $^3J_{H,H}$ = 2.0, 1H, H_{pz}), 6.30 (pt, $^3J_{H,H}$ = 2.1, 1H, H_{pz}), 6.11 (d, $^3J_{3,2}$ = 2.1, 1H, H_3 [Pt−Bn]), 6.07 (d, $^3J_{3,2}$ = 2.1, 1H, H_3 [Pt−Br]), 4.36−4.10 (m, 5H, CH_2 (Bn) and OCH_2CH_3), 3.73 (d, $^2J_{H,H}$ = 7.9, $^2J_{H,Pt}$ = 69.0, $^3J_{H,Pt}$ = 28.9, 1H CH_2 (Bn)), 3.07 (s, 3H, H_4 [Pt−Br]), 2.71 (s, 3H, H_4 [Pt−Bn]), 1.32 (t, $^3J_{H,H}$ = 7.3, 3H, OCH_2CH_3), 1.25 (t, $^3J_{H,H}$ = 7.3, 3H, OCH_2CH_3).$^{13}C\{^1H\}$ NMR plus HMBC and HSQC (101 MHz, CD_2Cl_2, 248 K): δ = 166.5 (s, 1C, C═O), 166.0 (s, 1C, C═O), 153.2 (s, $^1J_{C,Pt}$ = 1323.4, 1C, C_1 [Pt−Br]), 148.7 (s, $^1J_{C,Pt}$ = 1239.5, 1C, C_1 [Pt−Bn]), 148.1 (s, 1C, C_5 [Pt−Br]), 147.1 (s, 1C, C_{ipso}), 145.8 (s, 1C, C_5 [Pt−Bn]), 138.9, 137.2 and 134.4 (s, 3C, C_{pz}), 133.3 (s, 1C, C_7 [Pt−Br]), 132.1 (s, 1C, C_7 [Pt−Bn]), 131.9 (s, 1C, C_{pz}), 128.9 (s, 2C, C_{meta}), 127.0 and 126.9 (2C, C_9 [Pt−Bn] and C_{orto}), 125.7 (s, 1C, C_9 [Pt−Br]), 124.5 (s, 1C, C_{para}), 122.7 (s, 1C, C_3 [Pt−Bn]), 121.9 (s, 1C, C_3 [Pt−Br]), 114.1 and 113.9 (2C, C_2), 111.4 (s, 1C, C_{10} [Pt−Bn]), 110.1 (s, 1C, C_{10} [Pt−Br]), 105.8 and 105.7 (2C, C_{pz}), 61.3 and 61.0 (2C, OCH_2CH_3), 36.6 (s, 1C, C_4 [Pt−Br]), 36.1 (s, 1C, C_4 [Pt−Bn]), 15.2 (s, $^1J_{C,Pt}$ = 448.1, $^2J_{C,Pt}$ = 192.9, 1C, Pt-CH_2Ph), 14.3 (s, 2C, OCH_2CH_3). $^{195}Pt\{^1H\}$ NMR (85.6 MHz, CD_2Cl_2, 248 K): δ = −2693.6 (s br, Pt−Bn), −2742.8 (s, $^1J_{Pt,Pt}$ = 1028.9, Pt−Br,). MS (MALDI+): m/z = 1061.6 $[Br(EtO_2C\text{-}C\hat{}C^*)\text{-}Pt(\mu\text{-}pz)_2Pt(EtO_2C\text{-}C\hat{}C^*)]^+$, 1072.8 $[(C\hat{}C^*_A)Pt(\mu\text{-}pz)_2Pt(C\hat{}C^*_A)\text{-}Bn]^+$. IR (ATR, cm^{-1}) υ = 1700 (m, C═O).

Synthesis of [{Pt(C^C*$_A$)Bn(μ-pz)}$_2$(μ-Br)]Br (6a). A suspension of **5a** (95 mg, 0.082 mmol) in BnBr (5 mL) was heated 70 °C for 5 h. Then, the suspension was cooled down to room temperature, and the

https://doi.org/10.1021/acs.inorgchem.2c01441
Inorg. Chem. 2022, 61, 12559−12569

Scheme 2. Computed (PCM(MeCN)-M06/6-31G(d), MWB60(Pt), and MWB46(I)) Free Energy Profile (ΔG, kcal/mol) for the Thermal Conversion of 1a into 4a (or 5a) and Int′-R (Step i) and Int′-R into 2a (or 6a) (Step ii) Following S_N2 Mechanisms

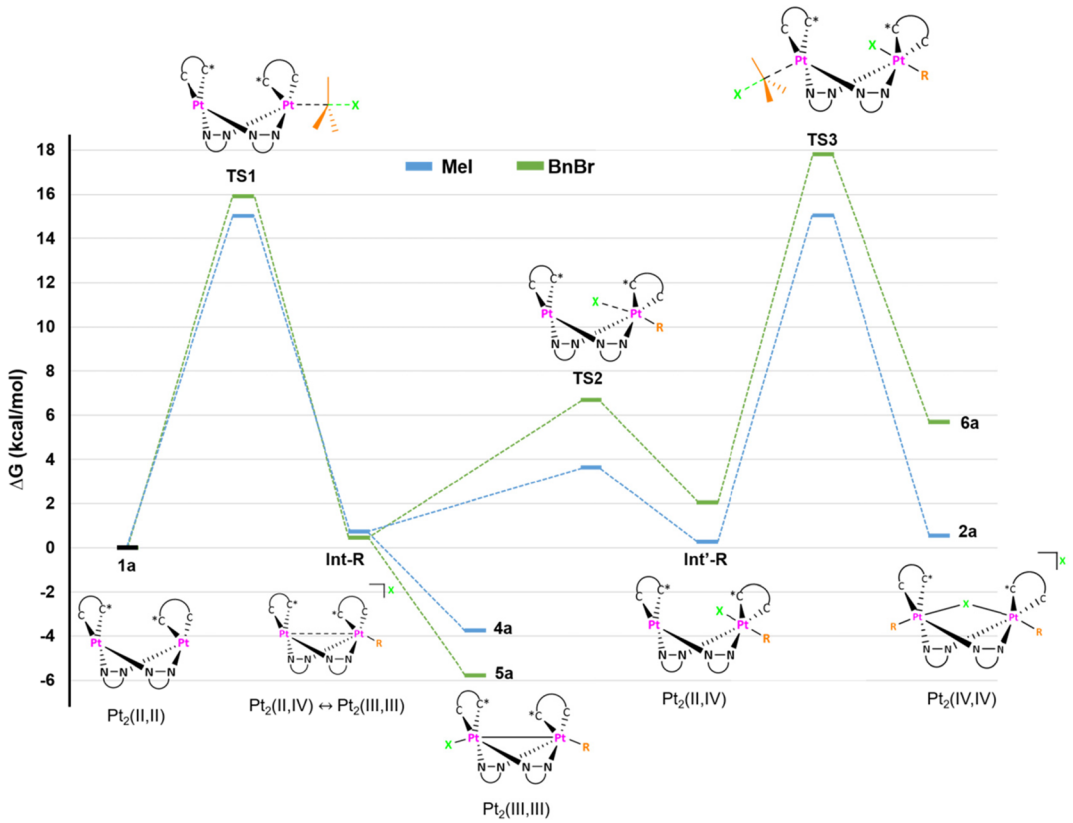

		Step i				Step ii			
		1a	TS1	Int-R	X-Pt-Pt-R	TS2	Int'-R	TS3	R-Pt-X-Pt-R
R=Me X=I	d(Pt-Pt) (Å)	3.16	3.04	2.83	2.79 (**4a**)	3.41	3.70	3.66	3.65 (**2a**)
	ΔG (kcal/mol)	0.00	15.02	0.72	-3.76 (**4a**)	3.64	0.27	15.05	0.55 (**2a**)
R=Bn X=Br	d(Pt-Pt) (Å)	3.16	2.93	2.81	2.76 (**5a**)	3.34	3.75	3.67	3.67 (**6a**)
	ΔG (kcal/mol)	0.00	15.92	0.45	-5.78 (**5a**)	6.69	2.05	17.81	5.69 (**6a**)

resulting solid was filtered and dried to give **6a**. Yield: 94.7 mg; 0.071 mmol; 87%. Anal. calcd for $C_{46}H_{46}Br_2N_8O_4Pt_2$: C, 41.70; H, 3.50; N, 8.46. Found: C, 41.38; H, 3.27; N, 8.44. ^{1}H NMR (400 MHz, CD_2Cl_2, 248 K): δ = 8.46 (s br, 2H, H_{pz}), 8.35 (s br, 2H, H_{pz}), 8.10 (d, $^4J_{7,9}$ = 1.1, $^3J_{H,Pt}$ = 37.5, 2H, H_7), 7.89 (dd, $^3J_{9,10}$ = 8.2, $^4J_{9,7}$ = 1.1, 2H, H_9), 7.18 (s, 2H, H_2), 7.15−7.03 (m, 6H, H_{10}, H_{para} and H_3), 6.88 (pt, $J_{H,H}$ = 7.6, 4H, H_{meta}), 6.79 (s br, 2H, H_{pz}), 6.64 (pd $J_{H,H}$ = 7.6, 4H, H_{orto}), 4.45−4.20 (m, 6H, CH_2 (Bn) and OCH_2CH_3), 4.02 (d, $^2J_{H,H}$ = 8.6, $^2J_{H,Pt}$ = 90.6, 2H, CH_2 (Bn)), 3.41 (s, 6H, H_4), 1.35 (t, $^3J_{H,H}$ = 7.3, 6H, OCH_2CH_3). ^{13}C{^{1}H} NMR plus HMBC and HSQC (101 MHz, CD_2Cl_2, 248 K): δ = 165.7 (s, 2C, C═O), 146.4 (s, 2C, C_5), 142.6 (s, 2C, $^1J_{C,Pt}$ = 1202.2, C_1), 141.1 (2C, C_{pz}), 141.0 (s, 2C, C_{ipso}), 138.4 (2C, C_{pz}), 132.2 (s, 2C, C_7), 128.8 (s, 2C, C_9), 128.7 (s, 2C, C_{meta}), 128.3 (s, 4C, $^3J_{C,Pt}$ = 23.0, C_{orto}), 127.1 (s, 2C, C_{para}), 124.5 (s, 2C, C_3), 116.5 (s, 2C, C_2), 113.6 (s, $^4J_{C,Pt}$ = 28.7, 2C, C_{10}), 107.4 (s, $^3J_{C,Pt}$ = 18.0, 2C, C_{pz}), 61.5 (s, 2C, OCH_2CH_3), 37.6 (s, 2C, C_4), 32.7 (s, $^2J_{C,Pt}$ = 521.4, 2C, Pt-CH_2Ph), 14.3 (s, 2C, OCH_2CH_3). ^{195}Pt{^{1}H} NMR (85.6 MHz, CD_2Cl_2, 248 K): δ = −2357.0 (s). MS (MALDI+): m/z = 1245.69 [{Pt(C^C*$_A$)Bn(μ-pz)}$_2$(μ-Br)]$^+$. IR (ATR, cm^{-1}) υ = 1715 (m, C═O).

RESULTS AND DISCUSSION

Reactivity of [{Pt^{II}(C^C*)(μ-pz)}$_2$](C^C*$_A$ 1a, C^C*$_B$ 1b) with MeI and BnBr: Experimental and Computational Investigations for the Mechanistic Studies. The reaction of [{Pt^{II}(C^C*$_A$)(μ-pz)}$_2$] (**1a**) with MeI in MeCN in the dark afforded the Pt_2(IV,IV) compound [{Pt^{IV}(C^C*$_A$)Me(μ-pz)}$_2$(μ-I)]I (**2a**) as result of a double OA of MeI, regardless the reactant molar ratio (Scheme 1, path a).

The use of other solvents such as acetone or dichloromethane does not change the nature of the final compound. Compound [I(C^C*$_A$)Pt^{III}(μ-pz)$_2$Pt^{III}(C^C*$_A$)Me] (**4a**), resulting from the bimetallic OA of one MeI molecule was just detected by ^{1}H NMR. To evaluate if the CO_2Et fragment plays a role in the redox behavior of complex **1a**, we prepared the new complex **1b** (Experimental Section in the Supporting Information and Figure S2). Then, it was reacted with MeI in DMF due to its low solubility in other organic solvents, giving rise to the Pt_2(IV,IV)

https://doi.org/10.1021/acs.inorgchem.2c01441
Inorg. Chem. 2022, 61, 12559−12569

complex $[\{Pt^{IV}(C\hat{}C^*_B)Me(\mu\text{-}pz)\}_2(\mu\text{-}I)]I$ (**2b**). This result indicates that the CO_2Et fragment does not affect the reactivity of these $Pt_2(II,II)$ complexes toward MeI; however, it increases their solubility, allowing for a better study of it. Complexes **2a** and **2b** were isolated as white solids in very good yields (92%, **2a**; 88%, **2b**) and fully characterized (Figures S3 and S4). Just two complexes with the same bridging system have been reported to date, $PPN[\{Pt^{IV}Me_3(\mu\text{-}pz)\}_2(\mu\text{-}I)]$[29] and $(PPh_4)[\{Pt^{IV}Me_2Br\text{-}(\mu\text{-}pz)\}_2(\mu\text{-}Br)]$,[30] both of them prepared by assembly of mononuclear Pt^{IV} fragments. Therefore, **2a** and **2b** are the first $Pt_2(IV,IV)$ derivatives obtained by OA of MeI to $\{Pt^{II}(\mu\text{-}pz)\}_2$ fragments.

Keeping in mind that compound **1a** is oxidized by CHX_3 (X = Br, I) in the dark through a radical mechanism,[26,27] we checked this possibility for MeI. The reaction of **1a** with MeI in MeCN-d_3 in the dark was performed with and without galvinoxyl (Gal·) as radical (R·) trap, and they were followed by ^1H NMR for 1 h. It resulted to be almost unaffected by the presence of Gal·(see Figure S5), which led us to dismiss a radical mechanism and to consider a S_N2 one for the first and the second OA of MeI to **1a**. For an in depth knowledge of these reaction mechanisms, we carried out a DFT study (see Computational Details in Supporting Information). The free energy profiles in MeCN have been represented in Scheme 2, the reference energy value being 0.0 kcal/mol for one of the $Pt_2(II,II)$ reactant, **1a**.

In the modeled mechanism, the first OA is a S_N2 reaction, $Nu + MeI \rightarrow NuMe^+ + I^-$, with the dinuclear compound **1a** acting as nucleophile (Nu) to give a cationic $[Pt(II)-Pt(IV)\ -Me]^+$ intermediate **Int-Me**. The reaction would proceed through a transition state TS1, with one imaginary frequency (436i cm^{-1}), which shows a hypervalent C atom with two long Pt···C and C···I distances. The energy barrier (Ea_{TS1} = 15.02 kcal/mol) is low enough to allow the reaction to proceed at room temperature in the dark. Once the intermediate **Int-Me** was formed, the migration of the halide to the Pt(II) center will afford the I−Pt(III) −Pt(III) −Me derivative (**4a**) while, if the halide bonds to the Pt(IV) center, Pt(II,IV) species (**Int′-Me**) will be generated.

The small barrier (2.92 kcal/mol) for the conversion of **Int-Me** into **Int′-Me** through the transition state TS2 (43i cm^{-1}) competes with the barrierless formation of **4a** (Figure S6). This along with the low free energy difference between **4a** and **Int′-Me** ($\Delta G_{Int'\text{-}Me\text{-}4a}$ = 4.03 kcal/mol) support the formation of the two species, **4a** and **Int′-Me** from **Int-Me**, which are believed to be in equilibrium in solution of MeCN at r.t.

The second OA reaction (Scheme 2) would start with the nucleophilic attack of the d_z^2 orbital of the Pt(II) center in complex **Int′-Me** to a second MeI molecule to give **2a** as the final product. This step could proceed through a transition state TS3 (423i cm^{-1}), with the energy barrier (Ea_{TS3} = 14.78 kcal/mol) being similar to that of the first OA and thus small enough to be surpassed at room temperature in the dark. Therefore, this calculated mechanism shows the feasible access to **Int′-Me**, which would explain the observed double OA of MeI to **1a** to give **2a**. Besides, it shows that **4a** is thermodynamically more stable than **2a**. Because of this, the scarce solubility of the latter in the reaction media is likely to be the driving force for **2a**, which will be the final product of the reaction of **1a** with MeI.

Species like **Int-Me** and **Int′-Me** have been proposed as intermediates in OA reactions of one or two RX molecules to $M_2(I,I)$ (M = Rh, Ir).[17,25] Besides, the mixed-valence species **Int′-Me** could also be available by a monometallic S_N2 OA of MeI to **1a**.[31] Aiming to test the proposed mechanism and to compare the structural and spectroscopic features of high-valent Pt_2 complexes, with the same core "$\{Pt(C\hat{}C^*_A)(\mu\text{-}pz)\}_2$" but with different oxidation states, we addressed the synthesis and characterization of additional compounds such as **3a′**, **4a**, and **Int′-Me** (Scheme S1 and Figures S7−S10).

First, to achieve our challenging tasks, **Int-Me** was prepared as the BF_4 salt, $[(C\hat{}C^*_A)Pt(\mu\text{-}pz)_2Pt(C\hat{}C^*_A)Me]BF_4$ (**3a′**), in a very good yield (85%) (see Scheme 1, path b) by reacting **1a** with Me_3OBF_4, at −25 °C in anhydrous CH_2Cl_2 in the dark, under argon atmosphere. Compound **3a′** resulted to be stable in the solid state and solution at room temperature and could be fully characterized (Figure S7). Then, **3a′** was reacted with KI in MeCN at low temperature (−25 °C) to favor the exothermic process (Scheme 1, path c). In these conditions, $[I(C\hat{}C^*_A)\text{-}Pt^{III}(\mu\text{-}pz)_2Pt^{III}(C\hat{}C^*_A)Me]$ (**4a**) precipitated in the reaction media and could be obtained as a pure species in a moderate yield (39%) and then characterized (Figure S8). A mixture of **4a** and **Int′-Me** remains in the mother liquor, as it was detected by ^1H NMR, which explains the low yield in the synthetic procedure. Further support for the simultaneous formation of both **4a** and **Int′-Me** along with the equilibrium between them was obtained following this reaction by NMR, as can be seen in Figure S9. At −30 °C, this reactions leads to the simultaneous formation of **4a** and **Int′-Me**, with the former being the major species, which becomes **Int′-Me** as the temperature raises, in such a way that after 24 h at room temperature, both species are present in the mixture in about a 1:1 molar ratio. To reach **Int′-Me** as pure species, we searched for solvents that give a smaller free energy difference between **Int′-Me** and **4a** than the one obtained in MeCN, so as to ensure a larger amount of **Int′-Me** in the equilibrium. As can be seen in Scheme 3, the computed

Scheme 3. Computed (PCM-M06/6-31G(d), MWB60(Pt), and MWB46(I)) Free Energy Profiles (ΔG, kcal/mol) in MeCN (ε = 35.688) and Anisole (ε = 4.2247) for the Thermal Conversion of 4a, Int-Me, and Int′-Me

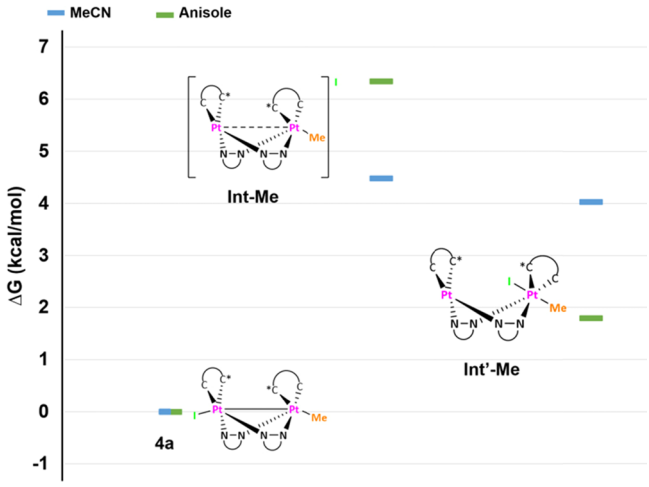

$\Delta G_{Int'\text{-}Me\text{-}4a}$ in anisole (1.79 kcal/mol) is clearly smaller than that in MeCN (4.03 kcal/mol). Accordingly, $[(C\hat{}C^*_A)Pt^{II}(\mu\text{-}pz)_2Pt^{IV}(C\hat{}C^*_A)(Me)I]$ (**Int′-Me**) was the single organometallic species detected by ^1H NMR in the reaction of **3a′** with Ph_4PI in anisole in the dark at 30 °C (Scheme 1, path d), although it was obtained from the reaction mixture unpurified with anisole and Ph_4PBF_4 (see Experimental section in the Supporting Information and Figure S10).

https://doi.org/10.1021/acs.inorgchem.2c01441
Inorg. Chem. 2022, 61, 12559−12569

Scheme 4. Reaction Pathway for OA Reactions of BnBr to 1a

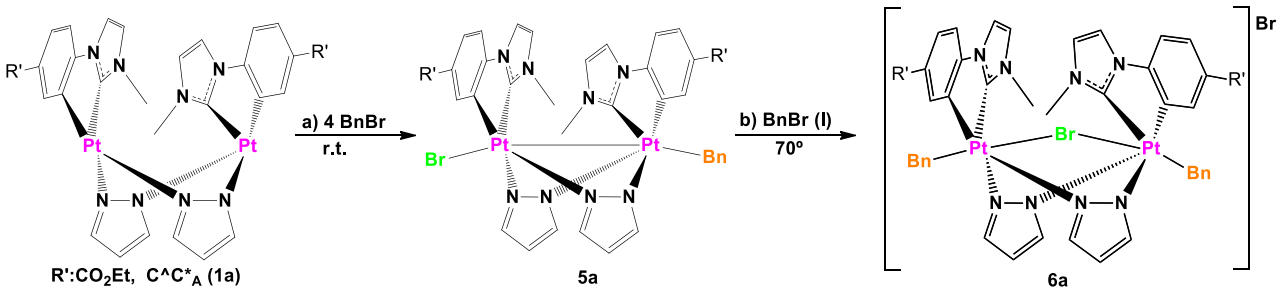

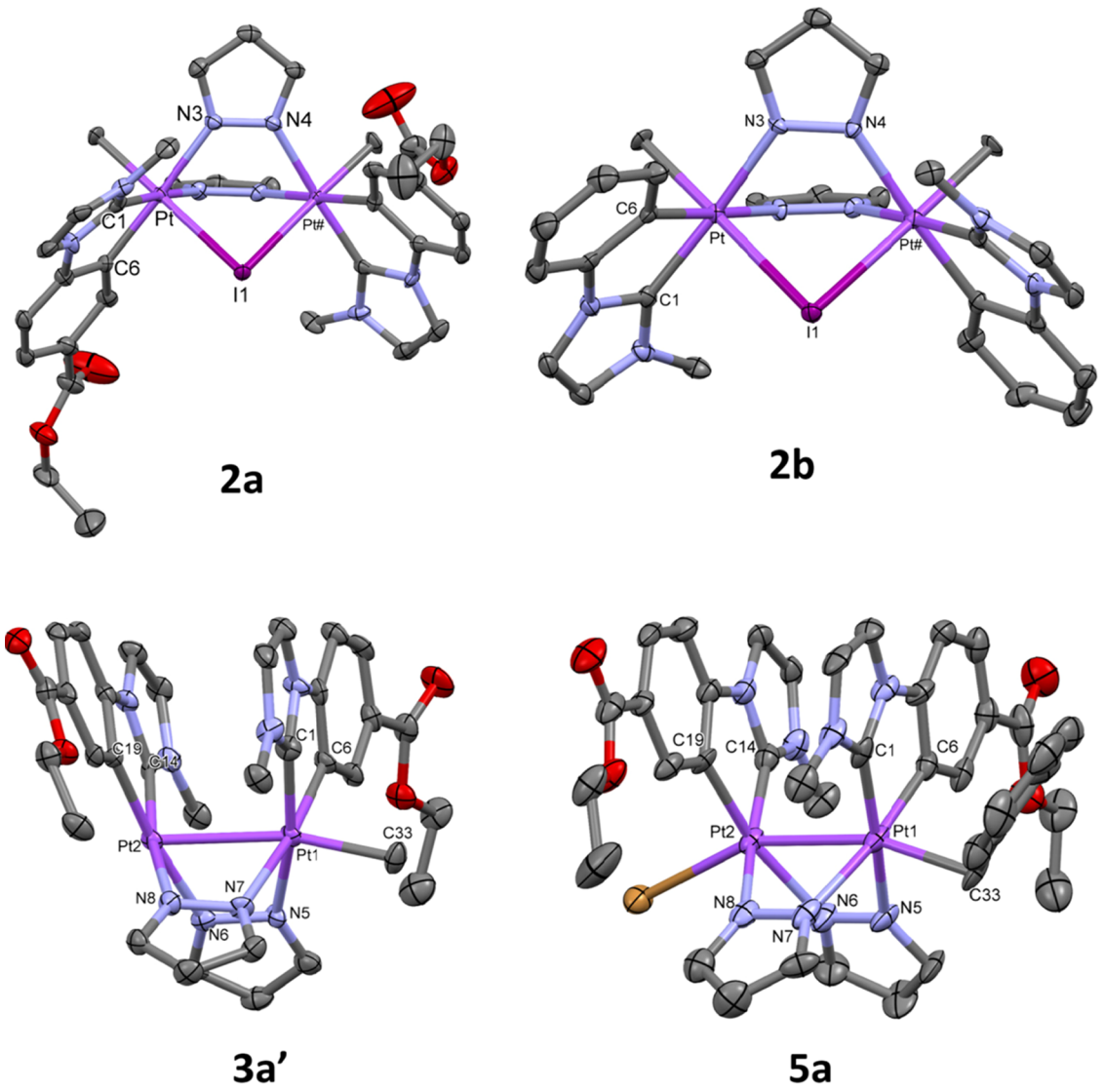

Figure 2. Molecular structure of the cationic complexes **2a**, **2b**, **3a′**, and **5a**. Ellipsoids are drawn at their 50% probability level; solvent molecules, I^- (**2a**, **2b**), BF_4^- (**3a′**), and hydrogen atoms have been omitted for clarity.

Additionally, **3a′** was reacted with MeI in acetonitrile at r.t., rendering **2a′** as the final product (Scheme 1, path e). This result is consistent with Pt_2(III,III) ↔ Pt_2(II,IV) formulations for **3a′**, the contribution of the Pt_2(II,IV) one being significant. Therefore, since all the intermediate species in the double OA of MeI to **1a** resulted to be experimentally available, the proposed mechanism, initiated with a bimetallic OA of MeI to the Pt_2(II,II) complexes **1a** and **1b**, seems suitable.

To expand these studies, we focused on the OA of benzyl bromide (BnBr) to $[\{Pt^{II}(C\hat{}C^*_A)(\mu\text{-pz})\}_2]$ (**1a**). The reaction of **1a** with BnBr in a 1:4 molar ratio in MeCN in the dark at r.t. rendered the Pt_2(III,III) complex $[Br(C\hat{}C^*_A)Pt^{III}(\mu\text{-pz})_2Pt^{III}(C\hat{}C^*_A)Bn]$ (**5a**) (Scheme 4, path a), which was isolated as an orange solid in very good yield (93%).

A second OA to give compound $[\{Pt^{IV}(C\hat{}C^*)Bn(\mu\text{-pz})\}_2(\mu\text{-Br})]Br$ (**6a**) was achieved by heating **5a** at 70 °C in BnBr(l) in the dark for 5 h. In these hard conditions, **6a** was obtained in

https://doi.org/10.1021/acs.inorgchem.2c01441
Inorg. Chem. 2022, 61, 12559−12569

Table 1. Relevant NMR Data for the New High Oxidation State Pt_2 Complexes[a]

compound	δ ^{195}Pt−X	δ ^{195}Pt−R	$^{1}J_{Pt-Pt}$	δ ^{1}H (Pt−R)	$^{2}J_{Pt-H}$	$^{3}J_{Pt-H}$
2a		−2688.0 (R = Me)		1.78	65.5	
2b		−2664.4[b] (R = Me)		1.80	66.1	
3a′	−3064.2 X = vacant	−2589.2 (R = Me)	1023.4	2.42	70.7	14.7
4a	−3018.8 (X = I)	−2848.2 (R = Me)	1239.8	1.48	61.0	14.5
Int′-Me	−3776.0 (Pt^{II})	−2697.0 (Pt^{IV})		1.75	65.9	
5a	−2742.8 (X = Br)	−2693.6 (R = Bn)	1028.9	3.73 (1H)[c]	69.0	28.9
6a		−2357.0 (R = Bn)		4.02 (2H)[c]	90.6	

[a]CD_2Cl_2, more details in experimental Section, δ (ppm); J (Hz). [b]Indirect detection by ^{1}H−^{195}Pt HMQC NMR. [c]An equal signal appears overlapped with OCH_2CH_3; δ ^{195}Pt = −3778.0 ppm (**1a**, acetone-d_6), −3767.4 ppm (**1b**, DMSO-d_6).

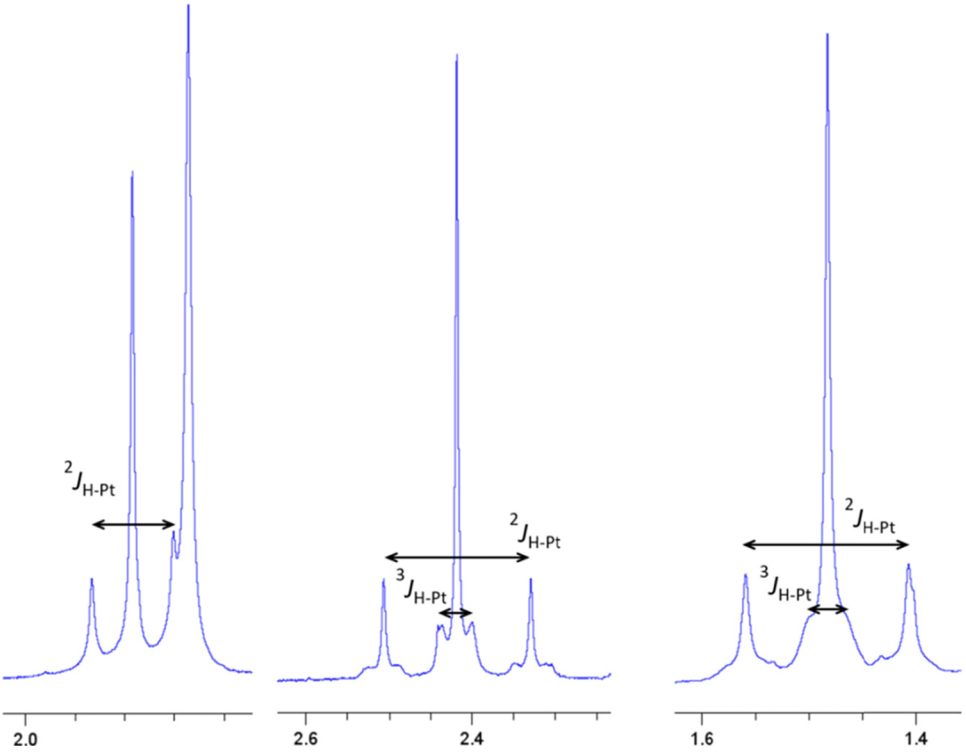

Figure 3. Expanded view of the ^{1}H NMR spectra of **2a** (left), **3a′** (middle), and **4a** (right) in CD_2Cl_2.

good yield (87%) (Scheme 4, path b). Then, **5a** and **6a** were fully characterized (Figures S11 and S12). The selective formation of **5a** in the presence of oxygen, an efficient radical trap, points to a S_N2 mechanism, like in the case of MeI (Figure S13), which was modeled by DFT in MeCN. For comparison, the free energy profiles obtained are represented in Scheme 2 and Figure S6.

The energy barrier for the first OA (Ea_{TS1} = 15.92 kcal/mol, TS1: 294i cm^{-1}) is low enough to enable the reaction go at r.t. in the dark, which is not much different from that for MeI. Once the **Int-Bn** was formed, species **5a** or **Int′-Bn** becomes available. Thermodynamically, the formation of **5a** from **1a** is clearly favored (calculated ΔG_{5a-1a} = −5.78 kcal/mol; $\Delta G_{Int'-Bn-1a}$ = 2.05 kcal/mol). Although the energy barrier (6.24 kcal/mol) for conversion of **Int-Bn** into **Int′-Bn** through TS2 (44i cm^{-1}) is in principle not large enough to prevent it to occur, experimentally, **5a** is the only species formed at r.t. in the dark. Therefore, it seems that the free energy difference between **5a** and **Int′-Bn** (calculated $\Delta G_{Int'Bn-5a}$ = 7.83 kcal/mol) hinders significant formation of **Int′-Bn**, thus preventing the second OA to occur at r.t. Only by heating at 70 °C in BnBr(l) is the formation of **Int′-Bn** achieved, enabling it to convert into **6a** through TS3 (260i cm^{-1}).

Again, in view of the lower stability of **6a** compared to **5a**, the scarce solubility of the former in the reaction media is likely the driving force for its formation.

The characterization of all these Pt_2 compounds has been addressed together for an overall perspective, as can be seen below.

Characterization of All New High-Valent {Pt(μ-pz)}$_2$ Complexes. In addition to elemental analysis, the most valuable information for the full characterization of these new complexes came from their ^{1}H and ^{195}Pt{^{1}H} NMR spectra in solution (Figures S2−S4 and S7−S12). All these Pt_2 complexes, except **1a**/**b** and **3a′**, are not stable in solution at r.t. without excess of RX in the media. Thus, the characterization of all these has been carried out at low temperature. Besides, single-crystal X-ray diffraction studies on complexes **2a**, **2b**, **3a′**, and **5a** have been carried out. Their molecular structures are depicted in Figure 2, and selected bond distances and angles are given in Tables S2 and S3.

As it can be seen in Figure 2, in all of them, the Pt_2N_4 rings exhibit a boat-like shape (angle between the Pt−N−N−Pt fragments being 73.0° **2a**, 71.7° **2b**, 89.32° **3a′**, and 89.64° **5a**) with an anti-configuration of the C^C* groups (C1−Pt−Pt#−

https://doi.org/10.1021/acs.inorgchem.2c01441
Inorg. Chem. 2022, 61, 12559−12569

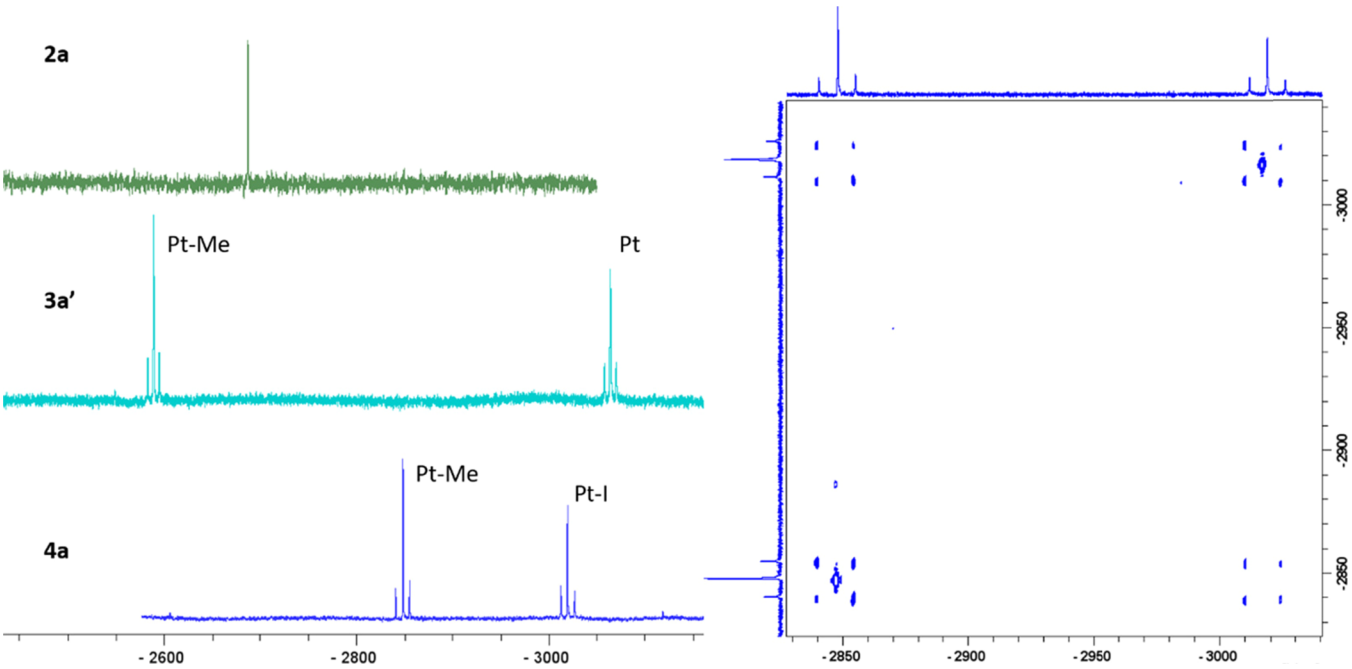

Figure 4. Left: ^{195}Pt{^{1}H} NMR spectra in CD_2Cl_2 of **2a**, **3a′**, and **4a**. Right: ^{195}Pt−^{195}Pt{^{1}H} COSY spectrum of **4a** in CD_2Cl_2.

C#1 torsion angles: 96.7(4)° **2a**, 96.1(2)° **2b**; C1−Pt1−Pt2−C14 torsion angles: 79.29° **3a′**, 72.92° **5a**).

The molecular structures of the cationic complexes, $[\{Pt^{IV}(C\text{^}C^*)Me(\mu\text{-}pz)\}_2(\mu\text{-}I)]^+$, in **2a** and **2b** consist of a Pt_2(IV,IV) core bridged by two pyrazolates and one iodide ligand. The intermetallic distances (d_{Pt-Pt}: 3.5909(9) Å **2a**, 3.6228(6) Å **2b**) are in between the observed ones in the Pt_2(IV,IV) compounds (PPN)$[\{Pt^{IV}Me_3(\mu\text{-}pz)\}_2(\mu\text{-}I)]$ (d_{Pt-Pt}: 3.706(1) Å)[29] and (PPh_4) $[\{Pt^{IV}Me_2Br(\mu\text{-}pz)\}_2(\mu\text{-}Br)]$ (d_{Pt-Pt}: 3.593(1) Å).[30] The Pt^{IV} centers exhibit octahedral $PtIN_2C_3$ coordination environments with the axial positions occupied by one Me group and the iodine bridge, the Pt−I−Pt angle being close to 80° (81.55(2) **2a**, 82.69(13) **2b**). The Pt−I, Pt−N, and Pt−C distances seem to be not affected by the metal oxidation state since they are quite similar to those observed in Pt_2(III,III) complexes containing the same kind of ligands.[26,27]

The cationic complex $[Pt_2(C\text{^}C^*_A)_2(\mu\text{-}pz)_2Me]^+$ in **3a′** and **5a** show short intermetallic distances (d_{Pt-Pt}: 2.6700(4) Å **3a′**, 2.6545(5) Å **5a**) indicative of the existence of a Pt−Pt bond in each of them. All bond distances and angles are very similar to those observed in analogous complexes with the $[(C\text{^}C^*)\text{-}Pt^{III}(\mu\text{-}pz)]_2$ core and octahedral environment at each Pt center.[26,27] In **3a′**, the platinum centers show different coordination environments: octahedral for Pt1 with the Pt2 and the methyl group (C33) in the *apex* positions and distorted square pyramidal for Pt2, with Pt1 in the *apex* position. The intermetallic distance in **3a′** is in the range reported for "$Pt_2^{III}(\mu\text{-}L)_2R$" species, no matter if they exhibit an octahedral environment of each Pt center [2.529(1)−2.7910(2) Å][32,33] or octahedral geometry at one and square pyramidal at the other center. The latter is exemplified by complex $[R(H_3N)_2Pt(\mu\text{-}L\text{-}N,O)_2Pt(NH_3)_2]^{3+}$ (L-*N*,*O*- = amidate or pyridonate) [2.676(1)−2.7542(11) Å].[34−41]

Regarding pyrazolate-bridged complexes, the intermetallic distance in **3a′** is a little longer than those in $[(CHX_2)(C\text{^}C^*)\text{-}Pt^{III}(\mu\text{-}pz)Pt^{III}(C\text{^}C^*)X]$,[26,27] ($d_{Pt-Pt}$ = 2.6302(4) Å X = Br; 2.6324(3) Å X = I) or in **5a**, which can be attributed to the larger *trans* influence of CH_3 compared to CHX_2 and CH_2Ph.

The NMR spectra of the Pt−Me derivatives, **2a**, **2b**, **3a′**, **4a**, and **Int′-Me**, as well as the Pt−Bn ones, **5a** and **6a**, were performed in CD_2Cl_2 solution (see Table 1 and Figures 3 and 4).

Their ^{1}H NMR and ^{195}Pt{^{1}H} NMR spectra showed that in all cases, the major isomer is that observed in the X-ray single-crystal structures, with the C^C* groups in an *anti*-conformation, which provided structurally relevant details. In agreement with the absence of metal−metal interactions and their symmetry, the Pt_2(IV,IV) complexes **2a**, **2b**, and **6a** show the coupling to just one ^{195}Pt nucleus (see $^{2}J_{Pt\text{-}H}$ in Table 1) of their corresponding Pt−R (R = CH_3, CH_2Ph) ^{1}H NMR signals. Besides, their ^{195}Pt{^{1}H} NMR spectra exhibit just one singlet in the typical spectral range for Pt(IV) compounds (see Table 1 and Figure 4 for **2a**).[42]

By contrast, in compounds **3a′**, **4a**, and **5a**, the NMR spectra denote the non-equivalence of two Pt fragments joined by a metal−metal bond. That is, each compound exhibits a signal due to the Pt-CH_3 (singlet) or Pt-CH_2Ph (doublet) flanked by two sets of ^{195}Pt satellites in its ^{1}H NMR spectrum and two singlets in the ^{195}Pt{^{1}H} NMR one, each one flanked by ^{195}Pt satellites.

The existence of a Pt−Pt bond was confirmed by a ^{195}Pt−^{195}Pt{^{1}H} COSY spectrum, which displays a crosspeak due to scalar coupling (Figure 4 right for **4a** and S6 for **3a′**).

The assignment of these resonances was made from ^{1}H−^{195}Pt HMQC and ^{1}H {selective^{195}Pt} NMR experiments.

All the ^{195}Pt signals appear clearly downfield-shifted with respect to those of the Pt_2(II,II) complexes, **1a** and **1b** (Table 1), according to the higher oxidation state of the metal centers. They appear more deshielded as the oxidation state is higher [see δ^{195}Pt for Pt^{IV}-CH_3 (**2a**) and Pt^{IV}-CH_2Ph (**6a**) vs Pt^{III}-CH_3 (**4a**) and Pt^{III}-CH_2Ph (**5a**)], and the electronegativity of the axial ligand is greater [see δ^{195}Pt for Pt−Br (**5a**) vs Pt−I (**4a**)]. Besides, a downfield shift of the ^{195}Pt-CH_2Ph resonances with respect to the ^{195}Pt−Me one is observed (see δ^{195}Pt for **6a** vs **2a**), which is attributed to the effect of the π system of the benzyl fragment.[43]

https://doi.org/10.1021/acs.inorgchem.2c01441
Inorg. Chem. 2022, 61, 12559−12569

The proposed structure for complex **Int′-Me** was based on its NMR data. The presence of two singlets in the spectral range expected for Pt^{II} and Pt^{IV} and the absence of platinum satellites in its $^{195}Pt\{^{1}H\}$ NMR spectrum denote the mixed-valence nature of **Int′-Me** and the absence of a metal−metal bond between the platinum centers. This fact was confirmed by its ^{1}H NMR spectrum, which shows only one singlet corresponding to the Pt−Me group flanked just by one set of platinum satellites (Table 1, Figure S10).

The complex cation in **3a′** deserves some additional attention. In this complex, the average oxidation number of the platinum centers is +3, but it can be regarded as a metal−metal bonded Pt_2(III,III) complex with just one axial ligand, or as a mixed valence Pt_2(II,IV) one[44] with the metals linked by a $Pt^{II} \rightarrow Pt^{IV}$ donor−acceptor bond. The short intermetallic distance (2.6700(4) Å) observed in the X-ray structure points to a Pt_2(III,III) formulation, while the NMR data (Figure S7) point to a $Pt^{II} \rightarrow Pt^{IV}$ one. In this sense, the different coordination environments of the Pt centers cause a big separation between the two ^{195}Pt resonances up to 480 ppm. The one corresponding to Pt−Me appears even more deshielded than that in the Pt_2(IV,IV) compounds (**2a** and **2b**), while the other is shielded 50 ppm with respect to the Pt−I resonance in the Pt_2(III,III) complex **4a**. To help determine the correct oxidation states of the Pt centers, we performed additional computational and electrochemical studies. The Mulliken population analysis in MeCN for **3a′** provided an estimated partial charge for the two platinum centers (0.49 Pt, 0.46 Pt−Me) not much different one to another, the difference (Δ = 0.03) being even lower than in the Pt_2(III,III) complex, **4a** (0.35 Pt−I, 0.40 Pt−Me, Δ = 0.05). The Pt−Pt MO bond order in **3a′** (0.38) is close to the calculated value for the Pt_2(II,II) complex **1a** (0.39) and smaller than that found for the Pt_2(III,III) complex **4a** (0.59). These calculations are consistent with a Pt_2(III,III) ↔ Pt_2(II,IV) formulations, the contribution of the Pt_2(II,IV) one being significant, in line with earlier calculations on catalytic processes involving $[\{Pd^{III}(C\text{^}N)(OAc)\}_2XY]$. They showed that when a strong σ-donor group is "axially" coordinated to one of the metal centers in dinuclear complexes, the dz^2 orbital from the other metal gets populated, increasing the M(II) character and favoring the Pt_2(II,IV) formulation.[45] Therefore, in our case, the presence of Me as the electron-donating group in **3a′** would increase the Pt_2(II,IV) contribution to this molecule.

In this sense, oxidative CV in MeCN showed for **3a′** an irreversible oxidation at 0.39 V (given vs the Fc+/Fc couple). The value is quite similar to that of **1a**, 0.44 V, measured under the same conditions and to the related cyclometalated pyrazolate-bridged dinuclear platinum(II) complexes,[46] while being far from the value observed for the Pt_2(III,III) complex $[\{Pt(C\text{^}C^*_A)(\mu\text{-pz})I\}_2]$ (Figure S14). In the Pt_2(II,II) complexes, the irreversibility of this oxidation process has been attributed to the square-planar geometry of each Pt(II) unit with little or no metal−metal interaction. In them, the metal centers are highly susceptible to nucleophilic attack by coordinating solvents, such as MeCN, resulting in permanent oxidized products. Therefore, a mixed-valence Pt_2(II,IV) formulation with the metals linked by a $Pt^{II} \rightarrow Pt^{IV}$ donor−acceptor bond seems to be the most likely for **3a′** in MeCN solution, which is also compatible with the observed metal−metal coupling.[47] According to that, we observed that compound **3a′** reacted with MeI in acetonitrile to give **2a′**.

CONCLUSIONS

Compound $[\{Pt^{II}(C\text{^}C^*_A)(\mu\text{-pz})\}_2]$ (**1a**) reacted with MeI and BnBr at room temperature in the dark to give the high-valent dinuclear complexes $[\{Pt^{IV}(C\text{^}C^*_A)Me(\mu\text{-pz})\}_2(\mu\text{-I})]I$ (**2a**) and $[Br(C\text{^}C^*_A)Pt^{III}(\mu\text{-pz})_2Pt^{III}(C\text{^}C^*_A)Bn]$ (**5a**), resulting from the double or single OA of RX, respectively. Also, $[\{Pt^{II}(C\text{^}C^*_B)(\mu\text{-pz})\}_2]$ (**1b**) reacted with MeI, affording $[\{Pt^{IV}(C\text{^}C^*_B)Me(\mu\text{-pz})\}_2(\mu\text{-I})]I$ (**2b**), indicating that the CO_2Et substituent in $C\text{^}C^*_A$ does not affect the redox behavior of these Pt_2(II,II) compounds **1a** and **1b**. DFT modeling of the S_N2 mechanisms for the OA of RX to **1a** proposed species such as $[(C\text{^}C^*_A)Pt(\mu\text{-pz})_2Pt(C\text{^}C^*_A)R]X$ (RX = MeI **Int-Me**, BnBr **Int-Bn**) as intermediates for the first OA reaction. Once formed, two species are accessible, $[X(C\text{^}C^*_A)Pt^{III}(\mu\text{-pz})_2Pt^{III}(C\text{^}C^*_A)R]$(RX = MeI **4a**, BnBr **5a**) and $[(C\text{^}C^*_A)\text{-}Pt^{II}(\mu\text{-pz})_2Pt^{IV}(C\text{^}C^*_A)(R)X]$ (RX = MeI **Int′-Me**, BnBr **Int′-Bn**), the latter being the intermediate for the second OA. Keeping in mind the small energy barrier for the transformation of **Int-R** into **Int′-R**, the free energy difference between the species Pt_2(III,III) (**4a** or **5a**) and Pt_2(II,IV) (**Int′-Me**, **Int′-Bn**) seems to determine the nature of the compounds obtained at r.t. When it is small ($\Delta G_{Int'\text{-}Me\text{-}4a}$ = 4.03 kcal/mol), the feasible formation of **Int′-Me** allows the second OA to occur, providing the Pt_2(IV,IV) complex, **2a**. When it is bigger ($\Delta G_{Int'\text{-}Bn\text{-}5a}$ = 7.83 kcal/mol), the reaction leads to the selective formation of the Pt_2(III,III) complex **5a**. In this case, the second OA to get $[\{Pt^{IV}(C\text{^}C^*_A)Bn(\mu\text{-pz})\}_2(\mu\text{-Br})]Br$ (**6a**) is possible under harder conditions. Species **Int-Me** could be prepared and isolated as the BF_4 salt, **3a′**, and then used to get **4a**, **Int′-Me**, and **2a′**, which indicate this computed mechanism as the most likely one and allow us to compare structural and spectroscopic data for complexes with the same core $[\{Pt(C\text{^}C^*)(\mu\text{-pz})\}_2]$ but different oxidation states.

ASSOCIATED CONTENT

Supporting Information

The Supporting Information is available free of charge at https://pubs.acs.org/doi/10.1021/acs.inorgchem.2c01441.

Information about general procedures and materials; X-ray structure determinations (CCDC 2160386−2160389); crystallographic data; DFT and electrochemistry methods; and multinuclear and NMR spectra and CV for characterization and mechanism's determination and selected bond angles and lengths in the X-ray structures of **2a**, **2b**, **3a′**, and **5a** (PDF)

Accession Codes

CCDC 2160386−2160389 contain the supplementary crystallographic data for this paper. These data can be obtained free of charge via www.ccdc.cam.ac.uk/data_request/cif, or by emailing data_request@ccdc.cam.ac.uk, or by contacting The Cambridge Crystallographic Data Centre, 12 Union Road, Cambridge CB2 1EZ, UK; fax: +44 1223 336033.

AUTHOR INFORMATION

Corresponding Authors

Daniel Escudero − *Department of Chemistry, KU Leuven, 3001 Leuven, Belgium;* orcid.org/0000-0002-1777-8578; Email: daniel.escudero@kuleuven.be

Sara Fuertes − *Departamento de Química Inorgánica, Facultad de Ciencias, Instituto de Síntesis Química y Catálisis Homogénea (ISQCH), CSIC − Universidad de Zaragoza,*

50009 Zaragoza, Spain; orcid.org/0000-0003-1812-3175; Email: sfuertes@unizar.es

Violeta Sicilia − *Departamento de Química Inorgánica, Escuela de Ingeniería y Arquitectura de Zaragoza, Instituto de Síntesis Química y Catálisis Homogénea (ISQCH), CSIC − Universidad de Zaragoza, 50018 Zaragoza, Spain;* orcid.org/0000-0002-0257-0483; Email: sicilia@unizar.es

Authors

Lorenzo Arnal − *Departamento de Química Inorgánica, Facultad de Ciencias, Instituto de Síntesis Química y Catálisis Homogénea (ISQCH), CSIC − Universidad de Zaragoza, 50009 Zaragoza, Spain;* orcid.org/0000-0002-0283-9307

Antonio Martin − *Departamento de Química Inorgánica, Facultad de Ciencias, Instituto de Síntesis Química y Catálisis Homogénea (ISQCH), CSIC − Universidad de Zaragoza, 50009 Zaragoza, Spain;* orcid.org/0000-0002-4808-574X

Complete contact information is available at: https://pubs.acs.org/10.1021/acs.inorgchem.2c01441

Author Contributions

The manuscript was written through contributions of all authors. All authors have given approval to the final version of the manuscript.

Funding

This work was supported by the Spanish Ministerio de Economia y Competitividad (Ministerio de Ciencia Innovacion y Universidades)/FEDER (Project PGC2018−094749-B-I00), by the Gobierno de Aragon (Grupo E17_20R: Química Inorgánica y de los Compuestos Organometálicos) and by Internal Funds KU Leuven and FWO.

Notes

The authors declare no competing financial interest.

■ ACKNOWLEDGMENTS

This work was supported by the Spanish Ministerio de Economia y Competitividad (Ministerio de Ciencia Innovacion y Universidades)/FEDER (Project PGC2018-094749-B-I00), by the Gobierno de Aragon (Grupo E17_20R: Química Inorgánica y de los Compuestos Organometálicos) and by Internal Funds KU Leuven and FWO. L.A. acknowledges the support of a grant from the Gobierno de Aragón. The authors thank Dr. I. Delso and Prof. Dr. J. M. Casas at the Instituto de Síntesis Química y Catálisis Homogénea (ISQCH) for their guidance on special NMR experiments and CV, respectively.

■ REFERENCES

(1) Powers, D. C.; Ritter, T. Bimetallic Redox Synergy in Oxidative Palladium Catalysis. *Acc. Chem. Res.* **2012**, *45*, 840−850.

(2) Souillart, L.; Parker, E.; Cramer, N. Highly Enantioselective Rhodium(I)-Catalyzed Activation of Enantiotopic Cyclobutanone C−C bonds. *Angew. Chem., Int. Ed.* **2014**, *53*, 3001−3005.

(3) Chen, B.; Fang, C.; Liu, P.; Ready, J. M. Rhodium-Catalyzed Enantioselective Radical Addition of CX_4 Reagents to Olefins. *Angew. Chem., Int. Ed.* **2017**, *56*, 8780−8784.

(4) Li, X.; Wu, H.; Lang, Y.; Huang, G. Mechanism, Selectivity, and Reactivity of Iridium- and Rhodium-Catalyzed Intermolecular Ketone α-Alkylation with Unactivated Olefins via an Enamide Directing Strategy. *Catal. Sci. Technol.* **2018**, *8*, 2417−2426.

(5) Heng, D.; Chen, H.; He, X.; Liu, S.; Zhu, L.; Zhong, K.; Zhang, T.; Bai, R.; Lan, Y. Synergistic Dinuclear Rhodium Induced Rhodium-Walking Enabling Alkene Terminal Arylation: A Theoretical Study. *ACS Catal.* **2021**, *11*, 3975−3987.

(6) Hetterscheid, D. G. H.; Chikkali, S. H.; de Bruin, B.; Reek, J. N. H. Binuclear Cooperative Catalysts for the Hydrogenation and Hydroformylation of Olefins. *ChemCatChem* **2013**, *5*, 2785−2793.

(7) Powers, I. G.; Uyeda, C. Metal−Metal Bonds in Catalysis. *ACS Catal.* **2016**, *7*, 936−958. and references therein

(8) Xu, W.; Li, M.; Qiao, L.; Xie, J. Recent Advances of Dinuclear Nickel- and Palladium-Complexes in Homogeneous Catalysis. *Chem. Commun.* **2020**, *56*, 8524−8536.

(9) Wang, W.; Ji, C. L.; Liu, K.; Zhao, C. G.; Li, W.; Xie, J. Dinuclear Gold Catalysis. *Chem. Soc. Rev.* **2021**, *50*, 1874−1912.

(10) Aghakhanpour, R. B.; Rashidi, M.; Hosseini, F. N.; Raoof, F.; Nabavizadeh, S. M. Oxidation of a Rollover Cycloplatinated(II) Dimer by MeI: a Kinetic Study. *RSC Adv.* **2015**, *5*, 66534−66542.

(11) Nabavizadeh, S. M.; Sepehrpour, H.; Kia, R.; Rheingold, A. L. Bis(diphenylphosphino) acetylene as Bifunctional Ligand in Cycloplatinated Complexes: Synthesis, Characterization, Crystal Structures and Mechanism of MeI Oxidative Addition. *J. Organomet. Chem.* **2013**, *745*−*746*, 148−157.

(12) Jamali, S.; Nabavizadeh, S. M.; Rashidi, M. Binuclear Cyclometalated Organoplatinum Complexes Containing 1,1′-Bis(diphenylphosphino)ferrocene as Spacer Ligand: Kinetics and Mechanism of MeI Oxidative Addition. *Inorg. Chem.* **2008**, *47*, 5441−5452.

(13) Roundhill, D. M.; Dickson, M. K.; Atherton, S. J. Thermal and Photochemical Addition of Alkyl and Aryl Halides to Tetrakis(μ-pyrophosphito) Diplatinum(II) Tetraanion. *J. Organomet. Chem.* **1987**, *335*, 413−422.

(14) Sicilia, V.; Baya, M.; Borja, P.; Martín, A. Oxidation of Half-Lantern Pt_2(II,II) Compounds by Halocarbons. Evidence of Dioxygen Insertion into a Pt(III)−CH3Bond. *Inorg. Chem.* **2015**, *54*, 7316−7324.

(15) Nabavizadeh, S. M.; Aseman, M. D.; Ghaffari, B.; Rashidi, M.; Hosseini, F. N.; Azimi, G. Kinetics and Mechanism of Oxidative Addition of MeI to Binuclear Cycloplatinated Complexes Containing Biphosphine Bridges: Effects of Ligands. *J. Organomet. Chem.* **2012**, *715*, 73−81.

(16) Jamali, S.; Nabavizadeh, S. M.; Rashidi, M. Oxidative Addition of Methyl Iodide to a New Type of Binuclear Platinum(II) Complex: a Kinetic Study. *Inorg. Chem.* **2005**, *44*, 8594−8601.

(17) Oro, L. A.; Sola, E.; López, J. A.; Torres, F.; Elduque, A.; Lahoz, F. J. Synthesis of $[Ir_2(\mu\text{-}Pz)_2(CH_3)(CO)_2(PiPr_3)_2]^+$. A key Intermediate in S_N2 Oxidative Addition of Halocarbons to Dinuclear Complexes. *Inorg. Chem. Commun.* **1998**, *1*, 64−67.

(18) Atwood, J. L.; Beveridge, K. A.; Bushnell, G. W.; Dixon, K. R.; Eadie, D. T.; Stobart, S. R.; Zaworotko, M. J. Pyrazolyl-Bridged Iridium Dimers. 6. Two-Fragment, Two-Center Oxidative Addition of Halogens and Methyl Halides to *trans*-Bis(triphenylphosphine)-dicarbonylbis(μ-pyrazolyl)diiridium(I). *Inorg. Chem.* **1984**, *23*, 4050−4057.

(19) Fjeldsted, D. O. K.; Stobart, S. R.; Zaworotko, M. J. Pyrazolyl-Bridged Iridium Dimers. 10. Sequential Addition at the Metal Centers in a Diiridium Configuration. Oxidatively Induced Relocation of a Bent, Terminal Nitrosyl Group to Occupy a Bridging Site. *J. Am. Chem. Soc.* **1985**, *107*, 8258−8259.

(20) Casado, M. A.; Pérez-Torrente, J. J.; Ciriano, M. A.; Dobrinovitch, I. T.; Lahoz, F. J.; Oro, L. A. Stereoselective Oxidative Additions of Iodoalkanes and Activated Alkynes to a Sulfido-Bridged Heterotrinuclear Early−Late ($TiIr_2$) Complex. *Inorg. Chem.* **2003**, *42*, 3956−3964.

(21) Kalck, P.; Bonnet, J. J. Oxidative Addition of Halogens to Thiolato-Bridged Dinuclear Iridium(I) Complexes. Preparation of Several Iridium(II) and Iridium(III) Species. X-ray Structure of $Ir_2(\mu\text{-}t\text{-}BuS)_2(CO)_2(PMe_2Ph)_2I_2$. *Organometallics* **1982**, *1*, 1211−1216.

(22) Kolel-Veetil, M. K.; Rheingold, A. L.; Ahmed, K. J. Oxidative Addition Reactions of the Bridging Amido Complex $Ir_2[\mu\text{-}NH(p\text{-}tolyl)]_2(CO)_4$: X-ray Crystal Structure of the 16e-18e Dimer

$Ir_2(Me)(I)[\mu$-NH(p-tolyl)$]_2(CO)_4\cdot 0.25C_6H_{14}$. *Organometallics* **1993**, *12*, 3439−3446.
(23) Schenck, T. G.; Milne, C. R. C.; Sawyer, J. F.; Bosnich, B. Bimetallic Reactivity. Oxidative-Addition and Reductive-Elimination Reactions of Rhodium and Iridium Bimetallic Complexes. *Inorg. Chem.* **1985**, *24*, 2338−2344.
(24) Tejel, C.; Ciriano, M. A.; Edwards, A. J.; Lahoz, F. J.; Oro, L. A. Metal Basicity of Dirhodium and Diiridium Complexes Induced by Isocyanide Ligands. Model for the Oxidative-Addition Reaction of Methyl Iodide with Dinuclear Complexes. *Organometallics* **1997**, *16*, 45−53.
(25) Tejel, C.; Ciriano, M. A.; López, J. A.; Lahoz, F. J.; Oro, L. A. Oxidative-Addition of Organic Monochloro Derivatives to Dinuclear Iridium Complexes: The Detection of Tautomeric Equilibria and Their Implications on the Reactivity. *Organometallics* **2000**, *19*, 4977−4984.
(26) Arnal, L.; Fuertes, S.; Martín, A.; Baya, M.; Sicilia, V. A Cyclometalated N-Heterocyclic Carbene: The Wings of the First Pt_2 (II,II) Butterfly Oxidized by CHI_3. *Chem. − Eur. J.* **2018**, *24*, 18743−18748.
(27) Sicilia, V.; Arnal, L.; Fuertes, S.; Martin, A.; Baya, M. Metal-Metal Cooperation in the Oxidation of a Flapping Platinum Butterfly by Haloforms: Experimental and Theoretical Evidence. *Inorg. Chem.* **2020**, *59*, 12586−12594.
(28) Sicilia, V.; Arnal, L.; Chueca, A. J.; Fuertes, S.; Babaei, A.; Igual Munoz, A. M.; Sessolo, M.; Bolink, H. J. Highly Photoluminescent Blue Ionic Platinum-Based Emitters. *Inorg. Chem.* **2020**, *59*, 1145−1152.
(29) Lindner, R.; Kaluđerović, G. N.; Paschke, R.; Wagner, C.; Steinborn, D. Synthesis and Characterization of Dinuclear Pyrazolato Bridged Platinum(IV) Complexes. *Polyhedron* **2008**, *27*, 914−922.
(30) Kelly, M. E.; Gómez-Ruiz, S.; Kluge, R.; Merzweiler, K.; Steinborn, D.; Wagner, C.; Schmidt, H. Studies of Mononuclear and Dinuclear Complexes of Dibromodimethylplatinum(IV): Preparation, Characterization and Crystal Structures. *Inorg. Chim. Acta* **2009**, *362*, 1323−1332.
(31) Tejel, C.; Ciriano, M. A.; Edwards, A. J.; Lahoz, F. J.; Oro, L. A. Oxidative-Addition of Organic Monochloro Derivatives to Dinuclear Rhodium Complexes: Mechanistic Considerations. *Organometallics* **2000**, *19*, 4968−4976.
(32) Yamaguchi, T.; Sasaki, Y.; Ito, T. Unusual C,O-Bridging Coordination of Acetate and Acetylacetonate Ligands in the Platinum Clusters, $[Pt^{III}_2(\mu\text{-}CH_2COO\text{-}C,O)_2(\mu\text{-}CH_3COO\text{-}O,O')_2Cl_2]^{2-}$ and $PtII_4(\mu\text{-}CH_3COO\text{-}O,O')_4(\mu\text{-}CH_3COCHCOCH_3\text{-}O,C^3)_4$. *J. Am. Chem. Soc.* **1990**, *112*, 4038−4040.
(33) Che, C. M.; Mak, T. C. W.; Gray, H. B. A Dimeric Platinum(III) System Containing a Long Metal-Metal Bond. Crystal Structure of $K_4[Pt_2(P_2O_5H_2)_4CH_3I]\cdot 2H_2O$. *Inorg. Chem.* **1984**, *23*, 4386−4388.
(34) Ochiai, M.; Fukui, K.; Iwatsuki, S.; Ishihara, K.; Matsumoto, K. Synthesis of Aryl-Platinum Dinuclear Complexes via ortho C−H Bond Activation of Phenol and Transmetalation of Arylboronic Acid. *Organometallics* **2005**, *24*, 5528−5536.
(35) Matsumoto, K.; Arai, S.; Ochiai, M.; Chen, W.; Nakata, A.; Nakai, H.; Kinoshita, S. Synthesis of the Pivalamidate-Bridged Pentanuclear Platinum(II,III) Linear Complexes with Pt···Pt Interactions. *Inorg. Chem.* **2005**, *44*, 8552−8560.
(36) Ochiai, M.; Lin, Y.-S.; Yamada, J.; Misawa, H.; Arai, S.; Matsumoto, K. Reactions of a Platinum(III) Dimeric Complex with Alkynes in Water: Novel Approach to α-Aminoketone, α-Iminoketone, and α,β-Diimine via Ketonyl−Pt(III) Dinuclear Complexes. *J. Am. Chem. Soc.* **2004**, *126*, 2536−2545.
(37) Matsumoto, K.; Ochiai, M. Organometallic Chemistry of Platinum-Blue Derived $Platinum^{III}$ Dinuclear Complexes. *Coord. Chem. Rev.* **2002**, *231*, 229−238.
(38) Lin, Y.-S.; Misawa, H.; Yamada, J.; Matsumoto, K. Synthesis of Ketonylplatinum(III) Dinuclear Complexes: Observation of the Competitive Radical vs Electrophilic Displacement in Pt(III)-Promoted C−H Bond Activation of Ketones. *J. Am. Chem. Soc.* **2001**, *123*, 569−575.
(39) Lin, Y.-S.; Takeda, S.; Matsumoto, K. Consecutive Double Nucleophilic Attacks on an Olefin Promoted by a Platinum(III) Dimeric Complex. *Organometallics* **1999**, *18*, 4897−4899.
(40) Matsumoto, K.; Nagai, Y.; Matsunami, J.; Mizuno, K.; Abe, T.; Somazawa, R.; Kinoshita, J.; Shimura, H. A Synthetic Route to Alkyl−Pt^{III} Dinuclear Complexes from Olefins and Its Implication on the Olefin Oxidation Catalyzed by Amidate-Bridged PtIII Dinuclear Complexes. *J. Am. Chem. Soc.* **1998**, *120*, 2900−2907.
(41) Matsumoto, K.; Matsunami, J.; Mizuno, K.; Uemura, H. Organometallic Chemistry of an Amidate-Bridged Dinuclear Pt(III) Complex: Axial Pt(III)−Alkyl σ-Bond Formation in the Reaction with Acetone. *J. Am. Chem. Soc.* **1996**, *118*, 8959−8960.
(42) Still, B. M.; Kumar, P. G.; Aldrich-Wright, J. R.; Price, W. S. ^{195}Pt NMR-Theory and Application. *Chem. Soc. Rev.* **2007**, *36*, 665−686.
(43) Priqueler, J. R. L.; Butler, I. S.; Rochon, F. D. An Overview of ^{195}Pt Nuclear Magnetic Resonance Spectroscopy. *Appl. Spectrosc. Rev.* **2006**, *41*, 185−226.
(44) Canty, A. J.; Gardiner, M. G.; Jones, R. C.; Rodemann, T.; Sharma, M. Binuclear Intermediates in Oxidation Reactions: $[(Me_3SiC{\equiv}C)Me_2(bipy)Pt{-}PtMe_2(bipy)]^+$ in the Oxidation of $Pt^{II}Me_2(bipy)$ (bipy = 2,2′-Bipyridine) by $IPh(C{\equiv}CSiMe_3)(OTf)$ (OTf = Triflate). *J. Am. Chem. Soc.* **2009**, *131*, 7236−7237.
(45) Ariafard, A.; Hyland, C. J.; Canty, A. J.; Sharma, M.; Brookes, N. J.; Yates, B. F. Ligand Effects in Bimetallic High Oxidation State Palladium Systems. *Inorg. Chem.* **2010**, *49*, 11249−11253.
(46) Chakraborty, A.; Deaton, J. C.; Haefele, A.; Castellano, F. N. Charge-Transfer and Ligand-Localized Photophysics in Luminescent Cyclometalated Pyrazolate-Bridged Dinuclear Platinum(II) Complexes. *Organometallics* **2013**, *32*, 3819−3829.
(47) Horiuchi, S.; Moon, S.; Ito, A.; Tessarolo, J.; Sakuda, E.; Arikawa, Y.; Clever, G. H.; Umakoshi, K. Multinuclear Ag Clusters Sandwiched by Pt Complex Units: Fluxional Behavior and Chiral-at-Cluster Photoluminescence. *Angew. Chem., Int. Ed.* **2021**, *60*, 10654−10660.

Global Discussion

Methodology

M.1. Synthetic Procedures and Materials

Unless otherwise stated, reactions and manipulations were carried out under open atmosphere. In the case of unstable products, they were carried out under pure argon using Schlenk techniques. Deaerated and anhydrous solvents were used from a solvent purification system (MBraun SPS-800) or treated with the corresponding molecular sieves. Deuterated solvents for NMR spectroscopy were also treated with activated molecular sieves and deaerated by Freeze-Pump technique.

All other chemicals were purchased from standard commercial suppliers and used as received. BnI was prepared by reaction of the BnOH with I_2 and PPh_3.[36]

Compounds [{Pt(C^C*$_{A/B}$)(μ-Cl)}$_2$] (EtO_2C-CH^C*= 1-(4-(ethoxycarbonyl)phenyl)-3-methyl-1*H*-imidazol-2-ylidene (**A**),[37] H-CH^C* = 1-phenyl-3-methyl-1*H*-imidazol-2-ylidene (**B**)[32]) were prepared by using a step by step synthetic procedure and were used as starting materials.

Synthesis of [Pt(C^C*$_A$)(3,5-dmpzH)$_2$Cl] (1a)

3,5-dmpzH (46.5 mg, 0.48 mmol) was added to a suspension of **A** (100.0 mg, 0.11 mmol) in acetone (30 mL) at r.t. and the mixture stirred for 24 h. Then the solvent was removed under reduced pressure. The residue was treated with n-hexane/Et_2O (20/1 mL) and the resulting solid was filtered, and washed with n-hexane to give **1a** as a yellow solid. Yield: 133.4 mg (61%).

Synthesis of [Pt(C^C*$_A$)(4-MepzH)$_2$Cl] (2a)

Complex **2a** was synthesized following the same procedure used for **1a** with 4-MepzH (22 µL, 0.27 mmol) and **A** (54 mg, 0.06 mmol). **2a**, yellow solid. Yield: 35.0 mg (64%).

Synthesis of [Pt(C^C*$_A$)(pzH)$_2$Cl] (3a)

Complex **3a** was synthesized following the same procedure used for **1a** with pzH (20.6 mg, 0.30 mmol) and **A** (61.3 mg, 0.07 mmol). **3a**, yellow solid. Yield: 31.4 mg (60%).

Synthesis of [Pt(C^C*$_A$)(3,5-dmpzH)$_2$]ClO$_4$ (1b)

$AgClO_4$ (45.5 mg, 0.22 mmol) was added to a stirred suspension of **A** (100.0 mg, 0.11 mmol) in acetone (50 mL) in the dark at r.t. After 2 h of reaction, 3,5-dmpzH (42.2 mg, 0.44 mmol) was added to the mixture and allowed to react for 16.5 h in the dark. Then, the resulting suspension was filtered through Celite and the solvent was removed under reduced pressure. The residue was treated with *n*-hexane/Et_2O (20 mL /1 mL) and filtered to give **1b** as a pale yellow solid. Yield: 110.7 mg (71 %).

Synthesis of [Pt(C^C*$_A$)(4-MepzH)$_2$]ClO$_4$ (2b)

$AgClO_4$ (45.5 mg, 0.22 mmol) was added to a stirred suspension of **A** (100.0 mg, 0.11 mmol) in acetone (50 mL) in the dark at r.t. After 3 h, 4-MepzH (36 μL, 0.44 mmol) was added to the mixture and allowed to react for 14 h in the dark. Then, the resulting suspension was filtered through Celite and the solvent was evaporated to dryness. The residue was treated with *n*-hexane/Et_2O (20 mL /1 mL)and filtered, to give **2b** as a pale yellow solid. Yield: 133.5 mg (89 %).

Synthesis of [Pt(C^C*$_A$)(pzH)$_2$]ClO$_4$ (3b)

Complex **3b** was synthesized following the same procedure used for **2b** with $AgClO_4$ (46.2 mg, 0.22 mmol), **A** (101.4 mg, 0.11 mmol) and pzH (30.0 mg, 0.44 mmol). **3b**, white solid. Yield: 114.0 mg (78 %).

Synthesis of [Pt(C^C*$_A$)(3,5-dmpzH)$_2$]PF$_6$ (1c)

$AgPF_6$ (44.0 mg, 0.17 mmol) was added to a stirred suspension of **A** (80.0 mg, 0.09 mmol) in acetone (50 mL) in the dark at r.t. After 3 h, 3,5-dmpzH (33.79 mg, 0.35 mmol) was added to the mixture and allowed to react for 14 h in the dark. Then, the resulting suspension was filtered through Celite and the solvent was evaporated to dryness. The residue was treated with *n*-hexane/Et_2O (20 mL /1 mL) and filtered to give **1c** as a pale yellow solid. Yield: 60.0 mg (45 %).

Synthesis of *syn-/anti*-[{Pt(C^C*$_A$)(μ-pz)}$_2$] (4)

Method A: Compound **A** (100.0 mg, 0.11 mmol) was added to a solution containing KOH (13.6 mg, 0.22 mmol) and pzH (14.8 mg, 0.22 mmol) in acetone/EtOH (16 mL /8 mL). After 24 h of reaction at r.t. the solvent was removed under reduced pressure, filtered and washed with 2 x 5 mL of H_2O to give **4-*anti* (92 %)/ 4-*syn* (8%)** as a yellow solid. Yield: 66.4 mg, 62 %.

Method B: NEt_3 (0.5 mL, 3.62 mmol) was added to a solution of **3b** (120 mg, 0.18 mmol) in acetone (40 mL) at r.t. After 2 h of reaction the solvent was removed in vacuo. The residue was treated with MeOH (5 mL), filtered, and washed to give **4-*anti* (86 %)/ 4-*syn* (14%)** as a yellow solid. Yield: 60.6 mg, 68 %.

Synthesis of *syn-/anti*- [{Pt(C^C*$_A$)(μ-4-Mepz)}$_2$] (5)

NEt_3 (0.5 mL, 3.62 mmol) was added to a solution of **2b** (133.5 mg, 0.19 mmol) in acetone (30 mL) at r.t. After 2 h of reaction the solvent was removed in vacuo to 2 mL. The solution was treated with H_2O (20 mL), filtered, and washed with H_2O to give **5-*anti* (83 %)/ 5-*syn* (17%)** as a yellow solid. Yield: 73.7 mg, 75 %.

Synthesis of *syn-/anti-* [{Pt(C^C*$_A$)(μ-3,5-dmpz)}$_2$] (6)

Compound **A** (106.3 mg, 0.12 mmol) was added to a solution containing NaO^{t}Bu (22.2 mg, 0.23 mmol) and 3,5-dmpzH (22.5 mg, 0.23 mmol) in acetone/EtOH (10 mL /5 mL). After 3 h of reaction at -10^{o}C, the solvent was removed to 3 mL under reduced pressure, filtered and washed with 2 x 5mL of H_2O to give **6-*anti* (80 %)/ 6-*syn* (20%)** as a yellow solid. Yield: 70 mg, 58 %.

Synthesis of *syn-/anti-* [{Pt(C^C*$_A$)(μ-3,5-dppz)}$_2$] (7)

$AgClO_4$ (52.7 mg, 0.25 mmol) was added to a stirred suspension of **A** (115.8 mg, 0.12 mmol) in acetone (30 mL) in the dark at r.t.. After 2 h of reaction, 3,5-dppzH (110.9 mg, 0.50 mmol) was added to the mixture and allowed to react overnight in the dark. Then, the resulting suspension was filtered through Celite and concentrated to *ca.* 20 mL. NEt_3 (0.5 mL, 3.62 mmol) was added to the reaction mixture and stirred for 2 h. Then, the solvent was removed in vacuo. The residue was treated with cold MeOH (5 mL) and filtered to give **7-*anti* (94%)/ 7-*syn* (6%)** as a yellow solid. Yield: 90.0 mg, 74 %.

Synthesis of [{Pt(C^C*$_A$)(3,5-dmpz)$_2$Ag}$_2$] (8)

To a solution of **1b** (150 mg, 0.21 mmol) in methanol (10 mL) was added $AgClO_4$ (45 mg, 0.21 mmol) and excess of NEt_3 (0.5 mL, 3.58 mmol). The solution was stirred for 1 h at r.t. in the dark. The resulted yellow precipitate was collected, washed with methanol, and dried in vacuum. **8**. Yield 116 mg (78%).

Synthesis of syn/*anti*-[{Pt(C^C*$_A$)(μ-pz)Cl}$_2$] (9-Cl)

Compound **4** (67.9 mg, 0.069 mmol) was allowed to react in $CHCl_3$ (15 mL) in ambient light at rt for 7.5 h. The resulting yellow solution was concentrated to *ca.* 5 mL, and 10 mL of *n*-hexane was added to the residue to give **9-Cl-*anti* (96%)/ 9-Cl-*syn* (4%)** as a yellow solid. Yield: 65 mg, 89%.

Synthesis of syn/*anti*-[{Pt(C^C*$_A$)(μ-pz)Br}$_2$] (9-Br)

$CHBr_3$ (38 μL, 0.10 mmol) was added to a solution of **4** (43 mg, 0.044 mmol) in acetone (10 mL) and allowed to react in ambient light at r.t. for 2 h. Then the solvent was removed under vacuum, the residue was treated with *n*-hexane, and this suspension was filtered to give **9-Br-*anti* (96%)/ 9-Br-*syn* (4%)** as a yellowish orange solid. Yield: 45 mg, 90%.

Synthesis of *anti*-[{Pt(C^C*$_A$)(μ-pz)I}$_2$] (9-I)

CHI_3 (83.4 mg, 0.21 mmol) was added to a solution of **4** (51.4 mg, 0.052 mmol) in acetone (15 mL) at r.t and sunlight. After 8 h of reaction the resulting suspension was concentrated to a volume of *ca*. 5 mL, filtered and washed with *n*-hexane (20 mL) to give **9-I** as a dark orange solid. Yield: 26.2 mg, 41 %.

NMR detection of *anti*- [ClPt(C^C*$_A$)(μ-pz)$_2$Pt(C^C*$_A$)CHCl$_2$] (10-Cl)

Compound **4** was allowed to react with $CHCl_3$ (1:4 molar ratio) in acetone-d_6 under argon atmosphere under UV-light (365 nm). Then, ^{1}H and ^{1}H-^{195}Pt HMQC NMR experiments were carried out at 193K.

Synthesis of *anti*- [BrPt(C^C*$_A$)(μ-pz)$_2$Pt(C^C*$_A$)CHBr$_2$] (10-Br)

$CHBr_3$ (29.0 μL, 0.33 mmol) was added in the dark to a solution of **4** (81.4 mg, 0.08 mmol) in deaerated acetone (7 mL) at rt under an argon atmosphere and allowed to react for 30 min. Then the solvent was removed under vacuum, the residue was treated with *n*-hexane, and this suspension was filtered to give **10-Br** as a yellow solid. Yield: 70.4 mg, 69%.

Synthesis of *anti*-[IPt(C^C*$_A$)(μ-pz)$_2$Pt(C^C*$_A$)CHI$_2$] (10-I)

CHI_3 (25.0 mg, 0.06 mmol) was added in the dark to a solution of **4** (50.0 mg, 0.05 mmol) in deaerated acetone (5 mL) at r.t under an argon atmosphere. After 30 min of reaction, an orange precipitate was filtered off and washed with n-hexane (5 mL) to give **10-I** as an orange solid. Yield: 30.1 mg, 43 %.

Synthesis of [{Pt(C^C*$_B$)(μ-pz)}$_2$] (4B)

$AgClO_4$ (55.1 mg, 0.263 mmol) was added to a stirred suspension of **B** (102.1 mg, 0.132 mmol) in acetone (40 mL) in the dark at r.t. After 2.5 h, pzH (35.8 mg, 0.527 mmol) was added to the mixture and allowed to react for 18.5 h in the dark. Then, the resulting suspension was filtered through Celite and the solution was concentrated to 20 mL. Afterwards, NEt_3 (0.5 mL, 3.62 mmol) was added to the solution at r.t. and let it to react for 2h. The suspension was concentrated to 15 mL and the solid was filtered and washed with 2 mL of acetone to give **4B** as a white solid. Yield: 74.0 mg, 0.088 mmol, 67%.

Synthesis of [{Pt(C^C*$_A$)Me(μ-pz)}$_2$(μ-I)]I (11)

CH_3I (26 μL, 0.403 mmol) was added to a solution of **4** (98.9 mg, 0.101 mmol) in anhydrous CH_2Cl_2 (5 mL) under argon atmosphere in the dark. After 14h of reaction, the precipitate was filtered, washed with Et_2O (4 x10 mL) and dried to give **11** as a white solid. Yield: 117.8 mg; 0.093 mmol; 92%.

Synthesis of [{Pt(C^C*$_B$)Me(μ-pz)}$_2$(μ-I)]I (11B)

CH_3I (18 μL, 0.286 mmol) was added to a suspension of **4B** (60 mg, 0.072 mmol) in anhydrous DMF (5 mL) under argon atmosphere in the dark. After 8h of reaction, 100 mL of Et_2O was added and the precipitate was filtered, washed with Et_2O (5 x 10 mL) and dried to give **11B** as a white solid. Yield: 70.7 mg; 0.063 mmol; 88 %.

Synthesis of [(C^C*$_A$)Pt(μ-pz)$_2$Pt(C^C*$_A$)Me]BF_4 (12')

Me_3OBF_4 (49.3 mg, 0.320 mmol) was added to a solution of **4** (262.0 mg, 0.267 mmol) in anhydrous CH_2Cl_2 (15 mL) under argon atmosphere in the dark at -25ºC. After 2h of reaction, the solution was dried in vacuo. The residue was treated with 20 mL of dried Et_2O and the resulting solid was filtered, washed with Et_2O (2 x 20 mL) and dried to give **12'** as a brown solid. Yield: 244.8 mg; 0.226 mmol; 85%.

Synthesis of [I(C^C*$_A$)Pt(μ-pz)$_2$Pt(C^C*$_A$)Me] (13)

KI (33.6 mg, 0.202 mmol) was added to a solution of **12'** (109.8 mg, 0.101 mmol) in MeCN (3 mL) in the dark at -25ºC. After 3h of reaction, the suspension was filtered, the solid was washed with water (7 x 10 mL) and dried to give **13** as a yellow solid. Yield: 44.0 mg; 0.039 mmol; 39%.

NMR detection of [(C^C*$_A$)Pt(μ-pz)$_2$Pt(C^C*$_A$)(Me)I] (Int'-Me(14))

PPh_4I (83.4 mg, 0.179 mmol) was added to a solution of **12'** (97.0 mg, 0.089 mmol) in anisole (5 mL) in the dark at 30ºC and the mixture was allowed to react for 2h. Then, the solvent was removed under vacuum and the residue was treated with H_2O. The resulting yellow solid was identified as [(C^C*$_A$)Pt(μ-pz)$_2$(C^C*$_A$)PtI(CH_3)] **(Int'-Me(14))** by ^1H and $^{195}Pt\{^1H\}$ NMR although anisole and PPh_4BF_4 were detected as impurities.

Synthesis of [Br(C^C*$_A$)Pt(μ-pz)$_2$Pt(C^C*$_A$)Bn] (15-Br)

BnBr (33 μL, 0.277 mmol) was added to a solution of **4** (68.0 mg, 0.069 mmol) in MeCN (20 mL) in the dark. After 3.5 h of reaction, the solvent was removed under vacuum. The residue was treated with a mixture of Et_2O and *n*-hexane (1 mL /20 mL) to give **15-Br** as an orange solid. Yield: 74.0 mg; 0.064 mmol; 93%.

Synthesis of [I(C^C*$_A$)Pt(μ-pz)$_2$Pt(C^C*$_A$)Bn] (15-I)

Compound **4** (71 mg, 0.072 mmol) was added to a solution of freshly prepared BnI (37 μL, 0.294 mmol) in MeCN (20 mL) in the dark. After 40 min of reaction, the solvent was removed under vacuum. The residue was treated with a mixture of Et_2O and *n*-hexane (1 mL /20 mL) to give **15-I** as an orange solid (75 mg; 0.062 mmol; 87 %).

Synthesis of [{Pt(C^C*$_A$)Bn(μ-pz)}$_2$(μ-Br)]Br (16)

A suspension of **15-Br** (95 mg, 0.082 mmol) in BnBr (5 mL) was heated at 70 ^{o}C for 5h. Then, the suspension was cooled down to r.t. and the resulting solid was filtered and dried to give **16**. Yield: 94.7 mg; 0.071 mmol; 87%.

M.2.Characterization Techniques

Different spectroscopic and analytical techniques have been used for the characterization of the compounds prepared in this Thesis. The equipment used and the procedures associated to each technique are shortly described in the following sections. However, specific details appear described in the Supporting Information of the papers collected in the Electronic Supplementary Material-Thesis LAV.

M.2.1.Nuclear Magnetic Resonance

In this Thesis, ^{1}H, ^{13}C, ^{19}F and ^{195}Pt NMR spectra were measured on Bruker NEO 400 or NEO 500 spectrometers, using the standard references: $SiMe_4$ for ^{1}H and ^{13}C, $CFCl_3$ for ^{19}F, and Na_2PtCl_6 in D_2O for ^{195}Pt. Most of the measurements were carried out at r.t., unless specified otherwise. All NMR data are given according to Scheme 3.

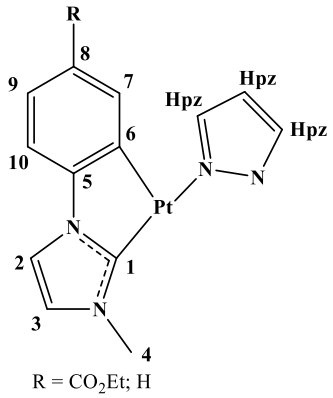

Scheme 3. Numerical scheme for NMR purpose.

As both direct and inverse experiments of ^{1}H and ^{13}C can be considered routine, we will focus on ^{195}Pt NMR experiments.

Platinum has 32 isotopes, but only ^{195}Pt presents nuclear spin 1/2. Its high natural abundance in addition to the large magnetogyric ratio (5.768×10^{7} $radT^{-1}$ s^{-1}) lead to a receptivity of 19 times that of ^{13}C.[38] Because of the large resonance window of ^{195}Pt (~ 15000 ppm) and the great shift of the signal with the oxidation state (δ_{Pt} (D_2O) = 0 ppm $[PtCl_6]^{2-}$; -1628 ppm $[PtCl_4]^{2-}$), and the bonded ligands (δ_{Pt}(D_2O) = -1628 ppm $[PtCl_4]^{2-}$; -4746 ppm $[PtCN_4]^{2-}$) the indirect detection of the ^{195}Pt signal (through ^{1}H-^{195}Pt HMQC experiments) was used prior to the $^{195}Pt\{^{1}H\}$ spectra.

In addition, for some asymmetric dinuclear metal-metal bonded platinum compounds of Chapter 2, ^{195}Pt-$^{195}Pt\{^{1}H\}$ COSY experiments were recorded. Platinum COSY experiments were optimized based on ^{1}H-^{1}H COSY (see Scheme 4[39]). As platinum coupling constants are much larger than proton ones, the t_1 increments have been set to 1 μs (the increments for a ^{1}H-^{1}H COSY are 3 μs). Additionally, a ^{1}H decoupling was added using the waltz16 sequence.

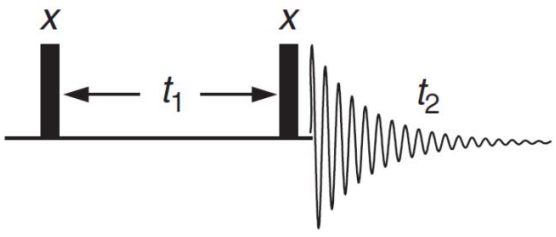

Scheme 4. ^{1}H-^{1}H COSY pulse sequence.

M.2.2.Infrared Spectroscopy

The IR spectra of the complexes presented in this Thesis were recorded on neat solid samples using a PerkinElmer Spectrum 100 FT-IR Spectrometer (ATR in the range 4000–250 cm^{-1}) equipped with an ATR (attenuated total reflectance) device, therefore avoiding any sample preparation.

M.2.3.Mass Spectrometry

Mass spectral analyses were performed with a Microflex MALDI-TOF Bruker or an Autoflex III MALDI-TOF Bruker instruments, using DCTB (*trans*-2-[3-(4-tert-butylphenyl)-2-methyl-2-propenylidene]malononitrile) as the matrix. All the analyses were performed by the Servicio de Espectrometría de Masas of the Centro de Química y Materiales de Aragón (CEQMA).

M.2.4. Single Crystal X-ray Diffraction

All X-ray structures showed in this Thesis were determined by Dr. Antonio Martín. X-ray intensity data were collected on an Oxford Diffraction Xcalibur or on a Bruker Apex Duo CCD diffractometers.

Single crystals suitable for X-ray diffraction analysis were obtained from a saturated solution of the corresponding compound either by slow evaporation of the solvent or by slow diffusion of a non-polar solvent into the solution, both solvents being miscible. Further crystallographic aspects are described in detail in the Supporting Information of the papers collected in the Electronic Supplementary Material-Thesis LAV.

M.2.5.Elemental Analyses

In this Thesis, elemental analyses were performed to check the purity of the samples. The C, H, and N analyses of all the compounds were carried out in a PerkinElmer 2400 CHNS/O Series

II microanalyzer. All the analyses were performed by the Servicio de Análisis Elemental of the Centro de Química y Materiales de Aragón (CEQMA).

M.2.6.Photophysical Properties

UV-vis Spectroscopy

UV-visible spectra in solution were recorded on a Unicam UV4 spectrophotometer using a 1cm or 1mm pathlength quartz cuvettes. Solid samples were measured by diffuse reflectance UV-vis (DRUV) spectroscopy on a Thermo electron corporation evolution 600 spectrophotometer equipped with a Praying Mantis integrating sphere. The solid samples were homogeneously diluted with $BaSO_4$.

Luminescence and QY

Steady-state photoluminescence spectra were recorded on a Jobin-Yvon Horiba Fluorolog FL-3-11 Tau 3 spectrofluorimeter. Phosphorescence lifetimes were recorded with a Fluoromax phosphorimeter accessory containing a UV xenon flash tube. Nanosecond lifetimes were recorded with a Datastation HUB-B with a nanoLed controller and software DAS6. The lifetime data were fitted using the Jobin-Yvon software package and the Origin Pro 8 program. Quantum yield (ϕ), in PMMA films and powdery samples were measured using a Hamamatsu Absolute PL Quantum Yield Measurement System C11347-11. PMMA films were prepared by drop-casting solutions 5% wt complex in PMMA (10^{-2} M, CH_2Cl_2) onto a quartz slide and allowing the solvent to evaporate.

M.2.7.Computational Calculations

Density functional theory (DFT) calculations were essential to understand the photophysical properties and the reactivity of the complexes described in this Thesis.

Theoretical DFT calculations were carried out on the ground (S_0) and triplet (T_1) states with the Gaussian 09[40] and 16[41] suite of programs, using the M06 hybrid density functional[42] (MUE

(M06) = 2.48 kcal/mol[43]) together with Grimme's D3 dispersion correction.[44] The SDD pseudopotential and associated basis set[45] was used for platinum (ECP-60-mwb) and iodine (ECP-46-mwb), and the 6-31G(d)[46-47] basis set were used for all other atoms. In certain cases, the basis set description was completed by using additional sets of f-type functions for platinum and d-type functions for iodine.[48-49]

In order to facilitate the theoretical study, a simplification was done on the real system, the ethoxycarboyl group on the cyclometalated ligand was modelled as a methoxycarboyl one. In some cases, besides, a privileged orientation of the methoxycarboyl groups, with their methyl pointing to the pyrazole bridging ligands.[50]

General geometry optimizations were performed without any symmetry restriction and, depending on the available computational resources, in gas phase and then adding the solvent in a single point [51] or in the corresponding solvent[50, 52-53] by using the polarizable continuum model (PCM).[54]

Frequency calculations were performed in order to determine the nature of the stationary points found in S_0 and T_1 (no imaginary frequencies for minima, only one imaginary frequency for Transition State).

Time-dependent density-functional (TD-DFT) calculations were also carried out in solution using PCM model.

Mulliken population analysis was carried out as implemented in the corresponding Gaussian package.[40-41] Molekel and ChemissianLab program packages were used for analysis and graphic representation of molecular structures and orbitals and for Mayer Bond Order analysis. Atomic charges were calculated by using the NBO analysis option as incorporated in Gaussian 9[40] and 16.[41]

M.2.8.Cyclic Voltammetry

Cyclic Voltammetry (CV) was performed using a VoltaLab PST050 electrochemistry work station in a conventional three-electrode arrangement. A saturated calomel electrode (SCE) was used as the reference electrode (RE); a platinum wire was used as working electrode (WE) and another platinum wire as counter electrode (CE).

In this Thesis, oxidation potentials were measured in deoxygenated MeCN solutions of the analyzed complex (5×10^{-4} M) and NBu_4PF_6 (0.1 M) contained in a home-made cell. Measurements were conducted with a scan rate of 100 mV/s and using ferrocenium/ferrocene (Fc+/Fc) as the internal standard.

Chapter 1

Mono and Dinuclear Platinum (II) Emitters

1.1.Introduction

Pyrazole/pyrazolate (RpzH/Rpz) are wide known to be versatile ligands having different coordination modes. In pyrazole complexes (RpzH) they show a monohapto coordination to the metal center[55-56] (Scheme 5, a). This kind of complexes has a significant interest in different fields such as medicine,[57] due to the anticancer activity, in catalysis,[58] in hydrogenation processes,[59] molecular architecture[60] or luminescence.[55, 61-62]

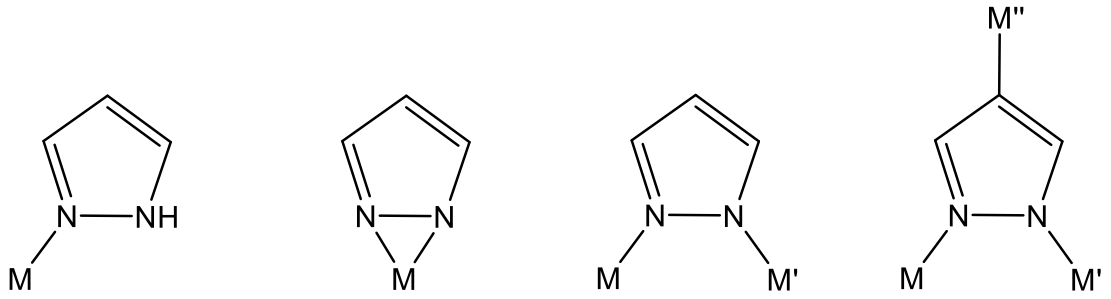

(a) (b) (c) (d)

Scheme 5. Coordination modes of pyrazole/pyrazolate ligands

Pyrazolates (Rpz), generated by the abstraction of the NH acidic proton from pyrazoles (RpzH), can exhibit *endo*-1,2-dihapto[63-64] (Scheme 5, b), *exo*-1,2-dihapto[65-66] (Scheme 5, c) or trihapto[67-68] (Scheme 5, d) coordination modes.

The *exo*-1,2-dihaptobridging Rpz ligands can hold two metal atoms in close proximity while permitting a wide range of structures and intermetallic separations with the strength of the metallophilic interactions affecting the emissive properties.[69-70]

The chemistry of pyrazolate-bridged dinuclear Pt(II) complexes has been deeply studied experimental and theoretically by Castellano,[71] Thompson,[69, 72] Ma,[73] and coworkers. Most studies addressed the control of the photoluminescence properties of complexes [{Pt(C^N)(μ-Rpz)}$_2$], dubbed "*molecular butterflies*". It was found that the Pt-Pt distance and the extent of the metallophilic interactions can be tuned by the bulkiness of the pyrazolate unit (*butterfly*

body), in such a way that when the bulkiness increases the cycloplatinated units (*butterfly wings*) are pushed closer together and the Pt···Pt interaction becomes stronger. As a result, the emissive triplet state can change from a monomer-based ^{3}IL/^{3}MLCT to a metal-metal-to-ligand charge transfer (^{3}MMLCT) (see Scheme 6), and then, the emission color can be tuned from blue to green or red.[24, 69]

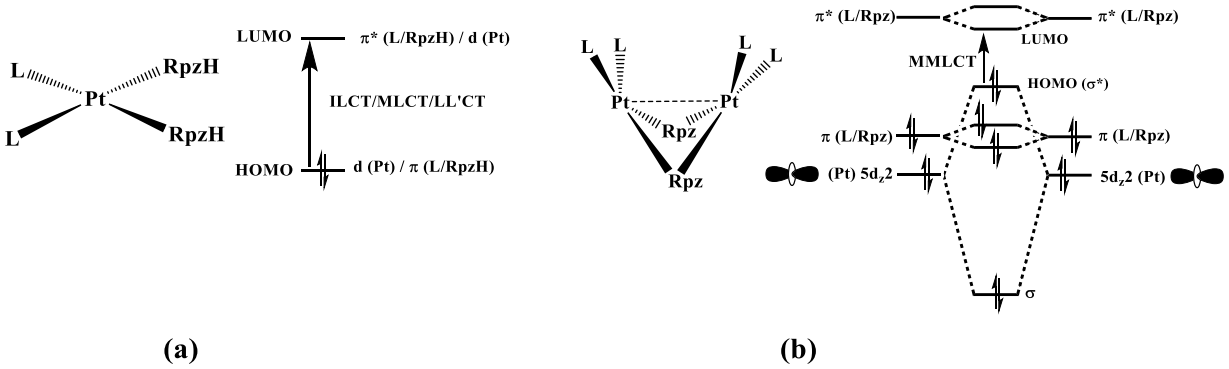

Scheme 6. (a) Generic molecular orbital for the HOMO-LUMO transition in a mononuclear pyrazole Pt(II) complex. (b) Simplified orbital diagram for a dinuclear Pt_2(II,II) pyrazole-bridged complex.

As an example, the blue, green, and red emission exhibited by [{Pt(C^N)(μ-3,5-dimethylpyrazolate)}$_2$], [{Pt(C^N)(μ-3-methyl-5-tert-butylpyrazolate)}$_2$], and [{Pt(C^N)(μ-3,5-bis(tert-butyl)pyrazolate)}$_2$] (C^N=2-(2,4-difluorophenyl)pyridyl) respectively.[69]

The unique *butterfly*-like structure of bis-pyrazolate bridge complexes allows additionally, the contraction of the Pt-Pt distance with temperature[70] and thus leading to solid-state thermochromism and thermoluminescence. This is the case of [{Pt(ppy)(μ-Ph_2pz)}$_2$],[74] which at low temperature exhibits monomer-based ^{3}LC/MLCT emission and it changes to excimer-like ^{3}MMLCT emission above 160 K.

Sometimes this kind of complexes exhibit in solution a photoinduced structural change (PSC) due to the existence of two local minima in the lower triplet-state potential energy surface (T_1-PES), leading to a fast change in the Pt-Pt distance and thereto on the color of the emission.

This flapping-*butterfly* behavior of those complexes in the T_1 state, which allows the contraction of the Pt-Pt distance, is sensible to both, the temperature[70] or the viscosity of the media.[75]

On the other hand, the existence of metal-metal interaction improves the QY due to the higher metal contribution to the frontier orbitals, which in fact implies an increase in the spin orbit coupling (SOC), making the emissive forbidden transition [T_1-S_0] more efficient.[76]

The cyclometalating groups play also an important role in the stability and the control of the photophysical properties.[77] In this sense, the platinum-*butterfly* complexes reported by Strassner *et al.*, [{Pt(C^C*)(μ-Rpz)}$_2$][78-79] (HC^C*= 3-Dibenzofuran-4-yl-1-methyl-3*H*-imidazo-2-ylidene, 1-Methyl-3-phenyl-imidazol-2-yliden[4,5-*b*]pyridine-κC2,κC2′; RpzH= pyrazole, 3,5-dimethylpyrazole, 3,5-bis(tert-butylpyrazole) are exemplary ones. They revealed that the cyclometalated N-heterocyclic carbenes (C^C*), forming two strong metal-carbon bonds, are excellent wings for the synthesis of highly efficient blue and orange emitters.

With all the above in mind, we addressed the synthesis, full characterization and deep study of the photophysical properties of highly efficient blue-light emitters, the mononuclear [Pt(C^C*$_A$)(RpzH)$_2$]$^+$ and the dinuclear complexes [{Pt(C^C* $_A$)(μ-Rpz)}$_2$] (RpzH = pyrazole (pzH), 4-methylpyrazole (4-MepzH), 3,5-dimethylpyrazole (3,5-dmpzH), 3,5-diphenylpyrazole (3,5-dppzH)), with the former being used as precursors of the dinuclear Pt_2(II,II) complexes. Exhaustive DFT and TD-DFT studies were performed to explain the chameleonic photo- and mechanoluminescence of the *butterfly*-like platinum (II) complexes, [{Pt(C^C*$_A$)(μ-Rpz)}$_2$].

This chapter is based on the following two peer-reviewed papers:

1.- Lorenzo Arnal; Sara Fuertes; Antonio Martín; Violeta Sicilia. The Use of Cyclometalated NHCs and Pyrazoles for the Development of Fully Efficient Blue Pt^{II}

Emitters and Pt/Ag Clusters. *Chemistry - A European Journal* **2018**, *24* (37), 9377-9384. DOI: 10.1002/chem.201800646. (ESM-1)

2.- Violeta Sicilia; Lorenzo Arnal; Daniel Escudero; Sara Fuertes; Antonio Martín. Chameleonic Photo- and Mechanoluminescence in Pyrazolate-Bridged NHC Cyclometalated Platinum Complexes. *Inorganic Chemistry* **2021**, *60* (16), 12274-12284. DOI: 10.1021/acs.inorgchem.1c01470. (ESM-2)

1.2.Synthesis of New Mononuclear Bis-pyrazole Complexes [Pt(C^C*$_A$)(RpzH)$_2$]X

The new mononuclear bis-pyrazole complexes [Pt(C^C*$_A$)(RpzH)$_2$]X were synthetized and isolated as the chloride (X=Cl^-, RpzH= 3,5-dmpzH **1a**, 4-MepzH **2a**, pzH **3a**), perchlorate (X=ClO_4^-, RpzH= 3,5-dmpzH **1b**, 4-MepzH **2b**, pzH **3b**) or hexafluorophosphate (X=PF_6^-, RpzH= 3,5-dmpzH **1c**) salts from **A** following the strategies indicated in Scheme 7.

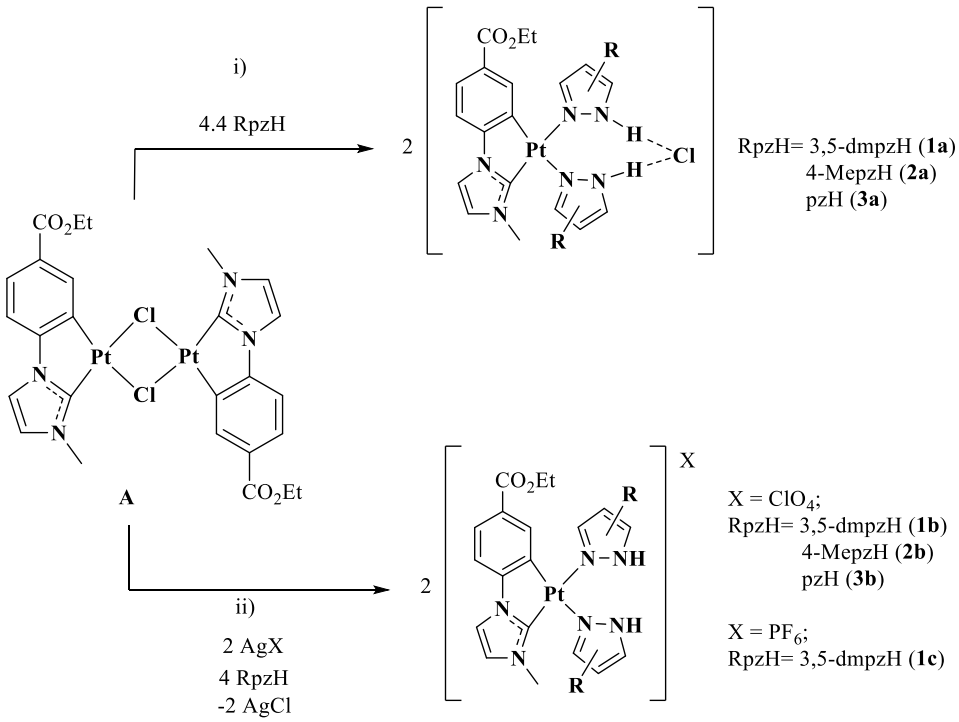

Scheme 7. Synthetic pathways for compounds **1a-3a**, **1b-3b**, and **1c**

Compounds **1a-3a** were obtained first, as pure solids in good yields (61% **1a**, 64% **2a**, 60% **3a**), by addition of an excess of RpzH to **A**, resulting in the breaking of the chloride-bridge and the substitution of the chloride ligand from the coordination sphere of the Pt centers (Scheme 7 i). Then, they were fully characterized.

The molecular structure of **1a** could be determined by single-crystal X-ray diffraction (see Figure 4). It shows the *cis* arrangement of the two pyrazole ligands and the presence of the chloride anion joined to the cation through two N-H···Cl hydrogen bonds.

The angle H4-Cl1-H6 (79.22(1.22)º) is almost the theoretical value for the lone pair of the chloride ligand (90º) and the parameters corresponding to the two H···Cl bonds are the expected for this kind of interactions (H4···Cl1=2.3164(361) Å, N4–H4···Cl1= 162.398º, H6···Cl1=2.2662(356) Å, N6–H6···Cl1=171.98º).[80-81]

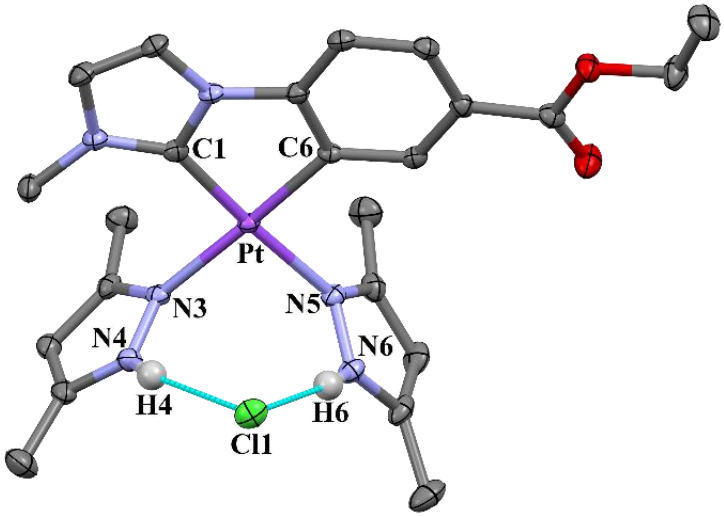

Figure 4. Molecular structure of **1a.**

The ^{1}H NMR spectra showed that unlike **1a**, in solution of CD_2Cl_2 complexes **2a** and **3a** co-exist with species [PtCl(C^C*$_A$)(RpzH)] (RpzH= 4-MepzH **2a'**, pzH **3a'**) in a dynamic equilibrium, such as the represented in Figure 5 for **2a**.

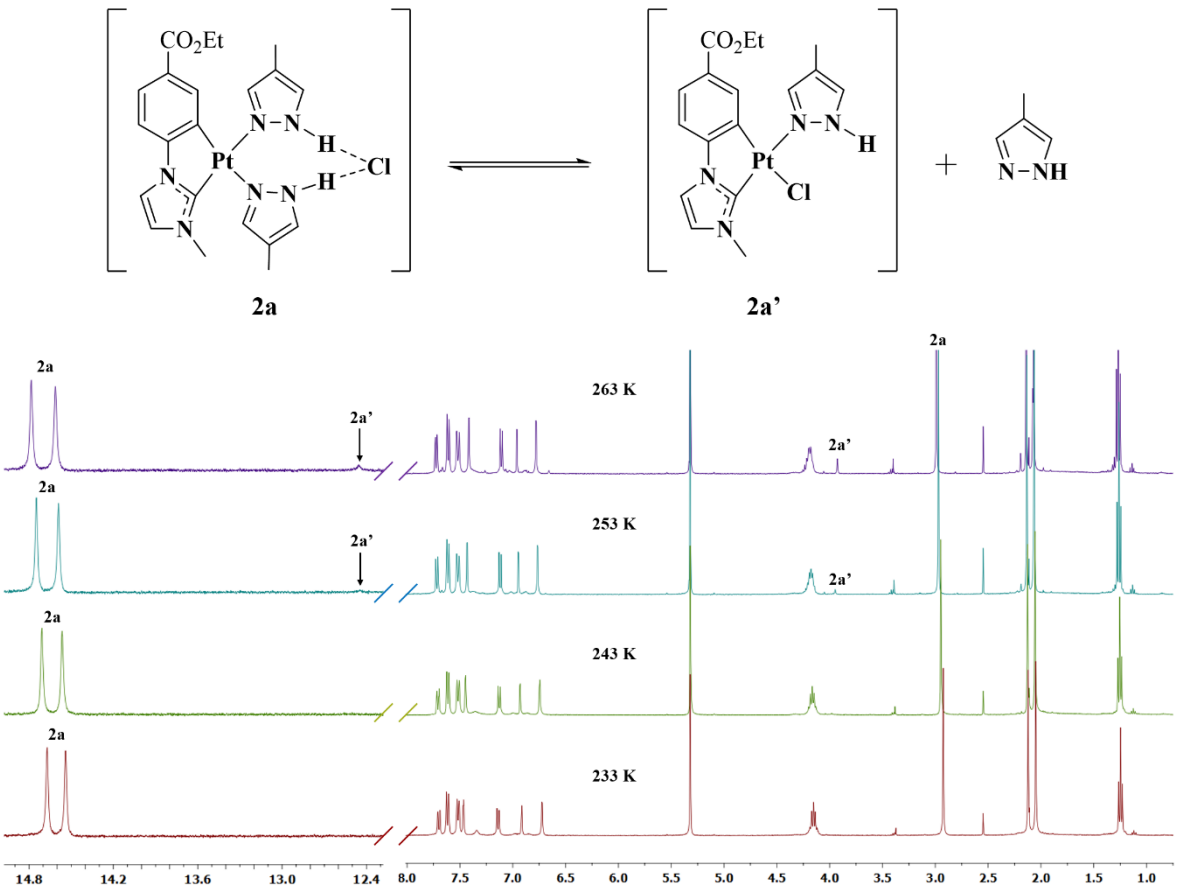

Figure 5. Variable temperature ^{1}H NMR of **2a** in CD_2Cl_2

These results illustrate the higher basicity of 3,5-dmpzH with respect to 4-MepzH and pzH, in agreement with the pKa values of their conjugate acids (3,5-dmpzH: 4.06, pzH: 2.83).

In agreement with the proposed equilibrium, addition of 4-MepzH/pzH to a solution of compound **2a/3a** in CD_2Cl_2 shifts this equilibrium to the left and the signals attributed to **2a'**/**3a'** disappear. Variable temperature ^{1}H NMR studies showed that as the temperature decreases the amount of **2a'**/**3a'** decreases, in such a way that **2a**/**3a** is the only species in solution (T < 243 K **2a**, 223 K **3a**). Because this equilibrium becomes spontaneous ($\Delta G = \Delta H - T\Delta S < 0$) when the temperature raises and $\Delta S > 0$, the dissociation must be an endothermic process. The values found for ΔS (93.7 J k^{-1} mol^{-1} **2a**, 111.2 J k^{-1} mol^{-1} **3a**) and ΔH (ΔH= 26.5 KJ mol^{-1} **2a**, 30.3 KJ mol^{-1} **3a**) confirmed these statements.

To prevent the above chemical equilibrium from occurring and be able to study the photophysical properties of these new bis-pyrazole complexes, we prepared these complexes as the salts of non-coordinating anions (ClO_4^- **1b-3b** and PF_6^- **1c**) following the procedure indicated in Scheme 7 ii. All compounds were synthetized as pure solids in good yields and were fully characterized (see Figure 6 for **2b**).

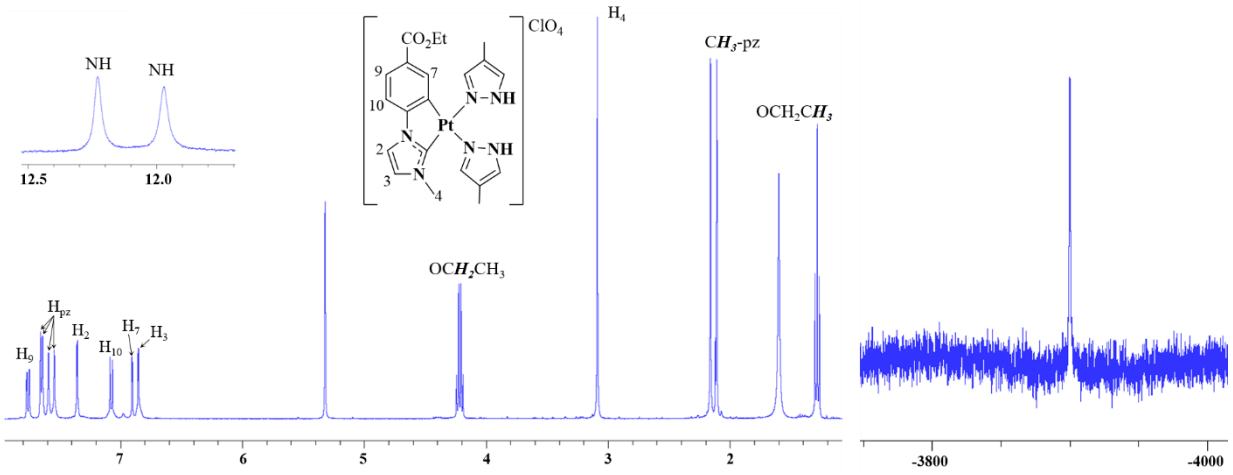

Figure 6. ^{1}H (left) and $^{195}Pt\{^{1}H\}$ (right) NMR spectra of **2b** in CD_2Cl_2. An accurate characterization using NOE ^{1}H NMR is described in *Chem. Eur. J.* **2018**, *24* (37), 9377-9384.

1.3.Reactivity of Bis-pyrazole Complexes towards Bases. Synthesis of Bis-pyrazolate-bridged Pt_2(II,II) Complexes

Compounds [{Pt(C^C*$_A$)(μ-Rpz)}$_2$] (RpzH= pzH **4**, 4-MepzH **5**, 3,5-dmpzH **6**, 3,5-dppzH **7**) were prepared following path i (for **4**, **5,** and **7**) or path ii (for **4** and **6**) in Scheme 8.

Treatment of the bis-pyrazole compounds, [Pt(C^C*$_A$)(RpzH)$_2$]ClO_4 with a large excess of NEt_3 (path i) proceeds with the elimination of acidic H atoms (NH) and to the release of a RpzH/ Rpz ligand from the platinum coordination sphere. That give rise to the complexes [{Pt(C^C*$_A$)(μ-Rpz)}$_2$] (RpzH= pzH **4**, 4-MepzH **5**, 3,5-dppzH **7**) and the formation of

$NHEt_3ClO_4$ and $NHEt_3Rpz$ as byproducts. For compound **7**, the starting bis-pyrazole complex was not isolated, but used from freshly prepared solutions of it in acetone.

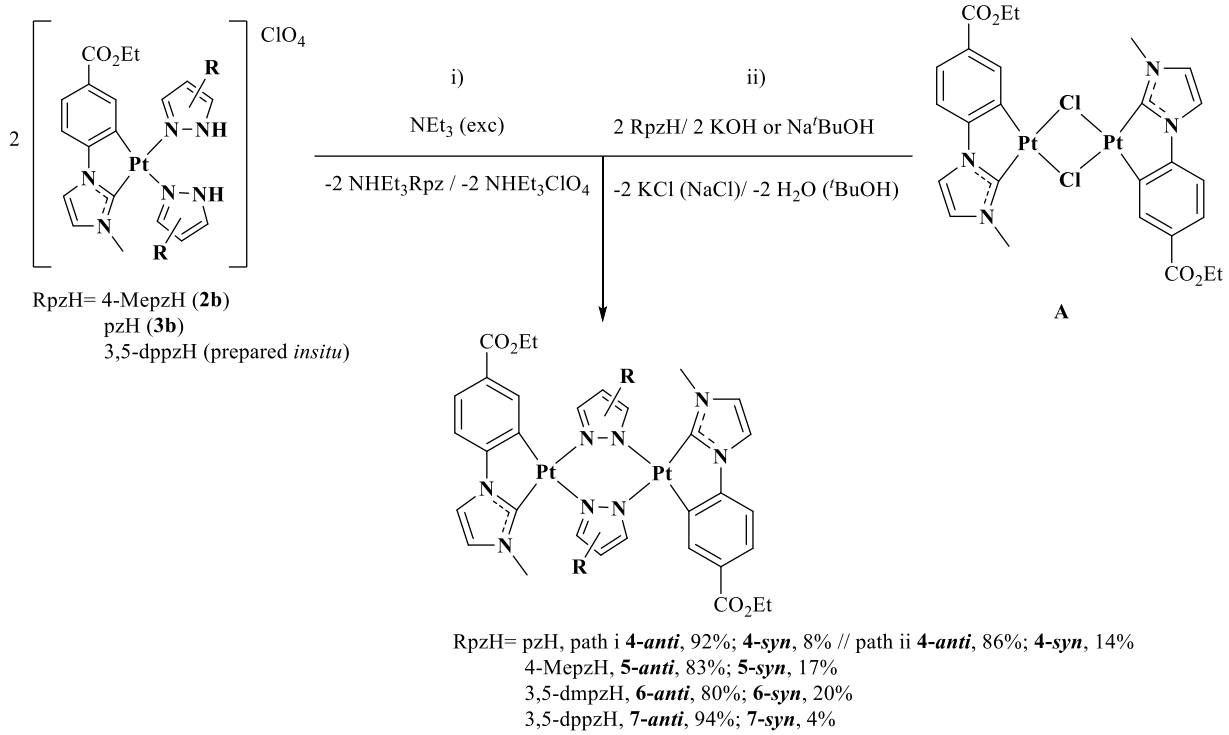

Scheme 8. Synthetic pathways for compounds **4-7** (Just the major isomer "*anti*" appears represented for clarity. Synthesis and characterization of compound **4** was described in L. Arnal *et al. Chem. Eur. J.* **2018**, *24* (70), 18743-18748.

Compound [{Pt(C^C*$_A$)(μ-3,5-dmpz)}$_2$](**6**) was not available by following path i, in agreement with the greater basicity of the 3,5-dmpzH with respect to the other RpzH, which prevents it from being removed from the coordination sphere of platinum. Therefore, the protocol should be modified using **A** and Na(3,5-dmpz), generated *in situ*, from 3,5-dmpzH and NaO^{t}Bu (path ii). This route was followed as well to get complex [{Pt(C^C*$_A$)(μ-pz)}$_2$](**4**), from **A**, pzH and KOH.

All complexes were obtained as a mixture of *anti*/*syn* isomers, considering the relative orientation of the cyclometalated C^C* groups, with the *anti* isomer being the major one. This agrees with DFT calculations carried out on complex **4**, which determined the *anti* isomer to be

3.1 kcal mol^{-1} lower in energy than the *syn* one. The two diastereoisomers (*anti*/*syn*) once formed do not transform one into the other. Therefore, complexes **4**-**7** were fully characterized as mixtures of *anti*/*syn* isomers, but we will focus on the major isomer: the *anti* one

^{1}H NMR spectra show the expected resonances for half of the molecule, see Figure 7 for **5**. Since H_7 and H_4 are very sensitive to both, steric and electronic changes in the environment,[27] these signals appear downfield shifted with respect to those of the corresponding bis-pyrazole complex. Additionally, the $J_{H7,Pt}$ becomes smaller.

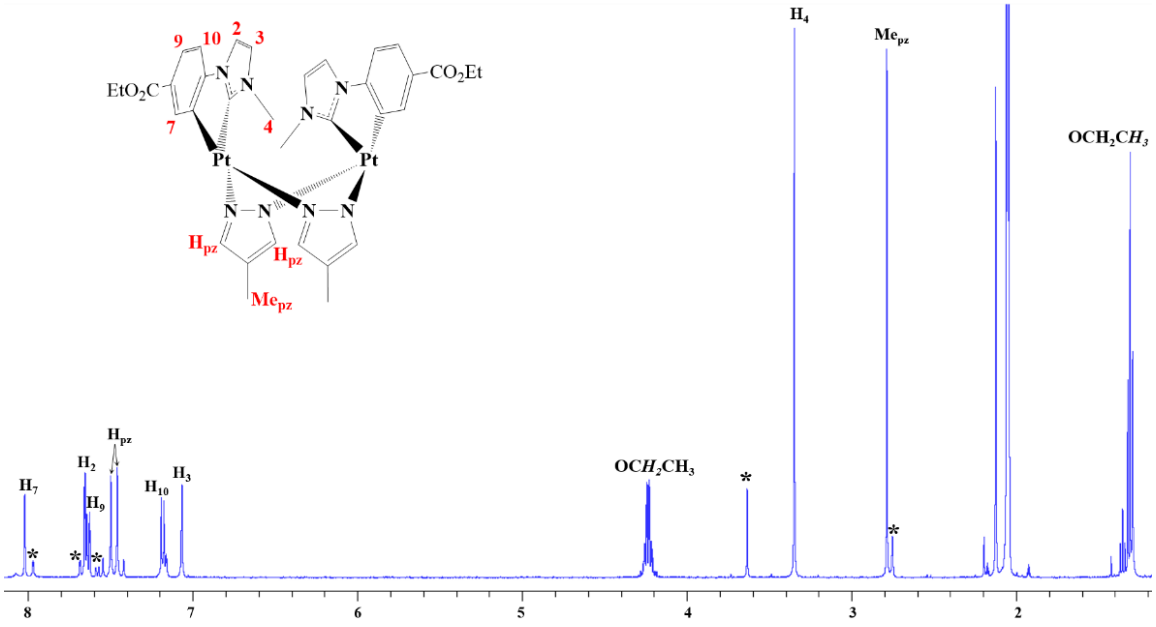

Figure 7. ^{1}H NMR spectrum of **5** in acetone-d_6. **syn* isomer resonances.

The ^{195}Pt{^{1}H} NMR spectra display the corresponding singlet, downfield shifted (*ca.* 200 ppm) with respect to that of the corresponding bis-pyrazole complex.

Single crystals were obtained for all complexes, but for **7** the quality was not good enough and only the connectivity of the atoms could be attained. Molecular structures of **4**, **5,** and **6** (Figure 8) present important differences. Compounds **4** and **5** have three different molecules in the asymmetric unit with a wide range of intermetallic distances ($d_{Pt\text{-}Pt}$ (Å) = 3.2294(4) **4A**, 3.2834(4) **4B**, 3.1210(3) **4C**; 3.355(4) **5A**, 3.224(3) **5B**, 3.156(3) **5C**), while **6** display only one molecule with a platinum-platinum distance of 3.131(17) Å. The presence of two molecules of

7 in the asymmetric unit with distances of 3.054 Å and 2.982 Å could be confirmed, despite the poor-quality of the crystal. All intermetallic separations are in the low range of distances published for other platinum-*butterfly*.[69, 79, 82] They are large enough to ruled out the existence of a metal-metal bond,[24, 34, 83] but not some intermetallic interaction.[23]

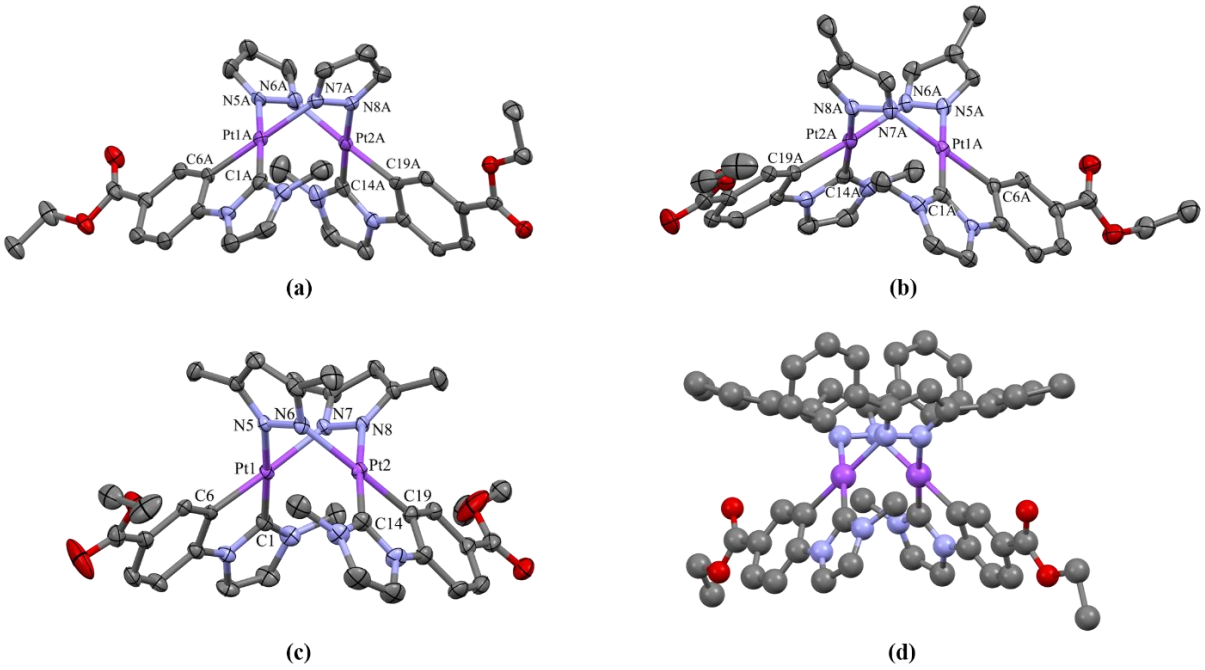

Figure 8. Molecular structure of **4A** (a), **5A** (b), **6** (c), and **7** (only atoms connectivity) (d).

These complexes, **4-7**, show supramolecular arrangements due to short π- π contacts (3.28-3.40 Å) between the NHC cyclometalated ligands, as can be seen in Figure 9 for **5** and **6**.

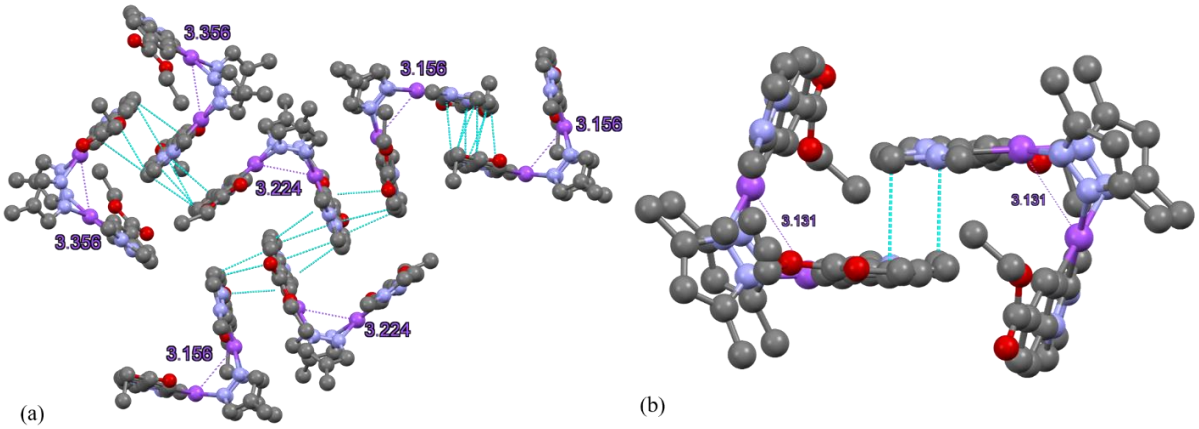

Figure 9. Supramolecular arrangement of complexes **5** (a) and **6** (b).

These contacts are more important in compounds **4** and **5**, in which the interactions take place on both internal and external faces of the molecules, while in complex **6** only the internal face is involved.

1.4.Reactivity of Bis-pyrazole Complexes to give [Pt_2Ag_2] Clusters

We explained above that the treatment of the bis-pyrazole complexes [Pt(C^C*$_A$)(RpzH)$_2$]ClO_4 (RpzH= pzH, 4-MepzH, 3,5-dppzH) with a large excess of NEt_3 give rise to the dinuclear complexes [{Pt(C^C*$_A$)(μ-Rpz)}$_2$] (RpzH= pzH **4**, 4-MepzH **5**, 3,5-dppzH **7**). However, this does not occur in the case of [Pt(C^C*$_A$)(3,5-dmpzH)$_2$]ClO_4 (**1b**), due to the higher basicity of 3,5-dmpzH with respect to the other RpzH.

Because of that, the reaction of complex [Pt(C^C*$_A$)(3,5-dmpzH)$_2$]ClO_4 (**1b**) with $AgClO_4$ (1:1 molar ratio) in the presence of NEt_3 resulted in the elimination of the acidic H atoms and their replacement by Ag(I) centers affording the tetranuclear cluster, [{Pt(C^C*$_A$)(3,5-dmpz)$_2$Ag}$_2$] (**8**).

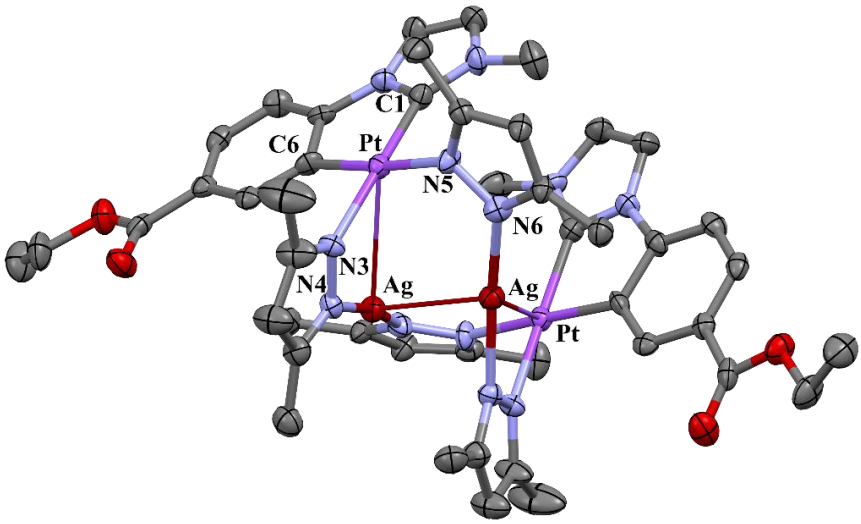

Figure 10. Molecular structure of **8**.

Its single-crystal X-ray diffraction structure (see Figure 10) showed that it consists of two subunits "Pt(C^C*$_A$)(3,5-dmpz)$_2$Ag", each one containing a Pt→Ag donor-acceptor bond,

joined through Ag-N bonds and argentophilic interactions[84-86] (d_{Ag-Ag} (Å) =3.2171(9)). The Pt-Ag distances, 3.2626(5) Å, are shorter than those observed in the related tetranuclear clusters $[Pt_2Ag_2(C\hat{}N)_2(Me_2pz)_4]^{0,\ 2+}$ (d_{Pt-Ag} > 3.4 Å).[84] The ^{1}H NMR spectrum of a freshly prepared solution of **8** in CD_2Cl_2 shows the expected resonances for half of the molecule with two set of signals due to the inequivalent pyrazolates of one "Pt(C^C*$_A$)(3,5-dmpz)$_2$Ag" fragment. The existence of the Pt→Ag donor-aceptor bond shifts upfield all resonances except that of H_7, which shifts downfield and reduce the value of the H-Pt coupling constant ($^3J_{H-Pt}$=51.2 Hz **8**, 59.2 **1b** Hz). Additionally, the ^{195}Pt resonance of **8** appears downfield-shifted when compared to that of **1b** ($\delta_{Pt,298K}$= -3920 ppm **1b**, $\delta_{Pt,183K}$= -3753 ppm **8**).

1.5.Optical Properties of New Complexes

The absorption and emission properties of all new platinum complexes were measured in different conditions (solution and solid for absorption; frozen solution, PMMA film, and solid for emission) and have been explained with the aid of theoretical calculations (DFT and TD-DFT).

1.5.1.Optical Properties of the Bis-pyrazole Compounds

The absorption spectra of compounds [Pt(C^C*$_A$)(RpzH)$_2$]X (X=Cl^-, RpzH= 3,5-dmpzH **1a**; X=ClO_4^-, RpzH= 3,5-dmpzH **1b**, 4-MepzH **2b**, pzH **3b**; X=PF_6^-, RpzH: 3,5-dmpzH **1c**) in CH_2Cl_2 (10^{-4} M) solutions (see Figure 11) show intense absorptions at high energy (λ < 300 nm), attributed to intraligand (^{1}IL) transitions of the C^C* ligand, along with weaker absorptions in the range of 314-320 nm with shoulders between 340 and 360 nm. Lower-energy absorptions show subtle differences due to the change of the counterion (Cl **1a** *vs*. ClO_4 **1b** and PF_6 **1c**) but not with the RpzH change (3,5-dmpzH **1b**, 4-MepzH **2b**, pzH **3b**) indicating their low participation in the corresponding transitions.

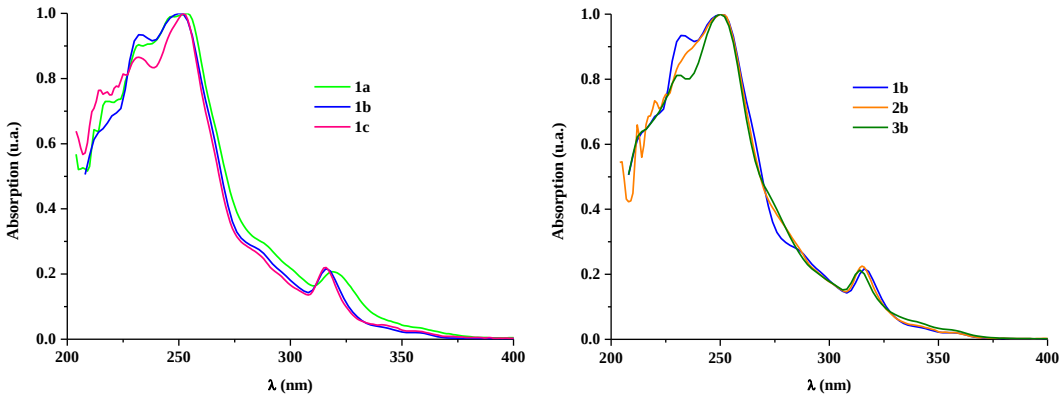

Figure 11. UV-vis absorption spectra of **1a-1c** (left) and **1b-3b** (right) in CH_2Cl_2 (10^{-4} M).

Time-dependent density functional theory calculations in CH_2Cl_2 solution (PCM-TD-DFT), indicate that the HOMO → LUMO transition is the only contribution to the calculated spin-allowed transition from S_0 to S_1 (see Table 1). Besides, they show that the frontier orbitals, HOMO and LUMO (Figure 12) are mainly centered in the NHC ligand and the platinum, with a marginal contribution of the RpzH ligands (less than 5%). Therefore, the lowest energy absorption in all compounds has been attributed to a metal-perturbed intraligand charge-transfer transition (ILCT) on the NHC with a small metal-to-ligand charge-transfer contribution MLCT.

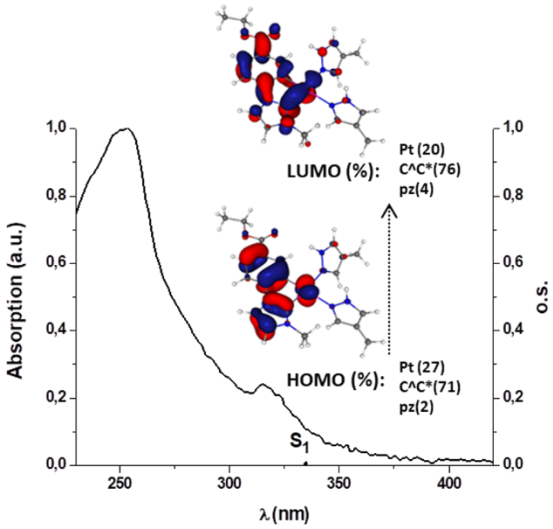

Table 1

	λcalc./nm	o.s.	Transition(%)	Assignment
1a	337.8	0.0084	H → L (95)	ILCT, MLCT
1b	337.3	0.0064	H → L (96)	ILCT, MLCT
2b	334.8	0.0051	H → L (96)	ILCT, MLCT
3b	334.6	0.0059	H → L (96)	ILCT, MLCT

Figure 12. UV/Vis absorption spectrum, calculated transition in CH_2Cl_2 (bar) and calculated frontier orbitals for **2b**. **Table 1.** S1 states calculated by TD-DFT in solution of CH_2Cl_2

Table 2. Photophysical data for **1a**–**3a**, **1b**–**3b**, and **1c**.

	Media (T/K)	λ_{ex}(nm)	λ_{em} (nm)	$\tau(\mu s)^b$	ϕ^c		Media (T/K)	λ_{ex}(nm)	λ_{em} (nm)	$\tau(\mu s)^b$	ϕ^c
	CH_2Cl_2[a](77)	322	454_{max}, 486, 514	14.0			CH_2Cl_2[a](77)	319	456_{max}, 488, 517	18.2	
1a	PMMA Film	360	449, 476_{max}, 504		0.66	**2b**	PMMA Film	360	446, 475_{max}, 500		0.99
	Solid (298)	362	448, 475_{max}, 505, 540_{sh}	17.7			Solid (298)	370	458, 487_{max}, 516	10.1	
2a[d]	CH_2Cl_2[a](77)	325	453_{max}, 481, 520	14.9		**3b**[e]	CH_2Cl_2[a](77)	316	451_{max}, 481, 511, 555_{sh}	19.7	
	Solid (298)	363	447, 477_{max}, 509, 546_{sh}				Solid (298)	366	460, 484_{max}, 515	15.9	
3a[d]	CH_2Cl_2[a](77)	325	454_{max}, 486, 518	12.3		**1c**	CH_2Cl_2*a*(77)	319	454_{max}, 482, 512_{sh}	21.2	
	Solid (298)	362	452, 483_{max}, 515, 550_{sh}				PMMA Film	360	455, 478_{max}, 512		1.00
	CH_2Cl_2[a](77)	319	453_{max}, 483, 512, 553_{sh}	21.6			Solid (298)	370	461, 487_{max}, 518_{sh}	12.9	
1b	PMMA Film	360	447, 475_{max}, 505,540_{sh}		1.00						
	Solid (298)	360	463, 489_{max}, 517, 560_{sh}	13.4	0.33						

[a] 10^{-5} M.; [b] Measurements at λ_{max}. [c] PMMA films in Ar atmosphere. [d] The dynamic equilibrium in solution hindered the PMMA film to be prepared conveniently for photophysical measurements. [e] QY in PMMA film has not been measured because **3b** evolves partially to [{Pt(C^C*$_A$)(μ-pz)}$_2$] in CH_2Cl_2 at r.t.

The emission spectra of compounds **1a-3a**, **1b-3b**, and **1c** in rigid matrix of CH_2Cl_2 (10^{-5} M solution at 77K) display highly structured emissions in the blue region with long lifetime decays (τ: 14-22 μs), which are neither affected by the nature of the RpzH ligand nor the anion (Table 2, Figure 13 left), as expected from the UV-vis spectra and theoretical calculations.

These phosphorescent emissions are similar to those of related compounds containing the same Pt(C^C*$_A$) fragment. In agreement with that and with theoretical calculations, they seem to originate in the monomeric species and to be intraligand charge- transfer (^{3}ILCT, [C^C*]) in nature.

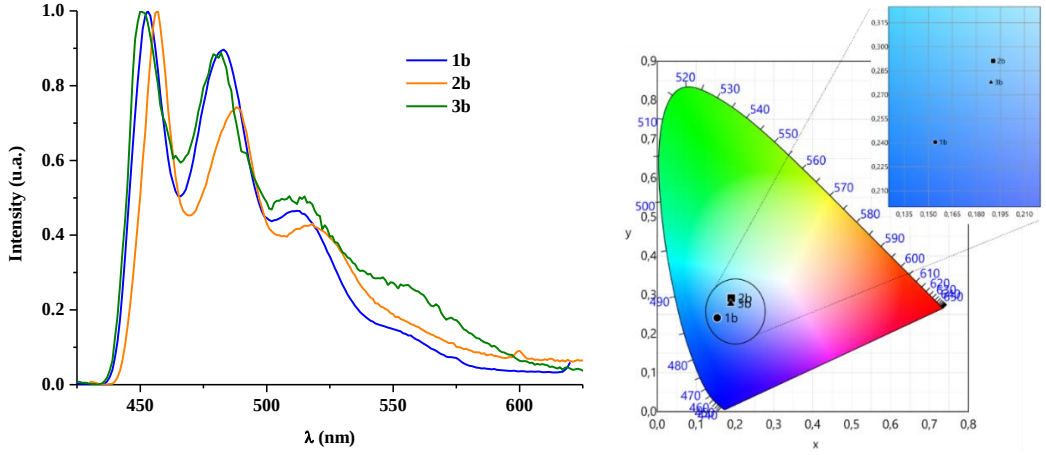

Figure 13. Left: Emission spectra of **1b-3b** CH_2Cl_2 solution at 77K (λex=319 nm). Right: CIE 1931 chromaticity diagram with the (x, y) positions of the emissions of **1b-3b** in PMMA films.

The emissions of **1a-c** and **2b** measured in PMMA film (5%) were found to be analogous to those recorded in rigid matrix of CH_2Cl_2. They exhibit quantum yields (QY) of up to 100% for **1b**, **1c**, and **2b** and Commission Internationale de L'Éclaire (CIE) coordinates of (0.15, 0.22) (Figure 13 right), which are very close to the desirable ones for blue emitters (0.15, 0.15). These mononuclear compounds are amongst the best blue light emitters of Pt(II), with PLQYs in PMMA films higher than those reported for [Pt(C^C*)(acac)] (Φ = 0.86[87] 0.90[88]), [Pt(C*^C^C*)Cl] (Φ = 0.32[89]), [Pt(C^X-L^L')] [C^X = phenyl methyl imidazole; L^L' = phenoxy pyridine, Φ = 0.58; L^L' = carbazolyl pyridine, Φ = 0.89; C^X = phenyl pyrazole;

L^L' = carbazolyl pyridine, Φ = 0.85],[90] and [Pt(R-C^C*)(acac)] (R= CN, Φ = 0.98, R=CO_2Et, Φ = 0.93).[29] Undoubtedly, the presence of an electron-withdrawing substituent in the *para* position to the carbene fragment guarantees a high emission efficiency.

In addition, the powdery solid samples display also a blue emission at 298 K, even a little more blueshifted when the anion is Cl^- (**1a**) instead of a non-coordinating anion (ClO_4^- (**1b**) and PF_6^- (**1c**)).

1.5.2.UV-vis and Luminescence Studies of [{Pt(C^C*$_A$)(μ-Rpz)}$_2$] (RpzH= pzH 4, 4-MepzH 5, 3,5-dmpzH 6, 3,5-dppzH 7). DFT and TD-DFT Calculations

The phophotophysical study of complexes **4-7** was carried out in 2-MeTHF because they were not stable in halogenated solvents. It was also detected that **4-7** loss the luminescence when treated with this kind of solvents. In view of this, the reactivity of complex **4** with haloforms was experimentally and theoretically studied. Metal-metal cooperation seemed to be the key for the [2c, 2e] oxidation of complex **4** by CHX_3 (X = Cl, Br, I), since MMLCT-based species, but not MLCT, are those which trigger these reactions, in the ground state (S_{0f}) for $CHBr_3$ and CHI_3, or in the first singlet excited state (S_{1f}) for its blue-light driven photooxidation by $CHCl_3$ (see Chapter 2). DFT and TD-DFT investigations were performed for an in-depth study of this unexpected reactivity and they were extended to compounds **5-7**, to decipher their intriguing luminescence and mechanoluminescence.

1.5.2.1.Theoretical Calculations

DFT calculations on the ground state (GS) and the lowest adiabatic triplet excited state (T_1) Potential Energy Surfaces (PESs) for **4-7** were performed, and the geometries of relevant stationary points, such as local minima and transition states (TS) were optimized, considering some solvents effects by using THF in the PCM model.

For all of the compounds two close-lying minima were optimized in the GS PES (see Figure 14): the *butterfly-spread* conformers **4s**-**7s**, which show long Pt-Pt distances and intramolecular C^C* separations (> 4.5 Å) and the *butterfly-folded* conformers **4f**-**7f**, which are characterized by shorter Pt-Pt distances (2.96 Å for **7f** < 2.97 Å for **6f**, 2.97 Å for **4f** < 2.98 Å for **5f**) and intramolecular C^C* contacts (< 3.8 Å).

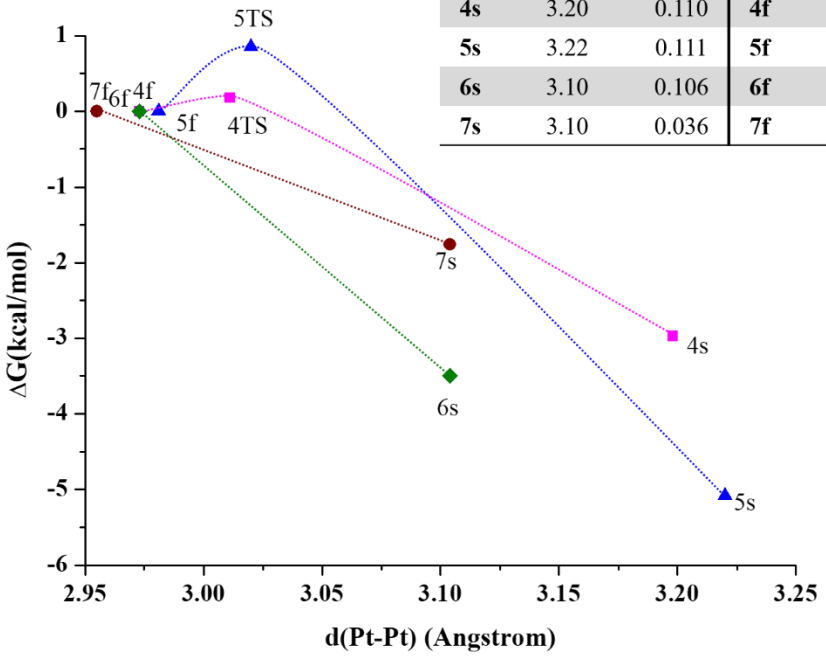

	d(Pt-Pt), Å	BO		d(Pt-Pt), Å	BO
4s	3.20	0.110	**4f**	2.97	0.228
5s	3.22	0.111	**5f**	2.98	0.233
6s	3.10	0.106	**6f**	2.97	0.174
7s	3.10	0.036	**7f**	2.96	0.170

Figure 14. Calculated relative energy profile (PCM(THF)-M06/6-31G(d) and MWB60(Pt)) and Bond Order (BO) in ground state for the interconversion between the **4f**-**7f** and **4s**-**7s** conformers. MUE (M06)= 2.48 kcal/mol.[43]

The computed energy profiles in the GS PES show that conformers **4s**-**7s** are more stable than **4f**-**7f**, especially in the case of **5s**. For complexes bearing the bulkier Rpz units (**6** and **7**), their **6s** and **7s** minima are stabilized at shorter Pt-Pt distances than **4s** and **5s**.

For complexes **4** and **5** both minima are connected by a transition state (TS). In the case of **4**, a small ΔG (**4s**/**4f**) value along with a small activation barrier supports, within the experimental

error, a fast thermal equilibration in the ground state PES, thus resembling an intramolecular *butterfly flapping-like* motion. For complexes **6** and **7** the interconversion between conformers likely occurs in a barrierless manner. So, these results are consistent with the presence of both conformers in solution, with the *butterfly-spread* molecules being the predominant ones.

DFT calculations on the lowest adiabatic triplet excited state (T_1) PES reveal the existence of two local minima (Figure 15) for all the complexes: the *butterfly-spread* conformers, which exhibit Pt-Pt distances and Pt-Pt bond orders (BO) similar to those observed for them in the GS, and the *butterfly-folded* conformers, which exhibit intermetallic distances shortened by *ca.* 0.22 Å and Pt-Pt BO increased by 0.4 with respect to those in the GS. Except for complex **7**, the two conformers are connected by a transition state.

	d(Pt-Pt), Å	BO		d(Pt-Pt), Å	BO
4s	3.21	0.099	**4f**	2.75	0.621
5s	3.20	0.110	**5f**	2.75	0.626
6s	3.09	0.116	**6f**	2.75	0.591
7s	3.02	0.102	**7f**	2.74	0.586

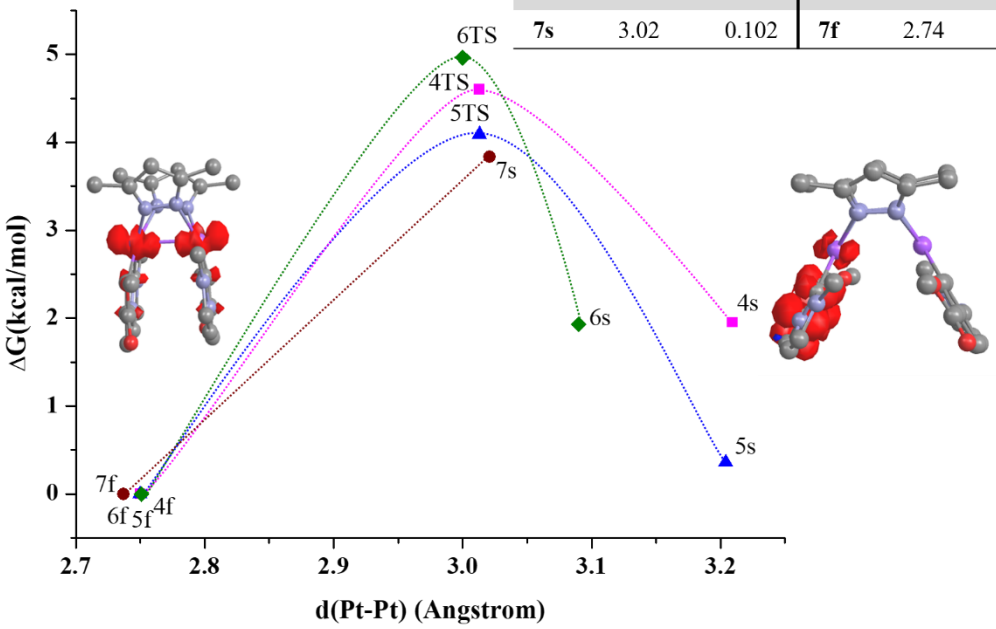

Figure 15. Calculated relative energy profile (PCM(THF)-M06/6-31G(d) and MWB60(Pt)) and Bond Order (BO) in first triplet excited state (T_1) for the interconversion between the **4f-7f** and **4s-7s** conformers. Spin density distribution plots of **6f** (left) and **6s** (right). MUE (M06)= 2.48 kcal/mol.[43]

The calculated spin density distribution for **4s**-**7s** indicates a mixed ^{3}IL/^{3}MLCT [π(C^C*)] → π*(C^C*)]/5d(Pt) → π*(C^C*)] character for their T_1 states, while a ^{3}MMLCT [dσ*(Pt-Pt) → π*(C^C*)] character for the T_1 states of **4f**-**7f** (see Figure 15 for **6s**/**6f**). Note that the changes in the Pt-Pt distances and the BO values from the GS to T_1 states in the *butterfly-folded* conformers **4f**-**7f**, almost agree with a one-electron excitation from the dσ*(Pt-Pt) orbital.

The change of excited state character when going from the **4s**-**7s** minima (^{3}IL/^{3}MLCT) to the **4f**-**7f** ones (^{3}MMLCT) leads to an extra stabilization of the latter conformers by 0.085 eV (1.95 kcal/mol), 0.015 eV (0.36 kcal/mol), 0.084 eV (1.93 kcal/mol), and 0.166 eV (3.83 kcal/mol) for complexes **4**-**7** respectively. Note also that certain amount of Pt-Pt bonding is only possible in the T_1 state but not in the GS.

A comparison reveals an opposite trend in the relative stability of folded and spread conformers, the former being more stabilized in their T_1 states, especially for complex **7**. The TSs for the interconversion between conformers in the T_1 state were located for complexes **4**-**6**, indicating that the energy barriers for PSC are larger than those for the flapping-like intramolecular motion in the GS.

Details about the absorption properties of **4**-**7** investigated with PCM-TD-DFT calculations in the presence of THF, the frontier molecular orbitals for **4s**-**7s** and **4f**-**7f** and the energies of their lowest singlet excited states can be found in the ESM-2. The lowest singlet excited states have predominant HOMO to LUMO character and can be described mainly as ^{1}MLCT/^{1}IL [5d(Pt) →π*(C^C*)]/ [π(C^C*)] →π*(C^C*)] for **4s**-**7s**, while some additional ^{1}MMLCT [dσ*(Pt-Pt) →π*(C^C*)] character is found for those of **4f**-**7f**. The vertical ΔSCF-M06 emission energies from the T_1 optimized geometries were calculated as well, rendering values of *ca.* 510 nm for **4s**-**7s** and of *ca.* 570 nm for **4f**-**7f** (see Table S4 ESM-2).

1.5.2.2.Absorption Spectra.

The absorption spectra of these compounds in 2-MeTHF (10^{-3} M **4-6**, 10^{-5} M **7**) show their lowest-energy absorption bands ($\varepsilon \sim 9 \cdot 10^3$ M^{-1} cm^{-1}) in the range 325- 390 nm. They match the $S_0 \rightarrow S_1$ transitions calculated for the predominant *butterfly-spread* molecules **4s-7s**. Their predominant HOMO to LUMO character (Figure 16) allows them to be described as ^{1}IL/ ^{1}MLCT. Despite the low contribution of the Rpz to the frontier molecular orbitals (FMOs), they play an important role in both, the metal-metal interaction and the $S_0 \rightarrow S_1$ transition, since the bulkier of R group on the bridging pyrazolate (4-Mepz ≈ pz < 3,5-dmpz < 3,5-dppz), the shorter the platinum-platinum distance and the larger the bathochromic shift in the low energy-bands. That is why, for complexes **6** and **7**, some ^{1}MMLCT/^{1}IL [dσ*(Pt-Pt) → π*(C^C*)] could be reasonably attributed.

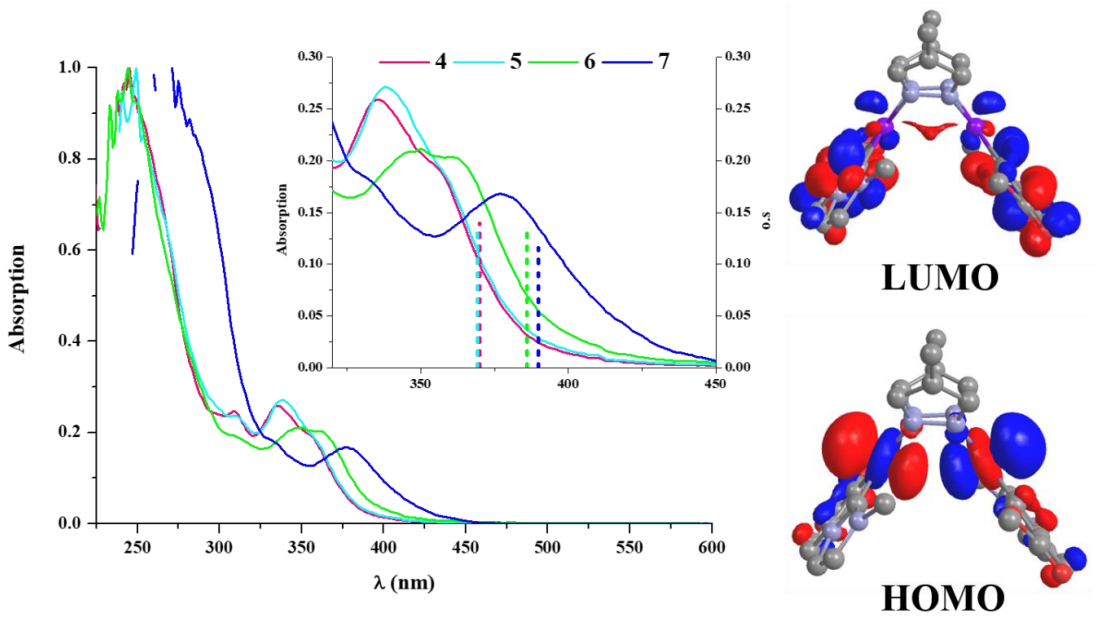

Figure 16. Left: UV-visible spectra (pathlength: 1mm) of **4-6** in 2-MeTHF 10^{-3} M and **7** in 2-MeTHF 10^{-5}M (pathlength: 1cm). Inset: Expanded view of the UV-Vis spectra and calculated spin allowed S0 → S1 transition (bars) of *butterfly spread* conformer. Right: Frontier MO (Isolvalue=0.03) for *butterfly spread* conformer of **5**.

1.5.2.3.Emission Spectra.

Upon excitation at $\lambda \leq 340$ nm, diluted solutions of complexes **4-7** in 2-MeTHF (10^{-5} M) at 77 K exhibit highly structured emission bands with $\lambda_{max} \sim 450$ nm (Figure 17). They are not affected by the nature of the Rpz ligands and agree with the computed ones for the conformers **4s-7s**. Therefore, they arise from an emissive state of ^{3}IL/ ^{3}MLCT character.

Complexes **4** and **7** show additional excitation and emission bands at lower energies ($\lambda_{exc} \sim 450$ nm, $\lambda_{em} > 600$ nm), attributable to the *butterfly-folded* molecules (calculated $S_1 \sim 426$ nm; $T_1 = 572$ nm for **4f**; and $S_1 \sim 429$ nm; $T_1 = 570$ nm for **7f**), although for **4** they are only perceptible in concentrated solutions (10^{-3} M) (Figure 17 right). The coexistence of *butterfly-spread* and *butterfly-folded* molecules for **4** and **7** agrees with the small ΔG value computed between the two conformers, **s**/**f** in the GS (ΔG: 0.076 eV (1.76 kcal/mol) **7s**/**7f**, 0.129 eV (2.97 Kcal/mol) **4s**/**4f**).

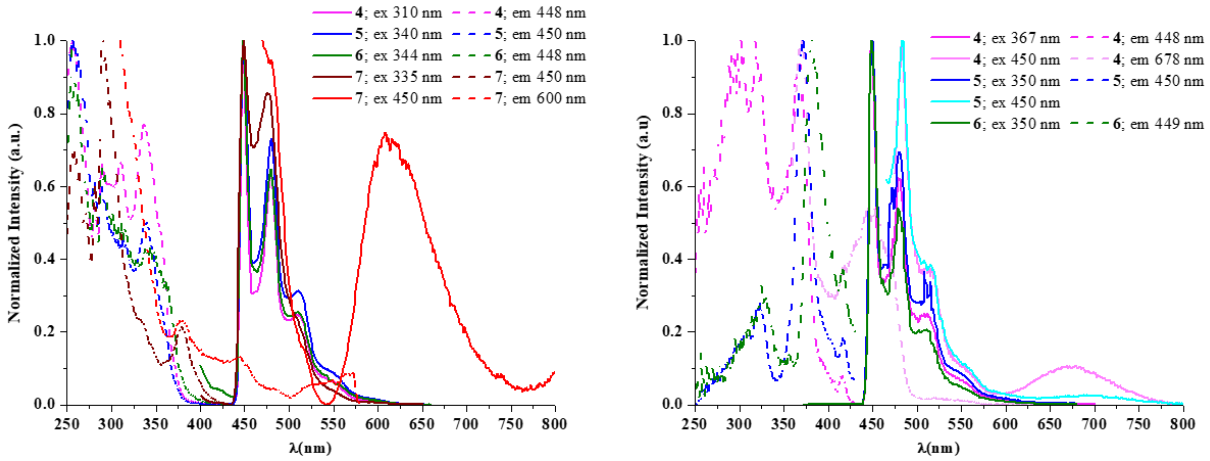

Figure 17. Normalized excitation (dotted lines) and emission (solid lines) spectra at 77K under Ar atmosphere, left: **4-7** in 2-MeTHF 10^{-5}M; right: **4-6** in 2-MeTHF 10^{-3}M.

In doped PMMA films (5%) in the air, complexes **4-7** afford intense sky-blue emissions (Complex **7** as an example in Figure 18), which match with those observed in 2-MeTHF (10^{-5}M) at 77K, with quantum yields of 72 % **4**, 83% **5**, 79% **6**, and 86% **7** (Table 3).

Table 3. Photophysical data for **4-7** in PMMA films and solid state in the air at 298K

	Media	λ_{exc} (nm)	λ_{em} (nm)	CIE (x;y)	τ (μs)	ϕ	k_r[b]	k_{nr}[c]
4	PMMA[a]	390	483_{max},517_{sh}, 567_{sh}	0.18; 0.32	3.7	0.20	$5.4\ 10^4$	$21.6\ 10^4$
	PMMA[a]	350	483_{max},517_{sh}, 567_{sh}	0.18; 0.32		0.72		
	Solid	390	469, 527_{sh}, 556_{max}	0.41; 0.52	0.4 (20%); 1.4 (80%)	0.03	$2.5\ 10^4$	$79.2\ 10^4$
5	PMMA[a]	390	469, 485_{max} ,524_{sh}	0.16; 0.29	3.5	0.54	$15.4\ 10^4$	$13.1\ 10^4$
	PMMA[a]	370	473, 492_{max} ,536_{sh}	0.16; 0.27		0.83		
	Solid	390	472, 527_{sh}, 559_{max}	0.41; 0.53	0.3 (22%); 1.1 (78%)	0.03	$3.2\ 10^4$	$103.2\ 10^4$
6	PMMA[a]	390	464, 484_{max} ,523_{sh}	0.15; 0.25	3.4	0.53	$15.7\ 10^4$	$13.8\ 10^4$
	PMMA[a]	380	464, 484_{max} ,523_{sh}	0.15; 0.25		0.79		
	Solid	390	468, 487_{max}	0.19; 0.35	0.3 (32%); 0.6 (68%)	0.16	$30.1\ 10^4$	$158.1\ 10^4$
	Grinded solid	390	468, 492_{max} , 519	0.29; 0.47	0.2 (20%); 0.6 (80%)	0.6	$11.2\ 10^4$	$175.4\ 10^4$
7	PMMA[a]	390	480_{max}	0.14; 0.26	2.2	0.69	$31.7\ 10^4$	$14.1\ 10^4$
	PMMA[a]	380	480_{max}	0.14; 0.26		0.86		
	Solid	390	469,482_{max} , 553_{sh}	0.24; 0.37	0.5 (30%); 1.1 (70%)	0.29	$32.9\ 10^4$	$80.7\ 10^4$
	Grinded solid	390	553_{max}	0.39; 0.55	1.1 (33%); 2.2 (67%)	0.51	$28.3\ 10^4$	$27.2\ 10^4$

[a] 5% wt. [b] Radiative decay rate constant given as $k_r = \phi/\tau_{exp}$; [c] $k_{nr} = (1-\phi)/\tau_{exp}$

Compounds **4-7** are scarcely luminescent at r.t., in solution, even in an argon atmosphere. However, at r.t. diluted solutions in 2-MeTHF (10^{-5}M) gives rise to a weak emission due to **4s** and **5s** for complexes **4** and **5**; a dual emission with maxima at 456 and 552 nm due to **6s** and **6f** for compound **6** and a broad band centered at 559 nm arising from **7f** for complex **7** (see Figure S13 ESM-2).

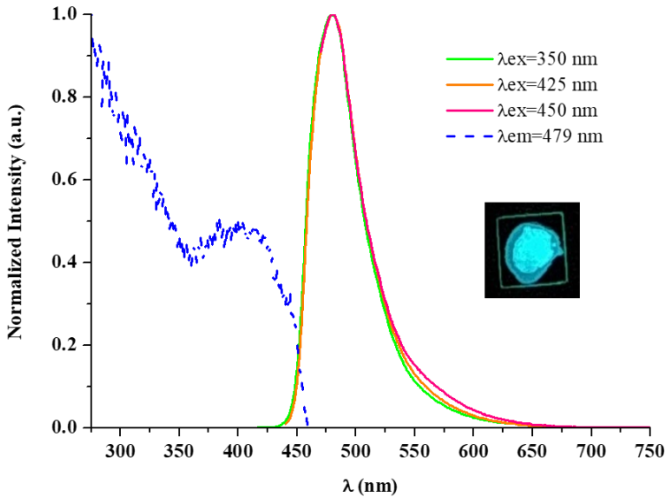

Figure 18. Normalized emission and excitation spectra of complex **7** in 5 wt % PMMA film in the air. Picture was taken under 365 nm UV light.

In summary, photoexcitation of complexes **4-7** at $\lambda < 380$ nm allows the major **4s-7s** conformers to reach the ^{1}IL/MLCT excited state; then, by a rapid intersystem crossing (ISC) the ^{3}IL/MLCT (T_s) state will be populated (see Scheme 9). In fluid solution, where the geometries of neither ground states nor those of the excited states are constrained, a photoinduced structural change (PSC) process between T_s and T_f conformers could happen depending on both, ΔG (T_f-T_s) and the PSC energy barrier. In the case of **7**, the computed barrierless PSC process along with the large ΔG values (T_{7f}-T_{7s} = -0.166 eV, -3.83 kcal) leads to T_{7f} almost in an exclusive manner. This piece of evidence explains why the emission from T_{7f} is the only one observed experimentally. In case of complex **6**, characterized by a smaller ΔG (T_{6f}-T_{6s} = -0.84 eV, -1.93 kcal) and a non-negligible PSC barrier (0.132 eV, 3.04 kcal), a thermal equilibrium between T_{6s} and T_{6f} is likely at r.t., and thus explaining its dual emission.

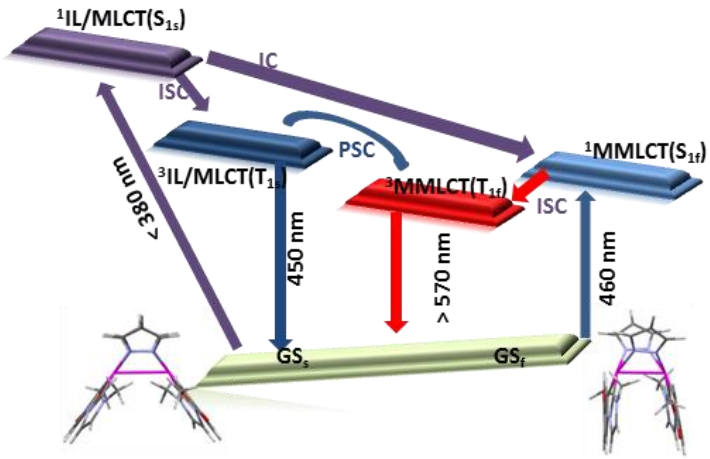

Scheme 9. Schematic diagrams of photophysical processes based on the steady-state excitation and emission spectra along with the results of the theoretical investigations

In the case of complex **5** with lower ΔG (T_{5f}-T_{5s}= -0.015 eV, -0.36 kcal), but larger energy barrier (0.162 eV, 3.73 kcal/mol) the PSC seems not to take place and the emission arises only from T_{5s}. For complex **4**, with ΔG (T_{4f}/T_{4s}= 0.085 eV, 1.95 kcal) and PSC energy barrier (0.115 eV, 2.65 kcal) on the same order of magnitude than those calculated for complex **6**, the PSC was expected to occur, but however, the emission arises only from T_{4s}. In this case, internal conversion (IC) from ^{1}IL/MLCT to ^{1}MMLCT competes with ISC to ^{3}IL/MLCT, and a faster quenching of the $^{1/3}$MMLCT states of complex **4**, as compared to that occurring in complexes **6** and **7**, enabled by the lack of steric hindrance of the reactive positions in complex **4**, could account for the absence of this low-energy emission.

In rigid media (2-MeTHF 10^{-5} M at 77K or PMMA films), photoexcitation of complexes **4**-**7** at λ < 380 nm leads in an analogous manner to the emission from the higher-lying triplet state ^{3}IL/MLCT, despite the greater stability of the ^{3}MMLCT state. This indicates that the energy barriers to connect the T_s/T_f wells are large enough to prevent the PSC in 2-MeTHF at 77K and it is also in agreement with PMMA being a rigid glass at r.t. (Tg = 378 K).[74] Notably, the frozen glass environment leads to a deceleration of the nonradiative pathways and thus leading to large PLQY values in PMMA films (see Table 3).

On the other hand, irradiation at $\lambda > 400$ nm will populate the low-energy states of the minor **4f-7f** conformers, ^{1}IL/MLCT with some ^{1}MMLCT character (see Scheme 9). A fast ISC to the close-lying triplet state ^{3}IL/MLCT,[91] would lead to the high-energy emission, which is the only one observed in 5% wt PMMA films of **4-7**. The low PLQYs when compared with those observed by irradiation at $\lambda < 380$ nm (see Table S27 ESM-2), agree with the low ratio of *butterfly-folded* molecules in the samples, but still being significant. Therefore, for complexes **5-7**, the existence of close-lying ^{1}IL/MLCT/MMLCT- ^{3}IL/MLCT states make possible to get intense blue-emissions (PLQY: 40%-60%) from doped films by irradiation with wavelengths in the visible region.

1.5.2.4.Mechanoluminescence in the Solid State.

The as-prepared powders of **4** and **5** are scarcely emissive and neither their excitation nor their emission spectra exhibit changes after grinding the solids with a mortar and pestle. However, complexes **6** and **7**, exhibit mechanoluminescence in the solid state. After grinding, the pale-yellow solids do not visually change their colours but their photoluminescence changes from blue to yellowish-green. Before to be grinded, a powdered sample of **6** exhibits a sky-blue emission, similar but weaker than that exhibited in PMMA film (5 % wt), which we attribute to ^{3}IL/MLCT. After grinding, the emission becomes green due to the presence of an intense lower-energy band with $\lambda \sim 540$ nm, that could be assigned to the ^{3}MMLCT state of molecules with *butterfly-folded* configuration in accordance with the theoretical calculations. However, in view of the intermolecular π-π interactions observed in the single-crystal X-ray structure of **6** (see Figure 9) and the decreased PLQY upon grinding, the participation of excimeric ^{3}π-π* states to the low-energy band cannot be ruled-out.[92-93]

In case of compound **7**, photoexcitation of as-prepared powder leads to a greenish-blue emission with λ_{max} at 480 nm and an incipient shoulder at 553 nm, that were assigned to ^{3}IL/MLCT and ^{3}MMLCT emissions respectively. Mechanical grinding resulted in a suppression of the

^{3}IL/MLCT band along with an increase of the ^{3}MMLCT one and an enhancement of the PLQY (see Figure 19). As a result, the photoluminescence of powdery samples of **7** is intensified and changed from greenish-blue to yellowish-green upon grinding.

This agrees with the *butterfly-spread* conformer, **7s** being the major one in the GS and the fact that no PSC can take place in rigid media. Mechanical grinding seems to induce changes in the GS, that somehow shorten the Pt-Pt distances and enforces the intramolecular Pt-Pt interactions, in such a way that in the grinded solid, **7-g** the phosphorescence arises mainly from **7f**.

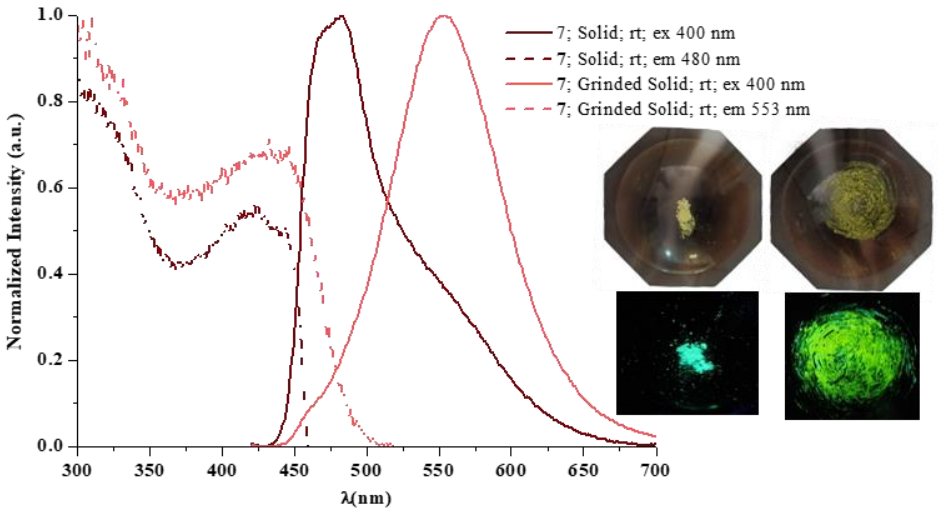

Figure 19. Normalized emission and excitation spectra of complex **7** in solid state in the air at r.t.; pictures were taken under 365 nm UV light.

Structural changes involving the intramolecular Pt-Pt separation in the GS as the origin of mechanoluminesce seems plausible on the bases of experimental and theoretical data and once other causes like desolvation or intermolecular interactions, were dismissed. The grinded solid, **7-g** undergoes the reverse change partially upon cooling to 77 K, as deduced from the emission and excitation spectra collected at r.t. and 77 K (Figure 20 left).

Structural changes involving the intramolecular Pt-Pt separation in the GS were reported for the thermochromic platinum-*butterfly* compound [{Pt(ppy)(μ-Ph$_2$pz)}$_2$],[74] but those induced by mechanical grinding had never been reported. In this case, like in complex **7** elongation of the

Pt-Pt distance occurs when the temperature drops. Also, the transformations resulted to be reversible by addition of THF, toluene or diethyl ether to the grinded samples of **6** and **7** that led to the recovery of the blue emission (see Figure 20 for **7**), and thus presumably restoring the previous structure arrangement.

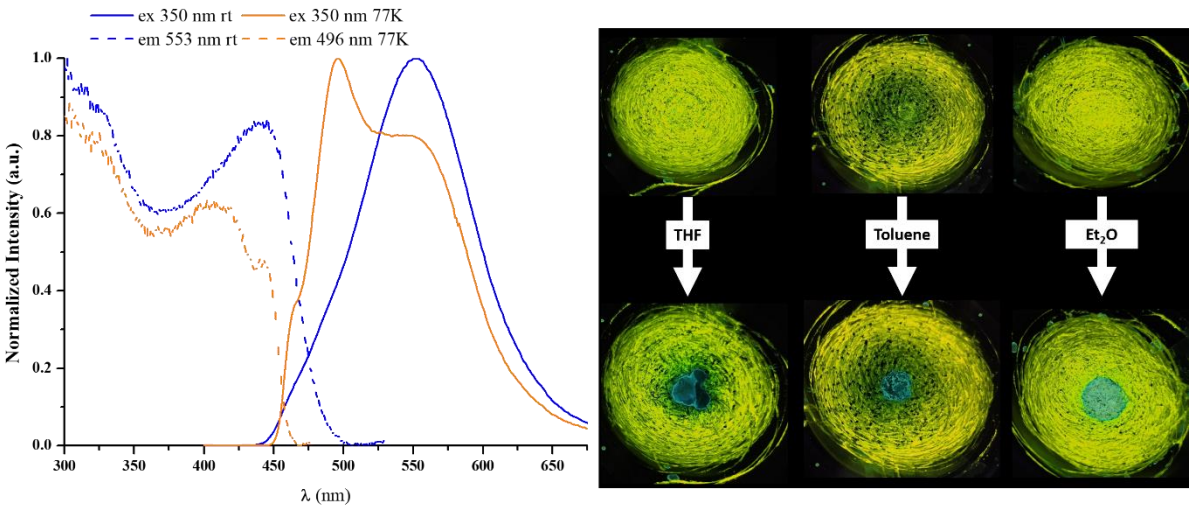

Figure 20. Left: Normalized emission and excitation spectra at r.t. and at 77K of the grinded solid, **7-g** in the air. Right: Pictures of mechanical grinding samples of **7** in response to solvent treatment taken under 365 nm-UV light

Therefore, it could be argued that the bulkiness of the μ-pyrazolates has a strong impact not only on the luminescence, but also on the mechanoluminiscence of these platinum *butterflies* in the solid state. As the bulkiness increases, the intermolecular π-π interactions become more hindered, affording a less efficient non-emissive deactivation channels and consequently a more efficient emission. In addition, as the steric demand of the μ-pyrazolates increases, the Pt-Pt interaction, enhanced by mechanical stimulation, causes a bathochromic shift of the emission (2750 cm^{-1}, **7**) along with a remarkable increment of its PLQY.

1.5.3.Comparative Study of the Photophysical Properties of Mono- and Dinuclear Complexes

In the bis-pyrazole complexes neither the lowest energy absorptions nor the emissions are affected by the nature of the RpzH ligands (**1b**-**3b**) and anions (**1a**-**1c**), in agreement with the marginal contribution of them to the frontier orbitals (FOs), HOMO and LUMO. Therefore, they were assigned mainly to intraligand charge transfer on the NHC ($^{1/3}$ILCT). These complexes exhibit in 5% doped PMMA films, intense blue phosphorescence with QY close to 100% and CIE coordinates close to the desirable ones for blue emitters upon excitation at $\lambda \leq$ 380 nm.

For the dinuclear pyrazolate-bridged complexes (**4**-**7**) two conformers, the *butterfly-spread* **4s**-**7s** and the *butterfly-folded* **4f**-**7f**, were optimized in the GS (S_0) and in the lowest adiabatic triplet excited state (T_1) PES, with the former being the more stable in the GS and the latter in the T_1. In these complexes the free energy difference between the two conformers, ΔG (s/f) and the energy barriers for the conversion of one into the other, as much in the GS as in the T_1, depend on the bulkiness of the Rpz groups and determine their absorption properties and their chameleonic photo- and mechanoluminescence.

So, the lowest-energy absorption match with the $S_0 \rightarrow S_1$ transitions calculated for the major *butterfly-spread* species, **4s**-**7s.** In complexes **6** and **7** it appears clearly red-shifted with respect to those in **4**, **5** and **1b**-**3b**, more as the bulkiness of the Rpz increases. The nature of this transition is mainly MLCT/ILCT with some MMLCT character.

In rigid media (2-MeTHF 10^{-5} M at 77K, PMMA films), complexes **4-7** exhibit sky-blue phosphorescence (λexc < 380 nm) arising from T_s, because the energy barriers to connect the T_s/T_f wells are large enough to prevent the PSC and show QYs up to 86% in 5% doped PMMA films in the air. By excitation at longer wavelengths (λexc ~ 450 nm), complexes **4** and **7** show the emission from T_f, at lower energy, although in case of **4** this is only perceptible at high concentration (10^{-3}M). In addition, in complexes **4**-**7**, it is possible to get intense blue-emissions

(PLQY: 40%-60%) under excitation with wavelengths in the visible region, up to 450 nm, which is due to the existence of close-lying ^{1}IL/MLCT/MMLCT- ^{3}IL/MLCT states of the **4f**-**7f** species.

In solid state (Figure 21), the bulkiness of the pyrazolate has a strong impact on the luminescence of **7,** which exhibits mechanoluminescence. That is, photoexcitation of as-prepared powder leads to a greenish-blue emission with λ_{max} at 480 nm and an incipient shoulder at 553 nm, from Ts (^{3}IL/MLCT) and T_f (^{3}MMLCT) respectively. Mechanical grinding causes the suppression of the ^{3}IL/MLCT band and the increase of the ^{3}MMLCT one, resulting in a bathochromic shift of the emission from greenish-blue (**7**) to yellowish-green (**7-g**) along with a remarkable increment of its PLQY. Therefore, the mechanoluminescence mechanism in **7**, associated with an intramolecular structural change in the GS that somehow shortens the Pt-Pt distances and enhances the Pt-Pt interactions, is clearly determined by the bulkiness of the 3,5-dppz bridging group.

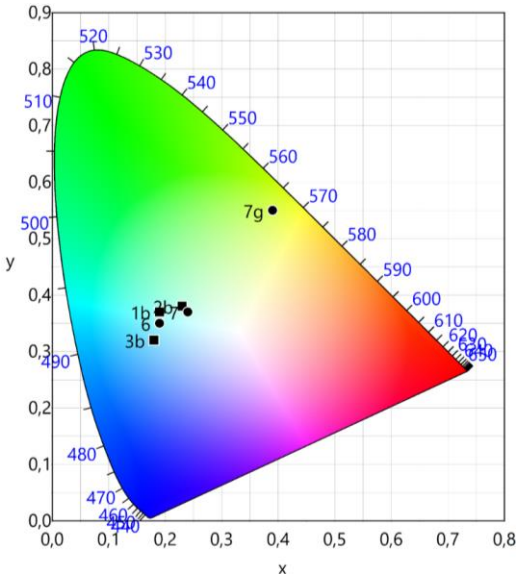

Figure 21. CIE 1931 diagram with the solid emissions of **1b-3b**, **6**, **7**, and **7g** as ground

1.5.4.Optical Properties of the New Cluster [Pt_2Ag_2] (8)

The most significant feature of **8** regarding its emissive behavior, is the blue shift of the emission band of powdery solid in relation to that of its precursor (λ_{max} = 483 nm **8**, 489 nm **1b**). This reflects the formation of the Pt → Ag dative bond since the electron density of the Pt center decreases upon bonding to Ag(I), lowering the energy of HOMO.[94-96] Likewise, there is a considerable reduction of the emission lifetime (6.4 μs **8**, 21.6 μs **1b**) and an increase of the QY values (0.55 **8**, 0.33 **1b**) in powdery solid samples. According to this and in line with similar compounds,[84, 97] this emission has been assigned to a mixed ^{3}IL/^{3}MLCT emissive state.

Chapter 2

Oxidation of the Flapping Platinum *Butterfly* [{Pt(C^C*$_A$)(μ-pz)}$_2$] by Halocarbons

2.1.Introduction

Cooperative effects between the adjacent d^8 metal centers in dinuclear complexes promote the formation of stabilizing metal-metal bonds in the intermediates of many catalytic reactions involving oxidative addition (OA)- reductive elimination processes.[98-100] Formation of low-energy metal-metal bonded intermediates enable reaction pathways and product unavailable from monometallic precursors.[101-104] Pd_2(III,III) or Rh_2(II,II) species are some examples of low energy transition states for C−H functionalization[4,5] or alkene hydroformylation[105] reactions, respectively.

In this context, dinuclear complexes of Rh(I) and Ir(I) have provided a very rich platform to C-X bond cleaving thermal or photoinduced chemistry. In the literature, it can be found many examples of haloalkanes, such as CH_3I or CH_2I_2, that are added to Ir_2(I,I) *via* a bimetallic S_N2 pathway,[106] yielding metal−metal bonded M_2(II,II) compounds. Sometimes these reactions follow a radical-like[107] mechanism or a monometallic S_N2 pathway resulting, in the second case, in mixed valence Ir(I)−Ir(III) compounds.[108] Few examples of OA of chloroalkanes (RCl) to Ir_2(I,I) compounds leading to metal−metal bonded complexes containing Cl−Ir(II)−Ir(II)-X (X = R, Cl) frameworks have been reported,[109-110] and in most circumstances they require visible- or UV-light irradiation. But relatively recently, the OA of RCl to [{Ir(μ-Pz)$(CNBut)_2$}$_2$] (R = CH_2COMe, CH_2CO_2Me, $CH(Me)CO_2Me$)[10] and [{Ir(μ-NH_2)$(cod)_2$}$_2$] (RCl = CH_2Cl_2, CH_3Cl)[111] have been reported in dark experimental conditions, rendering metal−metal bonded Ir(II)−Ir(II) compounds. The Ir_2(II,II) systems show relative inertness for further OA of haloalkanes, but when this occurs they render Ir_2(III,III) compounds with no metal−metal bond. Examples are illustrated by the double OA of MeI to complexes [$(L)_2$Ir(μ-pz)$_2$Ir$(CNBut)_2$][16] or $ClCH_2R$ (R= Ph, $CH{=}CH_2$) to [{Ir(μ-pz)$(CNBut)_2$}$_2$].[10]

Thus, as shown above, when the metal centers are held in proximity by bridging ligands, different kinds of mono- or bimetallic mechanisms can operate. The pathway of these reactions depends on many factors, such as the nature of the added molecule, the ligands and the metal.[112-113] Referring to the latter, the OA mechanism studies of halocarbons to Pt_2(II,II) complexes are still scarce in comparison to those reported for Rh_2(I,I) and Ir_2(I,I).

Square planar platinum(II) complexes are known to exhibit weak intramolecular and intermolecular interactions that lead to triplet metal–metal-to-ligand charge transfer $^3[5d\sigma^* \rightarrow \pi^*]$ and/or $^3[5d\sigma^* \rightarrow 6p\sigma]$ excited states.[114-116] The diradical character of such excited states with enhanced metal–metal bonding interactions renders these complexes capable of performing photocatalytic reactions.[117-119] The classic example, $[Pt_2(\mu\text{-}P_2O_5H_2)_4]^{4-}$, is a highly active species for the photoinduced dehydrogenation of alcohols to aldehydes/ketones.[114] Additionally, this complex can experience a thermal [2e, 2c] OA of RI (R = Me, Et, ^{n}Pr) through a radical mechanism, although contribution of S_N2-type one cannot be excluded for MeI.[35] Due to the uniqueness of the bridging pyrophosphito (pop) ligand, extending the photochemistry of $[Pt_2(pop)_4]^{4-}$, to other platinum(II) systems is a non-trivial task. In this regard, the lantern- or half-lantern compounds with short intermetallic distances (< 3 Å) are among the best suitors, such as $[Pt_2(pyt)_4]$,[120] (pytH = pyridine-2-thiol) $[Pt_2(ppy)_2(pyt)_2]$,[121] (ppy = 2-phenylpyridyl-H) or $[\{Pt(bzq)(\mu\text{-}N\text{^}S)\}_2]$[34] [bzq = benzo[h]quinoline, HN^S = 2-mercaptopyrimidine]; the latter undergoes [2e, 2c] thermal oxidations with CH_3I and CHX_3 (X = Br, I) following a bimetallic S_N2 or radical mechanism. On the other hand, complexes with flexible bridging ligands, $[Pt_2Me_2(C\text{^}N)_2(\mu\text{-}P\text{^}P)]$ [C^N = bzq, ppy; P^P = dppf (1,1′-bis-(diphenylphosphino)ferrocene), dppa (1,1′-bis-(diphenylphosphino)acetylene)],[122-124] and *cis*,*cis*-$[Me_2Pt(\mu\text{-}NN)(\mu\text{-}dppm)PtMe_2]$ (NN = phthalazine, dppm = bis-(diphenylphosphino)methane), reacted with CH_3I

in two steps, *via* a monometallic S_N2 mechanism. As a result, the dinuclear platinum(IV) derivatives $[Pt_2Me_4I_2(C\hat{}N)_2(\mu\text{-}P\hat{}P)]$ and $[Me_3Pt(\mu\text{-}I)_2(\mu\text{-dppm})PtMe_3]$ were obtained.[125]

In the chemistry of dinuclear pyrazolate-bridged complexes of platinum(II), such as $[\{Pt(N\hat{}E)(\mu\text{-Rpz})\}_2]^{2+}$ (E = N, diimines or pyridylpyrazolate; E = C, pyridyl-NHC),[82, 126-128] $[\{Pt(C\hat{}N)(\mu\text{-Rpz})\}_2]$(C^N= C,N-cyclometalated ligand),[129] and $[\{Pt(C\hat{}C^*)(\mu\text{-Rpz})\}_2]$ (C^C* =phenyl-NHC),[78] with long intermetallic distances (> 3 Å), most studies have been focused on the control of the photoluminescence properties of the "*butterfly*" complexes by tuning the Pt···Pt separation; they can be modulated by controlling the *butterfly body* (bulkiness of the bridging pyrazolates) and the *butterfly wings* (bulkiness and electronic properties of the C^N group) (see Introduction of Chapter 1). So, despite these pyrazolate ligands have shown a great ability to hold two Pt centers in close proximity allowing a wide range of intermetallic separations (2.83 - 3.48 Å), up to now, not [2c, 2e] oxidation processes have ever been reported.

The unexpected reactivity of the dinuclear pyrazolate complexes (**4**-**7**) with halogenated solvents along with the importance of high-valent organometallic species in many organic syntheses, encouraged us to explore the reactivity of platinum (II) complexes $[\{Pt(C\hat{}C^*_{A/B})(\mu\text{-}pz)\}_2]$ toward halogenated species, such as haloforms and haloalkanes. Supported by density functional theory (DFT) studies on the oxidation mechanisms, we were able to prepare dinuclear complexes with the same core "$\{Pt(C\hat{}C^*)(\mu\text{-}pz)\}_2$" but different oxidation states Pt_2(III,III), Pt_2(III,III) ↔ Pt_2(II,IV), and Pt_2(IV,IV). They allowed us to substantiate the modeled mechanisms and to compare their structural and spectroscopic data.

This chapter is based on the following three peer-reviewed papers:

3.- Lorenzo Arnal, Sara Fuertes, Antonio Martín, Miguel Baya, Violeta Sicilia. A Cyclometalated N-Heterocyclic Carbene: The Wings of the First Pt_2(II,II) Butterfly Oxidized by CHI_3. *Chemistry – A European Journal* **2018**, *24* (70), 18743-18748. DOI: 10.1002/chem.201804013. (ESM-3)

4.- Violeta Sicilia, Lorenzo Arnal, Sara Fuertes, Antonio Martin, Miguel Baya. Metal-Metal Cooperation in the Oxidation of a Flapping Platinum Butterfly by Haloforms: Experimental and Theoretical Evidence. *Inorganic Chemistry* **2020**, *59* (17), 12586-12594. DOI: 10.1021/acs.inorgchem.0c01701. (ESM-4)

5.- Lorenzo Arnal, Daniel Escudero, Sara Fuertes, Antonio Martin, Violeta Sicilia. High-Valent Pyrazolate-Bridged Platinum Complexes: A Joint Experimental and Theoretical Study. *Inorganic Chemistry* **2022**, *61* (32), 12559-12569. DOI: 10.1021/acs.inorgchem.2c01441. (ESM-5)

Some additionally results have been included in this Memory, such as the reactivity of [{Pt(C^C*$_A$)(μ-pz)}$_2$] (**4**) with benzyliodide and the reactivity of [X(C^C*$_A$)Pt(μ-pz)$_2$Pt(C^C*$_A$)Bn] (X= Br **15-Br**, I **15-I**) under UV-light. Experimental procedure is included in the section Methodology. All data for characterization and figures of these unpublished results are collected in ESM-6

Chapter 2A

Oxidation of the Flapping Platinum *Butterfly* [{Pt(C^C*$_A$)(μ-pz)}$_2$] by Haloforms: Experimental and Theoretical Studies

2.A.1.Reactivity of [{Pt(C^C*$_A$)(μ-pz)}$_2$] (4) with Haloforms. Synthesis and Characterization of New Metal-metal Bonded Pt$_2$(III,III) Complexes

The reaction of [{Pt(C^C*$_A$)(μ-pz)}$_2$] (**4**) with haloforms (CHX_3; X= Cl, Br, I) renders different kinds of metal-metal bonded Pt(III,III) complexes depending on the experimental conditions.

Compound **4** reacts with haloforms (CHX_3; X= Cl, Br, I, molar ratio 1:4) in the air and the sunlight to give [{Pt(C^C*$_A$)(μ-pz)X}$_2$] (X = Cl **9-Cl**, Br **9-Br**, I **9-I**) as result of its photochemical oxidation.

In the dark under Ar atmosphere, compound **4** adds oxidatively $CHBr_3$ and CHI_3 to give [BrPt(C^C*$_A$)(μ-pz)$_2$Pt(C^C*$_A$)$CHBr_2$] (**10-Br**) and [IPt(C^C*$_A$)(μ-pz)$_2$Pt(C^C*$_A$)CHI_2] (**10-I**) in a selective way. By contrast, in the dark compound **4** is air and thermally stable in the presence of $CHCl_3$, even in refluxing toluene (110 ^{o}C), with light being required for this reaction to occur (see Scheme 10). Because of that, the corresponding complex, due to the OA of $CHCl_3$ to **4**, [ClPt(C^C*$_A$)(μ-pz)$_2$Pt(C^C*$_A$)$CHCl_2$] (**10-Cl**) could be just detected by ^{1}H and ^{1}H-^{195}Pt HMQC NMR experiments from a reaction mixture performed under Ar atmosphere by irradiation with UV-light (365nm).

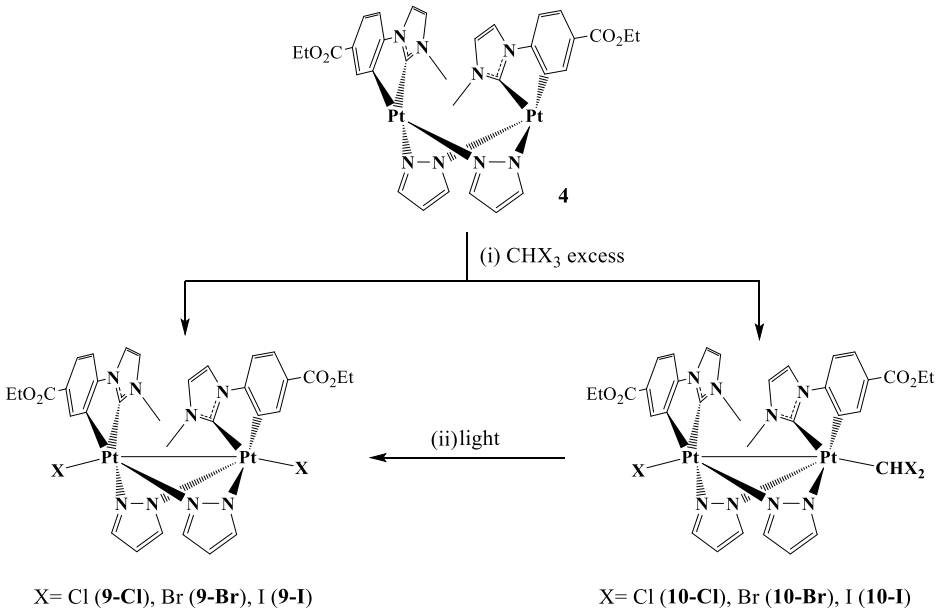

Scheme 10. Reaction pathways. For clarity, only the major isomer, the *anti* one, has been represented.

Compounds **9-Cl**, **9-Br**, **9-I**, **10-Br**, and **10-I** were isolated as yellow (**9-Cl** and **10-Br**) or orange (**9-Br**, **9-I** and **10-I**) solids in good yields, mostly as the *anti* isomer and then fully characterized.

The higher oxidation state of the platinum centers in these complexes with respect to those in complex **4** is evident from the dramatically downfield shift of the ^{195}Pt resonances ($\Delta\delta$(Pt) = 697-1348 ppm) and the great reductions of the $^{3}J_{H7,Pt}$ coupling constants (Table 4, Figure 22)

Structurally relevant for **10-Cl**, **10-Br**, and **10-I** is the presence of two separated ^{195}Pt signals, which evidences the presence of two non-equivalent platinum (III) fragments within each complex. In addition, their ^{1}H NMR spectra show characteristic singlets corresponding to the Pt-CHX_2 fragment (Figure 22 bottom for **10-Br**), flanked by two set of ^{195}Pt satellites, which agrees with a metal-metal bonded Pt_2(III,III) formulation for these derivatives.

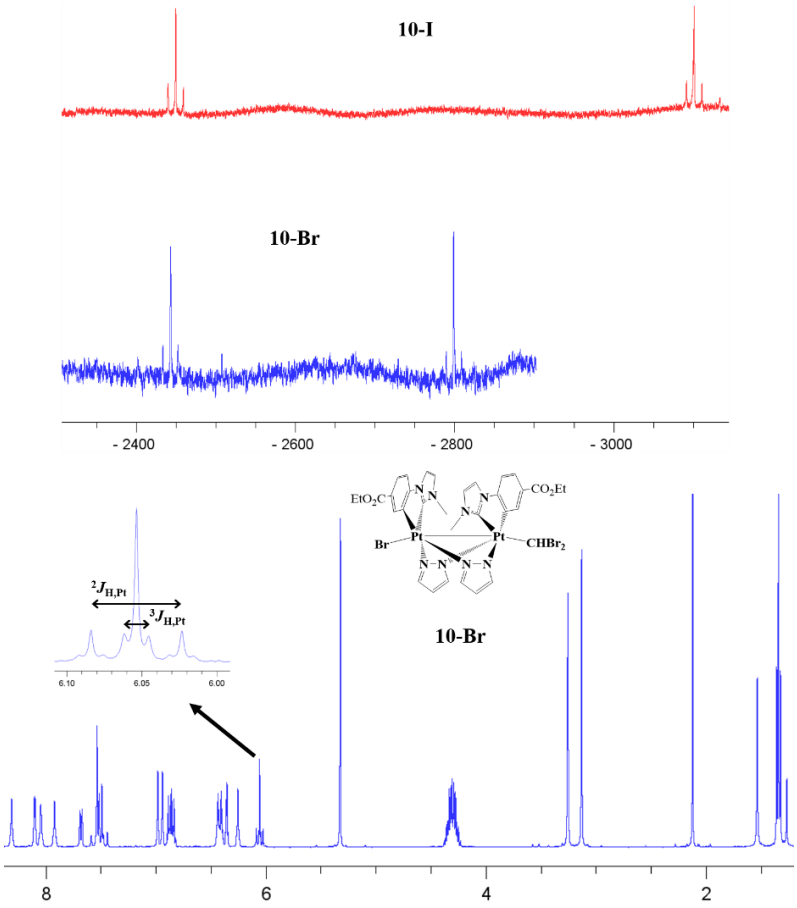

Figure 22. Top: ^{195}Pt NMR spectra of **10-Br** and **10-I**. Bottom: ^{1}H NMR spectrum of **10-Br** in CD_2Cl_2. Inset: Expanded view of the δH ($CHBr_2$) resonance.

Table 4. NMR data for Pt_2(III,III) complexes at rt in CD_2Cl_2. δ(ppm), *J*(Hz).

	Pt		**H_7**		**CHX_2**		
	δ	**$^1J_{Pt,Pt}$**	**δ**	**$^3J_{H7,Pt}$**	**δ**	**$^2J_{H,Pt}$**	**$^3J_{H,Pt}$**
4[a]	-3778		7.97	54.2			
9-Cl	-2441		7.50	39.6			
9-Br	-2675		7.49	40.0			
9-I	-3092		7.47	40.4			
10-Cl [a,b]	-2468(Cl); -2502 ($CHCl_2$)	-	-	-	6.59	28.7	2.47
10-Br	-2799(Br); -2443($CHBr_2$)	1633	7.51(Br); 7.48($CHBr_2$)	40.0($CHBr_2$)	6.05	24.2	6.3
10-I	-3107(I); -2454(CHI_2)	1674	7.54(I); 7.46(CHI_2)	44.9(I); 44.8(CHI_2)	6.40	30.4	5.9

[a] acetone-d_6. [b] Detected by ^{1}H and ^{1}H-^{195}Pt HMQC at 193K. Data for complex **4** have been included for comparison.

The molecular structures of **9-Cl**, **9-Br**, **9-I**, **10-Br**, and **10-I** were determined by single-crystal X-ray crystallography (see Figure 23 for **9-Br** and **10-Br**). They exhibit a similar boat-like shape with an *anti*-configuration of the "Pt(C^C*$_A$)" fragments. Besides, they exhibit an important shortening of the platinum-platinum distance (d(Pt-Pt), Å= 2.57446(18) (**9-Cl**), 2.5849(6) (**9-Br**), 2.6079(2) (**9-I**), 2.6302(4) (**10-Br**), 2.6324(3) (**10-I**)) with respect to **4**, indicative of the existence of a Pt^{III}- Pt^{III} bond in all of them. These distances increase with the *trans* influence of the ligands in the axial position (I_2CH > Br_2CH > I > Br > Cl), like it was observed in other Pt_2(III,III) complexes.[24, 83, 130-132] As far as we know, these were the only dinuclear metal-metal bonded $Pt^{III}(\mu\text{-pz})_2Pt^{III}$ compounds reported to date.

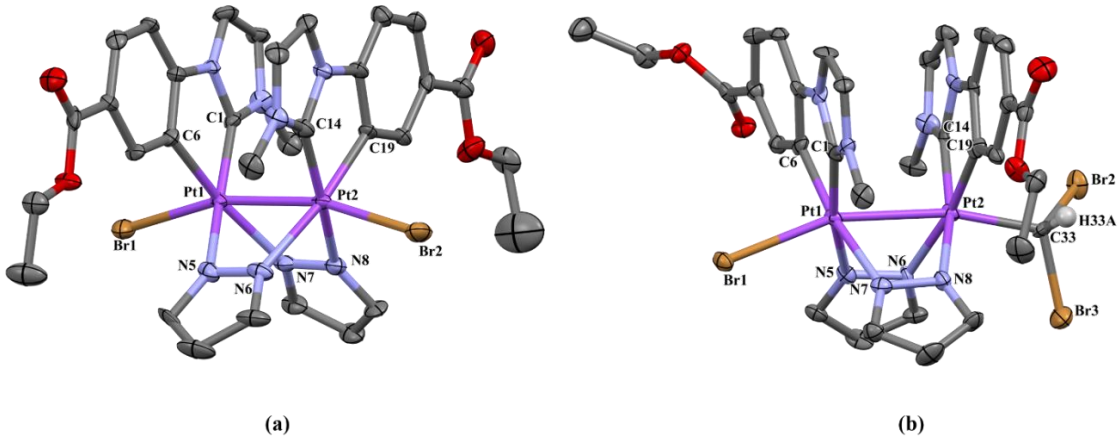

Figure 23. Molecular structures of complexes **9-Br** (a) and **10-Br** (b). Ellipsoids are drawn at the 50% probability level; solvent molecules and hydrogen atoms have been omitted for clarity

2.A.2.Mechanistic Study of the Reactivity of 4 with CHX_3 (X= Cl, Br, I).

2.A.2.1.Experimental Study

The mechanism of this unexpected [2c,2e] oxidation process was studied experimental and theoretically. To do that, solutions of **4** in acetone-d_6 were reacted with excess of haloforms (molar ratio 1:4 $CHBr_3$, CHI_3; 1:5 $CHCl_3$) in NMR tubes under different conditions and the reactions were followed by ^{1}H NMR spectroscopy (see Table 5). Comparative experiments

were carried out simultaneously in order to avoid environmental differences, e.g. temperature changes.

The thermally activated oxidation of **4** (8 x 10^{-3} M in acetone-d_6) with CHX_3 (X=Br, I) (molar ratio: 1:4) in the dark under Ar atmosphere are complete in few minutes, leading to **10-Br** (100%), **10-I** (93%), almost selectively. In the air, the reactions were less selective (see Scheme 10, path i, and Table 5).

Table 5. Data corresponding to the reaction of **4** with CHX_3 (X= Br, I) in acetone-d_6 (molar ratio 1:4).

Experimental Conditions	Ratio $CHBr_3$ (%) 4/ 9-Br/ 10-Br			Ratio CHI_3 (%) 4/ 9-I/ 10-I		
	15 min	3.5 h	24 h	15 min	3.5 h	24 h
Ar / dark	0/0/100	0/0/100	0/0/100	15/2/83	-	0/7/93
Ar / dark / Gal•	100/0/0	100/0/0	100/0/0	100/0/0	-	0/71/29
Air / dark	86/9/5	81/14/5	74/18/8	0/36/64		0/36/64
Air / sunlight	0/71/29	0/92/8	0/100/0	0/35/65	0/82/18	0/100/0

The simultaneous formation of Pt_2X_2 (**9-Br** and **9-I**) and $Pt_2X(CHX_2)$ (**10-Br** and **10-I**) species pointed to a radical mechanism for these thermal oxidations (eqs 2−5). The role of O_2 as a radical (R•) trap justifies the greater amount of **9-Br** or **9-I** in the final reaction mixtures (**9-Br /10-Br**; **9-I /10-I**) when the reactions were performed in the air, with respect to those performed under Ar atmosphere. This statement was confirmed making the reactions in the presence of Gal•, as radical (R•) scavenger. Once the starting material has completely reacted, these mixtures remain unreacted for at least 24h in the dark.

$$Pt_2 + RX \rightarrow Pt_2X\bullet + R\bullet \qquad \text{(eq.2)}$$

$$Pt_2 + R\bullet \rightarrow Pt_2R\bullet \qquad \text{(eq.3)}$$

$$Pt_2X\bullet + RX \rightarrow Pt_2X_2 + R\bullet \qquad \text{(eq.4)}$$

$$Pt_2R\bullet + RX \rightarrow Pt_2RX + R\bullet \qquad \text{(eq.5)}$$

By contrast, diluted solutions (10^{-4}-10^{-5}M) of **4** do not react with $CHBr_3$ in the dark, even after 45h, while under UV light (λ=365 nm) **4** is transformed completely into **9-Br.**

Considering that the reactions of **4** with CHX_3 (X=Br, I) lead to the selective formation of **10-Br**/**10-I** under Ar atmosphere and of **9-Br**/**9-I** in the air and the sunlight, we investigated the role of both, O_2 and UV light in the transformation of **10-Br** species into **9-Br** (Scheme 10, path ii).

With that purpose, we prepared two samples containing **10-Br** (obtained from **4** (8 x 10^{-3} M) and $CHBr_3$ (1:4) in acetone-d_6 under Ar in the dark) in J. Young NMR tubes. Then, one of the samples was freeze-pump-thaw degassed and placed under an O_2 atmosphere (1 atm). Subsequently, both samples were irradiated for 5 min with 365 nm-UV light, giving mixtures of **9-Br**/**10-Br** in different ratios (28%/ 72% in the O_2 free sample and 64%/ 36% in the O_2 containing one) (see Figure 24).

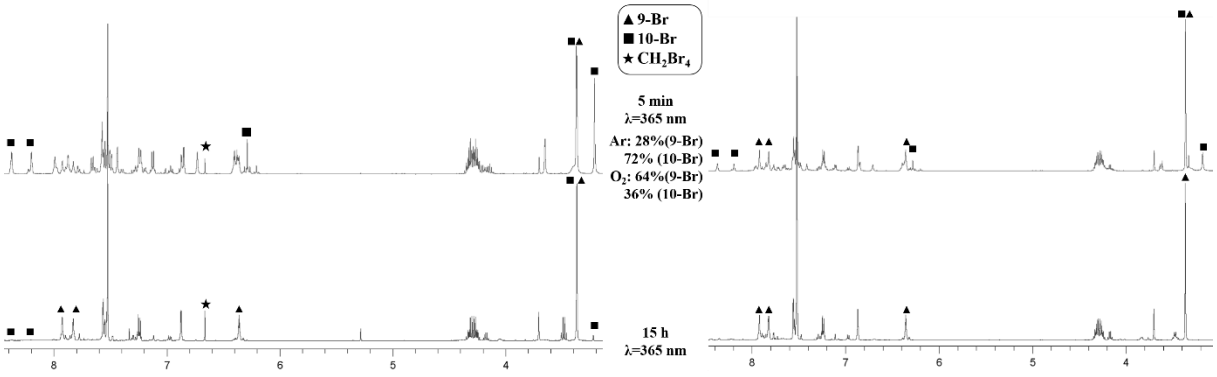

Figure 24. ^{1}H NMR spectra in acetone-d_6 of **10-Br** generated *in situ* and irradiated with 365 nm-UV light under Ar atmosphere (left) and under O_2 atmosphere (right).

As we see above, **10-Br** was stable under Ar in the dark and remains unchanged at least 24h, so the transformation of **10-Br** into **9-Br** was promoted by UV light with O_2 not being necessary, but making the process faster. In a thorough analysis of the ^{1}H NMR spectra, a singlet at 6,66 ppm was identified in the oxygen-free sample, which corresponds to $C_2H_2Br_4$, generated by •$CHBr_2$ radical coupling, which is indicative of a radical mechanism for path ii, as well. To

prove this early hint two samples of **10-Br** were prepared under Ar in the dark and galvinoxyl (Gal•) was added to one of them. After irradiation with 365-UV light, just the Gal•-free- sample displayed the singlet due to $C_2H_2Br_4$ and a faster transformation of **10-Br** into **9-Br**. Therefore, under Ar atmosphere, the photochemical bond homolysis of the Pt-$CHBr_2$ bond in **10-Br** promoted by UV light, followed by Br abstraction from $CHBr_3$ could account for the selective formation of **9-Br**. A similar mechanism is plausible for path ii in the reaction with CHI_3.

To study the oxidation of **4** with $CHCl_3$ two samples were prepared under Ar atmosphere in the dark, one of them with and the other without galvinoxyl (Gal•) (Table 6). Keeping in mind that this reaction needs light to take place, like for most oxidations of other platinum (II) complexes by chlorocarbons,[34, 133] the two samples were irradiated with 365 nm-UV light. These experiments showed that the presence of Gal• slows down the reaction and allows the selective formation of **9-Cl**, indicative of a radical mechanism, with Gal• acting as a radical scavenger.[35, 133] The role of molecular oxygen (O_2) as a radical trap, was confirmed by reacting **4** with $CHCl_3$ in the air under 365 nm light, which rendered **9-Cl** as the only oxidized species.

Table 6. Data corresponding to the reaction of **4** (8×10^{-3}M) with $CHCl_3$ (1:5) in acetone-d_6.

Experimental Conditions	**Ratio (%) 4/ 9-Cl/ 10-Cl**		
	15 min	**8 h**	**24 h**
Ar / λ=365 nm	89/ 8/ 3	-	35/ 33/ 32
Ar / λ=365 nm / Gal•	100/ 0/ 0	-	82/ 18/ 0
Air / λ=365 nm	83/ 17/ 0	34/ 66/ 0	0/ 100 /0
Air / λ=457 nm (blue LED)	80/ 20/ 0	8/ 92/ 0	0/ 100/ 0

In addition, we observed that in the air the reaction of **4** with $CHCl_3$ occurs by irradiation with blue LEDs (λ_{max}=457 nm) rendering **9-Cl** as the unique Pt_2(III,III) complex. However, under green (λ_{max}=510 nm) or red (λ_{max}=631 nm) LEDs, **4** remains unreacted. Besides, we observed that under blue light, this reaction goes faster than under 365 nm-UV light and that diluted

solutions (10^{-5}M) of **4** in acetone-d_6 in the air did not react with $CHCl_3$ under blue LEDs, but they did under 365 nm-UV light affording **9-Cl**.

2.A.2.2.DFT Calculations

To gain more in-depth knowledge about these reactions, DFT calculations were performed in a first stage, by Dr. Miguel Baya on the thermal oxidation of **4** by CHI_3 (see Scheme 11), and then extended to $CHBr_3$ and $CHCl_3$.

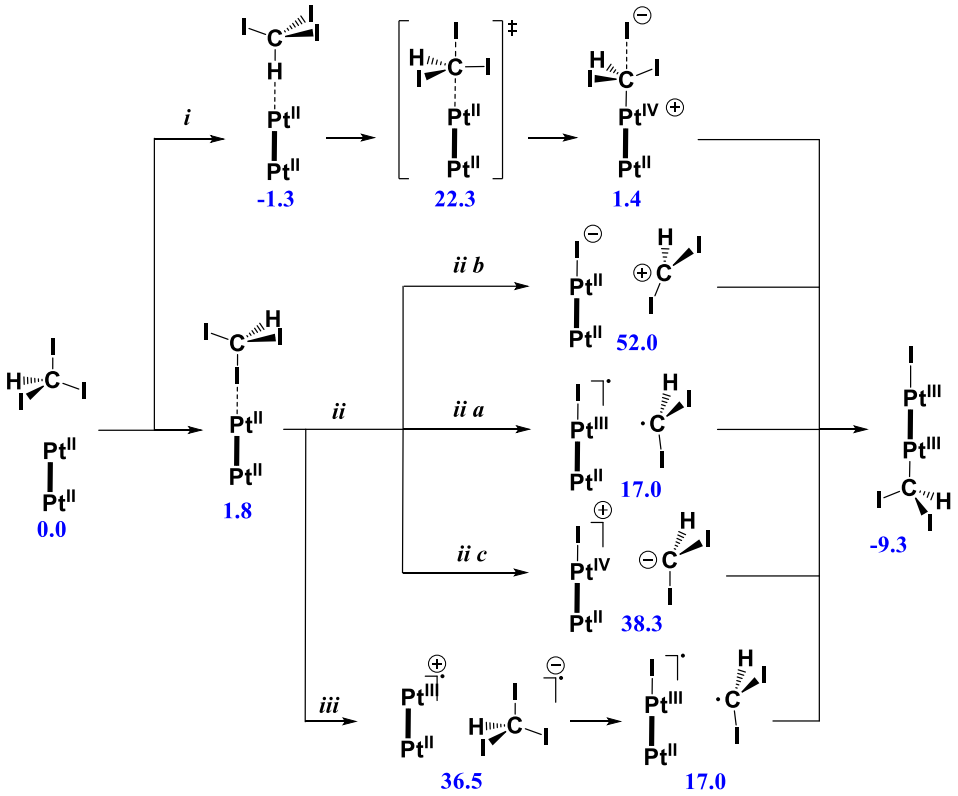

Scheme 11. DFT-calculated pathways and energy barriers (ΔG, kcal/mol, in blue, MUE (M06)= 2.48 kcal/mol[43]) for the thermal oxidation of **4** (S_{0s}, $d_{Pt\text{-}Pt}$ (Å) = 3.212) by CHI_3.

Thus, for the oxidation of **4** by CHI_3 under thermal conditions, three conceptually different metal oxidation pathways were considered: *i*) a classical S_N2 addition of iodoform to the Pt(II)-Pt(II) dimer; *ii*) an iodine-transfer from iodoform to the Pt(II)-Pt(II) dimer; *iii*) an electron-transfer from the Pt(II)-Pt(II) dimer to iodoform. The formation of either the Pt-Pt···CHI_3 or the Pt-Pt···$ICHI_2$ adducts as reaction intermediates is energetically feasible (Scheme 11). Interestingly, even though the S_N2 addition pathway (*i*) appears energetically accessible ($\Delta G^{\ddagger}$

= 23.6 kcal/mol), iodine-atom transfer to the platinum dimer (*iia*) is clearly favored (ΔG = 17.0 kcal/mol) and therefore emerges as the most likely reaction mechanism. Other variants as iodide transfer (*iib*), iodine-cation transfer (*iic*) and electron transfer from the platinum dimer to the iodoform (*iii*) are energetically disfavored processes.[107]

DFT calculations showed that pathway *iia* is energetically compatible with the experimental results. This means that the formation of the Pt(III)-Pt(III) compound **10-I** proceeds *via* a homolytic breakage of the I-C bond[134] in a S_0 [Pt-Pt···$ICHI_2$] adduct. Furthermore, the concomitant generation of radicals in the reaction media is consistent with the observed formation of the diiodide derivative **9-I** and also with the variable outcomes observed in the reactions carried out under argon atmosphere or in the presence of O_2 or galvinoxyl.

Subsequently, we extended the calculations to the reactions of **4** with $CHBr_3$ and $CHCl_3$ (Scheme 12). These calculations confirmed that a radical pathway, similar to the followed for CHI_3 is clearly the most favored option for the thermal oxidation of **4** by $CHBr_3$.

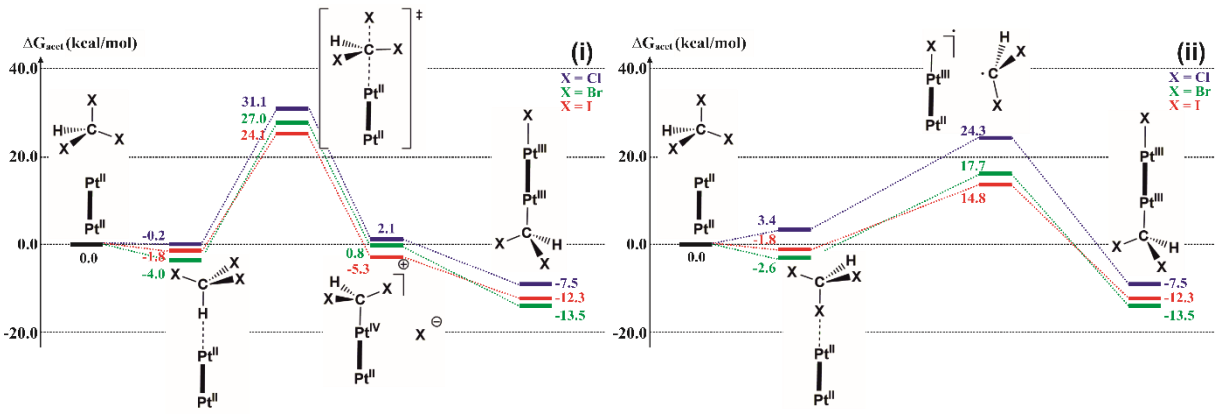

Scheme 12. Comparative DFT-calculated pathways and energy barriers (ΔG, kcal/mol) for the thermal conversion of **4** (S_{0s}) into **9-Cl/Br** and **10-Cl/Br** following a S_N2 (i) or a radical mechanism (ii). The values corresponding to the reaction of **4** with CHI_3 have been included for an overall picture of these reactions. MUE (M06)= 2.48 kcal/mol.[43]

They also showed a gradation for the X transfer process, which is increasingly favored with the heavier haloforms. Whereas the calculated barrier for the reaction with CHI_3 supports an easy

process happening in a wide diversity of conditions, the barrier for the reaction with $CHBr_3$ seems higher enough as to be sensitive to other kinetic factors such as the concentration of reagents, in good agreement with experimentally observed trends. Finally, the reaction with chloroform shows the highest barrier, and experimentally does not occur under thermal conditions. In this case, excited species, reached by irradiation, will trigger the photooxidation of **4** with $CHCl_3$ to give Pt_2(III,III) complexes following a radical mechanism.

Additional DFT calculations were further performed under the supervision of Dr. Daniel Escudero. These calculations aimed to reach a deeper knowledge about the nature of **4** trying to explain the excitation and emission spectra and its reactivity towards CHX_3. For that, DFT calculations on the ground state (GS) Potential Energy Surfaces (PESs) of **4** were performed in acetone solution. They shed results quite similar to those obtained in THF (see Chapter 1). Two close-lying minima were found, corresponding to the *butterfly-spread* conformer **4s**, and the *butterfly-folded* one **4f** (ΔG = 1.7 kcal/mol), with the former being the more stable one. A TS connecting these two minima (ΔG = 1.9 kcal/mol above **4-s** and 0.2 kcal/mol above **4-f**) was also located. The small energy difference between **4s**/**4f** and the low activation barrier support a fast thermal equilibration in the ground state PES, thus resembling an intramolecular *butterfly flapping-like* motion and the presence of both kinds of conformers in acetone solution.

The photophysical properties of **4**, described in Chapter 1, showed that diluted solutions (10^{-5} M, 2-MeTHF, 77K) of **4** display just one excited state at high energy, mostly reached by irradiation with a 365 nm UV light and corresponding to the major species **4-s**. Besides, compound **4** exhibits an additional excited state at low energy accessible by irradiation in the range 450−470 nm, corresponding to the minor species **4-f**, but this is only perceptible in concentrated solutions of **4** (10^{-3} M, 2-MeTHF, 77K) (see Chapter 1, section 1.5.2, Figure 17).

2.A.2.3.Discussion

The results shown above indicated that diluted solutions of **4** (10^{-5} M, 10^{-4} M) in acetone-d_6 react with CHX_3 (X = Cl, Br, I) under 365 nm UV-light. At higher concentrations (8 x 10^{-3} M), the reaction can be thermally (X= Br, I) or blue-light (X = Cl, $\lambda_{exc} \sim 460$ nm) initiated. These reactions follow a radical process (path i in Scheme 10 and eq. 2-5) rendering species **9**, **10** or mixtures of both, depending on the ambient conditions.

Since the reaction of **4** with $CHCl_3$ was promoted by 365nm-UV light (10^{-5} M, 10^{-4} M) and blue light (8 x 10^{-3}M), an haloform-initiated radical pathway can be excluded.[135] So the reaction should be initiated by platinum-based excited species, generated by irradiation of complex **4**. Consequently, when a concentrated sample of **4** was irradiated with blue LEDs (λ_{max} = 457 nm) under the experimental conditions the ^{1}MMLCT (λ = 460 nm) of species **4f** (S_{4f}) was reached and then excited states, ^{1}MMLCT or ^{3}MMLCT (reached by a quick ISC process), would likely initiate the fast reaction with $CHCl_3$. In order to investigate the singlet or triplet nature of the reactive [**4f**]* species, we used anthracene (E_S < 350 nm, E_T = 681 nm)[136] as quencher of the ^{3}MMLCT phosphorescence of **4**. So, we prepared two concentrated solutions of **4** one of them with (0.08 M) and the other without anthracene and allowed to react with $CHCl_3$ (molar ratio 1:5) under blue LEDs. In both samples the exciting light (λ_{max} = 457 nm) must be completely absorbed by complex **4** and no differences between them were detected by ^{1}H NMR, rendering only **9-Cl** after 24h in both cases (see Table 7). Since anthracene quenches the ^{3}MMLCT phosphorescence of **4** but not the photoreaction with $CHCl_3$, ^{1}[**4f**]* species, with a ^{1}MMLCT character, should be the reactive species (Scheme 9 in Chapter 1).

Therefore, under blue light, species ^{1}[**4f**]* would interact with $CHCl_3$, undergoing formation of Pt_2Cl• and •$CHCl_2$, starting the radical reaction.

Table 7. Percentages, based on ^{1}H NMR spectra, of species **4** and **9-Cl** in the reaction of **4** with $CHCl_3$ in acetone-d_6 (8x 10^{-3} M) in different conditions.

Time	365 nm-UV light		Blue-light		Blue-light, with anthracene	
	% 4	% 9-Cl	% 4	% 9-Cl	% 4	% 9-Cl
15 min	90.23	9.77	80.4	19.6	--	--
2h	62.27	37.73	50.74	49.26	52.61	47.39
6h	48.19	51.81	15.97	84.03	16.67	83.33
8h	33.78	66.22	8.26	91.74	7.41	92.59
24h	0	100	0	100	0	100

Additionally, this statement agrees with the observed effect of O_2 (E_{T1} = 1192 nm, E_{T2} = 773 nm) that quenches the phosphorescence of **4** (λ_{ex} = 400 nm) but not the photoreaction with $CHCl_3$.

At high concentration (8 x 10^{-3} M) under UV light (365 nm) the reaction goes slower than under blue light. In this case, the excitation will lead to the higher energy excited states (^{1}IL/MLCT), corresponding to ^{1}[**4s**]*, which by ISC or IC can relax and populate the ^{3}IL/MLCT or ^{1}MMLCT excited states respectively (Scheme 9 in Chapter 1). Since the ^{1}MMLCT excited states corresponding to species **4f** are those which promote the photochemical reaction, using UV light they will be only partially populated, slowing down the reaction with respect to the blue-light driven one. These processes explain that in diluted solutions (10^{-4} M, 10^{-5} M), with a mostly presence of species [**4s**], the reaction just occur under 365-UV light.

On the other hand, the thermally activated oxidative addition of CHX_3 (X=Br, I) only takes place in a concentrated solution (8 x 10^{-3}M) of **4**. This fact is explained if MMLCT-based species [**4f**] initiate the radical process, in such a way that their almost negligible presence in diluted solutions (10^{-4} M) slows down the thermal reaction, and it is not observed after 45 min. Therefore, experimental and theoretical calculations confirmed that MMLCT-based species [**4f**] are those which trigger the reactions of **4** with CHX_3, indicating the significance of metal-metal cooperation in the oxidation of the flapping platinum *butterfly*, **4**, by haloforms. These

reactions follow a radical pathway through the homolytic breakage of the X-C bond, in the S_0 for $CHBr_3$ and CHI_3 and in the S_1 state for $CHCl_3$ (path i, Scheme 10). The concomitant generation of Pt_2X• and •CHX_2 (R•) radicals is consistent with the simultaneous formation of complexes **9** and **10** (eq. 2-5) and the role of O_2 as radical (R•) trap explains the greater amount of **9** in the reaction mixtures when the reactions are performed in the air with respect to those performed under argon atmosphere. The negligible presence of species [**4f**] in diluted solutions (10^{-4} M) slows down the thermal reactions with $CHBr_3$ and CHI_3 and requires 365-UV-light for the reaction with $CHCl_3$ to occur.

Under UV-light species **10** convert into **9** following a radical pathway (path ii in Scheme 10) as well, which explains how in the ambient light **4** converts completely into **9-Cl/9-Br/9-I** in the presence of excess of CHX_3 (X = Cl, Br, I).

Chapter 2B

Oxidation of the Flapping Platinum *Butterfly* [{Pt(C^C*)(μ-pz)}$_2$] by Alkyl halides: Experimental and Theoretical Studies

2.B.1.Reactivity of [{Pt(C^C*)(μ-pz)}$_2$](C^C*$_A$ 4, C^C*$_B$ 4B) with MeI: Experimental and Computational Investigations for the Mechanistic Studies

The reaction of **4** with MeI in MeCN in the dark afforded the Pt_2(IV,IV) complex [{Pt^{IV}(C^C*$_A$)Me(μ-pz)}$_2$(μ-I)]I (**11**) as result of a double OA of MeI, regardless either, the reactants molar ratio (see Scheme 13 path a) or the use of different organic solvents, such as acetone or CH_2Cl_2. Compound [I(C^C*$_A$)Pt^{III}(μ-pz)$_2$$Pt^{III}$(C^C*$_A$)Me] (**13**), resulting from the bimetallic OA of one MeI molecule was just detected by ^{1}H NMR.

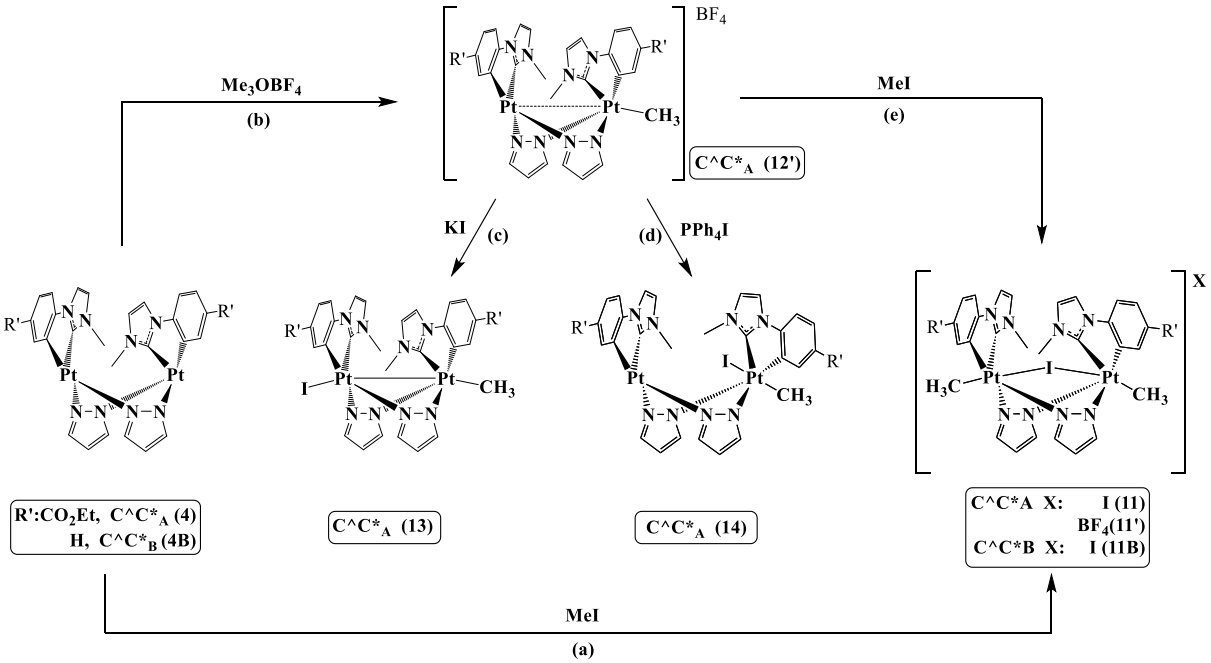

Scheme 13. Reaction pathway for OA reactions of MeI

To evaluate the influence of the CO_2Et fragment in the redox reactivity of complex **4**, we synthetized the new complex **4B**. Then, due to its low solubility, it was led to react with MeI in DMF rendering the complex [{Pt^{IV}(C^C*$_B$)Me(μ-pz)}$_2$(μ-I)]I (**11B**). This result indicates that the CO_2Et fragment does not affect the reactivity towards MeI; it only increases the solubility of the complexes, allowing a better study of them.

Complexes **11** and **11B** were isolated as white solids in very good yields (92%, **11**; 88%, **11B**) and fully characterized (Section 2.B.3). Just two complexes with the same bridging system have been reported to date, PPN[{$Pt^{IV}Me_3$(μ-pz)}$_2$(μ-I)][137] and (PPh_4)[{$Pt^{IV}Me_2Br$(μ-pz)}$_2$(μ-Br)],[56] but both of them were prepared by a different method, the assembly of mononuclear Pt(IV) fragments.

Keeping in mind Chapter 2A, we checked the possibility of a radical mechanism for MeI. The reaction of **4** with MeI in MeCN-d_3 in the dark was performed simultaneously with and without galvinoxyl (Gal•) as radical (R•) trap, and followed by ^{1}H NMR for 1 h. As a result, we could conclude it is almost unaffected by the presence of Gal•, which led us to dismiss a radical mechanism and to consider a S_N2 one for the first and the second OA of MeI to **4**. For a deeper knowledge of the reaction mechanisms, we carried out a DFT study.

The free energy profiles in MeCN have been represented in Scheme 14, the reference energy value being 0.0 kcal/mol for one of the Pt_2(II,II) reactant (**4**) and the two molecules of MeI.

In the modeled mechanism, the first OA is a S_N2 reaction with the dinuclear compound **4** acting as nucleophile (Nu) to give a cationic intermediate **Int-Me**. The reaction would proceed through a transition state TS1 (436i cm^{-1}), which shows a hypervalent C atom with two long Pt···C and C···I distances. The energy barrier (Ea_{TS1} = 15.02 kcal/mol) is low enough to allow the reaction to occur at r.t. in the dark. Once that intermediate was formed, the migration of the iodide to the Pt(II) center will afford the complex **13,** while if it bonds to the Pt(IV) center, Pt(II,IV) species (**Int′-Me(14)**) will be generated.

The small barrier (2.92 kcal/mol) for the interconversion of **Int-Me** into **Int′-Me(14)** through the transition state TS2 (43i cm^{-1}) competes with the barrierless formation of **13**. This, together with the low free energy difference between **13** and **Int′-Me(14)** ($\Delta G_{Int'\text{-}Me(14)\text{-}13}$ = 4.03 kcal/mol) support the formation of the two species from **Int-Me**, which are believed to be in equilibrium in solution of MeCN at r.t.

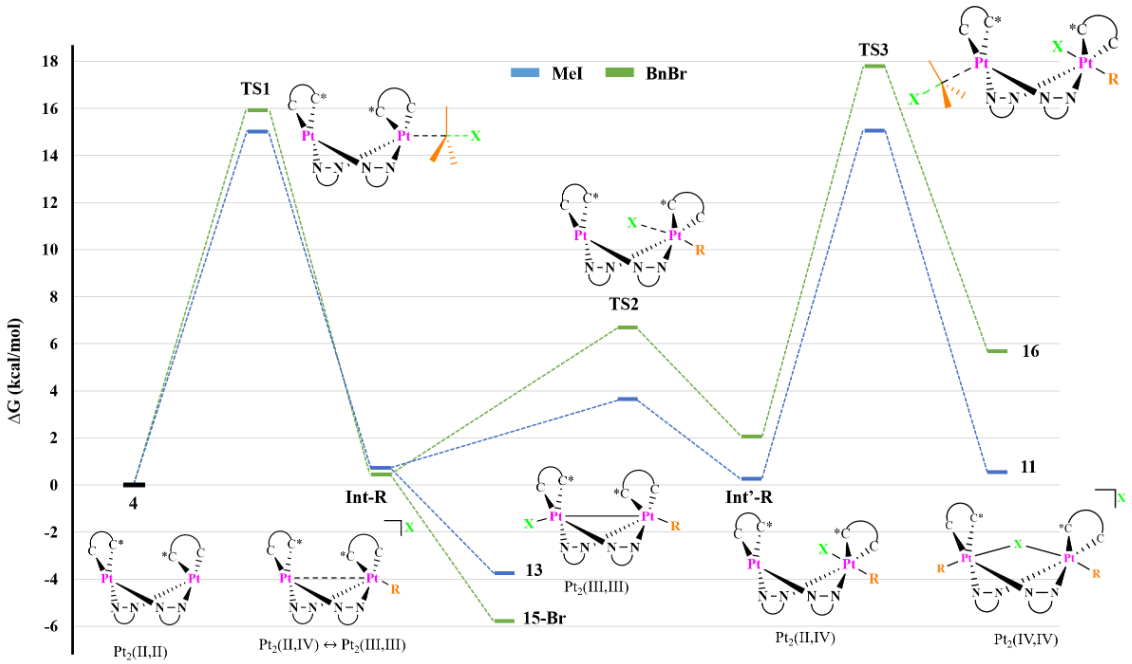

		Step i				Step ii			
		4	TS1	Int-R	X-Pt-Pt-R	TS2	Int'-R	TS3	R-Pt-X-Pt-R
R=Me X=I	d(Pt-Pt) (Å)	3.16	3.04	2.83	2.79 (**13**)	3.41	3.70	3.66	3.65 (**11**)
	ΔG (kcal/mol)	0.00	15.02	0.72	-3.75 (**13**)	3.64	0.27	15.05	0.55 (**11**)
R=Bn X=Br	d(Pt-Pt) (Å)	3.16	2.93	2.81	2.76 (**15-Br**)	3.34	3.75	3.67	3.67 (**16**)
	ΔG (kcal/mol)	0.00	15.92	0.45	-5.78 (**15-Br**)	6.69	2.05	17.81	5.69 (**16**)

Scheme 14. Computed ΔG profile (kcal/mol) for the thermal conversion of **4** into **13/15-Br** (Step i) and **Int′-R** into **11/16** (Step ii), following S_N2 mechanisms. MUE= 2.48 kcal/mol.[43]

The second OA reaction (Scheme 14) would start with the nucleophilic attack of the dz^2 orbital of the Pt(II) center in complex **Int′-Me(14)** to a second MeI molecule to give **11** as the final product. This step could proceed through a transition state TS3 (423i cm^{-1}), with the energy barrier (Ea_{TS3} = 14.78 kcal/mol) being similar to that of the first OA. Therefore, this calculated mechanism shows the feasible access to **Int′-Me(14)**, which could explain the observed double OA of MeI to **4** rendering **11**. Moreover, although **13** is thermodynamically more stable than **11**, the scarce solubility of the latter in the reaction media is likely to be the driving force of the reaction of **4** with MeI to give **11**.

Species similar to **Int-Me** and **Int′-Me(14)** were proposed as intermediates in OA reactions of one or two RX molecules to M_2(I,I) (M = Rh, Ir).[106, 113] Additionally, the mixed-valence species

Int′-Me(14) could also be available by a monometallic S_N2 OA of MeI to **4**.[138] In order to test the proposed mechanism and to compare the structural and spectroscopic features of high-valent dinuclear platinum complexes, with the same core "{Pt(C^C*$_A$)(μ-pz)}$_2$" but with different oxidation states, we carried out the synthesis and characterization of compounds **12'**, **13**, and **Int'-Me(14)** (See Scheme 13).

First, **Int-Me** was prepared as the BF_4 salt, [(C^C*$_A$)Pt(μ-pz)$_2$Pt(C^C*$_A$)Me]BF_4 (**12'**), in a very good yield (85%) (see Scheme 13, path b) by reacting **4** with Me_3OBF_4, at −25 °C in anhydrous CH_2Cl_2 in the dark, under argon atmosphere. This compound resulted to be stable in the solid state and solution at r.t. and could be fully characterized. Then, **12'** was allowed to react with KI in MeCN at low temperature (−25 °C) to favor the exothermic process (Scheme 13, path c). In these conditions, [I(C^C*$_A$)Pt^{III}(μ-pz)$_2$Pt^{III}(C^C*$_A$)Me] (**13**) precipitated in the reaction media and could be obtained as a pure species in a moderate yield (39%) and then characterized. A mixture of **13** and **Int'-Me(14)** remains in the mother liquor, as it was detected by ^{1}H NMR, which could explain the low yield of this synthetic procedure. Additional support for the simultaneous formation of both **13** and **Int'-Me(14)** along with the equilibrium between them was obtained following this reaction by NMR (See Figure 25).

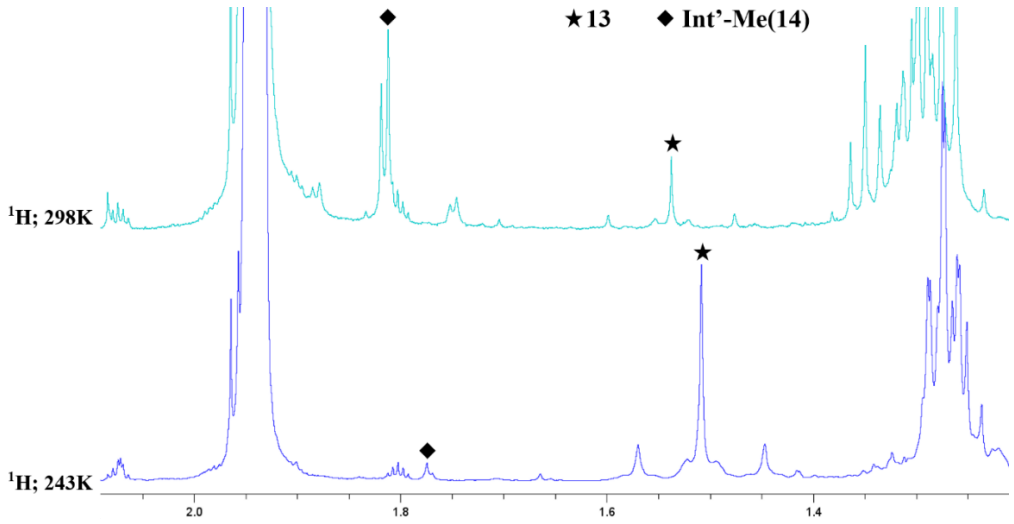

Figure 25. Expanded view of ^{1}H NMR spectra for the reaction of **12'** with KI at -30ºC in NMR tube recorded at 243 K (bottom) and after 24 h at 298 K (top).

At −30 °C, this reaction leads to the simultaneous formation of **13** and **Int'-Me(14)**, with the former being the major species, which becomes **14** as the temperature raises, in such a way that after 24 h at r.t., both species are present in the mixture in about a 1:1 molar ratio.

To obtain complex **Int'-Me(14)** as pure species, we investigated for solvents that give a smaller free energy difference between **Int'-Me(14)** and **13** than the one obtained in MeCN, so as to ensure a larger amount of **Int'-Me(14)** in the equilibrium.

As can be seen in Scheme 15, the computed $\Delta G_{Int'\text{-}Me(14)\text{-}13}$ in anisole (1.79 kcal/mol) is clearly smaller than that in MeCN (4.03 kcal/mol). Accordingly, [(C^C*$_A$)Pt^{II}(μ-pz)$_2$Pt^{IV}(C^C*$_A$)(Me)I] (**Int'-Me(14)**) was the single organometallic species detected by ^{1}H and ^{195}Pt{^{1}H} NMR in the reaction of **12'** with Ph_4PI in anisole in the dark at 30 °C (Scheme 13, path d).Unfortunately, it was obtained from the reaction mixture unpurified with anisole and Ph_4PBF_4 (see Figure S10 ESM-5).

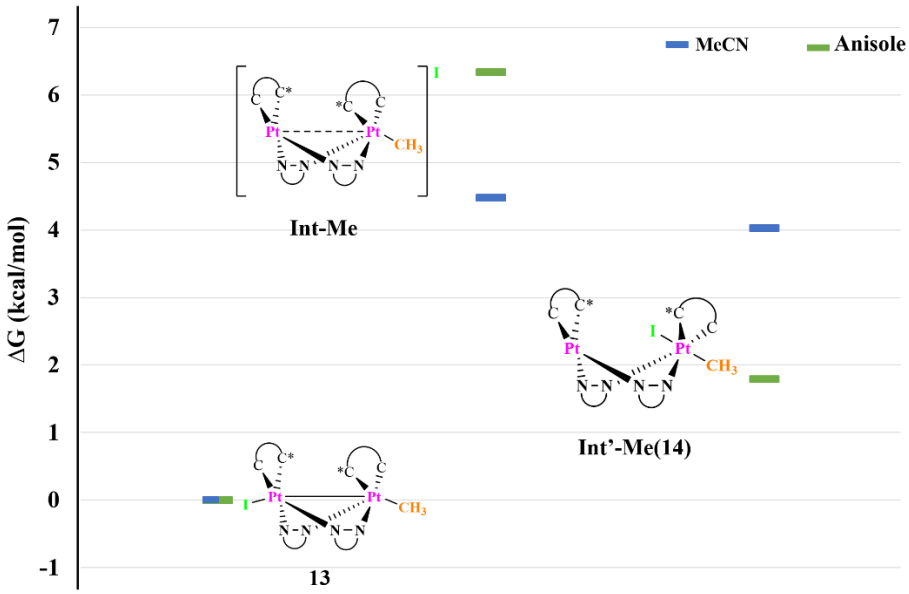

Scheme 15. Computed free energy profiles (ΔG, kcal/mol) in MeCN (ε = 35.688) and Anisole (ε = 4.2247) for the thermal conversion of **13**, **Int-Me** and **Int'-Me(14)**. MUE (M06)= 2.48 kcal/mol.[43]

Additionally, **12'** was reacted with MeI in acetonitrile at r.t., rendering **11'** as the final product (Scheme 13, path e). This result is consistent with Pt_2(III,III)↔Pt_2(II,IV) formulations for **12'**, the contribution of the Pt_2(II,IV) one being significant. Therefore, since all the intermediate species in the double OA of MeI to **4** resulted to be experimentally available, the proposed mechanism, initiated with a bimetallic OA of MeI to the Pt_2(II,II) complexes **4** and **4B**, seems suitable.

2.B.2.Reactivity of [{Pt(C^C$_A$*)(μ-pz)}$_2$](4) with BnBr and BnI: Experimental and Computational Investigations for the Mechanistic Studies

To expand these studies, we focused on the OA of benzyl halides (BnBr, BnI) to [{Pt(C^C*$_A$)(μ-pz)}$_2$] (**4**). The reaction of **4** with BnX (X=Br, I) in a 1:4 molar ratio in MeCN in the dark at r.t. rendered the Pt_2(III,III) complexes [X(C^C*$_A$)Pt^{III}(μ-pz)$_2$Pt^{III}(C^C*$_A$)Bn] (X=Br, **15-Br**; I, **15-I**) (Scheme 16, path a), which were isolated as orange solids in very good yields (93% **15-Br**, 87% **15-I**).

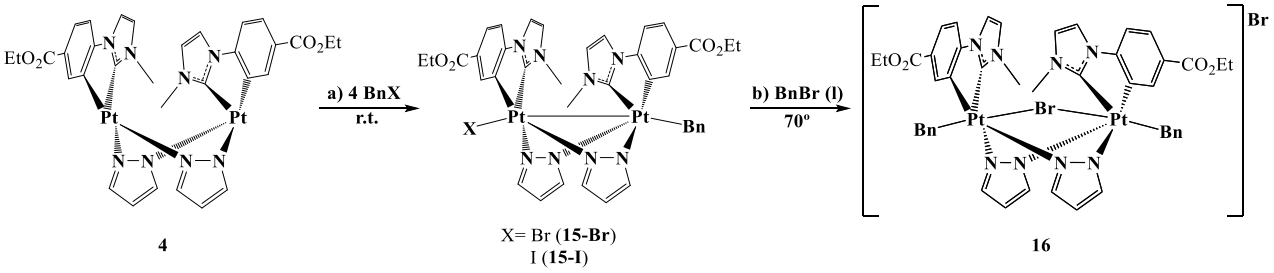

Scheme 16. Reaction Pathway for OA reactions of benzyl halides to **4**.

A second OA of BnBr, to give [{Pt (C^C$_A$*)Bn(μ-pz)}$_2$(μ-Br)]Br (**16**) was achieved by heating **15-Br** at 70ºC in BnBr(l) in the dark for 5h. In these hard conditions, **16** was obtained in good yield (87%) (Scheme 16, path b). Complexes **15-Br, 15-I, 16** were fully characterized (Section 2.B.3).The selective formation of the asymmetric complexes (**15-Br** and **15-I**) in the presence

of oxygen, an efficient radical trap, points to a S_N2 mechanism, like in the case of MeI. This mechanism was modeled by DFT in MeCN for BnBr and represented in Scheme 14 for comparison with the MeI one, the reference energy value being 0.0 kcal/mol for one of the Pt_2(II,II) reactant (**4**) and the two molecules of BnBr.

The energy barrier for the first OA (Ea_{TS1}= 15.92 kcal/mol, TS1: 294i cm^{-1}) is low enough to enable the reaction go at r.t. in the dark, being not much different from that for MeI. Once the **Int-Bn** was formed, species **15-Br** or **Int'-Bn** result available. Thermodynamically the formation of **15-Br** from **4** is clearly favored (calculated ΔG_{15Br-4}= -5.78 kcal/mol; $\Delta G_{Int'-Bn-4}$= 2.05 kcal/mol). Although the energy barrier (6.24 kcal/mol) for conversion of **Int-Bn** into **Int'-Bn** through TS2 (44i cm^{-1}) is in principle not large enough to prevent it to occur, experimentally **15-Br** is the only species formed at r.t. in the dark. Therefore, it seems that the free energy difference between **15-Br** and **Int'-Bn** (calculated $\Delta G_{Int'Bn-15Br}$= 7.83 kcal/mol) hinders **Int'-Bn** to be significantly formed, and thus preventing the second OA to occur at r.t. Only by heating at 70ºC in BnBr(l) the formation of **Int'-Bn** is achieved, enabling it to convert into **16** through TS3 (260i cm^{-1}).

Again, in view of the lower stability of **16** compared to **15-Br**, the scarce solubility of the former in the reaction media is likely as well, the driving force for it to be formed.

The characterization of all these dinuclear high-valent platinum compounds has been addressed together for an overall perspective, as can be seen below.

The Pt_2(III,III) complexes [X(C^C*$_A$)Pt^{III}(μ-pz)$_2$$Pt^{III}$(C^C*$_A$)Bn] (X=Br, **15-Br**; I, **15-I**) decomposed under UV-light (365 nm), to give the corresponding dihalogenated Pt_2(III,III) complexes (X=Br, **9-Br**; I, **9-I**), complex **4** and an organic compound (Figure S2 in ESM-6). In argon atmosphere 1,2-diphenylethane (Bn-Bn) could be isolated as the corresponding organic compound. Under an oxygen atmosphere the reaction yielded benzyl alcohol and the corresponding oxidized species, benzyl aldehyde. The mechanism reaction of this

transformations are under study. Then, the Pt_2(III,III) complexes obtained (**9-Br**, **9-I**) could be reduced using KC_8 recovering the Pt_2(II,II) complex **4** (Figure S3 in ESM-6).

2.B.3.Characterization of all New High-valent {Pt(μ-pz)}$_2$ Complexes

The most valuable information for the full characterization of these new complexes came from their ^{1}H and ^{195}Pt{^{1}H} NMR spectra in solution, being in most cases a picture of the chemical structure. All these dinuclear high-valent platinum complexes, except **12'**, are not stable in solution at r.t. without excess of RX in the media. Therefore, the characterization all of them has been carried out at low temperature. Additionally, single-crystal X-ray diffraction studies were carried out on complexes **11**, **11B**, **12'**, and **15-Br**. Their molecular structures have been depicted in Figure 26.

As it can be seen in Figure 26, in all of them, the Pt_2N_4 rings exhibit a boat-like shape (angle between the Pt−N−N−Pt fragments being 73.0° **11**, 71.7° **11B**, 89.32° **12'**, and 89.64° **15-Br**) with an anti-configuration of the C^C* groups (C1−Pt−Pt#−C#1 torsion angles: 96.7(4)° **11**, 96.1(2)° **11B**; C1−Pt1−Pt2−C14 torsion angles: 79.29° **12'**, 72.92° **15-Br**). In all four compounds, the Pt−I, Pt−N, and Pt−C bond distances and angles are very similar to those observed in analogous complexes with the same "{(C^C*)Pt(μ-pz)}$_2$" core.[50-51] Thus, they seem to be not affected by the metal oxidation state.

The molecular structures of the cationic complexes, [{Pt(C^C*)Me(μ-pz)}$_2$(μ-I)]$^+$, in **11** and **11B** consist of a Pt_2(IV,IV) core bridged by two pyrazolates and one iodide ligand. The intermetallic distances ($d_{Pt,Pt}$ (Å) = 3.5909(9) **11**, 3.6228(6) **11B**) are in between the observed ones in related Pt_2(IV,IV) systems (PPN)[{Pt^{IV}Me$_3$(μ-pz)}$_2$(μ-I)][137] ($d_{Pt,Pt}$ (Å) = 3.706(1)), and (PPh_4)[{Pt^{IV}Me$_2$Br(μ-pz)}$_2$(μ-Br)][56] ($d_{Pt,Pt}$ (Å) = 3.593(1)). The Pt(IV) centers exhibit octahedral coordination environments with the axial positions occupied by a Me group and a bridging iodine, which gives a Pt−I−Pt angle close to 80° (81.55(2) **11**, 82.69(13) **11B**).

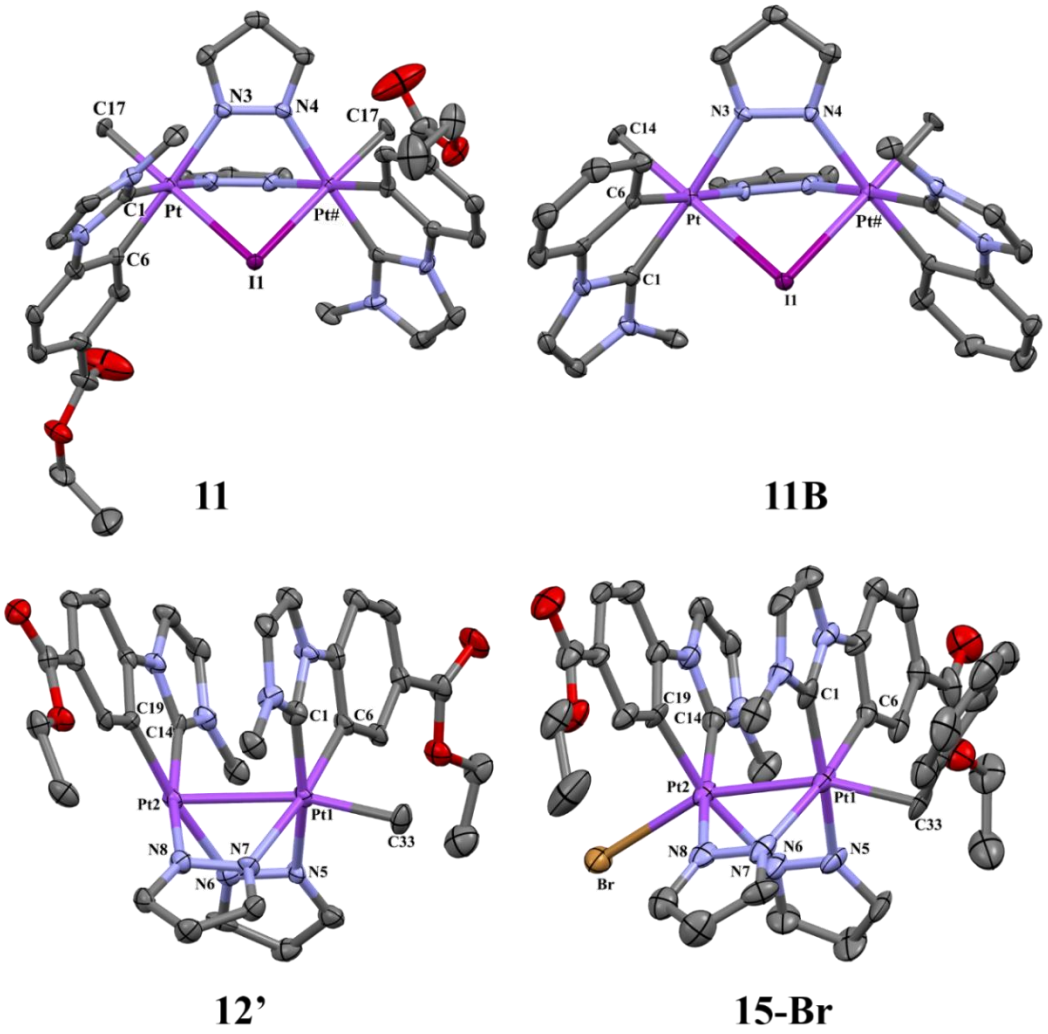

Figure 26. Molecular structures of the cationic complexes **11**, **11B**, **12'**, and **15-Br**. Ellipsoids are drawn at their 50% probability level; solvent molecules, I^- (**11**, **11B**), BF_4^- (**12'**), and hydrogen atoms have been omitted for clarity.

The cationic complex $[Pt_2(C\text{^}C^*_A)_2(\mu\text{-pz})_2Me]^+$ in **12'** and **15-Br** show short intermetallic distances ($d_{Pt,Pt}$ (Å) = 2.6700(4) **12'**, 2.6545(5) **15-Br**), indicative of the existence of a Pt−Pt bond. In **12'** it is a little longer than those in $[(CHX_2)(C\text{^}C^*)Pt^{III}(\mu\text{-pz})Pt^{III}(C\text{^}C^*)X]$,[50-51] ($d_{Pt-Pt}$ = 2.6302(4) Å X = Br (**10-Br**); 2.6324(3) Å X = I (**10-I**)) or in **15-Br**, which can be attributed to the larger *trans* influence of CH_3 compared to CHX_2 and CH_2Ph. The molecular structure of **12'** shows two different metal coordination environments: octahedral for Pt1 with the Pt2 and the methyl group (C33) in the *apex* positions and distorted square pyramidal for Pt2, with Pt1

in the *apex* position. The intermetallic distance is in the range reported for "$Pt_2^{III}(\mu\text{-}L)_2R$" species, regardless whether they exhibit octahedral environments for both Pt centers [2.529(1) −2.7910(2) Å][139-140] or an octahedral geometry at one and square pyramidal at the other center [2.676(1)−2.7542(11) Å].[141-148]

The NMR spectra of all these high-valent complexes (Pt−Me derivatives: **11**, **11B**, **12'**, **13**, **Int'-Me(14)**; Pt−Bn derivatives: **15-Br**, **15-I** (ESM-6), **16**) were performed in CD_2Cl_2 solution (see Table 8 and Figures 27 and 28).

Their ^1H NMR and $^{195}Pt\{^1H\}$ NMR spectra showed that in all cases, the major isomer is that observed in the X-ray single crystal structures, with the C^C* groups in an *anti* conformation, and provided structurally relevant details. In agreement with the absence of metal−metal interactions and their symmetry, in the Pt_2(IV,IV) complexes, **11**, **11B**, and **16**, the protons of the corresponding Pt−R (R = CH_3, CH_2Ph) display only one ^{195}Pt coupling constant, $^2J_{H\text{-}Pt}$ (see Table 8). Accordingly, their $^{195}Pt\{^1H\}$ NMR spectra exhibit just one singlet in the typical spectral range for Pt(IV) compounds (see Table 8 and Figure 28).[149]

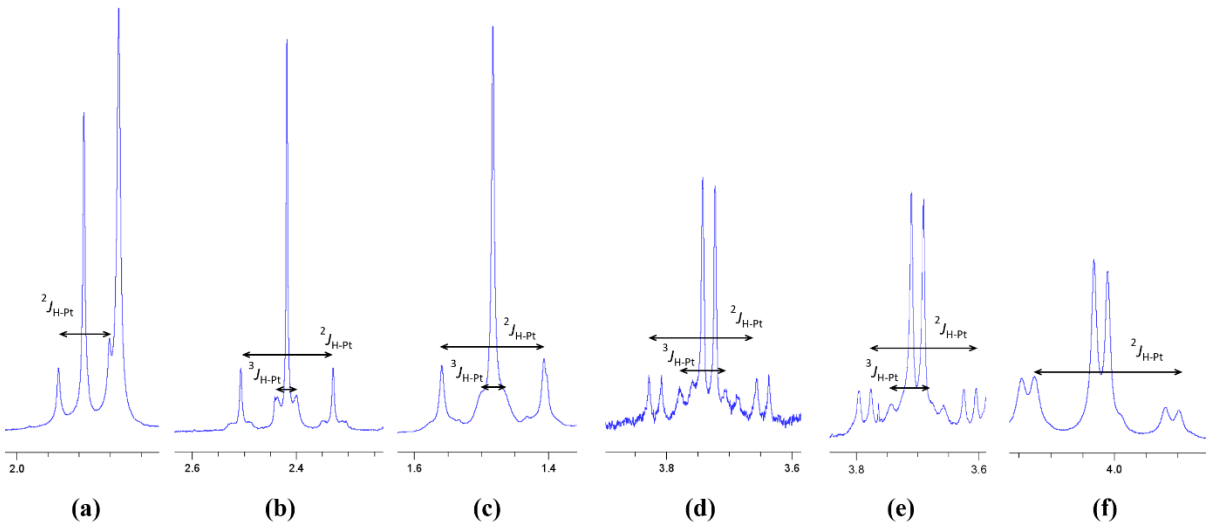

Figure 27. Expanded view of the ^1H NMR spectra corresponding to the Pt-R fragment of **11** (a), **12'** (b), **13** (c), **15-Br** (d), **15-I** (e), and **16** (f).

Table 8. NMR data for the new dinuclear high-valent platinum complexes in CD_2Cl_2. δ(ppm), *J*(Hz).

	Pt		Pt-R		
	δ	**$^1J_{Pt,Pt}$**	**δH**	**$^2J_{H,Pt}$**	**$^3J_{H,Pt}$**
11	-2688.0 (R=Me)	-	1.78	65.5	-
11B	-2664.4 (R=Me)[a]	-	1.80	66.1	
12'	-3064.2 (X=Vacant); -2589.2 (R=Me)	1023.4	2.42	70.7	14.7
13	-3018.8 (X=I); -2848.2 (R=Me)	1239.8	1.48	61.0	14.5
Int-Me(14)	-3776.0 (Pt(II)); -2697.0 (Pt(IV))	-	1.75	65.9	-
15-Br	-2742.8 (X=Br); -2693.6 (R=Bn)	1028.9	3.73 (1H)[b]	69.0	28.9
15-I	-2980.9 (X=I); -2680.9 (R=Bn)	1276.7	3.70 (1H)[b]	68.7	27.4
16	-2357.0 (R=Bn)	-	4.02 (2H)[b]	90.6	-

[a] Indirect detection by $^1H–^{195}Pt$ HMQC NMR. [b] An equal signal appears overlapped with OCH_2CH_3; δ ^{195}Pt = −3778.0 ppm (**4**, acetone-d_6), −3767.4 ppm (**4B**, DMSO-d_6).

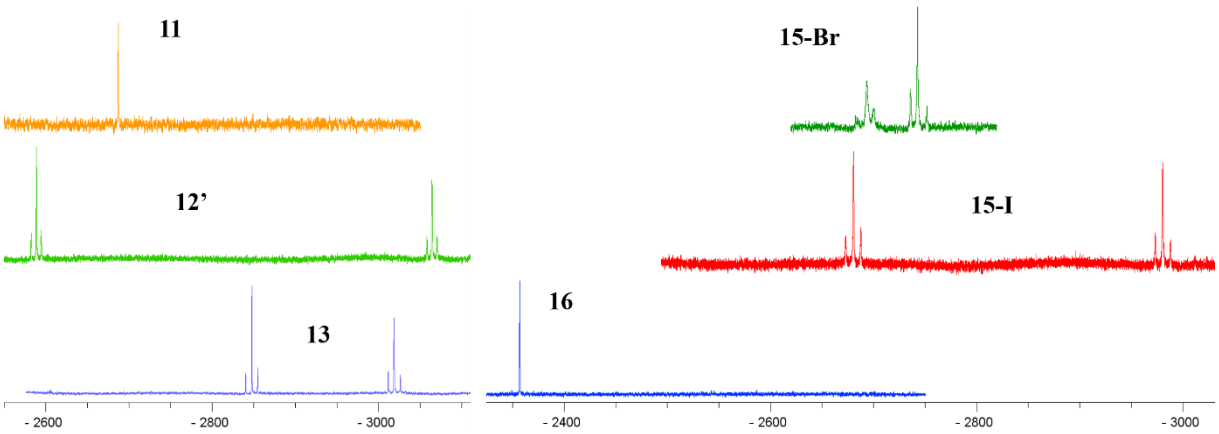

Figure 28. $^{195}Pt\{^{1}H\}$ NMR spectra in CD_2Cl_2 of **11**, **12'**, **13**, **15-Br**, **15-I**, and **16**

On the other hand, the NMR spectra of complexes **12'**, **13**, **15-Br**, and **15-I** indicate the non-equivalence of two Pt fragments joined by a metal−metal bond. Therefore, the ^{1}H NMR spectrum of each compound exhibits a signal due to the Pt-CH_3 (singlet) or Pt-CH_2Ph (doublet) flanked by two sets of ^{195}Pt satellites. Accordingly, the $^{195}Pt\{^{1}H\}$ NMR spectra display two singlets with their corresponding $^{1}J_{Pt,Pt}$ coupling constants (*ca*. 1023-1200 Hz).

The existence of the Pt−Pt bond in each case, was also confirmed by a ^{195}Pt–$^{195}Pt\{^{1}H\}$ COSY spectrum, which displays a crosspeak due to scalar coupling (Figure 29). The assignment of each platinum fragment resonance was made from ^{1}H–^{195}Pt HMQC and ^{1}H {selective^{195}Pt} NMR experiments.

All the ^{195}Pt signals appear clearly downfield-shifted with respect to those of the Pt_2(II,II) complexes, **4** and **4B** (Table 8), according to the higher oxidation state of the metal centers. Thus, they appear more deshielded as the oxidation state is higher (–2357.0 (Pt^{IV}-Bn, **16**) *vs.* –2693.6 ppm (Pt^{III}-Bn, **15-Br**)) and the electronegativity of the axial ligand is greater (–2742.8 (Pt-Br, **15-Br**) *vs.* –2980.9 ppm (Pt-I, **15-I**)). In addition, a downfield shift of the *Pt*-CH_2Ph resonances with respect to the *Pt*−Me one is observed, which is attributed to the effect of the π system of the benzyl fragment.[38]

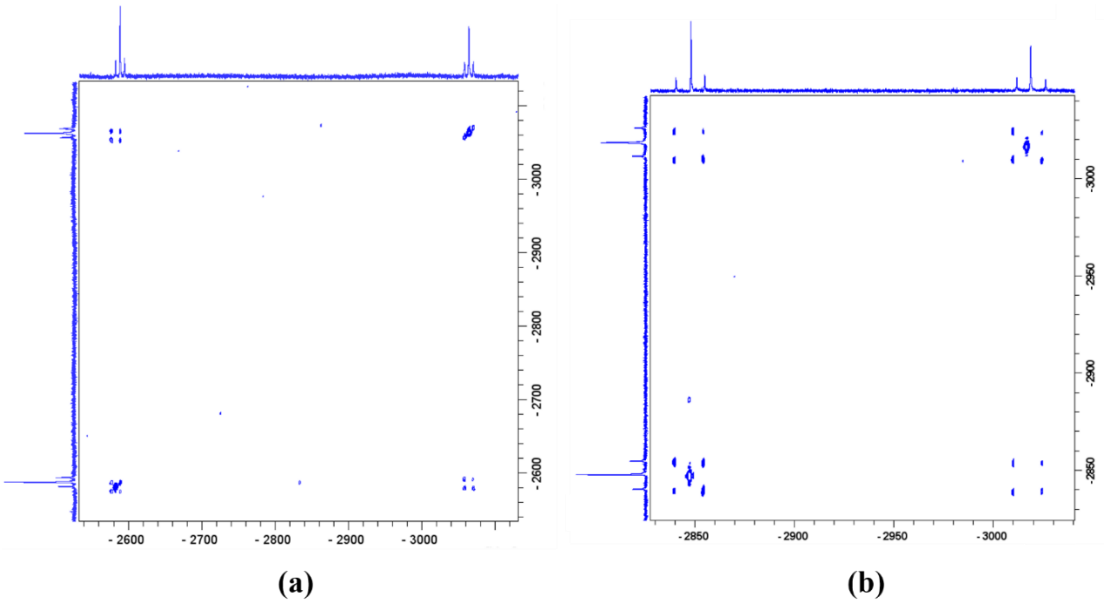

Figure 29. ^{195}Pt-^{195}Pt{^{1}H} COSY spectra of **12'** (a) and **13** (b) in CD_2Cl_2.

The proposed structure for complex [(C^C*$_A$)Pt^{II}(μ-pz)$_2$Pt^{IV}(C^C*$_A$)(Me)I] (**Int'-Me(14)**) was based on NMR data. The presence of two singlets in the spectral range expected for Pt(II) and Pt(IV)[149] (Table 8 and Figure 30 left) and the absence of platinum satellites in its ^{195}Pt{^{1}H} NMR spectrum suggest a mixed-valence nature of **Int'-Me(14)** and the absence of a metal−metal bond between the platinum centers. This fact was confirmed by its ^{1}H NMR spectrum, which shows only one singlet corresponding to the Pt−Me group flanked just by one set of platinum satellites (Table 8 and Figure 30 right).

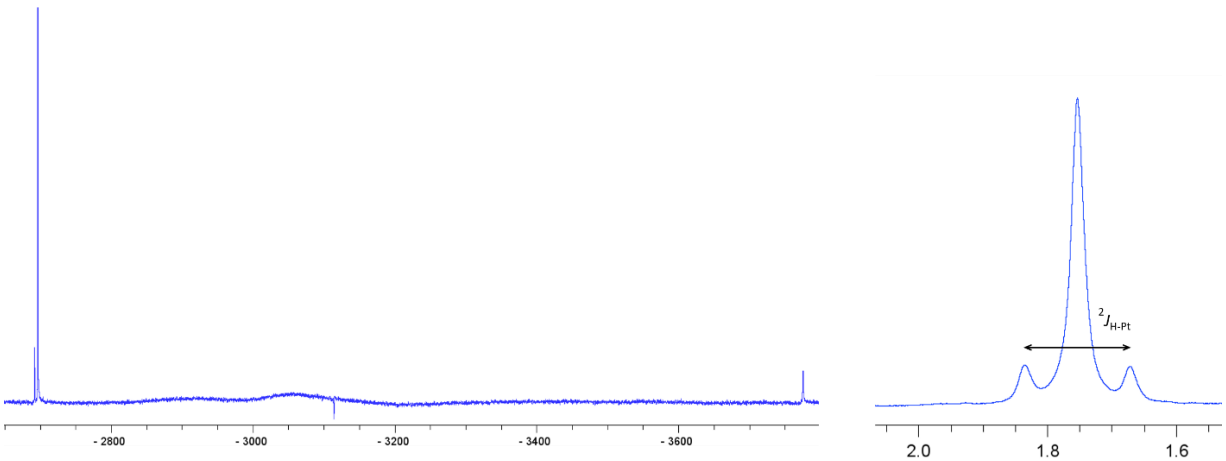

Figure 30. Left: ^{195}Pt{^{1}H} NMR spectrum. Right: Expanded view of the ^{1}H NMR of **Int'-Me(14)** in CD_2Cl_2.

The complex cation in **12'** deserves some additional attention. Analyzing this complex, the average oxidation number of the platinum centers is +III, but it can be considered as a metal−metal bonded Pt_2(III,III) complex with just one axial ligand, or as a mixed valence Pt_2(II,IV) one[150] with the metals linked by a Pt(II) → Pt(IV) donor−acceptor bond. The short intermetallic distance (2.6700(4) Å) observed in the X-ray structure points to a Pt_2(III,III) formulation, while the ^{195}Pt NMR data (Figure 28 and Figure 29 (a)) point to a Pt(II) → Pt(IV) one. In this sense, the different coordination environments of the Pt centers cause a big separation between the two ^{195}Pt resonances up to 480 ppm. The one corresponding to Pt−Me appears even more deshielded than that in the Pt_2(IV,IV) compounds (**11** and **11B**), while the other is shielded 50 ppm with respect to the Pt−I resonance in the Pt_2(III,III) complex **13**.

In order to determine the oxidation states of the metal centers, we performed additional computational and electrochemical studies. The Mulliken population analysis in MeCN for **12'** provided a similar estimated partial charge for the two platinum centers (0.49 Pt, 0.46 Pt−Me), being the difference (Δ = 0.03) even lower than in the Pt_2(III,III) complex, **13** (0.35 Pt−I, 0.40 Pt−Me, Δ = 0.05). The Pt−Pt MO bond order in **12'** (0.38) is close to the calculated value for the Pt_2(II,II) complex **4** (0.39) and smaller than that found for the Pt_2(III,III) complex **13** (0.59). These calculations are consistent with a Pt_2(III,III) ↔ Pt_2(II,IV) formulations, the contribution of the Pt_2(II,IV) one being significant, in line with earlier calculations on catalytic processes involving [{Pd(C^N)(OAc)}$_2$XY]. They showed that when a strong σ-donor group is "axially" coordinated to one of the metal centers in dinuclear complexes, the dz^2 orbital from the other metal gets populated, increasing the M(II) character and favoring the Pt_2(II,IV) formulation.[151] Consequently, in our case, the presence of Me as the electron-donating group in **12'** would increase the Pt_2(II,IV) contribution to this complex.

Considering all above, we performed the Cyclic Voltammetry (CV) (see Metodology) for complexes **4**, **12'**, and **9-I** in MeCN. The oxidative CV of **12'** showed an irreversible oxidation at 0.39 V, which is quite similar to that of **4**, 0.44 V, measured under the same conditions and

to the related cyclometalated pyrazolate-bridged dinuclear platinum(II) complexes,[77] while being far from the value observed for the Pt_2(III,III) complex **9-I** (Figure 31).

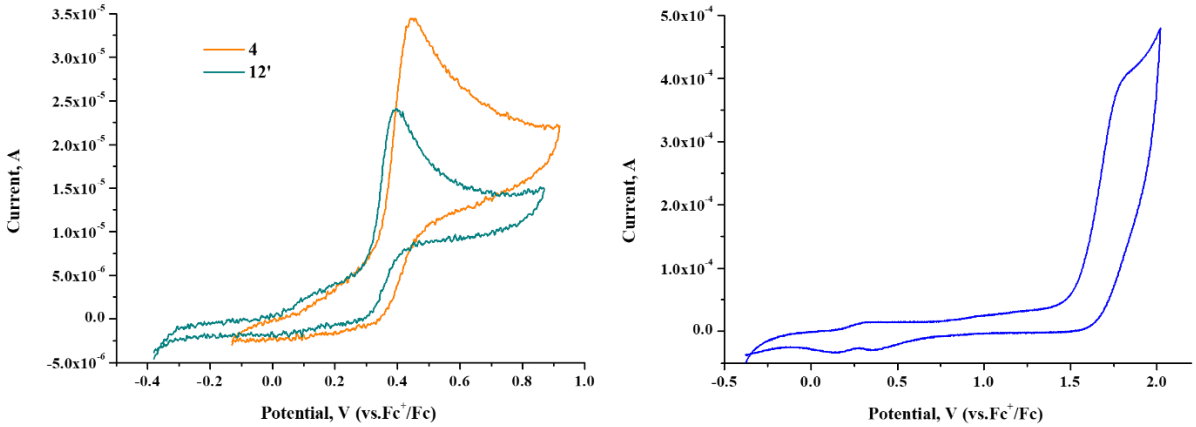

Figure 31. Cyclic Voltammogram for oxidation of **4**, **12'** (Left) and **9-I** (Right).

In the Pt_2(II,II) complexes, the irreversibility of this oxidation process has been attributed to the square-planar geometry of each Pt(II) unit with little or no metal−metal interaction. These metal centers are highly susceptible to nucleophilic attack by coordinating solvents, such as MeCN, resulting in permanent oxidized products. Therefore, a mixed-valence Pt_2(II,IV) formulation with the metals linked by a Pt(II) → Pt(IV) donor−acceptor bond seems to be the most likely for **12'** in MeCN solution, which is also compatible with the observed metal−metal coupling.[62] According to that, we observed that compound **12'** reacted with MeI in acetonitrile to give **11'** (see Scheme 13, path e).

Conclusions

1.-The cyclometalated N-heterocyclic carbene compound [{Pt(C^C*$_A$)(μ-Cl)}$_2$](**A**) (HC^C* = 1-(4-(ethoxycarbonyl)phenyl)-3-methyl-1*H*-imidazol-2-ylidene) works as an excellent starting material to get the new bis-pyrazole complexes [Pt(C^C*)(RpzH)$_2$]X (RpzH = pzH, 4-MepzH, 3,5-dmpzH) as chloride (Cl^-), perchlorate (ClO_4^-) or hexafluorophosphate (PF_6^-) salts.

2.-The stability of the three chloride compounds, [Pt(C^C*)(RpzH)$_2$]Cl, in solution depends on the solvent and the RpzH nature. In solvents, such as methanol, acetone or THF these compounds coexist with the corresponding [Pt(C^C*)(RpzH)Cl] and RpzH species in a dynamic equilibria which can be avoided by lowering the temperature to *ca*. 220 K. In CH_2Cl_2 solution at r.t. [Pt(C^C*)(3,5-dmpzH)$_2$]Cl (**1a**) is stable while the 4-MepzH and pzH derivatives exhibit the same behaviour than in other solvents, illustrating the higher basicity of the 3,5-dmpzH with respect to 4-MepzH and pzH.

3.-A new series of platinum-*butterflies* [{Pt(C^C*$_A$)(μ-Rpz)}$_2$] (RpzH= pzH **4**, 4-MepzH **5**, 3,5-dmpzH **6**, 3,5-dppzH **7**) containing a cyclometalated NHC in their wings, are mostly available by both, the treatment of the perchlorate salts [Pt(C^C*)(RpzH)$_2$]ClO_4 (RpzH= pzH **3b**, 4-MepzH **2b**, 3,5-dppzH) with NEt_3 and the treatment of compound [{Pt(C^C*$_A$)(μ-Cl)}$_2$](**A**) with a strong base in the presence of RpzH (RpzH= pzH, 3,5-dmpzH).

4.-Compound **1b** has been proved to behave as a useful synthon to reach the [Pt_2Ag_2] cluster, **8**, by the replacement of the acidic H of 3,5-dmpzH by Ag^+.

5.-Experimental data and theoretical calculations showed that both, the anion and the substituent of the ancillary ligands (RpzH) do not deeply affect the nature of the emission of these bis-pyrazole compounds which can be mainly assigned to ^{3}ILCT transitions on the NHC with some ^{3}MLCT character.

6.-The perchlorate and hexafluorophosphate derivatives (**1b, 2b, 1c**) are fully efficient blue-light emitters with QY up to 100% in PMMA films and CIE coordinates (0.15, 0.22) close to the desirable ones for blue emitters (0.15, 0.15) upon excitation at $\lambda \leq 380$ nm.

7.-DFT calculations on the dinuclear pyrazolate-bridged complexes (**4**-**7**) optimized two close-lying minima, the *butterfly-spread* **4s**-**7s** and the *butterfly-folded* **4f**-**7f**, which are characterized by long and short Pt-Pt separations respectively, as much in the ground state (GS) as in the lowest adiabatic triplet excited state (T_1) PES.

8.-The *butterfly-spread* **4s**-**7s** conformers are the more stable in the GS PES. Low ΔG (*s/f*) and low energy barriers in solution of THF or acetone support a fast thermal equilibration in the GS PES, thus resembling an intramolecular *butterfly* flapping-like motion. The *butterfly-folded* **4f**-**7f** conformers are instead, the most stable in the T_1 PES.

9.-In complexes **4**-**7**, the free energy difference between the two conformers, ΔG (*s/f*) and the energy barriers for the conversion of one into the other, as much in the GS as in the T_1, depend on the bulkiness of the Rpz groups and determine their absorption properties and their chameleonic photo- and mechanoluminescence.

10.- In 5% wt doped PMMA films in the air, complexes **4**-**7** show intense sky-blue emissions (PLQY: 72% - 86%) upon excitation at $\lambda \leq 380$ nm, which match with those observed in 2-MeTHF at 77 K. They mainly arise from emissive ^{3}IL/MLCT excited states, corresponding to the major *butterfly-spread* conformer **4s**-**7s**, according with no PSC occurring in a rigid matrix. In 2-MeTHF at 77 K, complexes **4** and **7** show additional excitation and emission bands at lower energies (λexc ~ 450 nm, λem> 600 nm), attributable to the *butterfly-folded* molecules although for **4** they are only perceptible in concentrated solutions (10^{-3} M). The existence of close-lying ^{1}IL/MLCT/MMLCT- ^{3}IL/MLCT states for the **4f**-**7f** species enables to get intense blue-emissions (PLQY: 40%-60%) under excitation with wavelengths in the visible region, up to 450 nm.

11.-The bulkiness of the μ-pyrazolates has also a strong impact on the mechanoluminescence of the 3,5-dppz derivative, **7** in solid state. Mechanical grinding of **7** causes a bathochromic shift of the emission from greenish-blue to yellowish-green along with a remarkable increment of its PLQY. This mechanoluminescence mechanism has been associated with an

intramolecular structural change in the GS that somehow shortens the Pt-Pt distances and enhances the Pt-Pt interactions, in such a way that the thermal *butterfly-flapping* can be induced by mechanical grinding.

12.-The complex [{Pt(C^C*$_A$)(μ-pz)}$_2$] (**4**) is the first and unique *butterfly* platinum compound oxidized by halocarbons reported to date. These oxidation reactions yield different high-valent dinuclear platinum complexes depending on both, the halocarbon nature and the experimental conditions.

13.-In diluted solutions in acetone-d_6, complex [{Pt(C^C*$_A$)(μ-pz)}$_2$] (**4**) reacts with CHX_3 (X = Cl, Br, I) under 365 nm UV-light to give [{Pt(C^C*$_A$)(μ-pz)X}$_2$] (X = Cl **9-Cl**, Br **9-Br**, I **9-I**). At higher concentrations (8 x 10^{-3} M), these reactions also take place by irradiation with blue LEDs (λ_{max}=457 nm).

14.-In concentrated solutions, complex **4** adds oxidatively $CHBr_3$ and CHI_3 in the dark under Ar atmosphere, to give selectively [XPt(C^C*$_A$)(μ-pz)$_2$Pt(C^C*$_A$)CHX_2] (X = Br **10-Br**, I **10-I**), but it renders mixtures of **9**/**10** if the reactions occur in the air. By contrast, complex **4** is air and thermally stable in the presence of $CHCl_3$ in such a way that complex [ClPt(C^C*$_A$)(μ-pz)$_2$Pt(C^C*$_A$)$CHCl_2$] (**10-Cl**) could be just detected by ^{1}H and ^{1}H-^{195}Pt HMQC NMR experiments from a reaction mixture of **4** and $CHCl_3$ irradiated with 365 nm-UV light under Ar atmosphere.

15.-Compounds **9-Cl**, **9-Br**, **9-I, 10-Cl**, **10-Br**, **10-I** were the first reported dinuclear metal−metal bonded Pt^{III}(μ-pz)$_2$$Pt^{III}$ compounds. They result from the [2c, 2e] oxidations of **4** by CHX_3 (X = Cl, Br, I) following a radical mechanism.

16.-In concentrated solutions of **4** in acetone, the MMLCT-based **4-f** species are those, which trigger the thermal- or blue-light driven-oxidation, in the S_0 with $CHBr_3$ and CHI_3 and in the S_1 state with $CHCl_3$, respectively. In diluted solutions, where the ratio of species **4-f** is lower, the reactions require 365 nm-UV light to occur. In this case, the excitation lead to the ^{1}IL/MLCT

excited states, corresponding to the major species **4-s**, which by IC can populate the ^{1}MMLCT state and then, promote the reaction.

17.-Under UV-light species **10** convert into **9** following a radical pathway as well, which explains how in the ambient light **4** converts completely into **9-Cl/ 9-Br/ 9-I** in the presence of excess of CHX_3 (X = Cl, Br, I).

18.-Compound **4** reacts with alkyl halides (RX = MeI, BnBr, BnI), *via* single or double OA, to give high-valent dinuclear complexes. Depending on the nature of RX or the reaction's conditions, the oxidation afford the metal-metal bonded Pt_2(III,III) complexes [X(C^C_A*)Pt^{III}(μ-pz)$_2$$Pt^{III}$(C^$C_A$*)Bn] (X = Br, **15-Br**; I, **15-I**), or go further up to the Pt_2(IV,IV) derivatives, [{RPt^{IV}(C^C_A*)(μ-pz)}$_2$(μ-X)]X (R= Me, X = I **11**; R= Bn, X = Br **16**).

19.-The presence of the CO_2Et substituent on the N-heterocyclic carbene does not affect the redox behavior of these Pt_2(II,II) compounds, since complex **4B,** with no substituent on the C^C_B* fragment, reacts with MeI in the same way than **4**, yielding an analogous compound, **11B**. The presence of the CO_2Et substituent increases the solubility of the compounds allowing a better characterization by NMR in solution.

20.-DFT modeling of the S_N2 mechanisms for the OA of MeI and BnBr to **4** proposed species such as [(C^C*$_A$)Pt(μ-pz)$_2$Pt(C^C*$_A$)R]X (RX = MeI **Int-Me**, BnBr **Int-Bn**) as intermediates for the first OA reaction. Once formed, two species are accessible, [X(C^C*$_A$)Pt^{III}(μ-pz)$_2$$Pt^{III}$(C^C*$_A$)R] (RX= MeI **13**, BnBr **15-Br**) and [(C^C*$_A$)Pt^{II}(μ-pz)$_2$$Pt^{IV}$(C^C*$_A$)(R)X] (RX= MeI **Int'-Me(14)**, BnBr **Int'-Bn**), the latter being the intermediate for the second OA.

21.-Keeping in mind the small energy barrier for the transformation of **Int-R** into **Int'-R**, the free-energy difference between the Pt_2(III,III) (**13**, **15-Br**) and the Pt_2(II,IV) (**Int'-Me(14)**, **Int'-Bn**) species seems to determine the nature of the compounds obtained at r.t. When it is small ($\Delta G_{Int'\text{-}Me(14)\text{-}13}$ = 4.03 kcal/mol), the feasible formation of **Int'-Me** allows the second OA to occur rendering the Pt_2(IV,IV) complex, **11**. When it is bigger ($\Delta G_{Int'\text{-}Bn\text{-}15\text{-}Br}$ = 7.83 kcal/mol), the reaction leads to the selective formation of the Pt_2(III,III) complex **15-Br**. In this case, the

second OA to get [{Pt^{IV}(C^C*$_A$)Bn(μ-pz)}$_2$(μ-Br)]Br (1**6**) is possible under harder conditions. Species **Int-Me** could be prepared and isolated as the BF_4 salt, [(C^C*$_A$)Pt(μ-pz)$_2$Pt(C^C*$_A$)CH_3]BF_4 (**12'**). Then, it was used to get **13**, **Int'-Me (14)** and [{MePt^{IV}(C^C_A*)(μ-pz)}$_2$(μ-X)] BF_4 (**11'**), which sustains the computed mechanism and allowed to compare structural and spectroscopic data for complexes with the same core "{(C^C*)Pt(μ-pz)}$_2$" but different oxidation states.

22.-Direct ^{195}Pt{^{1}H}, ^{195}Pt–^{195}Pt{^{1}H} COSY and indirect ^{1}H-^{195}Pt HMQC NMR experiments have been revealed as effective and very powerful tools for monitoring oxidative additions and are in most cases a picture of the chemical structure. They show a great sensitivity to the oxidation state of the Pt centers and to the metal coordination environment. The ^{195}Pt signal undergoes a gradual downfield shift as the oxidation state increases, from Pt_2(II,II) to Pt_2(IV,IV) and as the electronegativity of the axial ligand is greater, from Pt-I to Pt-Cl. Furthermore, ^{195}Pt–^{195}Pt{^{1}H} COSY experiments also confirmed the existence of metal-metal bond.

23.-Compounds **15-Br** and **15-I** decompose under UV-light to give an organic species and the corresponding dihalogenated complexes (**9-Br** and **9-I**), from which **4** could be recover using KC_8.

24.-The high basicity of the cyclometalated N-heterocyclic carbene (C^C*) seems to increase the nucleophilic character of the Pt centers in these pyrazolate-bridged compounds. This, and the cooperative effects between the two adjacent platinum (II) centers located in close proximity in the *butterfly-folded* species **4-f,** appear to be crucial in promoting the oxidation processes with CHX_3 and RX.

25.-Therefore, the [2c, 2e] oxidations of this *butterfly* Pt complex, **4**, by halocarbons are the first examples ever reported, showing a reactivity similar to that observed for lantern and half-lantern C^N-cyclometalated Pt(II) complexes, [{Pt(bzq)(μ-N^S)}$_2$], with shorter intermetallic distances.

Conclusiones

1.-El compuesto [{Pt(C^C*$_A$)(μ-Cl)}$_2$](**A**) (HC^C* = 1-(4-(etoxicarbonil)fenil)-3-metil-1*H*-imidazol-2-ilideno) es un excelente producto de partida para la obtención de nuevos complejos bis-pirazol [Pt(C^C*)(RpzH)$_2$]X (RpzH = pzH, 4-MepzH, 3,5-dmpzH) con cloruro (Cl^-), perclorato (ClO_4^-) o hexafluorofosfato (PF_6^-) como contra-aniones.

2.-La estabilidad de los tres derivados [Pt(C^C*)(RpzH)$_2$]Cl en disolución depende del disolvente y de la naturaleza del RpzH. En metanol, acetona o THF, estos compuestos coexisten con las especies [Pt(C^C*)(RpzH)Cl] y RpzH libre, formando parte de un equilibro que tiene lugar a temperaturas mayores de 220 K. En disolución de CH_2Cl_2 a temperatura ambiente [Pt(C^C*)(3,5-dmpzH)$_2$]Cl (**1a**) es estable mientras que los derivados de 4-MepzH y pzH presentan el mismo comportamiento que en los otros disolventes, demostrando la mayor basicidad del ligando 3,5-dmpzH.

3.-Los complejos dinucleares de platino de tipo *mariposa* [{Pt(C^C*$_A$)(μ-Rpz)}$_2$] (RpzH= pzH **4**, 4-MepzH **5**, 3,5-dmpzH **6**, 3,5-dppzH **7**) se pueden preparar por dos vías, haciendo reaccionar las sales de perclorato [Pt(C^C*)(RpzH)$_2$]ClO_4 (RpzH= pzH **3b**, 4-MepzH **2b**, 3,5-dppzH) con trietilamina o por ruptura de los puentes cloro en el complejo [{Pt(C^C*$_A$)(μ-Cl)}$_2$](**A**) con el pirazolato correspondiente (generado *in situ* por reacción de RpzH (RpzH= pzH, 3,5-dmpzH) con una base fuerte).

4.-El compuesto **1b** ha demostrado ser un buen sintón para la preparación del cluster [Pt_2Ag_2], **8**, siendo remplazados los hidrógenos ácidos del 3,5-dmpzH por iones Ag^+.

5.-Los estudios experimentales y teóricos muestran que tanto el anión como el ligando pirazol apenas afectan a la naturaleza de la emisión que se puede asignar a transiciones ^{3}ILCT centradas en el ligando NHC con algo de carácter ^{3}MLCT.

6.-Los complejos **1b**, **2b** y **1c**, en films de PMMA al 5%wt, son emisores muy eficientes de luz azul, con QY cercanos al 100% y con coordenadas CIE (0,15; 0,22) cercanas a las deseables para emisiones azules (0,15; 0,15).

7.-En los complejos de tipo *mariposa* se optimizaron, mediante cálculos DFT, dos mínimos de energía próximos entre sí, correspondientes a los confórmeros *alas-extendidas* **4s**-**7s** y *alas-plegadas* **4f**-**7f**, con distancias Pt-Pt largas y cortas respectivamente, tanto en el estado fundamental (GS-PES) como en el estado excitado triplete de menor energía (T_1-PES).

8.-Los confórmeros **4s**-**7s** son los más estables en el estado fundamental (GS-PES). El pequeño valor de ΔG (*s/f*) y las pequeñas barreras de energía en disolución de THF o acetona apoyan los equilibrios térmicos en el estado fundamental, que recuerdan al aleteo de una *mariposa*. Por otra parte, los confórmeros de tipo *mariposa alas-plegadas* **4f**-**7f** son los más estables en el estado triple (T_1 PES).

9.-En los complejos **4**-**7**, la diferencia de energía libre entre los dos confórmeros, y las barreras energéticas para la interconversión entre ellos, tanto en el estado fundamental como en el T_1, dependen del impedimento estérico en los grupos Rpz y determinan las propiedades de fotofísicas.

10.-Los compuestos dinucleares en films de PMMA (5%wt) presentan una intensa emisión azul cielo (QY: 72% - 86% al aire) al excitar a $\lambda \leq 380$ nm, que concuerda con la que se observa en 2-MeTHF a 77K. Estas emisiones proceden de estados excitados de tipo ^{3}IL/MLCT, que corresponden con el confórmero mayoritario, *alas-extendidas*, ya que en matriz rígida no tiene lugar el PSC. En 2-MeTHF a 77 K, los complejos **4** y **7** muestran unas bandas de emisión y excitación adicionales a baja energía (λexc ~ 450 nm, λem> 600 nm), que se atribuyen a las moléculas *alas-plegadas*, aunque en el caso de **4** solo se detecta en disoluciones concentradas (10^{-3} M). La existencia de estados excitados próximos entre sí de tipo ^{1}IL/MLCT/MMLCT-^{3}IL/MLCT para las especies **4f**-**7f** permiten obtener emisiones intensas en el azul (QY: 40%-60%) usando longitudes de onda de excitación del rango visible (hasta 450 nm).

11.-El impedimento estérico de los pirazolatos puente tiene un mayor impacto en la mecanoluminiscencia del derivado de 3,5-dppz en estado sólido, **7**. Al moler el sólido se provoca un desplazamiento batocrómico de la emisión desde el azul-verde a verde-amarillo así

como un incremento en el QY. Este fenómeno se asocia con un cambio estructural intramolecular en el estado fundamental que acorta las distancias Pt-Pt y potencia las interacciones metal-metal, de tal manera que el *aleteo* se puede inducir mecánicamente.

12.-El complejo [{Pt(C^C*$_A$)(μ-pz)}$_2$] (**4**) es el primer y único compuesto de platino de tipo *mariposa* que se oxida con reactivos halocarbonados descrito hasta la fecha. Estas oxidaciones dan lugar a diferentes compuestos dinucleares de platino en altos estados de oxidación, dependiendo tanto de la naturaleza del reactivo halocarbonado así como de las condiciones experimentales.

13.-En disoluciones diluidas de acetona-*d*$_6$, el complejo [{Pt(C^C*$_A$)(μ-pz)}$_2$] (**4**) reacciona con CHX_3 (X = Cl, Br, I) usando luz UV (365nm) para dar [{Pt(C^C*$_A$)(μ-pz)X}$_2$] (X = Cl **9-Cl**, Br **9-Br**, I **9-I**). A concentraciones más altas (8 x 10^{-3} M), estas reacciones se pueden llevar a cabo usando LEDs azules (λ_{max}=457 nm).

14.-En disoluciones concentradas, el complejo **4** adiciona oxidativamente $CHBr_3$ y CHI_3. En la oscuridad y bajo atmósfera de argón, se consigue selectivamente [XPt(C^C*$_A$)(μ-pz)$_2$Pt(C^C*$_A$)CHX_2] (X = Br **10-Br**, I **10-I**), pero si la reacción ocurre al aire se obtienen mezclas de **9**/**10**. Por otro lado, el complejo **4** en la oscuridad es térmicamente estable al aire en presencia de $CHCl_3$. Así que el derivado [ClPt(C^C*$_A$)(μ-pz)$_2$Pt(C^C*$_A$)$CHCl_2$] (**10-Cl**) solo se puede detectar por RMN en el medio de reacción al irradiar con luz UV de 365 nm en atmósfera de argón.

15.-Los compuestos **9-Cl**, **9-Br**, **9-I, 10-Cl**, **10-Br**, **10-I** son los primeros complejos dinucleares con enlace metal-metal de tipo $Pt^{III}(\mu\text{-pz})_2Pt^{III}$ descritos en la bibliografía. Estos se forman como resultado de una oxidación [2c, 2e] de **4** con CHX_3 (X = Cl, Br, I) siguiendo un mecanismo radicalario.

16.-En disoluciones concentradas de **4**, las especies **4f** de tipo MMLCT son las que desencadenan la oxidación térmica o inducida por luz azul, en el estado S_0 con $CHBr_3$ y CHI_3 o en el S_1 con $CHCl_3$. En disoluciones diluidas donde la presencia de estas especies **4f** es menor,

la reacción necesita luz UV de 365 nm. En este caso, en la excitación se alcanzan estados ^{1}IL/MLCT, correspondientes a la especie mayoritaria **4s**, a partir de los cuales por IC se puede poblar el estado ^{1}MMLCT que desencadena la reacción.

17.-Al irradiar con luz UV el compuesto **10** se convierte en **9** siguiendo un mecanismo radicalario, lo que explica por qué **4** se transforma completamente para dar **9-Cl/ 9-Br/ 9-I** en presencia de luz ambiente y un exceso de CHX_3 (X = Cl, Br, I).

18.-El compuesto **4** reacciona con halogenuros de alquilo (RX= MeI, BnBr, BnI), a través de una o dos adiciones oxidantes obteniéndose compuestos dinucleares en alto estado de oxidación. Dependiendo de la naturaleza del RX o de las condiciones de reacción, la oxidación da lugar a los compuestos Pt_2(III,III) con enlace metal-metal [X(C^C_A*)Pt^{III}(μ-pz)$_2$$Pt^{III}$(C^$C_A$*)Bn] (X = Br, **15-Br**; I, **15-I**), o avanza hasta los derivados Pt_2(IV,IV), [{RPt^{IV}(C^C_A*)(μ-pz)}$_2$(μ-X)]X (R= Me, X = I **11**; R= Bn, X = Br **16**).

19.-La presencia del sustituyente CO_2Et en el NHC no afecta a las reacciones redox del compuesto Pt_2(II,II), ya que el complejo **4B**, sin sustituyente en el fragmento C^C_B*, reacciona con MeI de la misma manera que **4**, dando lugar al compuesto análogo, **11B**. La presencia del sustituyente CO_2Et aumenta la solubilidad de los complejos permitiendo una mejor caracterización por RMN en disolución.

20.-El mecanismo S_N2 calculado por DFT para la adicción oxidante de MeI y BrBr a **4** propone especies [(C^C*$_A$)Pt(μ-pz)$_2$Pt(C^C*$_A$)R]X (RX = MeI **Int-Me**, BnBr **Int-Bn**) como intermedios en la primera adición oxidante. Una vez formados, dos complejos son accesibles, [X(C^C*$_A$)Pt^{III}(μ-pz)$_2$$Pt^{III}$(C^C*$_A$)R] (RX= MeI **13**, BnBr **15-Br**) y [(C^C*$_A$)Pt^{II}(μ-pz)$_2$$Pt^{IV}$(C^C*$_A$)(R)X] (RX= MeI **Int'-Me(14)**, BnBr **Int'-Bn**), siendo este último un intermedio en la segunda adición oxidante.

21.-Teniendo en cuenta la pequeña barrera de energía necesaria para la transformación de **Int-R** en **Int'-R**, la diferencia de energía libre entre las especies Pt_2(III,III) (**13**, **15-Br**) y Pt_2(II,IV) (**Int'-Me(14)**, **Int'-Bn**) parece determinar la naturaleza del compuesto obtenido a temperatura

ambiente. Cuando esta diferencia es pequeña ($\Delta G_{Int'\text{-}Me(14)\text{-}13}$ = 4.03 kcal/mol), es posible la formación de **Int'-Me** permitiendo que se produzca la segunda adicción oxidante dando lugar al complejo **11**, Pt_2(IV,IV). Cuando la barrera es más grande ($\Delta G_{Int'\text{-}Bn\text{-}15\text{-}Br}$ = 7.83 kcal/mol), se forma selectivamente el complejo **15-Br**. En este caso, la segunda adición oxidante para obtener [{Pt^{IV}(C^C*$_A$)Bn(μ-pz)}$_2$(μ-Br)]Br (**16**) se puede llevar a cabo utilizando condiciones más enérgicas. El compuesto **Int-Me** se puede aislar como la sal de BF_4, [(C^C*$_A$)Pt(μ-pz)$_2$Pt(C^C*$_A$)CH_3]BF_4 (**12'**). Posteriormente, se puede utilizar para obtener los complejos **13**, **Int'-Me (14)** y [{$MePt^{IV}$(C^C_A*)(μ-pz)}$_2$(μ-X)] BF_4 (**11'**) que permiten corroborar el mecanismo calculado, pudiendo además, comparar estructural y espectroscópicamente los complejos con un mismo esqueleto "{Pt(C^C*)(μ-pz)}$_2$" pero diferentes estados de oxidación.

22.-Los experimentos de RMN de detección directa ^{195}Pt{^{1}H}, ^{195}Pt–^{195}Pt{^{1}H} COSY e inversa ^{1}H-^{195}Pt HMQC han demostrado ser una potente herramienta a la hora de seguir reacciones de adición oxidante mostrando en la mayoría de casos una imagen de la estructura química del complejo estudiado. Estos experimentos muestran una gran sensibilidad al estado de oxidación de los centros de platino así como al entorno de coordinación del metal. La señal de ^{195}Pt sufre un desplazamiento gradual a bajo campo conforme aumenta el estado de oxidación del metal, de Pt_2(II,II) a Pt_2(IV,IV), y se incrementa la electronegatividad del ligando en posición axial, de Pt-I a Pt-Cl. Adicionalmente, el experimento ^{195}Pt–^{195}Pt{^{1}H} COSY confirma la existencia de un enlace metal-metal.

23.-Los compuestos **15-Br** y **15-I** descomponen al ser irradiados con luz UV para dar lugar a una especie orgánica y al correspondiente complejo de platino dihalogenado (**9-Br** y **9-I**), a partir de los cuales por reacción con KC_8 se puede recuperar **4**.

24.-La gran basicidad de los NHC ciclometalados, que incrementa la nucleofilia del centro de platino, junto con los efectos cooperativos entre los metales adyacentes en las especies *alas-plegadas* **4f**, son cruciales en la oxidación con CHX_3 y RX.

25.-Las oxidaciones de [2c, 2e] de este complejo de Pt de tipo *mariposa*, **4**, con reactivos halocarbonados son similares a las observadas para los complejos de Pt(II) de tipo lantern y half-lantern con C^N ciclometalados, [{Pt(bzq)(μ-N^S)}$_2$], que muestran distancias intermetálicas más cortas.

References

(1) Che, C. M.; Kwok, C. C.; Kui, C. F.; Lai, S. L.; Low, K. H. Luminescent Coordination and Organometallic Complexes for OLEDs. In *Comprehensive Inorganic Chemistry II*, Reedijk, J., Poeppelmeier, K. Eds.; Elsevier, 2013; pp 607-655. DOI: 10.1016/B978-0-08-097774-4.00808-1.

(2) Liao, J.-L.; Chi, Y.; Wang, J.-Y.; Chen, Z.-N.; Tsai, Z.-H.; Hung, W.-Y.; Tseng, M.-R.; Lee, G.-H. Pt(II) Phosphors Featuring Both Dicarbene and Functional Biazolate Chelates: Synthesis, Luminescent Properties, and Applications in Organic Light-Emitting Diodes. *Inorg. Chem.* **2016**, *55* (13), 6394-6404. DOI: 10.1021/acs.inorgchem.6b00097.

(3) Cebrian, C.; Mauro, M. Recent Advances in Phosphorescent Platinum Complexes for Organic Light-Emitting Diodes. *Beilstein J. Org. Chem.* **2018**, *14*, 1459-1481. DOI: 10.3762/bjoc.14.124.

(4) Weber, K. T.; Karikis, K.; Weber, M. D.; Coto, P. B.; Charisiadis, A.; Charitaki, D.; Charalambidis, G.; Angaridis, P.; Coutsolelos, A. G.; Costa, R. D. Cunning Metal Core: Efficiency/stability Dilemma in Metallated Porphyrin Based Light-Emitting Electrochemical Cells. *Dalton Trans.* **2016**, *45* (34), 13284-13288. DOI: 10.1039/c6dt02293f.

(5) Shafikov, M. Z.; Tang, S.; Larsen, C.; Bodensteiner, M.; Kozhevnikov, V. N.; Edman, L. An Efficient Heterodinuclear Ir(III)/Pt(II) Complex: Synthesis, Photophysics and Application in Light-emitting Electrochemical Cells. *J. Mater. Chem. A* **2019**, *7* (34), 10672-10682. DOI: 10.1039/c9tc02930c.

(6) Shigeta, Y.; Kobayashi, A.; Yoshida, M.; Kato, M. Stability Tuning of Vapor-Adsorbed State of Vapochromic Pt(II) Complex by Introduction of Chiral Moiety. *Inorg. Chem.* **2019**, *58* (11), 7385-7392. DOI: 10.1021/acs.inorgchem.9b00533.

(7) Jain, A. Multifunctional, Heterometallic Ruthenium-Platinum Complexes with Medicinal Applications. *Coord. Chem. Rev.* **2019**, *401*. DOI: 10.1016/j.ccr.2019.213067.

(8) Zhong, Y.-F.; Zhang, H.; Mu, G.; Liu, W.-T.; Cao, Q.; Tan, C.-P.; Ji, L.-N.; Mao, Z.-W. Nucleus-localized Platinum(II)–triphenylamine Complexes as Potent Photodynamic Anticancer Agents. *Inorg. Chem. Front.* **2019**, *6* (10), 2817-2823. DOI: 10.1039/c9qi00738e.

(9) Law, A. S.; Lee, L. C.; Yeung, M. C.; Lo, K. K.; Yam, V. W. Amyloid Protein-Induced Supramolecular Self-Assembly of Water-Soluble Platinum(II) Complexes: A Luminescence Assay for Amyloid Fibrillation Detection and Inhibitor Screening. *J. Am. Chem. Soc.* **2019**, *141* (46), 18570-18577. DOI: 10.1021/jacs.9b09515.

(10) Mitra, K.; Lyons, C. E.; Hartman, M. C. T. A Platinum(II) Complex of Heptamethine Cyanine for Photoenhanced Cytotoxicity and Cellular Imaging in Near-IR Light. *Angew. Chem. Int. Ed. Engl.* **2018**, *57* (32), 10263-10267. DOI: 10.1002/anie.201806911.

(11) Montalti, M., Credi, A., Prodi, L., & Gandolfi, M.T. . Handbook of Photochemistry. 3rd ed.; CRC Press/Taylor & Francis Group, 2006; pp 617-623. DOI: 10.1201/9781420015195.

(12) Williams, J. A. G. Photochemistry and Photophysics of Coordination Compounds II. In *Top. Curr. Chem.*, 1st ed.; S, B. V. C. Ed.; Vol. 281; Springer, 2007; pp 205-268. DOI: 10.1007/978-3-540-73349-2.

(13) To, W.-P.; Wan, Q.; Tong, G. S. M.; Che, C.-M. Recent Advances in Metal Triplet Emitters with d^6, d^8, and d^{10} Electronic Configurations. *Trends in Chemistry* **2020**, *2* (9), 796-812. DOI: 10.1016/j.trechm.2020.06.004.

(14) Huo, S.; Carroll, J.; Vezzu, D. A. K. Design, Synthesis, and Applications of Highly Phosphorescent Cyclometalated Platinum Complexes. *Asian J. Org. Chem.* **2015**, *4* (11), 1210-1245. DOI: 10.1002/ajoc.201500246.

(15) Lu, G. Z.; Tu, Z. L.; Liu, L.; Zheng, Y. X.; Zhao, Y. Two Platinum(II) Complexes with a 4-phenyl-4*H*-1,2,4-Triazole Derivative as An Ancillary Ligand For Efficient Green Oleds. *Dalton Trans.* **2019**, *48* (5), 1892-1899. DOI: 10.1039/c8dt04750b.

(16) Ortiz, R. J.; Braun, J. D.; Williams, J. A. G.; Herbert, D. E. Brightly Luminescent Platinum Complexes of *N^C*^*N* Ligands Forming Six-Membered Chelate Rings: Offsetting Deleterious

Ring Size Effects Using Site-Selective Benzannulation. *Inorg. Chem.* **2021**, *60* (22), 16881-16894. DOI: 10.1021/acs.inorgchem.1c02551.

(17) Maisuls, I.; Wang, C.; Gutierrez Suburu, M. E.; Wilde, S.; Daniliuc, C. G.; Brunink, D.; Doltsinis, N. L.; Ostendorp, S.; Wilde, G.; Kosters, J.; et al. Ligand-controlled and Nanoconfinement-boosted Luminescence Employing Pt(II) and Pd(II) Complexes: from Color-tunable Aggregation-enhanced Dual Emitters Towards Self-referenced Oxygen Reporters. *Chem. Sci.* **2021**, *12* (9), 3270-3281. DOI: 10.1039/d0sc06126c.

(18) Fuertes, S.; Chueca, A. J.; Arnal, L.; Martín, A.; Giovanella, U.; Botta, C.; Sicilia, V. Heteroleptic Cycloplatinated N-Heterocyclic Carbene Complexes: A New Approach to Highly Efficient Blue-Light Emitters. *Inorg. Chem.* **2017**, *56*, 4829-4839. DOI: 10.1021/acs.inorgchem.6b02826.

(19) Strassner, T. Phosphorescent Platinum(II) Complexes with C^C* Cyclometalated NHC Ligands. *Acc. Chem. Res.* **2016**, *49* (12), 2680-2689. DOI: 10.1021/acs.accounts.6b00240.

(20) Soellner, J.; Strassner, T. Diaryl-1,2,3-Triazolylidene Platinum(II) Complexes. *Chem. Eur. J.* **2018**, *24* (21), 5584-5590. DOI: 10.1002/chem.201705738.

(21) Soellner, J.; Strassner, T. The "Enders Triazole" Revisited: Highly Efficient, Blue Platinum(II) Emitters. *Organometallics* **2018**, *37* (12), 1821-1824. DOI: 10.1021/acs.organomet.8b00191.

(22) Tronnier, A.; Wagenblast, G.; Munster, I.; Strassner, T. Phosphorescent Platinum(II) Complexes with C^C* Cyclometalated NHC Dibenzofuranyl Ligands: Impact of Different Binding Modes on the Decay Time of the Excited State. *Chem. Eur. J.* **2015**, *21* (37), 12881-12884. DOI: 10.1002/chem.201502087.

(23) Forniés, J.; Sicilia, V.; Borja, P.; Casas, J. M.; Díez, A.; Lalinde, E.; Larraz, C.; Martín, A.; Moreno, M. T. Luminescent Benzoquinolate-Isocyanide Platinum(II) Complexes: Effect of Pt···Pt and π···π Interactions on their Photophysical Properties. *Chem. Asian J.* **2012**, *7* (12), 2813-2823. DOI: 10.1002/asia.201200585.

(24) Sicilia, V.; Forniés, J.; Casas, J. M.; Martín, A.; López, J. A.; Larraz, C.; Borja, P.; Ovejero, C.; Tordera, D.; Bolink, H. Highly Luminescent Half-Lantern Cyclometalated Platinum(II) Complex: Synthesis, Structure, Luminescence Studies, and Reactivity. *Inorg. Chem.* **2012**, *51* (6), 3427-3435. DOI: 10.1021/ic201910t.

(25) Forniés, J.; Fuertes, S.; López, J. A.; Martín, A.; Sicilia, V. New Water Soluble and Luminescent Platinum(II) Compounds, Vapochromic Behavior of $[K(H_2O)][Pt(bzq)(CN)_2]$, New Examples of the Influence of the Counterion on the Photophysical Properties of d^8 Square-Planar Complexes. *Inorg. Chem.* **2008**, *47* (16), 7166-7176. DOI: 10.1021/ic800265q.

(26) Fuertes, S.; Garcia, H.; Peralvarez, M.; Hertog, W.; Carreras, J.; Sicilia, V. Stepwise Strategy to Cyclometallated Pt-II Complexes with N-Heterocyclic Carbene Ligands: A Luminescence Study on New beta-Diketonate Complexes. *Chem. Eur. J.* **2015**, *21* (4), 1620-1631. DOI: 10.1002/chem.201404915.

(27) Fuertes, S.; Chueca, A. J.; Sicilia, V. Exploring the Transphobia Effect on Heteroleptic NHC Cycloplatinated Complexes. *Inorg. Chem.* **2015**, *54* (20), 9885-9895. DOI: 10.1021/acs.inorgchem.5b01655.

(28) Fuertes, S.; Chueca, A. J.; Martín, A.; Sicilia, V. New NHC Cycloplatinated Compounds. Significance of The Cyclometalated Group on the Electronic and Emitting Properties of Bis-cyanide Compounds. *J. Organomet. Chem.* **2019**, *889*, 53-61. DOI: 10.1016/j.jorganchem.2019.03.012.

(29) Fuertes, S.; Chueca, A. J.; Martín, A.; Sicilia, V. Pt_2Tl Building Blocks for Two-Dimensional Extended Solids: Synthesis, Crystal Structures, and Luminescence. *Cryst. Growth. Des.* **2017**, *17* (8), 4336-4346. DOI: 10.1021/acs.cgd.7b00662.

(30) Sicilia, V.; Fuertes, S.; Chueca, A. J.; Arnal, L.; Martín, A.; Perálvarez, M.; Botta, C.; Giovanella, U. Highly Efficient Platinum-based emitters for Warm White Light Emitting Diodes. *J. Mater. Chem. A* **2019**, *7* (15), 4509-4516. DOI: 10.1039/c9tc00747d.

(31) Jaime, S.; Arnal, L.; Sicilia, V.; Fuertes, S. Cyclometalated NHCs Pt(II) Compounds with Chelating P^P and S^S Ligands: From Blue to White Luminescence. *Organometallics* **2020**, *39* (20), 3695-3704. DOI: 10.1021/acs.organomet.0c00510.

(32) Sicilia, V.; Arnal, L.; Chueca, A. J.; Fuertes, S.; Babaei, A.; Igual Munoz, A. M.; Sessolo, M.; Bolink, H. J. Highly Photoluminescent Blue Ionic Platinum-Based Emitters. *Inorg. Chem.* **2020**, *59* (2), 1145-1152. DOI: 10.1021/acs.inorgchem.9b02782.

(33) Fuertes, S.; Mardegan, L.; Martínez, I.; Ventura, S.; Ara, I.; Tordera, D.; Bolink, H. J.; Sicilia, V. Green Light-emitting Electrochemical Cells Based on Platinum(II) Complexes with a Carbazole-appended Carbene Ligand. *J. Mater. Chem. A* **2022**, *10* (41), 15491-15500, 10.1039/D2TC02539F. DOI: 10.1039/D2TC02539F.

(34) Sicilia, V.; Baya, M.; Borja, P.; Martín, A. Oxidation of Half-Lantern Pt_2(II,II) Compounds by Halocarbons. Evidence of Dioxygen Insertion into a Pt(III)–CH_3 Bond. *Inorg. Chem.* **2015**, *54* (15), 7316-7324. DOI: 10.1021/acs.inorgchem.5b00846.

(35) Roundhill, D. M.; Dickson, M. K.; Atherton, S. J. Thermal and Photochemical Addition of Alkyl and Aryl Halides to Tetrakis(μ-pyrophosphito) Diplatinum(II) Tetraanion. *J. Organomet. Chem.* **1987**, *335* (3), 413-422. DOI: 10.1016/S0022-328X(00)99415-4.

(36) Alvarez-Manzaneda, E. J.; Chahboun, R.; Cabrera Torres, E.; Alvarez, E.; Alvarez-Manzaneda, R.; Haidour, A.; Ramos López, J. M. Reaction of Allylic and Benzylic Alcohols and Esters with PPh_3/I_2: One-pot Synthesis of β,γ-Unsaturated Compounds. *Tetrahedron Letters* **2005**, *46* (21), 3755-3759. DOI: 10.1016/j.tetlet.2005.03.132.

(37) Fuertes, S.; Chueca, A. J.; Perálvarez, M.; Borja, P.; Torrell, M.; Carreras, J.; Sicilia, V. White Light Emission from Planar Remote Phosphor Based on NHC Cycloplatinated Complexes. *ACS Appl. Mater. Interfaces* **2016**, *8*, 16160-16169. DOI: 10.1021/acsami.6b03288.

(38) Priqueler, J. R. L.; Butler, I. S.; Rochon, F. D. An Overview of ^{195}Pt Nuclear Magnetic Resonance Spectroscopy. *Appl. Spectrosc. Rev.* **2006**, *41* (3), 185-226. DOI: 10.1080/05704920600620311.

(39) Claridge, T. D. W. *High-Resolution NMR Techniques in Organic Chemistry*; Elsevier 2016. 3rd ed.

(40) Frisch, M. J.; Trucks, G. W.; Schlegel, H. B.; Scuseria, G. E.; Robb, M. A.; Cheeseman, J. R.; Scalmani, G.; Barone, V.; Mennucci, B.; Petersson, G. A.; *et al.* Gaussian 09. **2009**.

(41) Frisch, M. J.; Trucks, G. W.; Schlegel, H. B.; Scuseria, G. E.; Robb, M. A.; Cheeseman, J. R.; Scalmani, G.; Barone, V.; Petersson, G. A.; Nakatsuji, H.; *et al.* Gaussian 16 Rev. C.01. **2016**.

(42) Zhao, Y.; Truhlar, D. G. The M06 Suite of Density Functionals for Main Group Thermochemistry, Thermochemical Kinetics, Noncovalent Interactions, Excited States, and Transition Elements: Two New Functionals and Systematic Testing of Four M06-class Functionals and 12 Other Functionals. *Theor. Chem. Acc.* **2008**, *120* (1), 215-241. DOI: 10.1007/s00214-007-0310-x.

(43) Wang, Y.; Verma, P.; Jin, X.; Truhlar, D. G.; He, X. Revised M06 Density Functional for Main-Group and Transition-Metal Chemistry. *Proc.Natl. Acad. Sci.* **2018**, *115* (41), 10257. DOI: 10.1073/pnas.1810421115.

(44) Grimme, S.; Antony, J.; Ehrlich, S.; Krieg, H. A Consistent and Accurate Ab Initio Parametrization of Density Functional Dispersion Correction (DFT-D) for the 94 Elements H-Pu. *J. Chem. Phys.* **2010**, *132* (15), 154104. DOI: 10.1063/1.3382344.

(45) Andrae, D.; Häußermann, U.; Dolg, M.; Stoll, H.; Preuß, H. Energy-adjustedab Initio Pseudopotentials for the Second and Third Row Transition Elements. *Theoret. Chim. Acta* **1990**, *77* (2), 123-141. DOI: 10.1007/BF01114537.

(46) Ditchfield, R.; Hehre, W. J.; Pople, J. A. Self-Consistent Molecular-Orbital Methods. IX. An Extended Gaussian-Type Basis for Molecular-Orbital Studies of Organic Molecules. *J. Chem. Phys.* **1971**, *54* (2), 724-728. DOI: 10.1063/1.1674902.

(47) Hariharan, P. C.; Pople, J. A. The Influence of Polarization Functions on Molecular Orbital Hydrogenation Energies. *Theoret. Chim. Acta* **1973**, *28* (3), 213-222. DOI: 10.1007/BF00533485.

(48) Ehlers, A. W.; Böhme, M.; Dapprich, S.; Gobbi, A.; Höllwarth, A.; Jonas, V.; Köhler, K. F.; Stegmann, R.; Veldkamp, A.; Frenking, G. A Set of f-polarization Functions for Pseudo-potential Basis Sets of the Transition Metals Sc-Cu, Y-Ag and La-Au. *Chem. Phys. Lett.* **1993**, *208* (1), 111-114. DOI: 10.1016/0009-2614(93)80086-5.

(49) Höllwarth, A.; Böhme, M.; Dapprich, S.; Ehlers, A. W.; Gobbi, A.; Jonas, V.; Köhler, K. F.; Stegmann, R.; Veldkamp, A.; Frenking, G. A Set of d-polarization Functions for Pseudo-potential Basis Sets of the Main Group Elements Al-Bi and f-type Polarization Functions for Zn, Cd, Hg. *Chem. Phys. Lett.* **1993**, *208* (3), 237-240. DOI: 10.1016/0009-2614(93)89068-S.

(50) Sicilia, V.; Arnal, L.; Fuertes, S.; Martín, A.; Baya, M. Metal-Metal Cooperation in the Oxidation of a Flapping Platinum Butterfly by Haloforms: Experimental and Theoretical Evidence. *Inorg. Chem.* **2020**, *59* (17), 12586-12594. DOI: 10.1021/acs.inorgchem.0c01701.

(51) Arnal, L.; Fuertes, S.; Martín, A.; Baya, M.; Sicilia, V. A Cyclometalated N-Heterocyclic Carbene: The Wings of the First Pt_2(II,II) Butterfly Oxidized by CHI_3. *Chem. Eur. J.* **2018**, *24* (70), 18743-18748. DOI: 10.1002/chem.201804013.

(52) Arnal, L.; Fuertes, S.; Martín, A.; Sicilia, V. The Use of Cyclometalated NHCs and Pyrazoles for the Development of Fully Efficient Blue Pt^{II} Emitters and Pt/Ag Clusters. *Chem. Eur. J.* **2018**, *24* (37), 9377-9384. DOI: 10.1002/chem.201800646.

(53) Sicilia, V.; Arnal, L.; Escudero, D.; Fuertes, S.; Martin, A. Chameleonic Photo- and Mechanoluminescence in Pyrazolate-Bridged NHC Cyclometalated Platinum Complexes. *Inorg. Chem.* **2021**, *60* (16), 12274-12284. DOI: 10.1021/acs.inorgchem.1c01470.

(54) Tomasi, J.; Mennucci, B.; Cammi, R. Quantum Mechanical Continuum Solvation Models. *Chem. Rev.* **2005**, *105* (8), 2999-3094. DOI: 10.1021/cr9904009.

(55) Forniés, J.; Fuertes, S.; Martín, A.; Sicilia, V.; Lalinde, E.; Moreno, M. T. Homo- and Heteropolynuclear Platinum Complexes Stabilized by Dimethylpyrazolato and Alkynyl Bridging Ligands: Synthesis, Structures, and Luminescence. *Chem. Eur. J.* **2006**, *12* (32), 8253-8266. DOI: 10.1002/chem.200600139.

(56) Lindner, R.; Kaluđerović, G. N.; Paschke, R.; Wagner, C.; Steinborn, D. Synthesis and Characterization of Dinuclear Pyrazolato Bridged Platinum(IV) complexes. *Polyhedron* **2008**, *27* (3), 914-922. DOI: 10.1016/j.poly.2007.11.020.

(57) Keter, F. K.; Darkwa, J. Perspective: the Potential of Pyrazole-based Compounds in Medicine. *BioMetals* **2012**, *25* (1), 9-21. DOI: 10.1007/s10534-011-9496-4.

(58) Suna, Y.; Himeda, Y.; Fujita, E.; Muckerman, J. T.; Ertem, M. Z. Iridium Complexes with Proton-Responsive Azole-Type Ligands as Effective Catalysts for CO_2 Hydrogenation. *ChemSusChem* **2017**, *10* (22), 4535-4543. DOI: 10.1002/cssc.201701676 (acccessed 2022/10/18).

(59) Nakahara, Y.; Toda, T.; Matsunami, A.; Kayaki, Y.; Kuwata, S. Protic NNN and NCN Pincer-Type Ruthenium Complexes Featuring (Trifluoromethyl)pyrazole Arms: Synthesis and Application to Catalytic Hydrogen Evolution from Formic Acid. *Chem. Asian J.* **2018**, *13* (1), 73-80. DOI: 10.1002/asia.201701474.

(60) Brandi-Blanco, P.; Sanz Miguel, P. J.; Lippert, B. Expected and Unconventional Ag^+ Binding Modes in Heteronuclear Pt,Ag Coordination Polymers Derived from *trans*-$[Pt(methylamine)_2(pyrazole)_2]^{2+}$. *Eur. J. Inorg. Chem.* **2012**, *2012* (7), 1122-1129. DOI: 10.1002/ejic.201101197.

(61) Su, N.; Meng, F.; Chen, J.; Wang, Y.; Tan, H.; Su, S.; Zhu, W. Near-infrared Emitting Pyrazole-bridged Binuclear Platinum Complexes: Synthesis, Photophysical and

Electroluminescent Properties in PLEDs. *Dyes Pigm.* **2016**, *128*, 68-74. DOI: 10.1016/j.dyepig.2016.01.014.

(62) Horiuchi, S.; Moon, S.; Ito, A.; Tessarolo, J.; Sakuda, E.; Arikawa, Y.; Clever, G. H.; Umakoshi, K. Multinuclear Ag Clusters Sandwiched by Pt Complex Units: Fluxional Behavior and Chiral-at-Cluster Photoluminescence. *Angew. Chem. Int. Ed.* **2021**, *60* (19), 10654-10660. DOI: 10.1002/anie.202101460.

(63) Yélamos, C.; Gust, K. R.; Baboul, A. G.; Heeg, M. J.; Schlegel, H. B.; Winter, C. H. Early Transition Metal Complexes Containing 1,2,4-Triazolato and Tetrazolato Ligands: Synthesis, Structure, and Molecular Orbital Studies. *Inorg. Chem.* **2001**, *40* (25), 6451-6462. DOI: 10.1021/ic0109389.

(64) El-Kadri, O. M.; Siddique, A. A.; Eaton, M. D.; Nath, N. K. Synthesis and Characterization of Two Dioxidomolybdenum(VI) Complexes Bearing Amidinato and Pyrazolato Ligands and Their Use in Thin Film Growth and Oxygen Atom Transfer Reactions. *Polyhedron* **2018**, *147*, 36-41. DOI: 10.1016/j.poly.2018.03.009.

(65) Cinninger, L. M.; Bastatas, L. D.; Shen, Y.; Holliday, B. J.; Slinker, J. D. Luminescent Properties of a 3,5-diphenylpyrazole Bridged Pt(II) Dimer. *Dalton Trans.* **2019**, *48* (26), 9684-9691. DOI: 10.1039/c9dt00795d.

(66) Horiuchi, S.; Tanaka, S.; Moon, S.; Sakuda, E.; Ito, A.; Arikawa, Y.; Umakoshi, K. A Heteropolynuclear Pt–Ag System Having Cycloplatinated Rollover Bipyridyl Units. *Inorg. Chem.* **2021**, *60* (3), 1513-1522. DOI: 10.1021/acs.inorgchem.0c02843.

(67) R. Falvello, L.; Forniés, J.; Martín, A.; Navarro, R.; Sicilia, V.; Villarroya, P. Synthesis and Molecular Structure of [{$Pd_2(CH_2C_6H_4P(o\text{-tolyl})_2\text{-}\kappa C,P)_2(\mu_3\text{-3,5-dmpz-}N,N',C_4)_2Ag(\mu\text{-}ClO_4)\}_2$] (3,5-dmpz = 3,5-dimethylpyrazolato), a Silver Derivative Showing unprecedented η^1-Azolato Coordination. *Chem. Commun.* **1998**, (22), 2429-2430. DOI: 10.1039/A805938A.

(68) Forniés, J.; Martín, A.; Sicilia, V.; Martín, L. F. Polynuclear Palladium Complexes with 3,5-Dimethylpyrazolate Exhibiting Three Different Coordination Modes. *Chem. Eur. J.* **2003**, *9* (14), 3427-3435. DOI: 10.1002/chem.200204648.

(69) Ma, B.; Li, J.; Djurovich, P. I.; Yousufuddin, M.; Bau, R.; Thompson, M. E. Synthetic Control of Pt···Pt Separation and Photophysics of Binuclear Platinum Complexes. *J. Am. Chem. Soc.* **2005**, *127* (1), 28-29. DOI: 10.1021/ja044313w.

(70) Han, M.; Tian, Y.; Yuan, Z.; Zhu, L.; Ma, B. A Phosphorescent Molecular "Butterfly" that undergoes a Photoinduced Structural Change allowing Temperature Sensing and White Emission. *Angew. Chem. Int. Ed.* **2014**, *53* (41), 10908-10912. DOI: 10.1002/anie.201405293.

(71) Brown-Xu, S. E.; Kelley, M. S.; Fransted, K. A.; Chakraborty, A.; Schatz, G. C.; Castellano, F. N.; Chen, L. X. Tunable Excited-State Properties and Dynamics as a Function of Pt-Pt Distance in Pyrazolate-Bridged Pt(II) Dimers. *J. Phys. Chem. A* **2016**, *120* (4), 543-550. DOI: 10.1021/acs.jpca.5b11233.

(72) Ma, B.; Djurovich, P. I.; Garon, S.; Alleyne, B.; Thompson, M. E. Platinum Binuclear Complexes as Phosphorescent Dopants for Monochromatic and White Organic Light-Emitting Diodes. *Adv. Funct. Mater.* **2006**, *16* (18), 2438-2446. DOI: 10.1002/adfm.200600614.

(73) Zhou, C.; Tian, Y.; Yuan, Z.; Han, M.; Wang, J.; Zhu, L.; Tameh, M. S.; Huang, C.; Ma, B. Precise Design of Phosphorescent Molecular Butterflies with Tunable Photoinduced Structural Change and Dual Emission. *Angew. Chem. Int. Ed.* **2015**, *54* (33), 9591-9595. DOI: 10.1002/anie.201505185.

(74) Rachford, A. A.; Castellano, F. N. Thermochromic Absorption and Photoluminescence in $[Pt(ppy)(\mu\text{-}Ph_2pz)]_2$. *Inorg. Chem.* **2009**, *48* (23), 10865-10867. DOI: 10.1021/ic901156z.

(75) Zhou, C.; Yuan, L.; Yuan, Z.; Doyle, N. K.; Dilbeck, T.; Bahadur, D.; Ramakrishnan, S.; Dearden, A.; Huang, C.; Ma, B. Phosphorescent Molecular Butterflies with Controlled Potential-Energy Surfaces and Their Application as Luminescent Viscosity Sensor. *Inorg. Chem.* **2016**, *55* (17), 8564-8569. DOI: 10.1021/acs.inorgchem.6b01108.

(76) Yersin, H.; Rausch, A. F.; Czerwieniec, R.; Hofbeck, T.; Fischer, T. The Triplet State of Organo-transition Metal Compounds. Triplet Harvesting and Singlet Harvesting for Efficient OLEDs. *Coord. Chem. Rev.* **2011**, *255* (21-22), 2622-2652. DOI: 10.1016/j.ccr.2011.01.042.

(77) Chakraborty, A.; Deaton, J. C.; Haefele, A.; Castellano, F. N. Charge-Transfer and Ligand-Localized Photophysics in Luminescent Cyclometalated Pyrazolate-Bridged Dinuclear Platinum(II) Complexes. *Organometallics* **2013**, *32* (14), 3819-3829. DOI: 10.1021/om400276v.

(78) Pinter, P.; Unger, Y.; Strassner, T. Cyclometalated N-Heterocyclic Carbene Platinum(II) Complexes with Bridging Pyrazolates: Enhanced Photophysical Properties of Binuclear Blue Emitters. *ChemPhotoChem* **2017**, *1* (4), 113-115. DOI: 10.1002/cptc.201600065.

(79) Pinter, P.; Soellner, J.; Strassner, T. Photophysical Properties of Phosphorescent Mono- and Bimetallic Platinum(II) Complexes with C^C* Cyclometalating NHC Ligands. *Organometallics* **2021**, *40* (4), 557-563. DOI: 10.1021/acs.organomet.0c00790.

(80) Steiner, T. Lengthening of the Covalent X−H Bond in Heteronuclear Hydrogen Bonds Quantified from Organic and Organometallic Neutron Crystal Structures. *J. Phys. Chem. A* **1998**, *102* (35), 7041-7052. DOI: 10.1021/jp981604g.

(81) Martín, A. Hydrogen Bonds Involving Transition Metal Centers Acting As Proton Acceptors. *J. Chem. Educ.* **1999**, *76* (4), 578. DOI: 10.1021/ed076p578.

(82) Moon, S.; Horiuchi, S.; Sakuda, E.; Ito, A.; Arikawa, Y.; Umakoshi, K. Synthesis and Photophysical Properties of Butterfly-shaped Dinuclear Pt(II) Complex Having NHC-based Chelate Ligands. *Inorg. Chim. Acta* **2019**, *493*, 43-48. DOI: 10.1016/j.ica.2019.04.045.

(83) Sicilia, V.; Borja, P.; Casas, J. M.; Fuertes, S.; Martín, A. Selective Synthesis of New Half-lantern Benzoquinolate Platinum Complexes. DFT and Photophysical Studies on the Platinum(II,II) Derivative. *J. Organomet. Chem.* **2013**, *731*, 10-17. DOI: 10.1016/j.jorganchem.2013.01.027.

(84) Nishihara, K.; Ueda, M.; Higashitani, A.; Nakao, Y.; Arikawa, Y.; Horiuchi, S.; Sakuda, E.; Umakoshi, K. Different Structural Preference of Ag(I) and Au(I) in Neutral and Cationic Luminescent Heteropolynuclear Platinum(II) Complexes: Z (U)-shaped Pt_2M_2 Type *vs.* Trinuclear PtM_2 Type. *Dalton Trans.* **2016**, *45* (12), 4978-4982. DOI: 10.1039/c6dt00320f.

(85) Akatsu, S.; Kanematsu, Y.; Kurihara, T.-A.; Sueyoshi, S.; Arikawa, Y.; Onishi, M.; Ishizaka, S.; Kitamura, N.; Nakao, Y.; Sakaki, S.; et al. Syntheses and Luminescent Properties of 3,5-Diphenylpyrazolato-Bridged Heteropolynuclear Platinum Complexes. The Influence of Chloride Ligands on the Emission Energy Revealed by the Systematic Replacement of Chloride Ligands by 3,5-Dimethylpyrazolate. *Inorg. Chem.* **2012**, *51* (15), 7977-7992. DOI: 10.1021/ic202663q.

(86) Fornies, J.; Sicilia, V.; Casas, J. M.; Martin, A.; Lopez, J. A.; Larraz, C.; Borja, P.; Ovejero, C. Pt-Ag Clusters and their Neutral Mononuclear Pt(II) Starting Complexes: Structural and Luminescence Studies. *Dalton Trans* **2011**, *40* (12), 2898-2912. DOI: 10.1039/c0dt01451f.

(87) Hudson, Z. M.; Sun, C.; Helander, M. G.; Chang, Y. L.; Lu, Z. H.; Wang, S. N. Highly Efficient Blue Phosphorescence from Triarylboron-Functionalized Platinum(II) Complexes of N-Heterocyclic Carbenes. *J. Am. Chem. Soc.* **2012**, *134* (34), 13930-13933. DOI: 10.1021/Ja3048656.

(88) Unger, Y.; Meyer, D.; Molt, O.; Schildknecht, C.; Münster, I.; Wagenblast, G.; Strassner, T. Green–Blue Emitters: NHC-Based Cyclometalated [Pt(C^C*)(acac)] Complexes. *Angew. Chem. Int. Ed.* **2010**, *49* (52), 10214-10216. DOI: 10.1002/anie.201001316.

(89) Fleetham, T.; Wang, Z.; Li, J. Efficient Deep Blue Electrophosphorescent Devices Based on Platinum(II) bis(n-methyl-imidazolyl)benzene Chloride. *Organic Electronics* **2012**, *13* (8), 1430-1435. DOI: 10.1016/j.orgel.2012.03.041.

(90) Hang, X. C.; Fleetham, T.; Turner, E.; Brooks, J.; Li, J. Highly Efficient Blue-emitting Cyclometalated Platinum(II) Complexes by Judicious Molecular Design. *Angew. Chem. Int. Ed.* **2013**, *52* (26), 6753-6756. DOI: 10.1002/anie.201302541.

(91) Kim, P.; Kelley, M. S.; Chakraborty, A.; Wong, N. L.; Van Duyne, R. P.; Schatz, G. C.; Castellano, F. N.; Chen, L. X. Coherent Vibrational Wavepacket Dynamics in Platinum(II) Dimers and Their Implications. *J. Phys. Chem. C* **2018**, *122* (25), 14195-14204. DOI: 10.1021/acs.jpcc.8b01636.

(92) Le Bras, L.; Chaitou, K.; Aloïse, S.; Adamo, C.; Perrier, A. Aggregation-caused Quenching Versus Crystallization Induced Emission in Thiazolo[5,4-*b*]thieno[3,2-*e*]pyridine (TTP) Derivatives: Theoretical Insights. *Phys. Chem. Chem. Phys.* **2019**, *21* (1), 46-56. DOI: 10.1039/C8CP04730H.

(93) Zhao, Z.; Zhang, H.; Lam, J. W. Y.; Tang, B. Z. Aggregation-Induced Emission: New Vistas at the Aggregate Level. *Angew. Chem. Int. Ed.* **2020**, *59* (25), 9888-9907. DOI: 10.1002/anie.201916729.

(94) Díez, Á.; Lalinde, E.; Moreno, M. T. Heteropolynuclear Cycloplatinated Complexes: Structural and Photophysical Properties. *Coord. Chem. Rev.* **2011**, *255* (21-22), 2426-2447. DOI: 10.1016/j.ccr.2010.12.024.

(95) Fornies, J.; Ibanez, S.; Martin, A.; Sanz, M.; Berenguer, J. R.; Lalinde, E.; Torroba, J. Influence of the Pt -> Ag Donor-Acceptor Bond and Polymorphism on the Spectroscopic and Optical Properties of Heteropolynuclear Benzoquinolateplatinum(II) Complexes. *Organometallics* **2006**, *25* (18), 4331-4340. DOI: 10.1021/om0604526.

(96) Moret, M.-E.; Chen, P. Interaction of Organoplatinum(II) Complexes with Monovalent Coinage Metal Triflates. *J. Am. Chem. Soc.* **2009**, *131* (15), 5675-5690. DOI: 10.1021/ja900449y.

(97) Ueda, M.; Horiuchi, S.; Sakuda, E.; Nakao, Y.; Arikawa, Y.; Umakoshi, K. Reversible Formation and Cleavage of Pt-->Ag Dative Bonds in a Pre-organized Cavity of a Luminescent Heteropolynuclear Platinum(II) Complex. *Chem. Commun.* **2017**, *53* (48), 6405-6408. DOI: 10.1039/c7cc03447d.

(98) Li, X.; Wu, H.; Lang, Y.; Huang, G. Mechanism, Selectivity, and Reactivity of Iridium- and Rhodium-catalyzed Intermolecular Ketone *α*-alkylation with Unactivated Olefins *via* an Enamide Directing Strategy. *Catal. Sci. Technol.* **2018**, *8* (9), 2417-2426. DOI: 10.1039/c8cy00290h.

(99) Huang, B.; Hu, M.; Toste, F. D. Homogeneous Gold Redox Chemistry: Organometallics, Catalysis, and Beyond. *Trends in Chemistry* **2020**, *2* (8), 707-720. DOI: 10.1016/j.trechm.2020.04.012.

(100) Kornecki, K. P.; Berry, J. F.; Powers, D. C.; Ritter, T. Metal-Metal Bond-Containing Complexes as Catalysts for C-H Functionalization. In *Progress in Inorganic Chemistry*, 2014; pp 225-302. DOI: 10.1002/9781118792797.ch04.

(101) Powers, D. C.; Ritter, T. Bimetallic Redox Synergy in Oxidative Palladium Catalysis. *Acc. Chem. Res.* **2012**, *45* (6), 840-850. DOI: 10.1021/ar2001974.

(102) Powers, I. G.; Uyeda, C. Metal–Metal Bonds in Catalysis. *ACS Catal.* **2017**, *7* (2), 936-958. DOI: 10.1021/acscatal.6b02692.

(103) Wang, W.; Ji, C. L.; Liu, K.; Zhao, C. G.; Li, W.; Xie, J. Dinuclear Gold Catalysis. *Chem. Soc. Rev.* **2021**, *50* (3), 1874-1912. DOI: 10.1039/d0cs00254b.

(104) Buchwalter, P.; Rosé, J.; Braunstein, P. Multimetallic Catalysis Based on Heterometallic Complexes and Clusters. *Chem. Rev.* **2015**, *115* (1), 28-126. DOI: 10.1021/cr500208k.

(105) Fernando, R. G.; Gasery, C. D.; Moulis, M. D.; Stanley, G. G. Bimetallic Homogeneous Hydroformylation. In *Homo- and Heterobimetallic Complexes in Catalysis: Cooperative Catalysis*, Kalck, P. Ed.; Springer International Publishing, 2016; pp 1-29. DOI: 10.1007/3418_2015_147.

(106) Oro, L. A.; Sola, E.; López, J. A.; Torres, F.; Elduque, A.; Lahoz, F. J. Synthesis of $[Ir_2(\mu\text{-}Pz)_2(CH_3)(CO)_2(P^iPr_3)_2]^+$. A Key Intermediate in S_N2 Oxidative Addition of Halocarbons to Dinuclear Complexes. *Inorg. Chem. Commun.* **1998**, *1* (2), 64-67. DOI: 10.1016/S1387-7003(98)00017-3.

(107) Casado, M. A.; Pérez-Torrente, J. J.; Ciriano, M. A.; Dobrinovitch, I. T.; Lahoz, F. J.; Oro, L. A. Stereoselective Oxidative Additions of Iodoalkanes and Activated Alkynes to a Sulfido-Bridged Heterotrinuclear Early−Late ($TiIr_2$) Complex. *Inorg. Chem.* **2003**, *42* (12), 3956-3964. DOI: 10.1021/ic034278e.

(108) Kolel-Veetil, M. K.; Rheingold, A. L.; Ahmed, K. J. Oxidative Addition Reactions of the Bridging Amido Complex $Ir_2[\mu\text{-NH}(p\text{-tolyl})]_2(CO)_4$: X-ray Crystal Structure of the 16e-18e Dimer $Ir_2(Me)(I)[\mu\text{-NH}(p\text{-tolyl})]_2(CO)_4\cdot 0.25C_6H_{14}$. *Organometallics* **1993**, *12* (9), 3439-3446. DOI: 10.1021/om00033a014.

(109) Ciriano, M. A.; Pérez-Torrente, J. J.; Oro, L. A. Synthesis and Reactivity of Binuclear 7-Azaindolate Complexes of Iridium: II. Oxidative-addition Reactions of Halogens and Halocarbons to $[\{Ir(\mu\text{-aza})(CO)_2\}_2]$. *J. Organomet. Chem.* **1993**, *445* (1), 273-281. DOI: 10.1016/0022-328X(93)80216-X.

(110) Caspar, J. V.; Gray, H. B. Photoinduced Oxidative Addition Chemistry of bis(1,5-cyclooctadiene)bis(μ-pyrazolyl)diiridium(I). *Chem. Soc. Rev.* **1984**, *106* (10), 3029-3030. DOI: 10.1021/ja00322a046.

(111) Mena, I.; Jaseer, E. A.; Casado, M. A.; García-Orduña, P.; Lahoz, F. J.; Oro, L. A. Terminal and Bridging Parent Amido 1,5-Cyclooctadiene Complexes of Rhodium and Iridium. *Chem. Eur. J.* **2013**, *19* (18), 5665-5675. DOI: 10.1002/chem.201204391.

(112) Tejel, C.; Bordonaba, M.; Ciriano, M. A.; Edwards, A. J.; Clegg, W.; Lahoz, F. J.; Oro, L. A. Oxidative-Addition Reactions of Diiodine to Dinuclear Rhodium Pyrazolate Complexes. *Inorg. Chem.* **1999**, *38* (6), 1108-1117. DOI: 10.1021/ic980650s.

(113) Tejel, C.; Ciriano, M. A.; López, J. A.; Lahoz, F. J.; Oro, L. A. Oxidative-Addition of Organic Monochloro Derivatives to Dinuclear Iridium Complexes: The Detection of Tautomeric Equilibria and Their Implications on the Reactivity. *Organometallics* **2000**, *19* (24), 4977-4984. DOI: 10.1021/om000314v.

(114) Roundhill, D. M.; Gray, H. B.; Che, C. M. Pyrophosphito-bridged Diplatinum Chemistry. *Acc. Chem. Res.* **1989**, *22* (2), 55-61. DOI: 10.1021/ar00158a002.

(115) Che, C. M.; Yam, V. W. W.; Wong, W. T.; Lai, T. F. Spectroscopy and X-ray Crystal Structure of Luminescent bis[bis(diphenylphosphino)methane]tetracyanodiplatinum. *Inorg. Chem.* **1989**, *28* (15), 2908-2910. DOI: 10.1021/ic00314a007.

(116) Miskowski, V. M.; Houlding, V. H. Electronic Spectra and Photophysics of Platinum(II) Complexes with *a*-Diimine Ligands Solid-state effects. 2. Metal-metal Interaction in Double Salts and Linear Chains. *Inorg. Chem.* **1991**, *30* (23), 4446-4452. DOI: 10.1021/ic00023a032.

(117) Sun, C.-Y.; To, W.-P.; Hung, F.-F.; Wang, X.-L.; Su, Z.-M.; Che, C.-M. Metal–Organic Framework Composites with Luminescent Pincer Platinum(II) Complexes: ^{3}MMLCT Emission and Photoinduced Dehydrogenation Catalysis. *Chem. Sci.* **2018**, *9* (8), 2357-2364. DOI: 10.1039/C7SC04528J.

(118) Li, Z.; Han, Y.; Gao, Z.; Wang, F. Supramolecular Engineering of Discrete Pt(II)···Pt(II) Interactions for Visible-Light Photocatalysis. *ACS Catal.* **2017**, *7* (7), 4676-4681. DOI: 10.1021/acscatal.7b00709.

(119) Zhong, J.-J.; Yang, C.; Chang, X.-Y.; Zou, C.; Lu, W.; Che, C.-M. Platinum(II) Photocatalysis for Highly Selective Difluoroalkylation Reactions. *Chem. Commun.* **2017**, *53* (64), 8948-8951. DOI: 10.1039/C7CC03823B.

(120) Umakoshi, K.; Kinoshita, I.; Ichimura, A.; Ooi, S. Binuclear platinum(II) and -(III) Complexes of Pyridine-2-thiol and its 4-methyl Analog. Synthesis, Structure, and Electrochemistry. *Inorg. Chem.* **1987**, *26* (21), 3551-3556. DOI: 10.1021/ic00268a027.

(121) Koshiyama, T.; Omura, A.; Kato, M. Redox-controlled Luminescence of a Cyclometalated Dinuclear Platinum Complex Bridged with Pyridine-2-thiolate Ions. *Chem. Lett.* **2004**, *33* (10), 1386-1387. DOI: 10.1246/cl.2004.1386.

(122) Nabavizadeh, S. M.; Sepehrpour, H.; Kia, R.; Rheingold, A. L. Bis(diphenylphosphino)acetylene as Bifunctional Ligand in Cycloplatinated Complexes:

Synthesis, Characterization, Crystal Structures and Mechanism of MeI Oxidative Addition. *J. Organomet. Chem.* **2013**, *745–746*, 148-157. DOI: 10.1016/j.jorganchem.2013.07.032.

(123) Jamali, S.; Nabavizadeh, S. M.; Rashidi, M. Binuclear Cyclometalated Organoplatinum Complexes Containing 1,1′-Bis(diphenylphosphino)ferrocene as Spacer Ligand: Kinetics and Mechanism of MeI Oxidative Addition. *Inorg. Chem.* **2008**, *47* (12), 5441-5452. DOI: 10.1021/ic701910d.

(124) Nabavizadeh, S. M.; Aseman, M. D.; Ghaffari, B.; Rashidi, M.; Hosseini, F. N.; Azimi, G. Kinetics and Mechanism of Oxidative Addition of MeI to Binuclear Cycloplatinated Complexes Containing Biphosphine Bridges: Effects of Ligands. *J. Organomet. Chem.* **2012**, *715*, 73-81. DOI: 10.1016/j.jorganchem.2012.05.026.

(125) Jamali, S.; Nabavizadeh, S. M.; Rashidi, M. Oxidative Addition of Methyl Iodide to a New Type of Binuclear Platinum(II) Complex: a Kinetic Study. *Inorg. Chem.* **2005**, *44* (23), 8594-8601. DOI: 10.1021/ic0511064.

(126) Umakoshi, K.; Kimura, K.; Kim, Y. H.; Tsukimoto, Y.; Arikawa, Y.; Onishi, M.; Ishizaka, S.; Kitamura, N. Pyrazolato- and 3,5-Dimethylpyrazolato-bridged Dinuclear Platinum(II), Palladium(II), and Their Mixed-Metal Complexes of 2,2′-Bipyrimidine. Syntheses, Structures, and Luminescent Properties. *Bull. Chem. Soc. Jpn.* **2010**, *83* (12), 1504-1510. DOI: 10.1246/bcsj.20100208.

(127) Sakai, K.; Sato, T.; Tsubomura, T.; Matsumoto, K. Di-(*m*-pyrazolato-N:N')-bis[(2,2'-bipyridine-N,N')platinum(II)] Bis(tetrafluoroborate) Monohydrate. *Acta Crystallographica Section C* **1996**, *52* (4), 783-786. DOI: 10.1107/S0108270195014326.

(128) Sun, Q.-F.; Wong, K. M.-C.; Liu, L.-X.; Huang, H.-P.; Yu, S.-Y.; Yam, V. W.-W.; Li, Y.-Z.; Pan, Y.-J.; Yu, K.-C. Self-Assembly, Structures, and Photophysical Properties of 4,4′-Bipyrazolate-Linked Metallo-Macrocycles with Dimetal Clips. *Inorg. Chem.* **2008**, *47* (6), 2142-2154. DOI: 10.1021/ic701344p.

(129) Saito, K.; Nakao, Y.; Sakaki, S. Theoretical Study of Pyrazolate-Bridged Dinuclear Platinum(II) Complexes: Interesting Potential Energy Curve of the Lowest Energy Triplet Excited State and Phosphorescence Spectra. *Inorg. Chem.* **2008**, *47* (10), 4329-4337. DOI: 10.1021/ic702367f.

(130) Bennett, M. A.; Bhargava, S. K.; Bond, A. M.; Edwards, A. J.; Guo, S.-X.; Privér, S. H.; Rae, A. D.; Willis, A. C. Synthesis, Characterization, and Electrochemical Relationships of Dinuclear Complexes of Platinum(II) and Platinum(III) Containing Ortho-Metalated Tertiary Arsine Ligands. *Inorg. Chem.* **2004**, *43* (24), 7752-7763. DOI: 10.1021/ic0498790.

(131) Bennett, M. A.; Bhargava, S. K.; Cheng, E. C.-C.; Lam, W. H.; Lee, T. K.-M.; Privér, S. H.; Wagler, J.; Willis, A. C.; Yam, V. W.-W. Unprecedented Near-Infrared (NIR) Emission in Diplatinum(III) (d^7–d^7) Complexes at Room Temperature. *J. Am. Chem. Soc.* **2010**, *132* (20), 7094-7103. DOI: 10.1021/ja1002313.

(132) Sicilia, V.; Borja, P.; Martín, A. Half-Lantern Pt(II) and Pt(III) Complexes. New Cyclometalated Platinum Derivatives. *Inorganics* **2014**, *2* (3), 508-523. DOI: 10.3390/inorganics2030508.

(133) Vogler, A.; Kunkely, H. Photooxidation of 1,2-dithiolene Complexes of Nickel, Palladium, and Platinum in Chloroform. *Inorg. Chem.* **1982**, *21* (3), 1172-1175. DOI: 10.1021/ic00133a057.

(134) Wade, L. G., Jr.; Simek Jan, W. *Organic Chemistry*; Pearson Education, 2016. 9th ed.

(135) Hoggard, P. E.; Vogler, A. The Photooxidation of Tetrachloroplatinate(II) in Chloroform. *Inorg. Chim. Acta* **2003**, *348*, 229-232. DOI: 10.1016/S0020-1693(03)00004-5.

(136) Sandrini, D.; Maestri, M.; Balzani, V.; Chassot, L.; Von Zelewsky, A. Photochemistry of the Orthometalated *cis*-bis[2-(2-thienyl)pyridine]platinum(II) Complex in Halocarbon Solvents. *J. Am. Chem. Soc.* **1987**, *109* (25), 7720-7724. DOI: 10.1021/ja00259a021.

(137) Kelly, M. E.; Gómez-Ruiz, S.; Kluge, R.; Merzweiler, K.; Steinborn, D.; Wagner, C.; Schmidt, H. Studies of Mononuclear and Dinuclear Complexes of

dibromodimethylplatinum(IV): Preparation, Characterization and Crystal Structures. *Inorg. Chim. Acta* **2009**, *362* (4), 1323-1332. DOI: 10.1016/j.ica.2008.06.025.

(138) Tejel, C.; Ciriano, M. A.; Edwards, A. J.; Lahoz, F. J.; Oro, L. A. Oxidative-Addition of Organic Monochloro Derivatives to Dinuclear Rhodium Complexes: Mechanistic Considerations. *Organometallics* **2000**, *19* (24), 4968-4976. DOI: 10.1021/om0003133.

(139) Yamaguchi, T.; Sasaki, Y.; Ito, T. Unusual C,O-bridging Coordination of Acetate and Acetylacetonate Ligands in the Platinum Clusters, $[Pt^{III}_2(\mu\text{-}CH_2COO\text{-}C,O)_2(\mu\text{-}CH_3COO\text{-}O,O')_2Cl_2]^{2-}$ and $Pt^{II}_4(\mu\text{-}CH_3COO\text{-}O,O')_4(\mu\text{-}CH_3COCHCOCH_3\text{-}O,C^3)_4$. *J. Am. Chem. Soc.* **1990**, *112* (10), 4038-4040. DOI: 10.1021/ja00166a051.

(140) Che, C. M.; Mak, T. C. W.; Gray, H. B. A Dimeric Platinum(III) System Containing a Long Metal-metal Bond. Crystal Structure of $K_4[Pt_2(P_2O_5H_2)_4CH_3I]\cdot 2H_2O$. *Inorg. Chem.* **1984**, *23* (25), 4386-4388. DOI: 10.1021/ic00193a058.

(141) Ochiai, M.; Fukui, K.; Iwatsuki, S.; Ishihara, K.; Matsumoto, K. Synthesis of Aryl-Platinum Dinuclear Complexes via ortho C−H Bond Activation of Phenol and Transmetalation of Arylboronic Acid. *Organometallics* **2005**, *24* (23), 5528-5536. DOI: 10.1021/om050316l.

(142) Matsumoto, K.; Arai, S.; Ochiai, M.; Chen, W.; Nakata, A.; Nakai, H.; Kinoshita, S. Synthesis of the Pivalamidate-Bridged Pentanuclear Platinum(II,III) Linear Complexes with Pt···Pt Interactions. *Inorg. Chem.* **2005**, *44* (23), 8552-8560. DOI: 10.1021/ic050942a.

(143) Ochiai, M.; Lin, Y.-S.; Yamada, J.; Misawa, H.; Arai, S.; Matsumoto, K. Reactions of a Platinum(III) Dimeric Complex with Alkynes in Water: Novel Approach to α-Aminoketone, α-Iminoketone, and *α,β*-Diimine via Ketonyl−Pt(III) Dinuclear Complexes. *J. Am. Chem. Soc.* **2004**, *126* (8), 2536-2545. DOI: 10.1021/ja0302634.

(144) Matsumoto, K.; Ochiai, M. Organometallic Chemistry of Platinum-blue Derived $Platinum^{III}$ Dinuclear Complexes. *Coord. Chem. Rev.* **2002**, *231* (1), 229-238. DOI: 10.1016/S0010-8545(02)00125-X.

(145) Lin, Y.-S.; Misawa, H.; Yamada, J.; Matsumoto, K. Synthesis of Ketonylplatinum(III) Dinuclear Complexes: Observation of the Competitive Radical vs Electrophilic Displacement in Pt(III)-Promoted C−H Bond Activation of Ketones. *J. Am. Chem. Soc.* **2001**, *123* (4), 569-575. DOI: 10.1021/ja9943041.

(146) Lin, Y.-S.; Takeda, S.; Matsumoto, K. Consecutive Double Nucleophilic Attacks on an Olefin Promoted by a Platinum(III) Dimeric Complex. *Organometallics* **1999**, *18* (24), 4897-4899. DOI: 10.1021/om990756a.

(147) Matsumoto, K.; Nagai, Y.; Matsunami, J.; Mizuno, K.; Abe, T.; Somazawa, R.; Kinoshita, J.; Shimura, H. A Synthetic Route to Alkyl−Pt^{III} Dinuclear Complexes from Olefins and Its Implication on the Olefin Oxidation Catalyzed by Amidate-Bridged Pt^{III} Dinuclear Complexes. *J. Am. Chem. Soc.* **1998**, *120* (12), 2900-2907. DOI: 10.1021/ja971129k.

(148) Matsumoto, K.; Matsunami, J.; Mizuno, K.; Uemura, H. Organometallic Chemistry of an Amidate-Bridged Dinuclear Pt(III) Complex: Axial Pt(III)−Alkyl σ-Bond Formation in the Reaction with Acetone. *J. Am. Chem. Soc.* **1996**, *118* (37), 8959-8960. DOI: 10.1021/ja961151y.

(149) Still, B. M.; Kumar, P. G.; Aldrich-Wright, J. R.; Price, W. S. ^{195}Pt NMR-theory and application. *Chem. Soc. Rev.* **2007**, *36* (4), 665-686. DOI: 10.1039/b606190g.

(150) Canty, A. J.; Gardiner, M. G.; Jones, R. C.; Rodemann, T.; Sharma, M. Binuclear Intermediates in Oxidation Reactions: $[(Me_3SiC{\equiv}C)Me_2(bipy)Pt{-}PtMe_2(bipy)]^+$ in the Oxidation of $Pt^{II}Me_2(bipy)$ (bipy = 2,2′-Bipyridine) by $IPh(C{\equiv}CSiMe_3)(OTf)$ (OTf = Triflate). *J. Am. Chem. Soc.* **2009**, *131* (21), 7236-7237. DOI: 10.1021/ja902799u.

(151) Ariafard, A.; Hyland, C. J.; Canty, A. J.; Sharma, M.; Brookes, N. J.; Yates, B. F. Ligand Effects in Bimetallic High Oxidation State Palladium Systems. *Inorg. Chem.* **2010**, *49* (23), 11249-11253. DOI: 10.1021/ic1020912.

La realización de esta Tesis ha sido posible gracias a la siguiente financiación:

- Contrato del Gobierno de Aragón para Personal Investigador Predoctoral en Formación para el Período 2019-2023.
- Beca Erasmus+ del Campus Iberus, Curso 2019-2020
- Proyecto PGC2018-094749-B-I00
- Proyecto PID2021-122869NB-I00
- Financiación a Grupos del Gobierno de Aragón, Grupo E17_20R: Química Inorgánica y de los Compuestos Organometálicos.